Bulletin
of
The Geological Society of America

VOLUME 61 September 1950 NUMBER 9

CONTENTS

Pages

Geophysical investigations in the emerged and submerged Atlantic Coastal Plain: Part V: Woods Hole, New York, and Cape May sections. By Maurice Ewing, J. L. Worzel, N. C. Steenland, and Frank Press 877–892

Geology of Gatun Lake and vicinity, Panama. By Stewart M. Jones 893–922

Structural petrology of the Wissahickon schist near Philadelphia, Pennsylvania. By Chi-shang Ch'ih 923–956

Petrology of Hakone volcano and adjacent areas, Japan. By Hisashi Kuno 957–1020

Short Notes

Volcanic geology of Toowa Valley, Southern Sierra Nevada, California. By Evans B. Mayo 1021–1022

Subscription $15 per year.

Publication Office: Mt. Royal & Guilford Aves., Baltimore 2, Md.

Communications for publication should be addressed to The Geological Society of America, Dr. H. R. Aldrich Secretary, 419 West 117th Street, New York 27, N. Y.

NOTICE.—Four weeks notice of change of address is necessary. In accordance with the rules established by the Council, claims for non-receipt of the preceding number of the Bulletin must be sent to the Secretary of the Society within three months of the date of the receipt of this number in order to be filled gratis.

Entered as second-class matter in the Post-Office at Baltimore, Md., under the Act of Congress of July 16, 1894.

Accepted for mailing at special rate of postage provided for in Section 1103 Act of October 3, 1917, authorized on July 8, 1918.

PAPERS IN PRESS FOR FORTHCOMING ISSUES

STRATIGRAPHY AND STRUCTURE OF THE OAK HILL SUCCESSION IN VERMONT. By Verne H. Booth
This paper is accompanied by a geological map, in color. Copies of the map (unfolded, in tubes) may be obtained. Price 25 cents. Remittance should accompany order.

PLEISTOCENE HISTORY OF COASTAL ALABAMA. By Charles W. Carlston

BLUE RIDGE FRONT—A FAULT SCARP. By William A. White

METAMORPHISM AND ASSOCIATED MINERALIZATION IN THE PHILIPSBURG REGION, MONTANA. By William T. Holser

TRACE-ELEMENT STUDIES, SANTA RITA, NEW MEXICO. By Donald L. Graf and Paul F. Kerr

SUBMARINE GEOLOGY OF BIKINI LAGOON AS INDICATED BY DISPERSION OF WATER-BORNE EXPLOSION WAVES. By Milton B. Dobrin

GEOLOGY OF THE BROKEN HILL ORE DEPOSIT, BROKEN HILL, N. S. W., AUSTRALIA. By J. K. Gustafson, H. C. Burrell, and M. D. Garretty

W
6
1
1
9
U

LOCATION OF SEISM

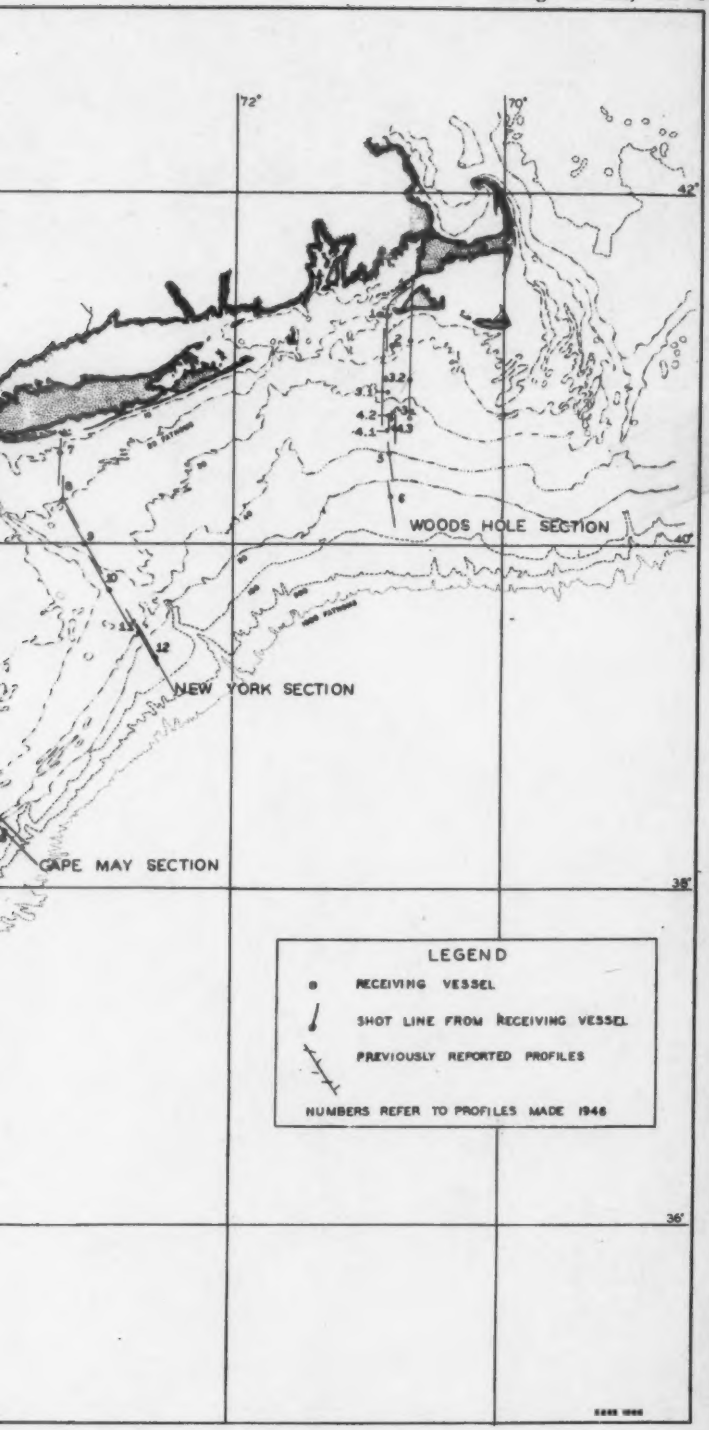

SEISMIC STATIONS

T
subs
cove
T
data
for

For
Abs
Intr
Ack
Loc
Met
Prin
Tra

Figu
1.
2.

Plat
1.
2.
3.
4.

S
line
alo
Ne
tiv
580
abo
the
wer

BULLETIN OF THE GEOLOGICAL SOCIETY OF AMERICA
VOL. 61, PP. 877–892, 2 FIGS., 6 PLS. SEPTEMBER 1950

GEOPHYSICAL INVESTIGATIONS IN THE EMERGED AND SUBMERGED ATLANTIC COASTAL PLAIN

PART V: WOODS HOLE, NEW YORK, AND CAPE MAY SECTIONS

By MAURICE EWING, J. L. WORZEL, N. C. STEENLAND, AND FRANK PRESS

FOREWORD

To avoid repetition of data and diagrams, the writers present the following seismic investigations of the subsurface geological structure in the northern submerged Atlantic Coastal Plain as one composite paper covering both the seismic investigation and the geological significance of the results.

The work was carried out by all the authors under the direction of Maurice Ewing. The reduction of the data was subdivided with J. Lamar Worzel primarily responsible for the Woods Hole profile, N. C. Steenland for the New York profile, and Frank Press for the Cape May profile.

CONTENTS

	Page
Foreward	877
Abstract	877
Introduction	878
Acknowledgments	878
Location of sections	878
Method of investigation	879
Principles of interpretation	879
Travel time data and geophysical results	881
General statement	881
Woods Hole profile	881
Summary of Woods Hole section	883
New York profile	883
Summary of New York profile	886
Cape May profile	886
Summary of Cape May profile	887
Geological significance of results	887
General statement	887
Geology, Woods Hole profile	887
Geology, New York profile	888
Geology, Cape May profile	888
Observed velocities	889
Geological history	889
Stratigraphic history	889
Structural history	891
Conclusion	891
References cited	891

ILLUSTRATIONS

Figure	Page
1. Atlantic Coastal Plain sections	884
2. Profile velocity variations	885

Plate	Facing page
5. Typical records for the Woods Hole, New York, and Cape May profiles	888
6. Subsurface contours on the basement	892

Plate	Facing page
1. Location of seismic stations	877
2. Travel time curve Woods Hole section	882
3. Travel time curve New York section	884
4. Travel time curve Cape May section	886

Table	Page
1. Locations of stations	879
2. Observed velocities and time intercepts	881
3. Velocities, thicknesses, and slopes of layers	882
4. Deep well tests, Maryland	890

ABSTRACT

Seismic refraction measurements from the coast line to the edge of the continental shelf were made along three lines of traverse: near Cape May, N. J., New York, N. Y., and Woods Hole, Mass., respectively. An unconsolidated layer with velocity about 5800 ft/sec, a semiconsolidated layer with velocity about 11,500 ft/sec, and a layer, considered to be the basement, with velocity about 18,000 ft/sec were traced across each traverse.

On the Cape May traverse, the thickness of the sedimentary column runs from about 5000 ft. near the beach to about 16000 ft. near the edge of the shelf, in general agreement with the findings on the Cape Henry traverse in 1935. The well on Cape Hatteras, which recently reached basement at 9878 feet, confirms the seismic results. The cross-section area of the sedimentary prism off Woods Hole is much less than that off New York, which in turn is less than that off Cape May. Depth to basement increases abruptly near the beach at Cape May,

and about 30 miles off shore at New York. The basement starts to slope gently upward at or just before the edge of the continental shelf on these two profiles.

Introduction

The writers present three seismic refraction profiles in the study of the submerged portion of the Atlantic Continental Shelf. Two of the profiles, Cape May and New York, are essentially continuations of profiles of the emerged portion of the continental shelf described in Part III and Part IV (Ewing *et al.*, 1939; Ewing *et al.*, 1940). The Woods Hole profile extends from the shore, which is almost at the Fall Line, here buried under glacial till, out to sea. Each profile was made along a line approximately perpendicular to the trend of the continental shelf and extended to the edge of the shelf.

Six sea seismic stations were occupied on the Woods Hole profile, six on the New York profile, and four on the Cape May profile (Pl. 1). Reverse profiles were made at all stations to determine the slopes of the seismic horizons. Except for two places, all slopes were gentle. Seaward basement dips of approximately 6° and 4°, respectively, were found about 10 miles off shore on the Cape May profile and about 30 miles off shore on the New York profile. The basement gradually deepened seaward on the Woods Hole profile. On both the New York and Cape May profiles, the basement deepened gradually seaward beyond the steep slope mentioned above, then reversed, shoaling somewhat towards the seaward ends.

The data obtained in this survey were far more complete than in our earlier ocean work, primarily because we could use a greatly increased number of shots. The accuracy of the subsurface information is correspondingly increased, and is adequate for reconnaissance purposes. The coverage is far less than that achieved in commercial operations.

The method of calculating the reversed profiles was that described in Part III (p. 262). For some stations on the New York and Cape May profiles, there was evidence of changes of velocity or slope within the reversed profiles, so that these were broken near the middle and calculated as two reversed profiles jn an attempt to bridge the gap between the interpretation methods of reconnaissance and detailed surveys.

As in previous work, certain seismic horizons in the overlying sediments could be traced accurately. All horizons on the New York and Cape May profiles may be connected to horizons under the emerged coastal plain without serious discrepancies. The Cape May profile and its landward continuation show a gradual velocity increase for the semi-consolidated layer from the Fall Line to the edge of the shelf.

The velocity variations of the basement rocks on these profiles is less than that observed in the earlier work.

Acknowledgments

The writers wish to express their deep appreciation for the financial aid furnished by the Penrose Bequest of the Geological Society of America, which made the work possible.

The Bureau of Ordnance of the U. S. Navy generously donated all the explosives used. In addition, the Naval Ordnance Laboratory, part of this Bureau, made a Mark I hydrophone available for this work and helped make the initial installation and adjustment of this gear.

We wish to thank the Watson Laboratories of the Army Air Forces for the loan of much of the equipment used in these observations, and for the privilege of sharing the use of a crash boat, which served as the receiving vessel.

The Woods Hole Oceanographic Institution served as the operating base, made the Research Vessels Balanus and Asterias available, and gave summer fellowships to Steenland and Worzel to make their participation possible.

G. P. Woollard and J. A. Peoples, Jr., assisted greatly in launching the field work and gave valuable advice throughout the field program. J. Mangin aided in the field operations.

The officers and crews of the P446, R. V. Balanus, and R. V. Asterias gave much valuable assistance.

Drs. W. H. Bucher and G. Marshall Kay of Columbia University were kind enough to critically review and discuss the manuscript before publication.

Location of Sections

The lines of sections were chosen to be as nearly perpendicular to the strike of the Coastal Plain structure as possible. Since reversed profiles were made at each station and the stations

(Table 1) overlap to some extent, information about slopes and depths was obtained nearly continuously along each profile. Plate 1 shows the relative positions of all seismic profiles established through 1946 in this study of the continental margin. On the profiles of the present investigation, the circles represent the positions of the receiving vessel and the lines cover the shot points.

Method of Investigation

The standard method of refraction seismic measurements described in Part I (Ewing, *et al.*, 1937, p. 759) was employed. The geophones and hydrophones were placed directly on the ocean bottom. All instruments were considerably improved, and octave filters were used to obtain further information about the frequencies of the water waves. The highest frequency water waves were used for distance determinations following the practice determined by Worzel and Ewing (1948). Bathythermograph observations were made at all stations to determine water velocities.

F. M. radios were used for intercommunication between ships and for the transmission of the instant of explosion, by interrupting a 1000-cycle tone by the same relay which fired the shot. Determinations of the error caused by this apparatus showed it to be negligible.

T. N. T. was used for most shots, but C-3 plastic explosive was used on a few occasions. No waterproofing of the explosives was needed. Shots were fired on bottom on all occasions except for the few shots in water depths greater than 100 fathoms where the lengths of cable available would not permit it.

Principles of Interpretation

The method employed was that described in Part III, but it is worthwhile to repeat the assumptions which form the basis of the derived formulae:

(1) Each layer is bounded top and bottom by planes and transmits seismic waves at a constant velocity.

(2) At the interface between two layers the path of the seismic wave is bent according to Snell's Law.

(3) A wave travelling in any layer with velocity, V, and incident upon the surface of the layer at an angle, α, with the normal has an apparent velocity, V/sin α, along the surface.

(4) Any travel time will be unchanged if the shot point and recording point are interchanged.

Table 1.—Location of Seismic Stations

No.	Latitude (N)	Longitude (W)
Woods Hole section		
1A	41°18.7′	70°52′
3.2	40°57.5′	70°52.5′
3A	40°43.3′	70°49.8′
4.3	40°40.0′	70°49.8′
5	40°30.9′	70°50′
6	40°16.9′	70°49.8′
New York section		
7	40°31.2′	73°17.8′
8	40°14.6′	73°16.2′
9	40°00.0′	73°06.6′
10	39°44.5′	72°54.3′
11	39°29.7′	72°41.7′
12	39°21.0′	72°34.6′
Cape May section		
13	39°00.0′	74°30.0′
14	38°49.6′	74°16.4′
15	38°36.4′	73°59.0′
16	38°20.8′	73°39.5′

From these assumptions it can be shown that the time-distance curves corresponding to each layer must satisfy three sets of conditions: (1) the reverse points (circled crosses on Pls. 2–4) for the two stations which are included in a reversed pair must be equal; (2) the time-intercepts at a single station should be equal for shot points both up-dip and down-dip from the station; and (3) the time-intercept points must be collinear. These conditions will not be met if the velocity or slope of a layer changes between the reversed station pair.

Points on the time-distance curves of the semi-consolidated and basement layers could be picked with certainty only when they occurred as first arrivals. Control over the slopes of these curves therefore extended only over a portion of the distance between the two stations of a reversed pair. In many cases, especially on the Cape May profile, a simple straight-line extension of the time-distance curve of the semi-consolidated layer violated condition (1), the

resulting reverse points being unequal. A straight-line extension from adjacent sides of a station of the time-distance curves of the basement layer occasionally violated condition (3) in that the discrepancies of the time-intercepts at the station were relatively large. For reasons given later, this discrepancy is attributed to a progressive velocity change in the semi-consolidated layer rather than to geometrical changes in the attitude of the layers. The reversed station pair 14S.–15N. illustrates this case. The time-distance curve for the first (unconsolidated) layer is fairly well determined over the range 14S.–15N. (Pl. 4). The second (semi-consolidated) layer is well determined for the forward direction in the range 14S.–14′N. but is not defined at all in the range 14′S.–15N. For the reverse direction, the second layer is determined only in the range 14′S.–15N. At distances large enough for the third (basement) layer to occur as first arrivals, its time-distance curves are well defined. Thus the velocity of the third layer is only determined for the forward direction in the range 14′S.–15N. and for the reverse direction in the range 14S.–14′N. A simple straight-line extension of the time-distance curves into the regions where they are not defined violates conditions (1) and (3).

To obtain an approximate adjustment of the data the following method was devised by Ewing. An artificial station 14′ is inserted near the break between the time-distance curves of the second and third layers. This gives two reversed station pairs, in each of which the velocities and dips of the layers are constant, in place of the original reverse station pair along which the velocity and dip vary.

The slopes of the travel-time curves corresponding to the second layer are broken near 14′ and altered so that the lines intersect an adjusted set of reverse points determined by averaging the original reverse points. This gives an apparent velocity for this layer in the reverse direction for the region 14S.–14′N. and an apparent velocity in the forward direction for 14′S.–15N. The forward apparent velocity for 14S.–14′N. and the reverse apparent velocity for 14′S.–15N. are determined by the original travel-time data.

The inequality of the time-intercepts at station 14 for the travel-time curves corresponding to the third layer was adjusted by altering the slopes of the curves at 13′ and 14′ so that they intersect at an adjusted intercept determined by successive trials to give plausible and concordant times, velocities, and depths.

In this manner apparent velocities in the forward and reversed directions are determined for the reversed pairs 14S.–14′N. and 14′S.–15N. Station 14′ is finally constructed by fitting time-distance curves to it having the velocities obtained by the above methods and fulfilling the additional condition of the equality of reverse points at 14–14′ and 14′–15, respectively. The formulae given by Ewing *et al.* (1939) are then applied to stations 14, 14′, and 15 to obtain depths and true velocities. The same methods are applied wherever artificial stations are required.

In all of our work the water-wave travel-time has been used to give the distance to the shot point, assuming the speed of sound in water derived from the temperature and salinity of the water. On the time-distance curves, the unit of distance is taken as the distance sound travels through the water in 1 second. Velocity changes along the length of a profile, and the lack of control over these changes because of difficulties in picking second arrivals, is the chief source of error in this investigation. The velocities of the unconsolidated, semi-consolidated, and basement layers are believed to be accurate to within 2 or 3 per cent. We are unwilling to claim an accuracy of greater than 10 per cent for the depth to basement, due to the well known possibility of masked layers.

The possibility that a layer of sediment overlying basement and matching it closely in velocity might be mistaken for basement has been pointed out many times, and the above estimate of accuracy includes no allowance for this possibility. At the present time there is little basis other than considerations of geological probability for taking a stand on this question. The reader who does not choose to join us in assuming that the third layer continues to represent basement as we proceed from land to sea may increase our values for basement depth by adding whatever thickness of "matching" sediments he considers justified.

TABLE 2.—OBSERVED VELOCITIES AND TIME INTERCEPTS

Sta. Pairs	V_1	V_{2a}	V_{2b}	V_{3a}	V_{3b}	T_{2a}	T_{2b}	T_{3a}	T_{3b}
Woods Hole Profile									
–1A	5600		19100				.20		
1A–3.2	5600	9800	9700	18400	19000	.24	.20	.19	.50
3.2–3A	6000	18800	19900			.48	.68		
4.2–4.3	5900	17700	19000			.68	.74		
4.3–5	6100	17800	18700			.74	.84		
5–6	6000	17600	20100			.84	1.44		
6–	6400	18000				1.44			
New York Profile									
–7	5600		19700				.65		
7–8	6100		12600	17100	17600		.67	.65	.82
8–9	5200	10600	11100	17200	22700	.67	.96	.82	2.33
9–9′	5750	11300	11300	17000	19600	.96	.93	2.33	2.80
9′–10	5750	11300	11300	20200	17200	.93	.90	2.80	2.32
10–11	5750	10900	11000	17200	18100	.90	1.03	2.32	2.60
11–12	5850	11700	12200	19000	17000	1.03	1.21	2.60	2.21
12–	5500	11500		17000		1.21		2.21	
Cape May Profile									
–13	5500		9600		23000		.72		2.40
13–13′	5450	10000	10200	17600	18300	.72	.84	2.40	2.49
13′–14	5450	10800	10900	17600	18300	.84	.92	2.49	2.63
14–14′	5250	11000	11000	17700	18000	.92	.93	2.63	2.63
14′–15	5250	11800	12100	17700	18100	.93	1.17	2.63	2.80
15–15′	5500	12700	13100	18400	18500	1.17	1.38	2.80	2.81
15′–16	5500	13400	14000	19100	18500	1.38	1.61	2.81	2.63
16–	5350	14700				1.61			

V_n: true velocity, ft/sec, of layer "n". The subscripts 1, 2, and 3 refer to the various seismic layers. Additional subscript "a" indicates apparent velocity at inshore end of a station-pair and "b" indicates offshore end. For example, V_{2a} for sta.-pair 8–9 is apparent velocity of second layer as determined at sta. 8.

T_{na} & T_{nb}: time-intercepts, secs., of travel-time curve for layer "n". "a" and "b" again designate determination at inshore and offshore ends of a sta.-pair, respectively.

TRAVEL TIME DATA AND GEOPHYSICAL RESULTS

General Statement

The travel-time data are all presented as profile-graphs in Plates 2–4. Apparent velocities and time-intercepts were determined from these lines (Table 2). The true velocities, slopes, and depths of the layers indicated by the travel-time profiles were then calculated (Table 3). Typical records for each profile are shown in plate 5.

Woods Hole Profile (Pl. 2)

Station 1A–N: There was land intervening between shot and receiving point for the five most distant points of this station, so that water-wave travel times could not be determined. (See Ewing *et al.*, 1946.) The distances are therefore somewhat uncertain since the ship's positions are relatively inaccurate for this type of work. This explains the divergence of the five most distant points from the line drawn to fit the points where observed water-wave times were available.

Station 1A–3.2: This reversed pair constitutes a very good determination. These stations were made towards the end of the season to compute a portion of the profile which had been omitted

TABLE 3.—VELOCITIES, THICKNESSES, AND SLOPES OF LAYERS

Station Pairs										Stations				
Number	V_1	V_2	V_3	W_{12}	W_{23}	h_{1a}	h_{1b}	h_{2a}	h_{2b}	Number	h_w	$\bar{h}_1$	$\bar{h}_2$	H
Woods Hole Profile														
1A	5600	18750*		−0.3			590							
1A–3.2	5600	9750	18700	0.2	−1.0	820	680	−510	1540	1A	70	700		770
3.2–3A	6000	19350		−0.5		1510	2150			3.2	160	680	1520	2360
3A–4.3	5900	18350		−0.7		2120	2300			3A	180	2140		2320
4.3–5	6100	18250		−0.5		2390	2720			4.3	220	2350		2570
5–6	6000	18750		−1.3		2660	4560			5	250	2690		2940
6	6400	19000*		−1.1		4890				6	390	4730		5120
New York Profile														
7	5600	18800*		−0.8			1910							
7–8	6100	17300		−0.3		2120	2180		550	7	80	2020		2100
8–9	5200	10800	19550	−0.7	−3.5	1980	2840	550	8310	8	110	2080	550	2740
9–9′	5750	11300	18150	0.0	−3.2	3210	3110	9120	12810	9	140	3030	8720	11890
9′–10	5750	11300	18550	0.0	3.5	3110	3010	12640	9450	9′	170	3110	12720	16000
10–11	5750	10900	17650	−0.2	−0.8	3040	3480	9140	10090	10	240	3030	9300	12570
11–12	5850	11900	17900	−0.7	4.6	3460	4060	11900	7200	11	210	3470	11000	14680
12	5500	11900*	17900*	−1.0	0.2	3750		7250		12	400	3910	7230	11540
Cape May Profile														
13	5500	9800*	19500*	0.8	−6.3		2392		8900					
13–13′	5450	10100	17950	−0.4	0.0	2330	3310	9710	8120	13	40	2330	9710	12080
13′–14	5450	10850	18150	−0.2	−0.5	2650	2900	10560	10970	13′	90	2980	9340	12410
14–14′	5250	11000	17850	0.1	−0.6	2750	2780	11380	11310	14	120	2830	11180	14130
14′–15	5250	11950	17900	−0.4	0.5	2700	3420	13160	12440	14′	140	2740	12240	15120
15–15′	5500	12900	18450	−0.4	1.2	3550	3890	14160	13170	15	160	3490	13300	16950
15′–16	5500	13700	18750	−0.6	2.9	4140	4840	12860	8920	15′	190	4020	13020	17210
16	5350	14200*		+0.8		4650				16	380	4750	8920	14050

V_n: true velocity, ft/sec, of layer "n".

W_{12} and W_{23}: slope, in degrees, of interface between layers 1 and 2, 2 and 3, respectively.

h_n: vertical thickness, feet, of layer "n". "a" and "b" designate determination at inshore and offshore ends of a station-pair, respectively.

h_w: depth of water, feet.

$\bar{h}_n$: mean vertical thickness, feet, of two determinations for layer "n".

H: vertical depth to basement below sea level, in feet.

* Assumed value.

The subscripts 1, 2, and 3 refer to the various seismic layers. Subscript "a" refers to the inshore station of a reverse pair and "b" to the offshore station. The subscript "w" refers to the water.

earlier in the season due to instrumental difficulties. This station pair shows practically the only arrivals from a consolidated layer on this profile. These arrivals are sharp and clear. This layer is missing at station 1A and again disappears 3 or 4 miles south of station 3.2. This is interpreted as a lens of semi-consolidated material overlying the basement. Ewing's observations (Part I) in 1935, 7 miles to the east, show a layer of about 12,000 ft./sec., somewhat higher than the 9,750 ft./sec. observed here. On the previous observations no slopes were determined, and only two points were available on which to base the velocity so that the present determination must be considered better.

Station 3.2–3A (4.2): Here the velocity determinations from 3.2 to the south are good, but

V6
1
1978
UI

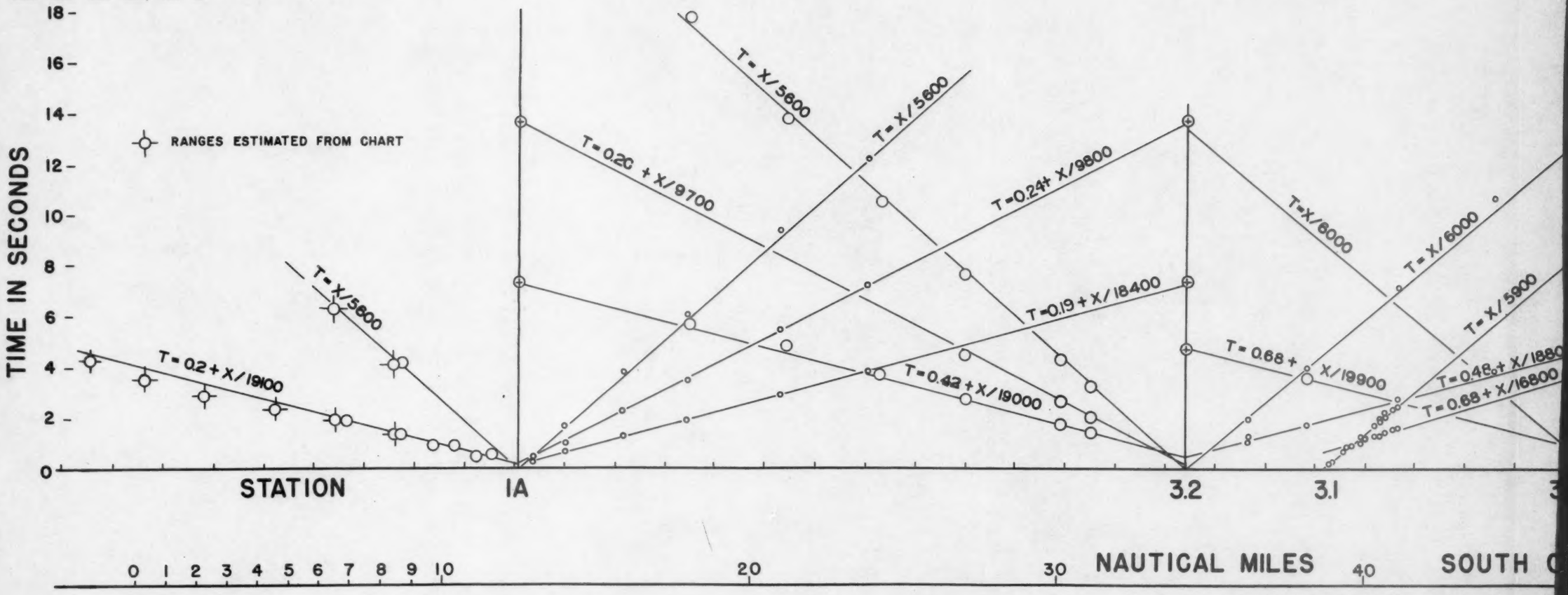

TRAVEL-TIME CURVES. W

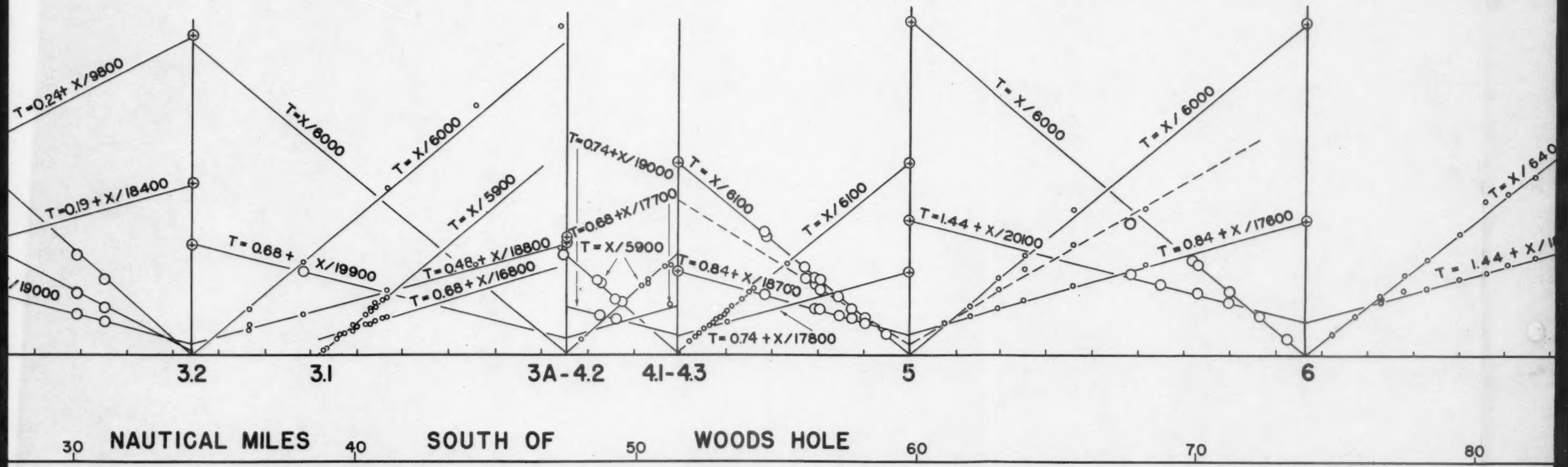

TRAVEL-TIME CURVES, WOODS HOLE SECTION

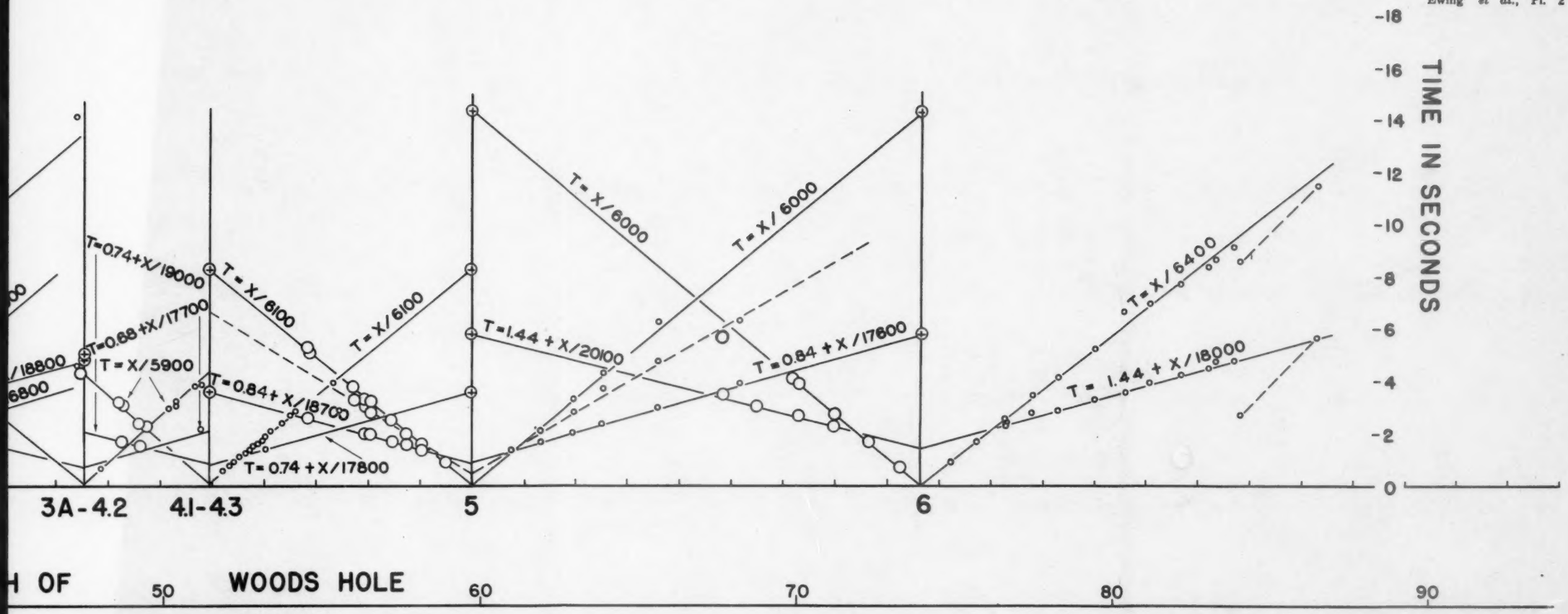

. WOODS HOLE SECTION

th
v
re
tr
e
m
g

w
w
n
H
d

c
tw
fo
cu
of
4.

th
yi
la

re
de
Th
th
th
5M
sm
tic
ev
in
ba
in

an
sol
of
sta

tio
loc
is
cha
los
tim
slo

there was no data available from 3A. The high velocity line was drawn on the basis of the reverse points from the shooting from 3.2 to true south and the time intercept at 3A as explained below. Station 3A is very poor and must be considered interpolated from the very good 3.2 and the fair 4.3.

Station 3.1W: The basement velocity is not well determined at station 3.1. Since the shots were fired to the west of the receiving point, no support can be given from other stations. Hence no calculations were made with these data.

Station 4.2(3A)–4.3N(4.1): This reverse pair constitutes a poor determination. There are only two points to determine the basement velocity for 4.3N. and only one poor point for 3AS. The curves for the basement are drawn on the basis of the support of 4.3S. and the two points for 4.3N.

Station 4.1W: Station 4.1W. was made during the period of instrumental difficulties and yielded only points from the unconsolidated layer.

Station 4.3S.(4.1)–5N: The 5N. station of this reversed pair is an excellent station with well-determined basement and unconsolidated layers. The 4.3S. station yielded only one point from the basement layer. The basement velocity for this station was drawn using the support of the 5N. station. There were some indications of a small lens of semi-consolidated material at station 5 both to the north and the south, but evidence was insufficient to include this layer in the calculations. If this lens is present, the basement depth may be somewhat greater than indicated here.

Station 5S.–6N: This reversed pair constitutes an excellent determination of both the unconsolidated and basement layers. The steepening of the basement slope begins between these stations.

Station 6S: This station is a good determination of the unconsolidated and basement velocities. The distance to the outermost points is somewhat in question, due to firing the charges hydrostatically, which involved serious loss in precision of the time break. The firing time is uncertain to ±0.2 sec. The basement slope indicated in 5S.–6N. is continued.

Summary of Woods Hole Section

This section has the poorest observations of any reported here. The central part of the profile is weakest. More recent work, soon to be reported, has filled in the poor part of this section and carried the Woods Hole and New York sections out to the 1500 fathom curve, as well as establishing a new profile from Portland, Maine, across George's Banks, also out to the 1500 fathom curve.

Figure 1 shows the cross section. Previous depth determinations by Ewing (1935) are also shown. The agreement is considered satisfactory since his stations were more to the east and based on meager data. The basement dips gently toward the sea at about 0.5° from 10 miles to 60 miles south of Woods Hole. From here to the end of the profile the slope steepens to about 1°.

Figure 2 shows the variations of true velocity along this profile. The velocity of the unconsolidated layer increases gradually towards the sea from about 5,500 ft./sec. to 6,500 ft./sec. The basement velocity shows no trend but varies from 18,000 ft./sec. to 19,400 ft./sec., averaging 18,700 ft./sec., the largest deviations occurring when the data are poorest.

New York Profile (Pl. 3)

Station 7N: This station has no reverse profile. The semi-consolidated layer is absent north of station 7. The northernmost basement arrival was recorded about 6 miles from station 7. The basement depth at that point can be made to coincide with the slopes drawn between the computed depths at 7 and the known depth off shore by assuming a value of the velocity of the basement rock of 18,800 ft./sec. This value is in good agreement with the V_3 values along the New York line, being 700 ft./sec. greater than the average value for the line.

The travel-time curve for the basement is well-defined by seven points, all of which have second arrivals which plot on a parallel curve and have a higher intercept. These later arrivals are interpreted as seismic waves which have followed normal refraction paths but have been reflected once at the surface of the water.

Stations 7S–8N: This station-pair was computed as though it were a two-layer case in

spite of the presence of three arrivals on the profile north of 8, apparently from the semi-consolidated layer.

The curves for the crystalline rock are well determined. The slope and velocity of the base-

the highest recorded for the basement on the New York section.

Coincident with the appearance of the semi-consolidated layer, the basement floor drops abruptly from a depth of 2740 feet at station

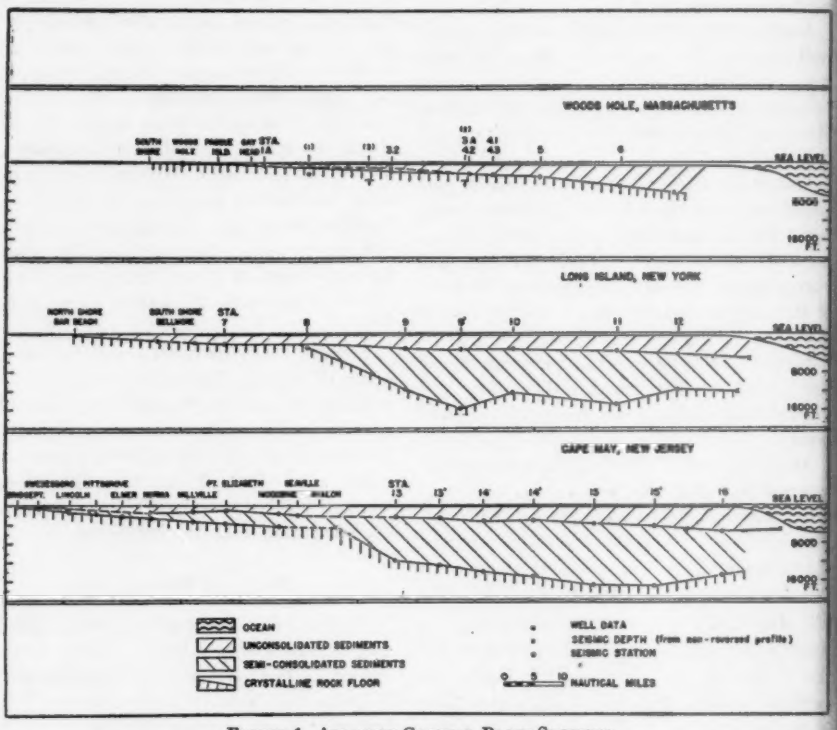

FIGURE 1. ATLANTIC COASTAL PLAIN SECTIONS

ment are 0.3° (seaward) and 17,300 ft./sec. This basement velocity is the lowest value on the New York profile. Parallel travel-time curves are again present, denoting the later arrival of a wave that has been reflected once at the surface of the water.

Stations 8S–9N: All three layers are present with the introduction of the layer of semi-consolidated sediments in this station-pair, and the three layers persist throughout the remainder of the profile. The semi-consolidated sediments are identified by their velocity, 10,800 ft./sec., which is well above that of the unconsolidated layer, 5200 ft./sec., and also well below that of the basement rock, 19,550 ft./sec.,

8 to 11,890 feet at 9, a slope of 4.2°. The top of the semi-consolidated sediments slopes gently seaward at 0.7°.

Stations 9S–10N: This station-pair is divided into two fictitious station-pairs, 9–9′ and 9′–10, according to the method previously described. The added detail was occasioned by the geometrical complexity of the structure, for the basement reverses the direction of its slope. The surface of the basement continues its sharp slope downward, 3.2°, and reaches a depth of 16,000 feet, the maximum on the New York line, at 9′. The surface then rises, at 3.5°, to a depth of 12,560 feet at station 10. The interface between

UM

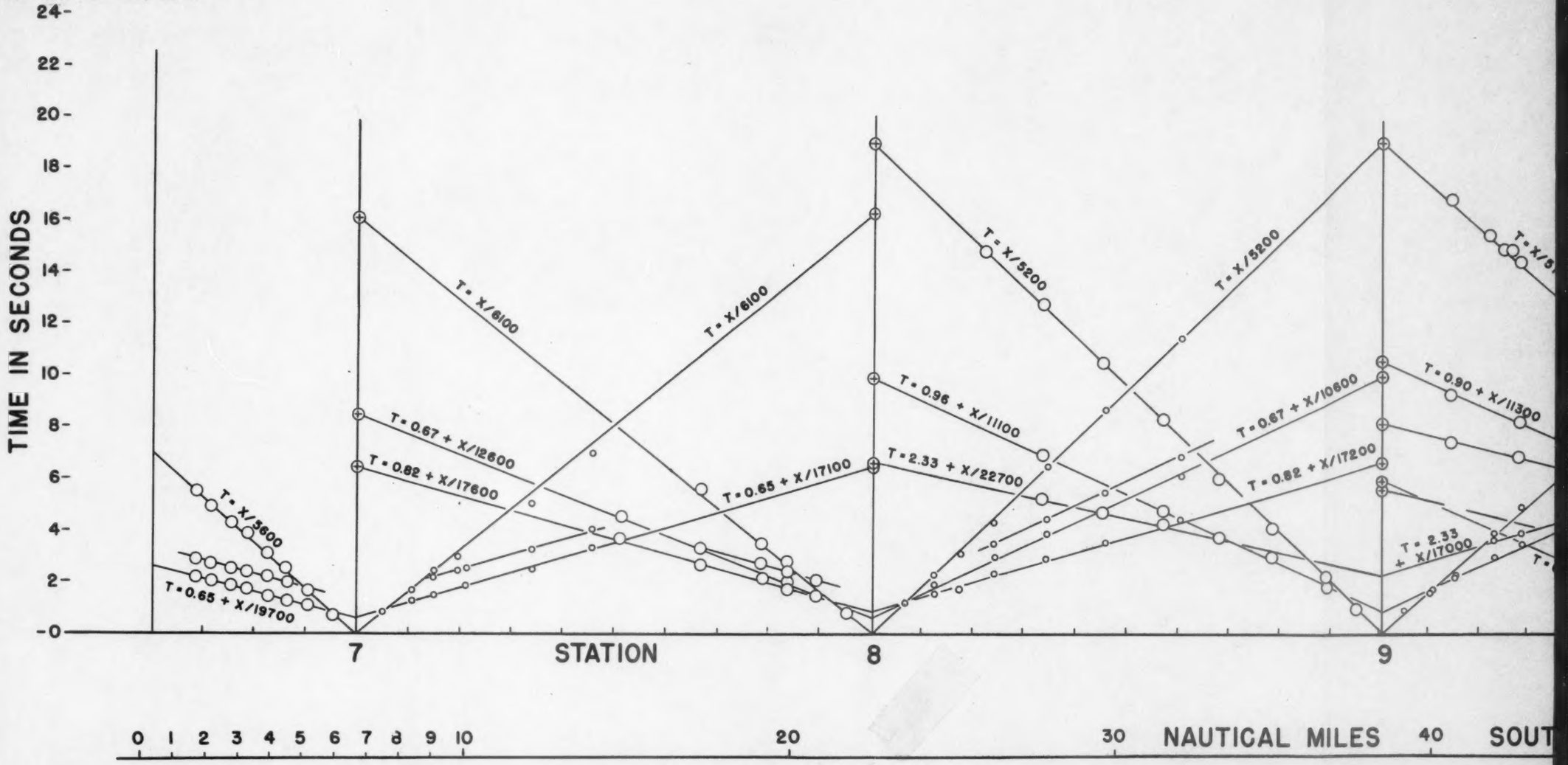
TIME IN SECONDS
24
22
20
18
16
14
12
10
8
6
4
2
0
T = X/6100
T = X/6100
T = X/5200
T = X/5200
T = 0.67 + X/12600
T = 0.82 + X/17600
T = 0.96 + X/11100
T = 2.33 + X/22700
T = 0.65 + X/17100
T = X/3600
T = 0.65 + X/19700
T = 0.67 + X/10600
T = 0.82 + X/17200
T = 0.90 + X/11300
T = 2.33 + X/17000
7
STATION
8
9
0 1 2 3 4 5 6 7 8 9 10
20
30
NAUTICAL MILES
40
SOUT

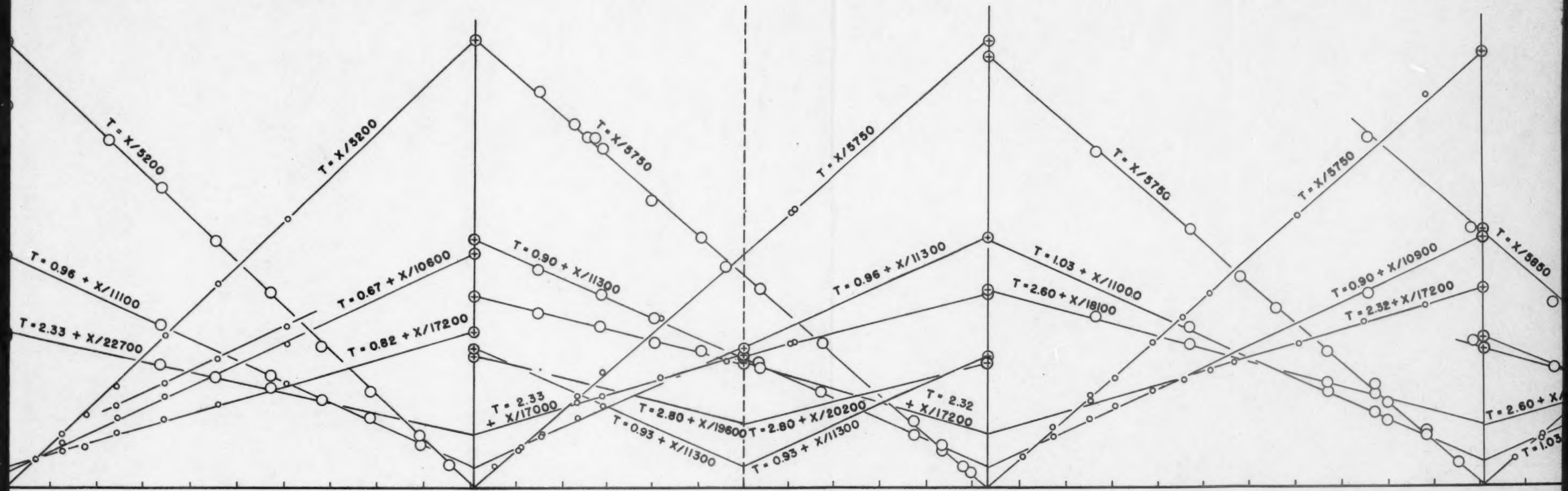

TRAVEL-TIME CURVES, NEW YORK SECTION

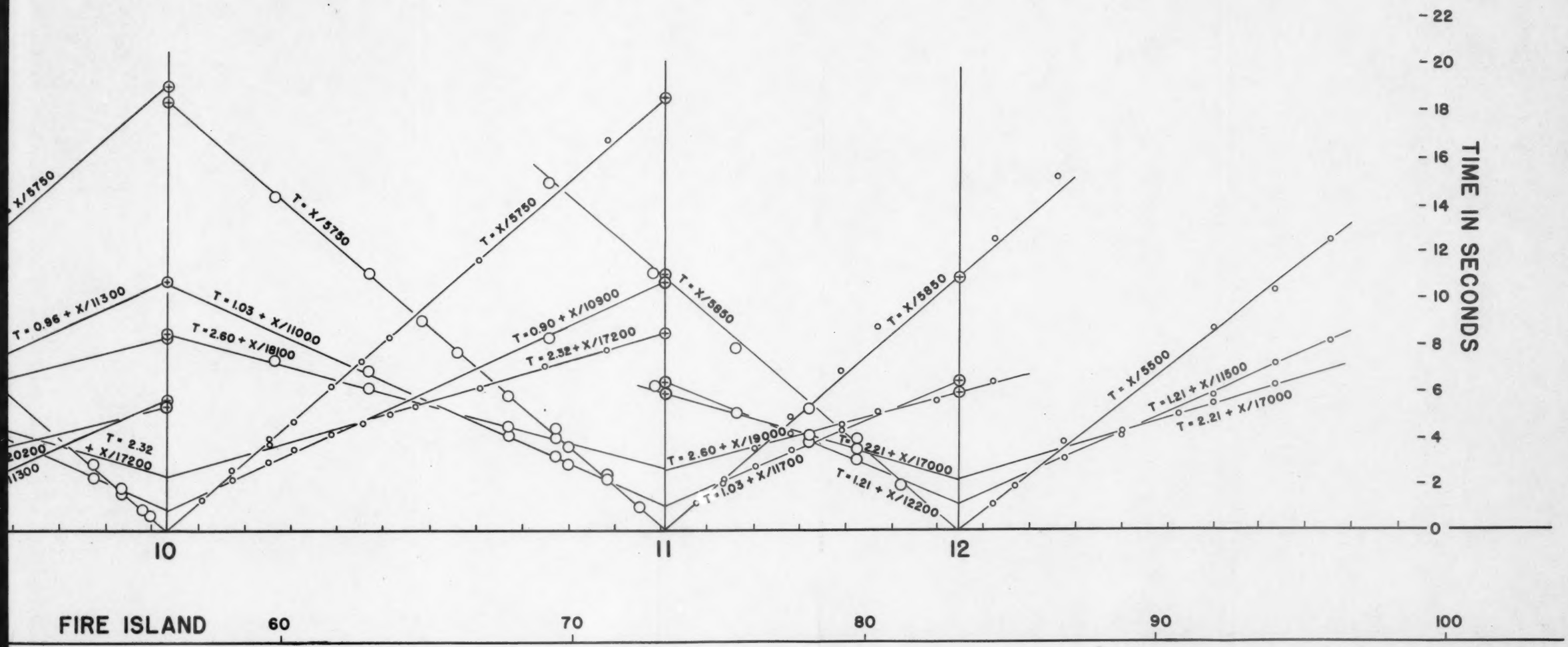
T = X/5750
T = 0.96 + X/11300
T = 1.03 + X/11000
T = 2.60 + X/18100
T = 2.32 + X/17200
T = X/5850
T = 0.90 + X/10900
T = 2.32 + X/17200
T = 2.60 + X/19000
T = 1.03 + X/11700
T = 1.21 + X/12200
T = 2.21 + X/17000
T = X/5500
T = 1.21 + X/11500
T = 2.21 + X/17000
TIME IN SECONDS
0
2
4
6
8
10
12
14
16
18
20
22
10
11
12
FIRE ISLAND
60
70
80
90
100

the
10,
T

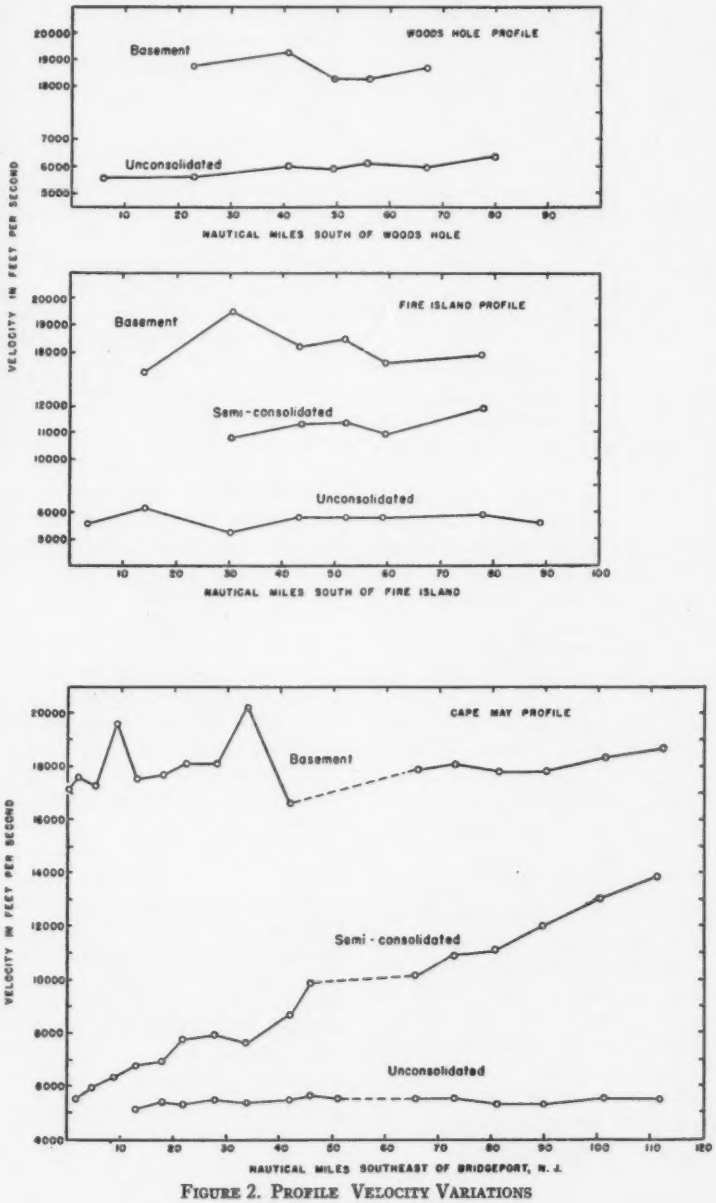

FIGURE 2. PROFILE VELOCITY VARIATIONS

the V_1 and V_2 layers is horizontal between 9 and 10, at a depth of approximately 3,200 feet.

The velocities do not vary significantly within the station pair. V_2 remains at 11,300 ft./sec. and V_3 is somewhat over 18,000 ft./sec.

Stations 10S–11N: The basement surface con-

tinues to slope seaward gently, at 1.5°. The V_1–V_2 interface is almost horizontal, sloping seaward at only 0.2°.

The velocity of the semi-consolidated layer decreased to 10,900 ft./sec., and the velocity of the basement rock to 17,650 ft./sec.

Stations 11S-12N: The depths and velocities are particulary well determined for this pair. The crystalline rock floor distinctly rises upward as it extends seaward, from 14,680 feet to 11,570 feet, a slope of 3.9°. The interface between layers one and two continues to dip gently seaward, however, the dip being 0.7° along the profile.

The velocity of the semi-consolidated layer attains its maximum value for the line, 11,900 ft./sec., but the velocity of the basement rock, 17,900 ft./sec., agrees very well with the previous values.

Station 12S: This station has no reverse profile. The V_2 and V_3 velocities were assumed to be the same as in the adjacent station pair. With these assumptions and good observational data, the crystalline rock floor appears to slope downward (0.8°) as the edge of the continental shelf is approached. The basement depth at the most seaward shot point, about 11 miles from station 12, is 12,030 feet. The top of the semi-consolidated layer continues to slope gently seaward. Its dip along the profile is 1.0°, and the thickness of the unconsolidated sediments is 5190 feet at the most seaward shot point.

Summary of New York Profile

The surface of the semi-consolidated layer dips gently seaward (Fig. 1). The basement floor dips seaward almost constantly from the north shore to approximately 20 miles south of the south shore of Long Island, where the crystalline rock surface bends sharply and increases its depth below sea level by 13,260 feet in 28 miles. At station 9′ there is a reversal in the basement slope, as the surface is only 12,560 feet deep at station 10. The surface then descends to 14,680 feet at station 11 only to rise again as the edge of the continental shelf is approached. The depth at 12 is only 11,560 feet.

The variations in the velocities V_1, V_2, and V_3, are small and without any consistent trend. The semi-consolidated layer shows the most consistent change, an overall increase of 1,100 ft./sec. between the ends of the profile (Fig. 2). The basement velocity averages 18,100 ft./sec.

Cape May Profile (Pl. 4)

Station 13N: This station has no reverse profile. Any reasonable estimate of true velocities (V_2 and V_3) gives a sharp seaward dip of the basement. For the assumed values of V_2 = 9800 ft./sec. and V_3 = 19,500 ft./sec. (V_3 being that determined at the corresponding flexure on the New York profile), the slope is of the order of magnitude of 6°. The sharp slope is further verified by the much shoaler basement depth obtained at the Woodbine station of the land profile of 1938 as described in Part IV. Here, as on the New York profile, the surface of the semi-consolidated layer does not show any abrupt change in slope at the place where the basement dip increases abruptly (Fig. 1).

Stations 13S.–14N: This pair is divided into two fictitious station pairs, 13S.–13′N. and 13′S.–14N. For stations 13S.–13′N., V_2 = 10,000 ft./sec. and V_3 = 17,950 ft./sec. V_2 shows a moderate increase to 10,850 ft./sec., whereas V_3 increases slightly to 18,150 ft./sec. at stations 13′S.–14N. The slope of the basement decreases to less than 1° for both pairs.

Station 14S.–15N.: The velocities V_2 and V_3 are particularly well determined at this station. V_2 shows a slight increase to 11,000 ft./sec. for 14S.–14′N. and increases more rapidly to 11,950 ft./sec. at 14′S.–15N. Only minor fluctuations of V_1 and V_3 are indicated at this pair of stations.

Stations 15S.–16N.: The semi-consolidated layer continues its gradual dip to the eastward. The progressive increase in the velocity of this layer is still present with V_2 = 12,900 ft./sec. for 15S.–15′N. and 13,700 ft./sec. for 15′S.–16N. The basement reaches its greatest depth of 17,210 feet at station 15′. Using the data of the pair, 15′S.–16N., the depth to the basement at station 16 shoals to 14,050 feet, denoting a reversal in direction of dip of the surface of the crystalline rocks.

Station 16S: Data are too meager to obtain depth to the basement. The semi-consolidated layer was computed by assuming a true velocity by extrapolation from the previous stations.

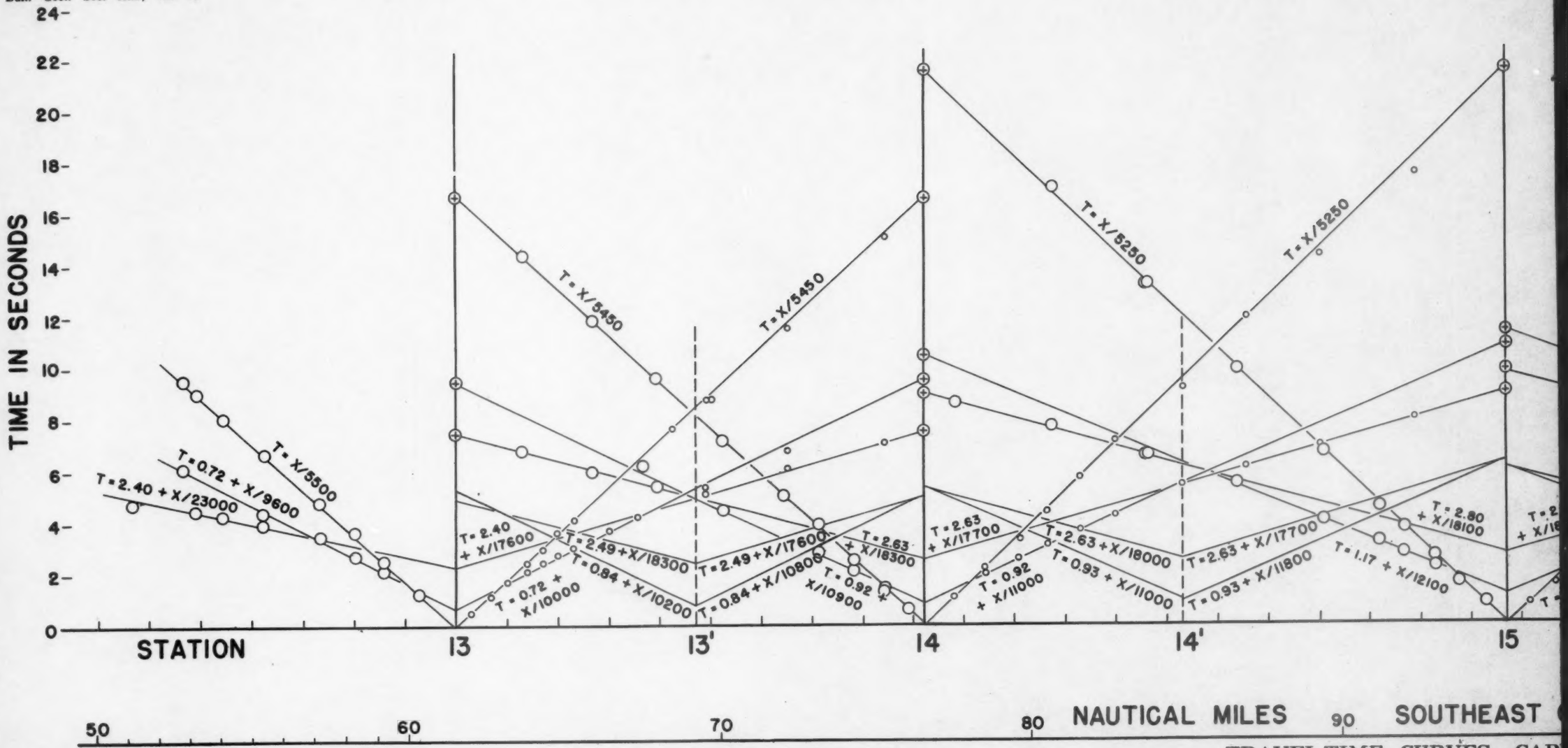

TRAVEL-TIME CURVES, CAP

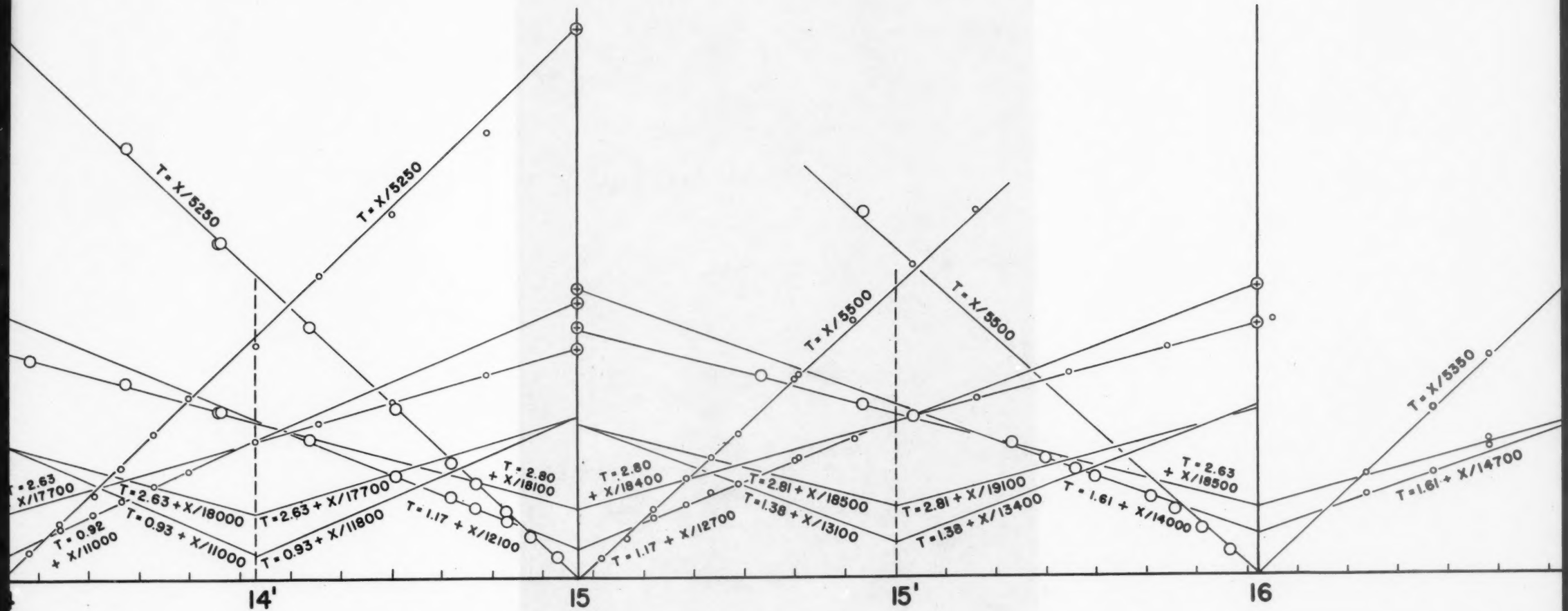

TRAVEL-TIME CURVES, CAPE MAY SECTION

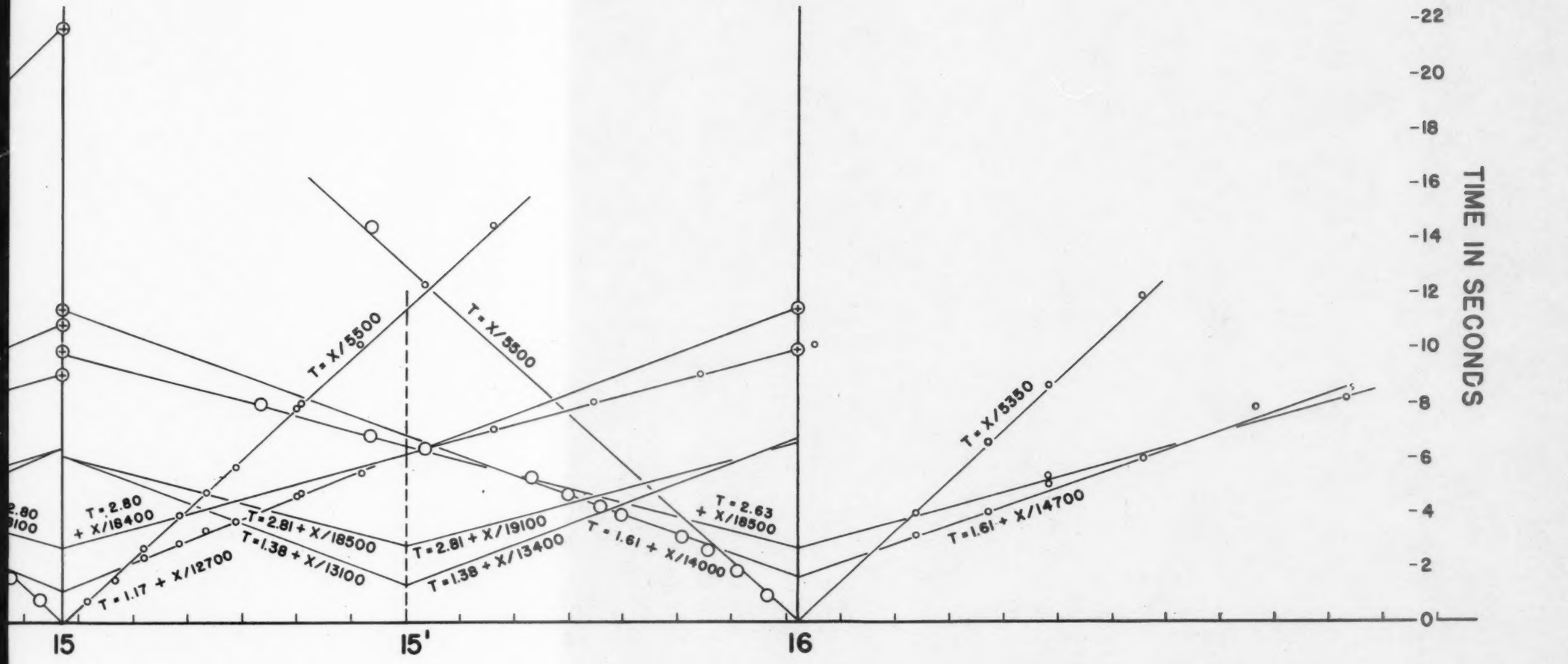

HEAST OF 100 BRIDGEPORT 110 120 130 140

ES, CAPE MAY SECTION

Summary of Cape May Profile

The surface of the semi-consolidated layer dips gradually to the east over the entire length of the profile (Fig. 1). The basement surface exhibits a sharp flexure between the first sea station and the Woodbine land station. The basement reaches its greatest depth of 17,210 feet at station 15′ and then shoals to 14,050 feet at station 16.

The unconsolidated and basement layers show an irregular fluctuation of velocity over the length of the profile. Excluding three land stations where there are larger deviations in measured velocity, the remaining 13 values of basement velocity average approximately 18,000 ft./sec. The extreme values are 17,150 ft./sec. and 18,750 ft./sec., and there is apparently a small systematic increase in velocity seaward. The velocity of the semi-consolidated layer increases progressively (Fig. 2) from V_2 = 7,750 ft./sec. at the Norma station of the land profile to V_2 = 13,700 ft./sec. at the outermost sea station.

Geological Significance of Results

General Statement

Two seismic refraction profiles in New Jersey and one in Virginia have already been presented (Parts I–IV). The Cape Henry profile is a land-sea section that extends from Petersburg, Virginia, almost to the edge of the continental shelf. The Cape May profile of this report is a continuation of a land profile across southern New Jersey (Part IV). These profiles, together with the Woods Hole and New York sections, are four of a series to be located at similar intervals along the Atlantic Coast from Newfoundland to Florida.

Geology, Woods Hole Profile

This section extends southward from a point just west of Martha's Vineyard, so the seismic results on this profile are interpreted by extrapolation from the known geology of Martha's Vineyard. According to Wigglesworth (Woodworth and Wigglesworth, 1934), the nature and depth of the pre-Cretaceous basement must be inferred from exposures on the southeastern mainland of Massachusetts. The basement rocks are probably crystalline rocks of Paleozoic age including metamorphosed conglomerate, sandstone, and shale. These rocks may of course contain additional intrusive rocks. Their surface, probably peneplaned in Cretaceous time, is estimated by Wigglesworth to lie 500 to 600 feet below sea level, which is in good agreement with the depth of 770 feet on the northernmost sea station of the Woods Hole refraction line. The basement depth determined in 1935 (Part I) at Woods Hole, 294 feet, plots well on the basement slope drawn between the outcrop on the south shore and the seismic determination at station 1A.

The overlying sedimentary section contains Upper Cretaceous, Tertiary, and Quaternary beds. The exposed pre-Pleistocene beds are all unconsolidated. The Cretaceous exposures represent only the lower half of the Upper Cretaceous system. They commence with beds of Magothy age (Berry, 1915), which are non-marine, plant-bearing strata. The succeeding Cretaceous beds are marine sands and clay that signify the sinking of the fluviatile regions of early Upper Cretaceous time. The less extensive Tertiary deposits are greensands of Miocene and Pliocene age. All of the pre-Pleistocene strata are greatly disturbed, exhibiting small scale folds and overthrusts directed to the southwest, produced presumably by the dragging of the Pleistocene ice sheets.

Pleistocene beds form the greater part of the exposed formations. These are also unconsolidated sands, gravels, clays, and tills. The deposits are of glacial and glacio-aqueous origin. The oldest beds are highly folded and distorted, apparently by Pleistocene ice drags.

Figure 1 shows the seismic profile from Woods Hole to a point 86 miles south. This section shows that the crystalline rock floor continues to slope seaward with a dip of approximately 1° along the profile. The overlying sediments are essentially all unconsolidated. Their thickness increases continuously to about 1 mile at the end of the section. The sediments must range from early Upper Cretaceous to Recent, judging fom the exposures on Martha's Vineyard. They are considered to be at least post-Raritan, on the basis of velocity comparison with the unconsolidated layer of the Cape May profile.

A section of semi-consolidated material was distinctly identified for station-pairs 1A–3.2 by its velocity, 9,750 ft./sec. This lens is 1520 feet thick at station 3.2 and becomes too thin to detect throughout the rest of the profile.

In previous investigations the interface between the unconsolidated and semi-consolidated sediments has been correlated with the Raritan-Magothy unconformable contact of early Upper Cretaceous time (Part III.)

Geology, New York Profile

This profile extends south from the east tip of Fire Island. Again the seismic results along the section are interpreted by an extrapolation of the geology of Long Island (Fuller, 1914; De Laguna and Brashears, 1948).

The pre-Cretaceous surface is exposed along the East River in the northwestern portion of Long Island. It consists of the Fordham gneiss of pre-Cambrian age. Well borings show that the surface of this metamorphic rock dips at an average rate of 100 feet per mile in western Long Island. The slope at the east end is considered by Fuller to be approximately 70 feet per mile.

The overlying sediments are of the same nature as those on Martha's Vineyard. They contain a complete series of Upper Cretaceous beds and some Tertiary and Quaternary deposits. Of the 1460 feet of sediments in the N 1927, U. S. Naval Receiving Station well on the south shore (De Laguna and Brashears, 1948), all but 150 feet are Upper Cretaceous deposits. The lower half of these beds is of Raritan and Magothy age and is predominantly clayey deposits of non-marine origin. The Magothy formation initiates the beginning of the late Cretaceous depression. This depression was more pronounced off the ancient shores of New Jersey where marls were forming. In the Long Island region, clays and sands were still being obtained from the near-by uplifted peneplane. All the formations thicken seaward and converge shoreward.

The unconsolidated sediments thicken continuously seaward until they attain a thickness of 3900 feet (Fig. 1). The semi-consolidated sediments, presumably pre-Magothy, are not detected until station 8. They then thicken abruptly to 8700 feet at station 9. Maximum recorded thickness is 12,700 feet, at station 9′. The thickness seems to decrease markedly as the edge of the continental shelf is approached; at station 12, the layer is only 7300 feet thick.

Geology, Cape May Profile

In this case, the sea section has a landward counterpart, and the general geology of the New Jersey Coastal Plain and its underlying basement structure has been previously discussed in Part III, p. 276.

The results on land have been described in Part IV. The interfaces determined at sea correlated perfectly with their landward counterparts. The seismic "V" horizon of the earlier land work was not detected by the investigations at sea. This was to be expected because of the probable effect of submergence on the overlying low velocity layer.

As on the Woods Hole and New York sections, the unconsolidated sediments of post-Raritan age dip continuously seaward and attain a maximum thickness of 4800 feet near the edge of the continental shelf. Contrary to the other two profiles, the Cape May section of unconsolidated sediments consists about equally of Cretaceous and Tertiary sediments. The Tertiary seas advanced over almost all of southern New Jersey, and intra-Tertiary erosional periods never produced complete denudation of the underlying Cretaceous deposits.

The Cape May section is also different from the two northern profiles because the semi-consolidated sediments are present beneath the emerged Coastal Plain. The Raritan-Magothy interface disappears seismically west of Norma because the velocity of the semi-consolidated layer is decreasing westward and becomes similar in value to the velocity of the unconsolidated layer. The thickening of the pre-Magothy sediments southward is noted in Part IV and attributed to the "probable . . . presence of lower Cretaceous sediments." The Potomac Group of Lower Cretaceous age is recognized in well-borings at Salem, New Jersey, (Richards, 1945) and crops out in Delaware. On the Cape May profile, these semi-consolidated sediments, apparently of pre-Magothy and post-Paleozoic age, thicken abruptly near the present shoreline, reach a maximum thickness of 13,300 feet at station 15, then thin to 8900 feet near

WOODS HOLE

1

2

3

4

NEW YORK

5

6

7

8

CAPE MAY

9

10

11

12

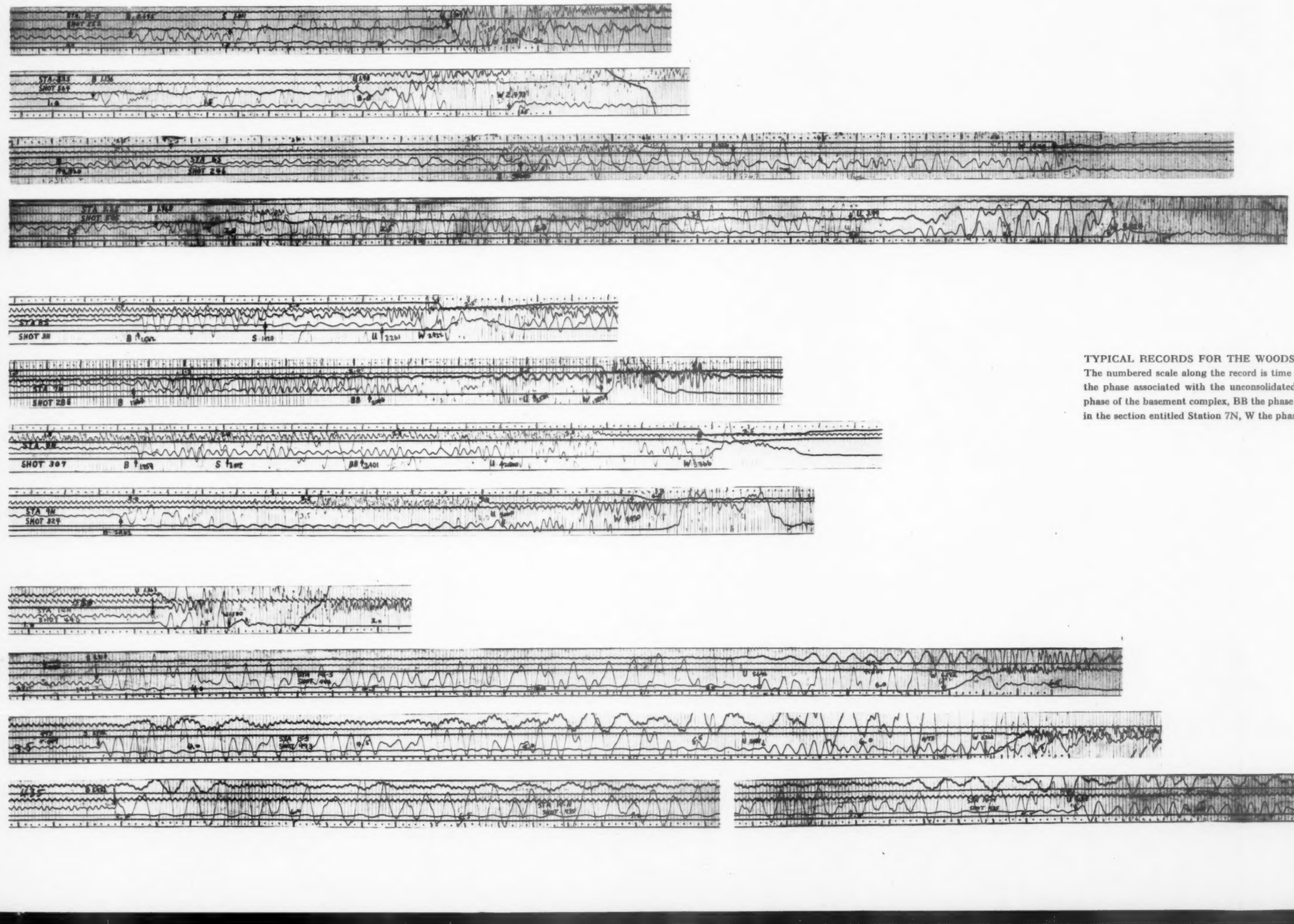

TYPICAL RECORDS FOR THE WOODS HOLE, NEW YORK, AND CAPE MAY PROFILES
The numbered scale along the record is time in seconds after the firing instant. The letter U indicates the phase associated with the unconsolidated layer, S the phase of the semiconsolidated layer, B the phase of the basement complex, BB the phase of the surface-reflected basement-refracted wave described in the section entitled Station 7N, W the phase of the water wave.

the edge of the continental shelf. The development of the semi-consolidated section of sediments is similar to that along the New York profile, but their continued existence under the emerged shelf in New Jersey illustrates that they are not confined to the basin structure of the submerged shelf.

Observed Velocities

The velocities of the unconsolidated sediments (Fig. 2) fluctuate to a minor extent and exhibit no trends except that the average velocity along each section increases to the north. The average value of V_1 for Cape May is 5400 ft./sec., 5700 for New York, and 5950 for Woods Hole. Perhaps this reflects the greater relative amount of younger (Tertiary) sediments along the southerly sections.

The velocities of the semi-consolidated sediments (Fig. 2) have an average value of 11,250 ft./sec. along the New York line and 11,750 ft./sec. along the sea portion of the Cape May line. Whereas the velocities show little variation on the New York profile, they continuously increase throughout the whole extent of the land and sea portions of the Cape May section. The velocity at Norma is 7760 ft./sec., and the velocity at station-pair 15′–16 is 13,700 ft./sec. The rate of increase is about 70 ft./sec./mile. This marked increase might be attributed to increasing compaction which decreases the porosity of the sediments, or to an increase in the calcareous content toward the seaward end of the profile.

The basement velocities (Fig. 2) fluctuate between 17,300 ft./sec. and 19,500 ft./sec., though mostly contained between much narrower limits. The variations are not of sufficient magnitude to warrant a correlation to various types of igneous and metamorphic rocks. The values are near the value of 18,000 ft./sec., assigned to the Wissahickon schist in Part IV. The basement velocity seems to be high in the region of the steep offshore dips on the New York and Cape May lines.

Geological History

The seismic refraction profiles disclose that the crystalline rock floor of the Atlantic Coastal Plain does not slope simply and constantly toward the ocean basin floor off the coasts of New Jersey and New York. It has a sharp downward flexure just off the present shoreline and on two of the sections an upward flexure as the edge of the continental shelf is approached. The basin thus developed is illustrated by contours drawn on the crystalline rock floor (Pl. 6).

Stratigraphic History

The off-shore basin is developed entirely within the semi-consolidated sediments (Fig. 1). On the New York profile, the top of the basin is almost coincident with the interface between unconsolidated and semi-consolidated material; on Cape May the interface is above the upper limit of the basin. This seismic interface has been correlated with the stratigraphic unconformity between the lower Upper Cretaceous, Raritan, and Magothy formations (Pts. III and IV) on the basis of deep well cores. Therefore, the basin was completely formed by Magothy time.

The pre-Magothy sediments on the emerged portion of the seismic profile have not been drilled into except in their upper portions (Pts. III–IV). However, the Lower Cretaceous has been recognized in southern New Jersey, Delaware, and Maryland, both in exposures and well-borings (Richards, 1945, 1948). Fuller describes them as occurring in a "fluviatile embayment into the Appalachian Mountains" (1944, p. 193). These beds are known as the Potomac Group. Fuller goes on to say that "the absence of marine shells and the presence of numerous leaves and other vegetable remains have led to the belief that the Potomac Group is a fresh or brackish water deposit". The lithologic character of these beds makes it difficult to establish horizons within the group, or the boundaries of the group.

Three deep wells recently completed in the Eastern Shore area of Maryland have not only shown an unusual thickness of Lower Cretaceous but these are underlain by shales and sandstones presumed to be of Triassic age (Table 4). Two of these wells (Pl. 6) penetrated basement rock (5472 and 7112 feet). The third, due east of these and on the shore line, reached a depth of 7710 feet and was still in Lower

Cretaceous (Anderson *et al.*, 1948; Richards, 1948).

These three wells show a marked increase in thickness to the east in the Triassic and Lower Cretaceous beds. Shales are more abundant in the Triassic of the Bethesda well than in the equivalent Hammond section. Anderson says "this would suggest that the Triassic basin of deposition lay to the east of the Hammond well".

The semi-consolidated sediments on the Virginia seismic profiles are clearly identified with the Raritan and Potomac Group formations (p. 287, Pt. III). Further south, in the Cape Hatteras area, additional evidences of a thick Lower Cretaceous section have been found in recent deep-well tests. Spangler, Skeels, and Ward of the Standard Oil Company of New Jersey, have kindly allowed the authors to review their report "Subsurface Geology of the Atlantic Coastal Plain of North Carolina with Geophysical Supplements", prior to publication*. In the borings of the Standard Oil Co. of N. J. Hatteras Light Esso No. 1 well (9854 on Pl. 5), they have identified 3,800 feet of Lower Cretaceous and 1,600 feet of pre-Magothy Upper Cretaceous. (Spangler, 1950). Furthermore the entire section, except for some "arkosic sands and varicolored shales", is considered to be of marine origin. Here there is a thick section of Lower Cretaceous beds, the marine counterpart of the non-marine facies found inshore.

TABLE 4.—DEEP WELL TESTS, MARYLAND

Well	Total depth	Age of beds	Thickness	Lithology
Ohio Oil Co. L. G. Hammond, No. 1	5472 ft.	Triassic	135 ft.	Non-fossiliferous. Conglomerate, arkosic sandstone, shales. Generally hard and indurated.
		Lower Cretaceous (Patuxent)	939 ft.	Fine to coarse, occasionally limy, arkosic sands.
		Upper Cretaceous (Patapsco-Arundel)	2111 ft.	Sandy. More clay shale and sandy shale than Patuxent.
		Upper Cretaceous (Raritan)	725 ft.	Clays and sandy clays.
		Upper Cretaceous (Magothy)	90 ft.	Dark clay, shales with interlaminated fine grain sands.
Socony-Vacuum Oil Co. James D. Bethesda No. 1	7112 ft.	Triassic	585 ft.	Conglomerate at base. Coarse to fine-grained sandstones above. Predominately shale in upper portion.
		Lower Cretaceous (Patuxent)	1690 ft.	Highly arkosic sands.
		Upper Cretaceous (Patapsco-Arundel)	2105 ft.	Predominately shale.
		Upper Cretaceous (Post-Patapsco)	1060 ft.	Raritan Position (87.6 ft.) is intercalated sand and shales.
Standard Oil Co of New Jersey Md. Esso No. 1	7710	Lower Cretaceous (Patuxent)	2310 ft.	Thick sand bodies with shales becoming thicker in lower portions. Occasional hard, calcareous beds.
		Upper Cretaceous (Patapsco-Arundel)	2070 ft.	Predominately shale.
		Upper Cretaceous (Post-Patapsco)	1200 ft.	Raritan is 850 feet of sand and shale. Magothy is 120 feet of sand.

*This paper appears under two titles (Spangler, 1950; Skeels, 1950).

To summarize, then: (1) the semi-consolidated section disclosed by the seismic investigations in Virginia was correlated with the introduction of a thick Lower Cretaceous series on the basis of well data along the section; (2) the semi-consolidated section disclosed by the Cape May seismic profile was designated to be mostly Lower Cretaceous on the basis of its similarity to the Virginia Section and the exposures of Lower Cretaceous in southern New Jersey; (3) the Hatteras well affirmed the presence of a Lower Cretaceous section and further disclosed the presence of an off-shore marine facies; (4) the Maryland deep-well tests not only contained a Lower Cretaceous series that thickened seaward but also indicated the existence of a Triassic section that similarly thickened seaward. The lithologic changes between the two Triassic sections suggested that a Triassic basin of deposition had existed east of the Hammond well.

We may infer, then, that the off-shore basin of semi-consolidated sediments discovered by the Cape May and New York seismic profiles over the submerged portion of the continental shelf contains a thick sequence of Lower Cretaceous beds. Triassic sediments probably exist there also. Because of the difficulties in establishing geologic age within these non-marine sediments, it is quite possible that Jurassic beds are likewise present. From the evidence of the Hatteras well and because of the increase in velocity seaward on the Cape May profile, we may also infer that the non-marine beds grade into marine, calcareous facies seaward.

Structural History

The seismic results yield no unique structural history that accounts for the formation of the off-shore basin. Three alternative processes are readily visualized.

(1) We may picture an off-shore platform which began to founder at the beginning of Mesozoic time and continued to do so until Magothy time in the lower Upper Cretaceous. During this time, deposition was probably continuous over the area. Just before Magothy time, this platform was bent into a gentle synclinorium, after which its surface was deeply eroded prior to the deposition of the Magothy formation.

(2) The platform may be thought of as being downwarped concurrent with the deposition of the pre-Magothy Mesozoic beds. Again the deposition is followed by a period of erosion prior to Magothy time.

(3) We may consider that the basin developed prior to deposition and the sediments were simply laid down in the off-shore depression. This case is somewhat less acceptable than the other two because the surface of the semi-consolidated sediments is so coincidental with the top of the basin on the New York section (Fig. 2).

The second process is an excellent example for the isostasists who would believe that the off-shore platform was downwarped in response to the additional load of sediments. However, no depression was found on the off-shore Cape Henry profile where a thick section of semi-consolidated sediments exists (Miller, 1937, Pt. II). This second process is also very suggestive of depositional conditions during the Triassic in the on-shore basins along the east coast, where deposition was continuous and simultaneous with the sinking of the basin.

Conclusion

The standard method of seismic refraction has disclosed the existence of a depression in the surface of the crystalline rocks beneath the submerged Atlantic Coastal Plain. This depression is filled with semi-consolidated sediments of probable pre-Upper Cretaceous age.

The depression was found along profiles extending seaward from Cape May and New York but not on a profile south of Woods Hole. Previous work (Pt. I) indicates that the depression does not exist under the submerged Coastal Plain on the Cape Henry line. Additional profiles are needed to learn whether the depression is closed on its ends or whether the outer upwarp is merely a flexure that plunges downward at both its northerly and southerly extremities.

References Cited

Anderson, J. L., et al. (1948) *Cretaceous and Tertiary Subsurface Geology*, St. of Md., Board Nat. Resources, Baltimore, Md.

Berry, E. W., (1915) *The age of the Cretaceous flora of southern New York and New England*, Jour. Geol., vol. 23, p. 608–618.

DeLaguna, W., and Brashears, M. L., Jr. (1948) *The configuration of the rock floor in western Long Island, N. Y.*, State of N. Y., Dept. Conserv. Water Power and Control Commission Bull. GW-13.

Ewing, Maurice, Crary, A. P., and Rutherford, H. M. (1937) *Geophysical investigations in the emerged and submerged Atlantic Coastal Plain*, Part I: *Methods and Results*, Geol. Soc. Am., Bull., vol. 48, p. 753–802.

———, Woollard, George P., and Vine, A. C., (1939), *Geophysical investigations in the emerged and submerged Atlantic Coastal Plain*, Part III: *Barnegat Bay, New Jersey, Section*, Geol. Soc. Am., Bull., vol. 50, p. 257–296.

———, ———, — ——— (1940) *Geophysical investigations in the emerged and submerged Atlantic Coastal Plain*, Part IV: *Cape May, New Jersey, Section*, Geol. Soc. Am., Bull., vol. 51, p. 1821–1840.

———, ———, Vine, A. C., and Worzel, J. L. (1946), *Recent results in submarine geophysics*, Geol. Soc. Am., Bull., vol. 57, p. 909–934.

Fuller, M. L. (1914) *The geology of Long Island, New York*, U. S. Geol. Survey, Prof. Paper 82, 231 pages.

Heiland, C. A. (1940) *Geophysical Prospecting*, New York

Kay, Marshall (1947) *Geosynclinal nomenclature and the craton*, Am. Assoc. Petrol. Geol., Bull., vol. 31, p. 1293.

Miller, B. L. (1937) *Geophysical investigations in the emerged and submerged Atlantic Coastal Plain*, Part II: *Geological significance of the geophysical data*, Geol. Soc. Am., Bull., vol. 48, p. 803–812.

Richards, H. G. (1945) *Subsurface stratigraphy of Atlantic Coastal Plain between New Jersey and Georgia*, Am. Assoc. Petrol. Geol., Bull., vol. 29, p. 885.

——— (1948) *Studies on the subsurface geology and paleontology of the Atlantic Coastal Plain*, Acad. Nat. Sci. Phila., Pr., vol. C.

Skeels, D.C. (1950) *Geophysical data on the North Carolina coastal plain*, Geophysics, vol. 15, p. 409–426.

Spangler, W. B. (1950) *Subsurface geology of Atlantic Coastal Plain of North Carolina*, Am. Assoc. Petrol. Geol., vol. 34, no. 1, p. 100–132.

Woodworth, J. B., and Wigglesworth, E. (1934) *Geography and geology of the region including Cape Cod, the Elizabeth Islands, Nantucket, Martha's Vineyard, No Man's Land, and Block Island*, Mus. Comp. Zool., Harvard College, Mem., vol. LII, Chap. II.

Worzel, J. L., and Ewing, Maurice (1948) *Explosion sounds in shallow water, part of "Propagation of Sound in the Ocean"*, Geol. Soc. Am., Mem. 27.

LAMONT GEOLOGICAL LABORATORY (COLUMBIA UNIVERSITY), PALISADES, N. Y.

MANUSCRIPT RECEIVED BY THE SECRETARY OF THE SOCIETY, JULY 18, 1949

LAMONT GEOLOGICAL OBSERVATORY CONTRIBUTION No. 7

CONTRIBUTION No. 480 OF WOODS HOLE OCEANOGRAPHIC INSTITUTION

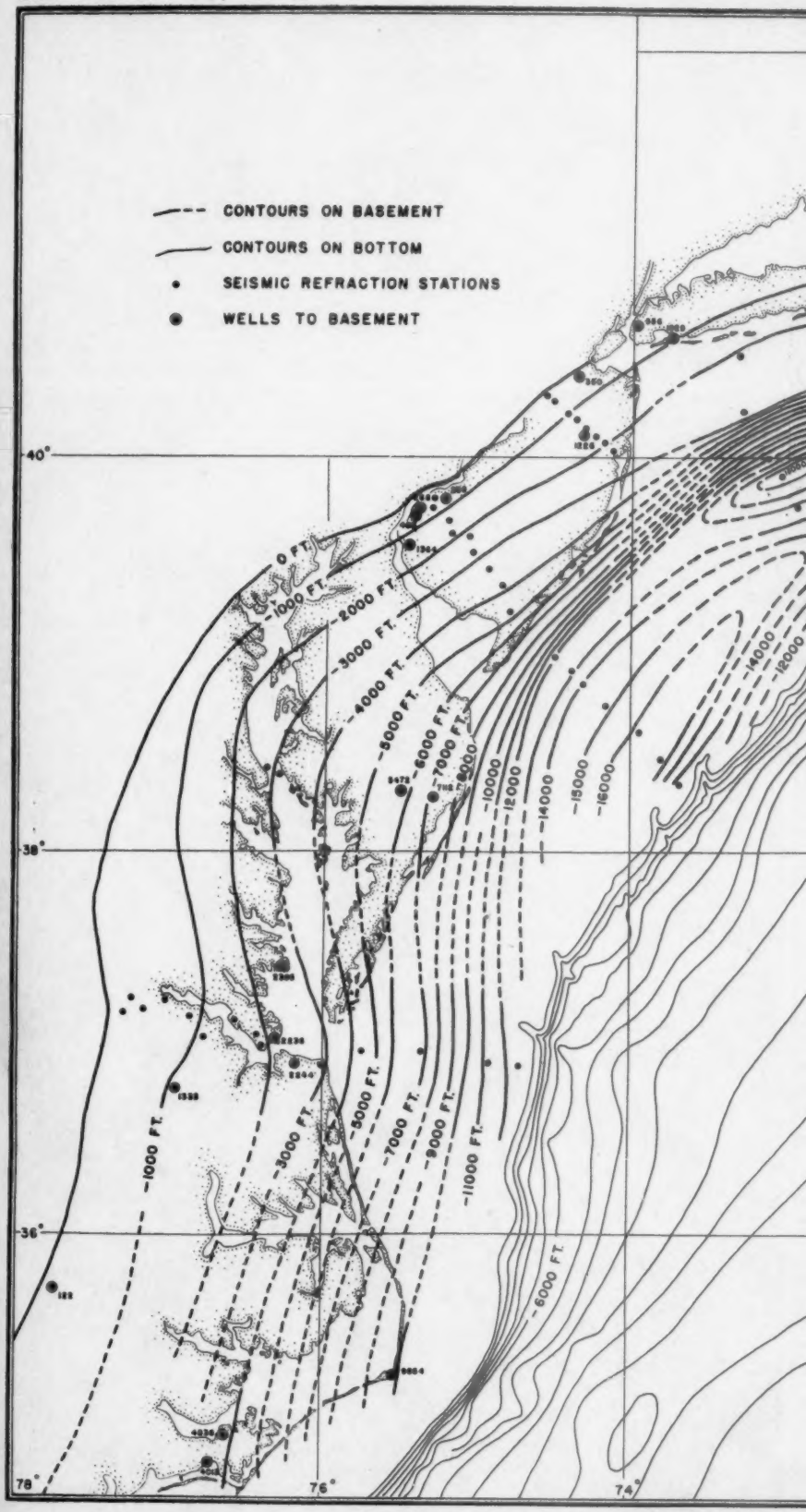

SUBSURFACE CONTOURS

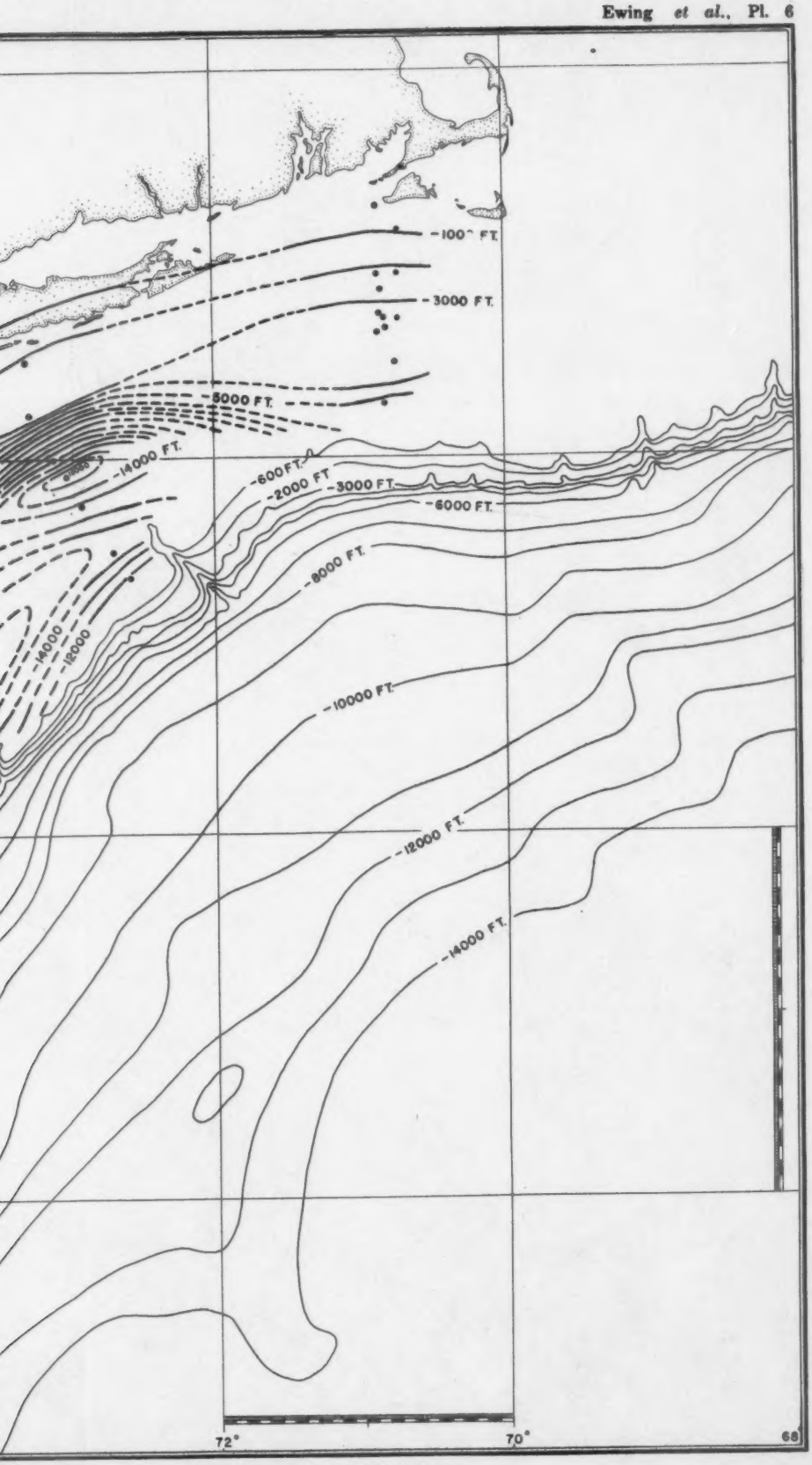

TOURS ON THE BASEMENT

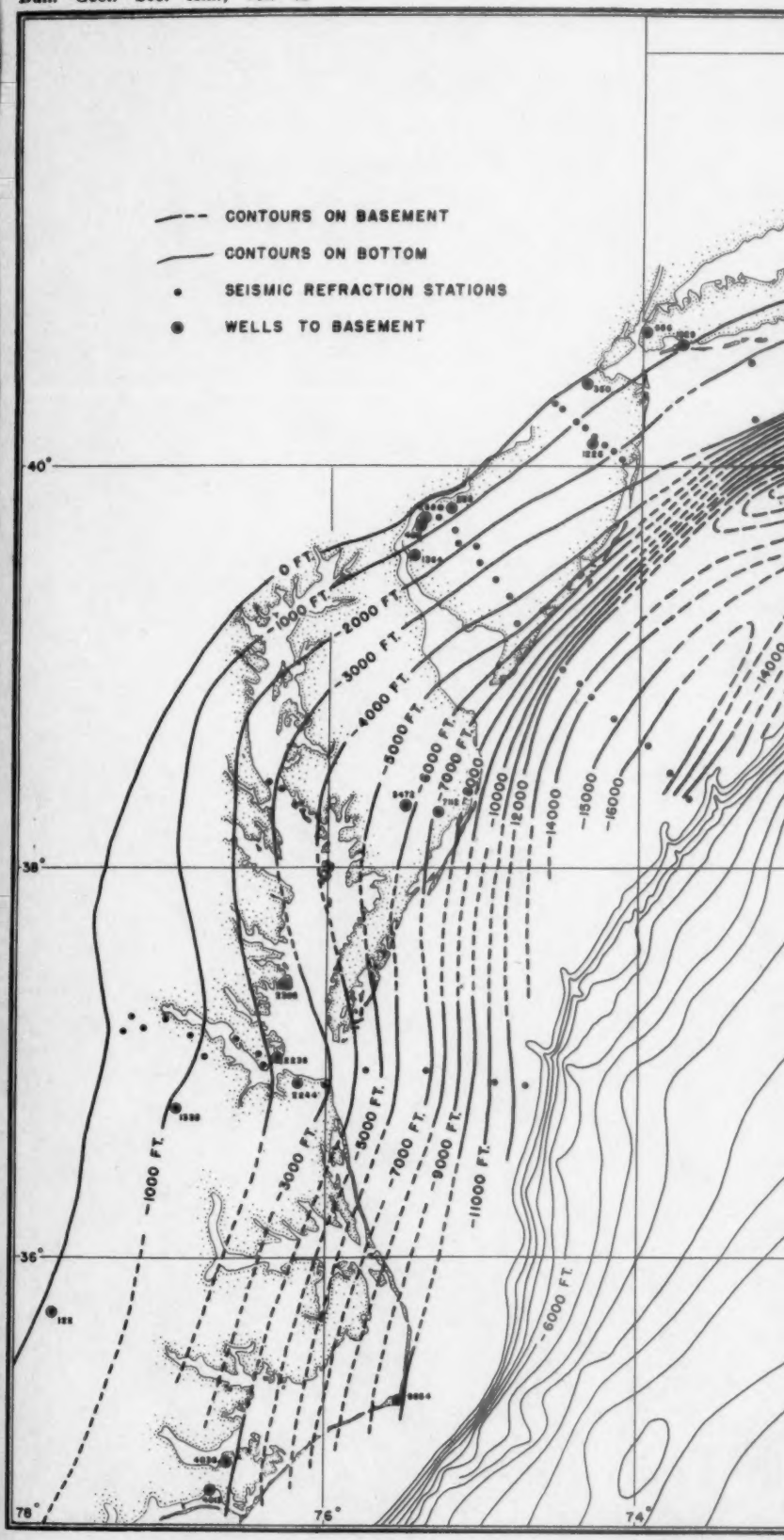

SUBSURFACE CONTOUR

NTOURS ON THE BASEMENT

Abs
Ack
Int
S
A
P
P
I
Str
S
W
C
Str
C
I
T
I
Figu
1.
2.
Tab
1.
2.

BULLETIN OF THE GEOLOGICAL SOCIETY OF AMERICA
VOL. 61, PP. 893-922, 2 FIGS., 2 PLS. SEPTEMBER 1950

GEOLOGY OF GATUN LAKE AND VICINITY, PANAMA

BY STEWART MCREDDIE JONES

CONTENTS

	Page
Abstract	894
Acknowledgement	895
Introduction	895
Scope	895
Area	895
Field methods	895
Previous work in the area	895
Local terminology of sedimentary rocks	896
Stratigraphy	897
Summary and conclusions	897
Vicinity of Gatun Lake	899
Basement Complex	899
Bohio formation	899
Las Cascadas formation	900
Caimito formation	900
Possible equivalents of the Caimito formation	901
Caraba facies of the Caimito formation	901
Bruja Island Dolerite, Cerro Gigante Basalt, and related basic igneous rocks	901
Gatun formation	902
Toro limestone	902
Chagres sandstone	902
Atlantic muck	904
Chagres alluvium	904
Outlying areas	904
General statement	904
Gatuncillo and Tranquilla formations	904
Quebrancha formation	905
"Alhajuela formation"	905
Sabanitas formation	905
Structure	905
General statement	905
Details of Fractures	905
The fracture pattern	909
General statement	909
North-south grain of the pre-Tertiary area	910
Permanency of the fracture pattern	910
Conclusion	910
Isthmian regional structure: relations and inferences	910
Tectonic axis	910
Volcanic axis	910
Basins and ridges adjoining the southern continental shelf	912
Uniform outline of the isthmus ridge of Panama	913
Topographic and structural affinities of the western Caribbean and the Ecuador basins	913
Correlation with the fracture pattern	913
Physiography	914
General character	914
Mountain areas	914
Intermontain areas	914
Swamp and lowland areas	914
Interlowland areas	914
Dissected highland areas	914
Hills region	914
Geologic history	915
Appendix 1—Description of beds in excavation for third locks at Gatun	916
Appendix 2—Physical data	917
General statement	917
Formations and Contacts	917
Basement Complex terrane and its bounding unconformity	917
Contact between Upper Eocene rocks and Caimito formation	918
Evolution of the name "Caimito formation"	918
Contacts above and below the Bohio formation	919
Evolution of the name "Bohio formation"	919
Unconformity and erosion surface over the Caimito formation	919
Contact between Gatun and Sabanitas formations	920
Contact between Sabanitas formation and Basement Complex	920
Contact between Gatun formation and Toro limestone	920
Contact between Toro limestone and Chagres formation	920
Limits of unconsolidated Pleistocene and Recent sediment	921
References cited	921
Maps and charts cited	921

ILLUSTRATIONS

Figure	Page
1. Location map	896
2. Major crustal setting	911

Plate	Facing page
1. Regional subaerial and submarine physiography	912
2. Areal geologic map, Gatun Lake and vicinity, Panama	920

TABLES

Table	Page
1. Local sedimentary rock classification	897
2. Correlation of stratigraphic columns, Canal Zone	898
3. Inter-relationship of beds exposed in Gatun Third Locks Cut	903
4. Index to fossil localities on Plate 2	920

Abstract

Gatun Lake and environs embraces about 650 square miles, in which the oldest rocks are closely jointed, folded, and partly metamorphosed pre-Tertiary Basement Complex. Over this old rock mass in the lower areas lies a Tertiary sequence of sedimentary, igneous, and pyroclastic rocks ranging from Eocene to late Upper Miocene. Quaternary deposits of unconsolidated sediments ranging from Pleistocene to Recent fill broad drowned areas and principal river valleys, locally to at least 300 feet below sea level. All sedimentary formations are fossiliferous. On a stratagraphic and lithologic basis, the following general correlation is made with other formations outside the lake area.

Gatun Lake Area	Pacific Cut Area
Gatun-Toro-Chagres Fms.	Missing
Upper Caimito Member	La Boca Fm. Cucaracha Fm.
Middle Caimito Member	Culebra Fm.
Lower Caimito Member	Las Cascada Fm.
Bohio Fm.	Obispo Fm.
Pre-Tertiary Complex	Missing

An exposure in an excavation at Gatun permitted more detailed stratigraphic and lithologic examination than was possible anywhere else in the area. Here a section of the Gatun formation 546 feet thick consists of marly, tuffaceous, highly fossiliferous sediments laid down in a shallow sea. At least three minor depositional cycles are represented.

Remote areas adjoining the Gatun Lake area contain previously mapped little-known formations. Among these are:

(1) The Eocene Tranquilla (Gatuncillo) formation. Discovery of its extension into the Gatun Lake area is the first record of Eocene sedimentary rock in the Canal Zone.

(2) The Oligocene-Lower Miocene Quebrancha formation, considered to be stratigraphically equivalent to the Caimito formation.

(3) The Lower Miocene Alhajuela member of the Caimito formation, which is the Gatun (?) formation of Reeves and Ross' Madden Dam Report.

(4) The Middle Miocene (?) Sabanitas formation, which is probably a continental and shallow-water facies of the lower Gatun formation.

The structure of this area is dominated by fractures, a few of uncertain nature but most believed or known to be faults. The greatest faults have a large normal throw. Numerous small faults apparently associated with Tertiary volcanic eruptions have a large strike-slip. The fracture pattern of the Gatun Lake Area, believed representative of the entire central Panamanian Isthmus, fits the view that the Panama Isthmus Ridge is a wide upwarp between the Caribbean and the Ecuador seas, possibly dating from the orogenic epoch of Senonian time.

The topography of the North Pacific Ocean and adjacent northwestern South America contrasts greatly with that of the Isthmus and the Caribbean Sea beyond, as if the southwestern rim of the Caribbean Basin (southern Isthmian continental slope and the line of its eastward extension) constituted a buttress against Cenozoic compressive force from the southwest and had been fractured and faulted by the force of the compression.

The Gatun Lake area is a physiographic basin flanked by high hills on the east and west and by low ones on the south. The highest hills rising over large areas to more than 1000 feet elevation are formed by pre-Tertiary Basement Complex. The main low part of the area is developed from Tertiary and Quaternary material and may be classified as:

1. Swamp and lowland areas up to 25 feet A.T.
2. Interlowland areas up to 300 feet A.T. (500 feet A.T. at extreme points).
3. Dissected highland up to 700 feet A.T.
4. Hills region up to 1100 feet A.T.

The history of the area is recorded in four sets of sediments separated by three major unconformities. The first set of sediments, those incorporated in the Basement Complex, is too folded, broken, and crushed to decipher. The second set, those of Upper Eocene through Lower Miocene, is moderately faulted and folded. The third set of sediments is the Middle Miocene and Upper Miocene (?) coastal plain beds which reveal a simple history that could be easily worked out in greater detail. The youngest set is composed of the Pleistocene and Recent unconsolidated sediments which are so young their short history is that of slight uplift.

The general faunal aspect at some of the rare fossil localities proved a welcome basis for distinguishing Upper Eocene, Oligocene, Lower, Middle, and Upper Miocene, and Quaternary deposits.

A system of sedimentary rock terminology suitable for use in geological mapping in this area of

pyroclastic, clastic, and chemical sedimentary rocks is described and used throughout the paper.

Acknowledgements

The following people generously helped in the completion of this article: Samuel K. Bartholomew who accompanied the writer during some of the field work; Lyle H. Henderson and Dr. W. P. Woodring, who discussed the geology and offered helpful advice on the work; Drs. John E. Allen, Ira S. Allison, H. N. Coryell, N. D. Newell, Sidney Paige, C. P. Ross, and G. G. Simpson who generously read and edited the manuscript; Dr. Walter H. Bucher who gave much time and thought to improving the presentation and interpretation of the data; William F. Jenks who generously supplied the unpublished information about extent of Cenozoic volcanoes in central Ecuador and southern Peru, which he permitted to be incorporated in Figure 2; Paul Wuenschel who permitted his gravity data to be examined and cited as evidence; N. B. Johnson who drafted Plate 2; Elizabeth, my wife, who proof-read the text; Mrs. Henry Nelson who typed the manuscript.

Introduction

Scope

This paper[1] describes the distribution of formations and faults in the northern half of the central Panamanian Isthmus. It correlates the formations with those previously described at various localities in the Canal Zone and adjacent parts of Panama and provides additional stratigraphic details concerning some of them. It demonstrates, for the first time, the presence of numerous fractures, faults, and master joints, in a definite and previously unsuspected pattern, sketches the physiographic features, and interprets the information in terms of geologic history.

Area

The area covers that portion of the Isthmus of Panama accessible by boat at the surface of Gatun Lake, and many inland places reached by streams and trails therefrom. It lies largely within the Canal Zone and extends north and west from Gamboa, C. Z., to the Caribbean Sea. It is slightly trapezoidal in outline and includes about 650 square miles (Fig. 1; Pl. 1).

The Trans-Isthmian Highway and the Panama Railroad constitute the land transportation through most of the region. The hill region between Gatun Lake and the Caribbean Sea has a sketchy road network which crosses a few trails. Although abundant in the Republic of Panama trails are scarce within the limits of the Canal Zone.

Bedrock projects through surficial deposits in only a few places and is deeply weathered; but locally one can surmise the character of the material underlying the extensive mantle by examination of the mantle alone.

Field Methods

The field work began on July 30, 1941, and was carried on intermittently until May 16, 1947. The maps used were waterproof acetate overlays of Panama Survey Army Topographic Sheets[2] on a scale of 1:20,000. Notes were penciled on the overlays in the field and later transferred to permanent records in the office. The field work was carried out on foot along shorelines, stream beds, trails, roads, and railroads, and in excavations such as quarries and the Gatun Third Locks Cut.

Previous Work in the Area

Extensive surface and subsurface exploration and study have been completed along narrow belts within the area under discussion, and the results thereof were utilized for background information. The earlier geologic information on the Gatun Lake area was derived largely from studies made for the French Canal companies, the Isthmian Canal Commission, and the Third Locks Project. The most helpful published papers are those by Dr. D. F. MacDonald. His determinations of stratigraphic sequence of formations in the Gatun Lake area (Mac-

[1] The writer obtained the information included herein in part during official investigations of the Third Locks Project and Interoceanic Canal Studies, 1947, and in part on field trips made on his own time. No expense was incurred by the U. S. Government in any way in the preparation of this article. (*See also* S. M. Jones, 1947b).

[2] Panama Survey Army Survey Topographic Sheets referred to in this article all are available in the library of the American Geographical Society, 156th St. and Broadway, N. Y. C., 32, N. Y., and may be examined by the general public.

FIGURE 1.—LOCATION MAP

Donald, 1913, p. 707–711) saved much time in mapping.

Local Terminology of Sedimentary Rocks

No generally accepted system of rock nomenclature could be found to distinguish adequately the sedimentary rocks of this area. The shortcomings of nomenclature encountered in early attempts to differentiate the Canal Zone Tertiary are summarized in the objections of Pettijohn (1949, p. 13, 14) to existing classifica-

tions. A megascopically applicable quantitative system of nomenclature suitable to this region, a modified composite of several pre-existing systems, (Wentworth and Williams, 1932; Wentworth, 1937), is presented here.

TABLE 1.—LOCAL SEDIMENTARY ROCK CLASSIFICATION

Grain size mm.	Predominantly inorganic						Predominantly organic ($CaCO_3$ more than half)	
	Less than half volcanic constituents				More than half volcanic constituents			
.004	Claystone	Mudstone	Clay shale	Shale	Tuff claystone			
(1/256 mm.)	Siltstone		Silt shale		Tuff siltstone	Tuff	Limestone	
0.06	fine-grained							
(1/16 mm.)								
0.2	medium-grained	Sandstone			Tuff sandstone			
0.6	coarse-grained						Coquina	
2.5								
(0.1 inch)	pebble						(Shell) breccia	Coquina
25.0								
(1.0 inch)	cobble	Conglomerate		Breccia		Agglomerate		
305.								
(1.0 foot)	boulder							

The combined forms of the rock names (Table 1) are made by hyphenation between two or three of them, proportions of which in the rock lie between 25 and 75 per cent. Under this taxonomy combined forms are mandatory where applicable, except where an inclusive term is present in the table in which case the inclusive term may be used instead of the combined form. Use of the adjectival forms of the rock names is optional but restricted to constituents composing up to 25 per cent of the rock.

Among the fine-grained sediments, claystone, siltstone, and mudstone are thickly to massively bedded; shales are fissile to thinly bedded; tuff-claystone and tuff-siltstone are thinly to massively bedded. The waxy luster of claystone distinguishes it from siltstone. The latter has a gritty, dull luster when cut with a knife.

In the sand-size range, fine grains are not readily visible to the naked eye but are easily seen with the aid of a 14× hand lens. Medium grains are readily visible to the naked eye but are not much over a half a mm. in diameter. Coarse grains are up to 2.5 mm. in diameter. Granules are not distinguished from pebbles.

Among the coarse sediments, "breccia" refers to fragments owing their angularity or subangularity to their most recent transportation or to intraformational activity; "agglomerate" refers to fragments initially of pyroclastic origin which still retain enough of their primary shape that their pyroclastic origin is apparent. Only some agglomerates are volcanic breccias. Volcanic breccias are but a small proportion of the coarse clastics.

Adjectives describing bedding thickness are used in the sense indicated below:

massive bedding—bedding partings more than 4 feet apart.

thick bedding—bedding partings 2–4 feet apart.

thin bedding—bedding partings 2 inches to 2 feet apart.

fissile bedding—bedding partings less than 2 inches apart.

STRATIGRAPHY

Summary and Conclusions

The rocks encountered in the Gatun Lake area include marine and fluviatile sediments and igneous flows and intrusives, ranging from Upper Eocene to Recent, all overlying a Basement Complex of probable pre-Tertiary age. All of the below named formations are described in the geologic literature on the Panama Canal Zone. The author's changes in concept of the stratigraphy of the Gatun Lake area are the result of observation of many more outcrops than previously found and of several discussions

TABLE 2.—CORRELATION OF STRATIGRAPHIC COLUMNS, CANAL ZONE

Age	Gatun Lake Area Formation	Thickness (in feet)	Pacific Area Formation
Recent Pleistocene	Chagres Alluvium & Chagres Gravel and Atlantic Muck	300	Chagres Alluvium & Chagres Gravel and Pacific Muck
Pliocene	Missing (?)		Missing
U. Miocene (?)	Chagres Fm.	1500	Missing
	Toro Ls.	500	Missing
M. Miocene	Gatun Fm.	3000	Missing
L. Miocene	Chorrera Basalt, Cerro Gigante Basalt, Bruja Dolerite, etc.	1000 1000	Miraflores and Sosa Hill Basalt
	upper Caimito Member	1750	La Boca Fm. Pedro / Miguel Agglomerate Cucaracha Fm.
U. Oligocene	Middle Caimito Member	450	Culebra Fm.
	Lower Caimito Member / Las Cascadas Fm.	300	Las Cascadas Fm.
L. Oligocene	Bohio Fm. Obispo Fm.	2500	Obispo Fm.
U. Eocene	? ? base not exposed ? ? ? ? ? ? base not exposed ? ? ? Gatuncillo Fm. west of Madden Basin only		
Pre-Tertiary	Basement Complex		not exposed

Legend: -O-O-O Unconformity
---- Conformity or disconformity
-o-o Local unconformity
\ Intergrading facies
? ? Contact not known

Modified slightly from Jones and Bartholomew (1946, Appendix A).

and field trips with Mr. H. G. Martin and Drs. D. F. MacDonald and W. P. Woodring. Woodring determined the ages of the fossil faunas (Woodring and Thompson, 1949). All the correlations (Table 2) were made by the author and T. G. Moran on the basis of lithologic sequences and the facies changes observed (Jones and Bartholomew, 1946, App. A).

The difference between these correlations (Table 2) and those of Woodring and Thompson (1949) is confined to the Oligocene-Lower Miocene sequence. It is attributed to the fact that the correlations of Woodring and Thompson are homotaxial, and that by suggestion only. The horizontal lines on their correlation chart should be interpreted as "suggested magnafacies" boundaries, especially in view of the tremendous environmental range evident from the lithologic and faunal variation from place to place in this sequence. The latitude inherent in the isochronal lines because of this "homotaxial" correlation is ample to allow the dating in Table 2 validity equal to that of the correlation chart of Woodring and Thompson (1949, p. 246).

The dating of the faunal facies of Woodring and

Thompson was done by comparing each facies with an already dated more or less similar facies often from a distant locality. The various facies used as standards for dating the local central Panama formations are scattered to such distances as Mexico, Peru, and the island of Antigua.

The correlations of Table 2 are local field correlations and therefore should be more reliable than those of Woodring and Thompson (1949). The latter were made on the basis of their suggested dating rather than by local field correlation. Not enough collecting has been done to make possible unambiguous correlation by direct comparison of local Oligocene and Lower Miocene faunas.

In order from oldest to youngest the formations present are:

1. Basement Complex—thought to be pre-Tertiary.
2. (Gatuncillo)* and Tranquilla formations—Upper Eocene.
3. Bohio and Obispo formations—Oligocene.
4. Las Cascadas formation—Upper Oligocene (?)
5. Caimito and (Quebrancha)* formations—Upper Oligocene and Lower Miocene.
6. Bruja Island Dolerite, Cerro Gigante Basalt,[1] and related basic igneous rocks—Lower Miocene.
7. Gatun and Sabanitas formations—Middle Miocene.
8. Toro Limestone—Upper Miocene (?).
9. Chagres formation—Upper Miocene (?)
10. Atlantic Muck and Chagres Alluvium—Pleistocene and Recent.

Vicinity of Gatun Lake

Basement Complex.—The Basement Complex is a pre-Tertiary (?) mass of basalts, metabasalts, metatuffs, hornfels, dacite porphyry, and possibly other quantitatively unimportant rock types. This mass of rock is closely jointed and complexly faulted. Closely spaced folding and steep tilting of the sediments were extensive prior to their secondary induration. All fresh bedrock exposures exhibit chloritization, silicification, kaolinization, and other similar alteration. In the typical case, joints stained by manganese oxide in the basalt and metabasalt are spaced less than 2 inches apart. The metasediments are even more closely jointed by platy bedding joints. The rocks are so altered that in some places igneous and sedimentary rocks cannot be megascopically divided. Exposures of fresh rock are rare because of the thick (50-foot) mantle of weathered material. Some roadcuts in this mantle have so disturbed the natural slopes or so cut the toes of dormant mudflows as to initiate active sliding of mudflow and structural types.

The Basement Complex is probably part of the Isthmian pre-Tertiary core which has long been below sea level in much of the Gatun Lake area. Exploration up the Mamoni and Capira rivers north and northwest of Chepo in the Republic of Panana show that this same terrane forms at least the south side of the Sierra de San Blas (Sierra de Chepo), the central Isthmian E-W core east of the Canal Zone. Extensive outcrops of similar appearance were seen during a visit to the north side of the Valiente Peninsula, but none have been reported between there and the Sierra de San Blas to the east.

Bohio Formation.—The Bohio formation is an early Upper or late Lower Oligocene series of siltstones, sandstones, and sandstone-conglomerates, very hard and massively bedded and jointed. It contains angular to rounded pebbles, cobbles, and boulders, locally up to as much as 6 feet in diameter, in a dark-gray, generally coarse-grained, angular-grained sandstone matrix. Both the sandstone matrix and conglomeratic fragments are notably basaltic. Some tuff-siltstone interbeds as much as 90 feet thick are present. Exposures of this formation show dips of 15° to 20°. The formation is characteristically transected by basalt intrusions ranging in width from a few inches to an observed maximum of 200 feet. These intrusions are more or less localized, being very numerous, for example, in the vicinities of Gamboa and Darien. They are so numerous and discontinuous that only the large ones are mappable units. The Bohio formation in localities containing numerous faults and basalt dikes has been highly indurated over broad areas by incomplete fusion and by other igneous effects. From Darien to Gamboa the overall outcrop picture is one of uneven increase in both coarseness of matrix and angularity of frag-

* Terms to be abandoned as the names of formations or members.

[1] "Basalt" is used throughout this paper as a field term applied to basic fine-grained igneous rocks including "andesite" and "basalt". Microscopic thin-section examination showed the abundance of both types.

ments of all sizes. At Darien some fused sandstone-agglomerate is present; at the Obispo High locality, some hard, friable sandstone-conglomerate is exposed. But eastward from Gamboa, angularity of fragments and induration of the Bohio formation by basalt intrusives are progressively greater to the extent that at Obispo Point, across the Chagres River Bridge from Gamboa, and at Bas Obispo and eastward therefrom, the rock is considered to be the Bas Obispo (agglomerate) formation. That the Bas Obispo and Bohio formations are different facies of the same stratigraphic sequence has become apparent through field mapping along the west bank of the present canal in the vicinity of and opposite from the town of Gamboa. Here numerous rock exposures have demonstrated a gradual change in character from that of the typical Obispo agglomerate to that of the Bohio sandstone-conglomerate.

The unconformity at the top of the Bohio formation is irregular and represents a period of erosion during which the Obispo-Bohio formation land surface was dissected to maturity with a relief of an undetermined number of scores or possibly hundreds of feet.

Las Cascadas Formation.—The Las Cascadas formation is an Upper Oligocene (?) series of massive to thin-bedded tuffs, tuff-conglomerates, and tuff-agglomerates of terrestrial origin. Matrix material ranges from tuff-claystone to coarse, finely agglomeratic tuff. Conglomerate fragments are pebbles, cobbles, and boulders of basalt and pebbles (rarely cobbles) of tuff. Basalt fragments are reworked from the underlying formations. They are generally rounded where they overlie the Bohio formation and sub-angular over the Obispo formation. All surface exposures are deeply and highly weathered. Only the centers of some of the larger cobbles and boulders show sound black basalt in outcrop. Fifty feet of weathered rock overburden is common over this formation. The Las Cascadas formation is a mass of reworked basic material from the underlying Bohio-Obispo formations mixed with proportions ranging from 0–100 per cent of the later acidic tuffs and agglomerates. Therefore some outcrops are impossible to distinguish from the supra- and subjacent formations except after consideration of outcrops over a broad area. Its distribution and variability are attributed to its origin as a formation of reworked material (in the Gatun Lake area) and to subsequent erosion, weathering, faulting, and intrusion by igneous bodies.

The upper contact was not found exposed. It is believed to be an unconformity in the vicinity of Gamboa and Darien where it is overlain by limestone, but a conformity in the vicinity of Barro Colorado where it grades up from a tuff-conglomerate into limy tuff-siltstone. Where conformable under the Caimito formation (apparently north and west of Darien), it has the lithologic characteristics of conglomeratic Caimito tuffs and is mapped with the Caimito formation. More detailed study in the future may separate this unit from the Caimito formation in the northwest Lake Area. On the other hand, the lower Caimito in this area appears to be a marine equivalent of the continental Las Cascadas formation and to be rightfully included in the Caimito formation. Its age is now inferred in accordance with its stratigraphic position with respect to over and underlying fossiliferous beds.

Caimito Formation.—The Caimito formation is an Upper Oligocene and Lower Miocene series of tuffs (here acidic tuff, the predominant constituent of this formation), tuff-agglomerates, tuff-conglomerates, and limestones, all thinly and thickly bedded and closely to moderately jointed. All are probably marine. Some beds contain sparse, poorly preserved, marine megascopic and microscopic fossils. The attitude of the beds is highly variable due to cross-lamination, faulting, and folding. Dips range from 5° to over 40°. The formation is divisible lithologically into three members: lower, middle, and upper.

The lower member, formerly designated "basal" phase (Jones, 1947b, p. 24), is a tuffaceous sandstone-conglomerate of local extent containing pebbles, cobbles, and boulders of basalt and pebbles of tuff. The basalt fragments are reworked from the underlying Bohio formation. All exposures are highly weathered indicating that this member of the Caimito formation either weathers very deeply upon exposure or was completely weathered during its deposition. It is present only along the bottoms and side slopes of the Bohio surface where the pebbles, cobbles, boulders, and some of the sand weathered out of the Bohio formation, were reworked and deposited with the first of the tuff which marked the new era of deposition. It is

probably a marine facies of the Las Cascadas formation.

The middle member, formerly designated "lower phase" (Jones, 1947b, p. 25), is a series of slightly fossiliferous tuffaceous sandstones and limestones. This member may be local and may intergrade in part with the lower member although the former is more widespread. But whether or not it was originally deposited throughout the Gatun Lake area has not been determined. The limestone beds within it are discontinuous. The zones of abundant *Lepidocyclina canellei, L. pancanalis,* and *L. vaughani* appear in this member and are found on the peninsula jutting into Zetek Bay, Barro Colorado Island, in the Panama Railroad cut at the east side of Bohio Peninsula, and at other points (Pl. 2).

The upper member (Jones, 1947b, p. 25) is a widely distributed series of tuffs and tuff-agglomerates, with sandy limestone beds interspersed throughout at irregular intervals. It is the thickest, most widely distributed part of the formation. When sufficiently detailed field mapping, laboratory study, or core drilling can be undertaken, it may be mappable as one or more other formations. The entire formation appears to be increasingly uniform and fine grained toward the northwest, away from Barro Colorado and Bohio Peninsula. In these areas it is essentially a tuff-siltstone series.

Possible equivalents of the Caimito Formation.—The author believes that the Pena Blanca Marls and Vamos-a-Vamos beds of earlier writers represent some of the finer-grained facies of the Caimito formation in the northwest Lake area (Jones, 1947b). This belief is based on the locations of fossil localities of these beds. Conversely, the Caimito formation becomes progressively coarser toward the southeast, presumably toward the higher summits of the Continental Divide. Thus the lower member is distinguishable as the Las Cascadas (tuff-agglomerate) formation south of Gamboa. Likewise north of Gamboa the Quebrancha formation and the "Alahuela formation" appear equivalent to all or parts of the middle and upper Caimito formation.

Caraba facies of the Caimito Formation.—A heretofore unrecognized facies presumably of parts of the middle and upper members of the Caimito formation was found typically exposed along the Rio Caraba southwest of Gamboa and in gullies along the south bank of Chagres Crossing Reach due south of Canal Beacons 29 and 30. The Rio Caraba exposure is good and reveals a thick massive, very sparsely jointed sandstone-conglomerate-breccia, overlain by a thick section of thin-bedded limestone and limy fine-grained sandstone. The sandstone-conglomerate-breccia of the Caraba facies is composed of angular to sub-angular grains. Composition is distinctive with a marked preponderance of quartz, hornblende, biotite, and pumice composing the matrix; while the psephytic components are essentially porphyritic and coarse-grained acidic igneous rocks of variable texture and composition but containing much quartz, hornblende, biotite, and albite. Rhyolite porphyry, dacite porphyry, tonalite, and granite are plentiful. Both the coarse constituents and the matrix are derived from a common source. Rhyolite dikes transect the facies locally. The limestone overlying the Caraba facies along the Rio Caraba has the fossil assemblage characteristic of the Caimito formation: *Lepidocyclina cf. L. canellei. cf. L. pancanalis,* and *cf. L. vaughani.* If this facies is later demonstrated to be a mappable unit it should be given formational status, although it is included in the Caimito formation on Plate 2.

Bruja Island Dolerite, Cerro Gigante Basalt, and related basic igneous rocks.—Under this heading are included Lower Miocene flows, plugs, and dikes of basic rock, hard and generally moderately jointed. Columnar jointing is pronounced at some localities, such as on the south side of Barro Colorado where columns as much as 6 feet in diameter have been observed. The most characteristic type of exposure is dark red-brown sandy and silty clay containing spheroidally weathered boulders as large as 6 feet in diameter with cores of hard, black basalt. The original basalt texture is observable in much of the undisturbed clay. The intrusives of this group of rocks transect every formation below the top of the Caimito formation; and the flows are found mostly on the unconformity over the Caimito formation (Jones, 1947b). South of the Gatun Lake area, exposed along roads north of Chorerra, R. de P., are a series of basalt flows interbedded with bentonitic clay layers presumed to be altered tuffs. If these tuffs are Caimitoan and the basalts are a southward continuation of those flows in the Lake Area, then the flows are merely the latest

and most extensive of a flow series interbedded in the Caimitoan (?) sediments to the south. Such an assumption would extend the time of eruption of the basic rocks back to include at least part of Caimitoan time. The best hard-rock quarry sites in the Gatun Lake Area are in rocks of this classification.

Gatun Formation.—The Gatun formation is a Middle Miocene series of sandstones, siltstones, conglomerates, and tuffs, all thickly and massively bedded. The siltstones, sandstones, and conglomerates are variably marly and tuffaceous, highly fossiliferous, and massively jointed, with nearly vertical joints spaced at intervals greater than 20 feet.

The tuffs are uniformly grained siltstones and claystones, except for local streaks sparsely scattered with pumice pebbles and cobbles. Jointing in the tuffs is well developed at moderate intervals. The formation has a thickness known to exceed 1400 feet (Thompson, 1943), and probably much more. The beds dip northwesterly to northerly at angles ranging uniformly from 2° near the shore of Limon Bay to as much as 20° in a few places near their southeastern border. The depth of overburden and weathered rock averages about 30 feet on this formation. The weathered rock is soft and grades imperceptibly into red clay soil.

The excavation for the Third Locks at Gatun afforded an unusual opportunity to study a 546-foot section of the Gatun formation. Observations of the sound rock section in this cut are summarized (Table 3) with the thicknesses and types of contact indicated. The detailed descriptions (Appendix 1) of each bed are based both upon field observations and microscopic examination of thin sections, loose grains, and small rock fragments. The details reveal some of the conditions extant in the Isthmian region during Gatunian time.

Toro Limestone.—The Toro limestone is an Upper Miocene (?) limy sandstone-coquina series, typically exposed at Toro Point across Limon Bay from Colon. The entire formation[4] is massively jointed and thickly to massively bedded without bedding parting. It is hard and well cemented with lime except where weathered to a poorly cemented, friable condition.

The matrix of the coquina is coarse-grained sandstone of rounded quartz sand and sand-size shell fragments. The coquina is of angular mollusc and coral fragments, all up to .03–.04 foot in diameter but averaging .01–.02 foot in diameter. Both matrix and psephitic fragments range in proportion from 0 to 100 per cent in the various beds. Some of the beds are made up of topset lenses overlying foreset lenses (dipping 30°–40°), in turn overlying bottomset lenses. The beds themselves have an average dip of 3¼ to 4° N 45–55° W at Toro Point, the type locality. This formation represents a beach sand deposit laid down by progressive overlaps and offlaps during extensive emergence and submergence between deposition of the Gatun and Chagres formations. The Toro limestone grades upward into the Chagres sandstone. The thickness of this formation (Table 1) was measured in the field on the slopes west of Gatun Dam.

Chagres Sandstone.—Chagres sandstone is an Upper Miocene (?)[5] sandstone and siltstone deposit, extremely massively bedded, soft and fine-grained. A few calcareous stringers all less than 1 foot thick are present. Practically no open joints exist in this formation. It contains a few fossils, principally pelecypods (Pecten) and gastropods. All fossils are excellently preserved, a few specimens even exhibiting some of the original shell pigmentation. The highly massive nature of the formation makes bedding difficult to determine. One core-drill hole extended for a depth of more than 300 feet into this formation with nearly 100 per cent core recovery without revealing any indication of bedding other than a few thin limestone stringers.

The contact between the Toro limestone and the Chagres formation is gradational where observed in detail in the hills on the southwest side of the lower Chagres River. Because of this gradational contact the above age was

[4] Relegated to the status of a member of the Chagres formation by Woodring and Thompson (1949, p. 244). Retained in full formational status in this report because considered an important mappable unit.

[5] Some authors in the past have called the Chagres formation Pliocene (?); but Dall and Woodring now consider optional the choice between Upper Miocene (?) and Pliocene (?) for the age of this formation.

TABLE 3.—INTER-RELATIONSHIP OF BEDS EXPOSED IN GATUN THIRD LOCKS CUT

Bed No.	Bed Letter	Thickess (variable)	Contacts and lithologic features
	A4	26.2′	Silty sandstone*
			Maximum thickness exposed.
			Top removed by erosion.
			Facies boundary.
12	A3	11′	Siltstone.
			Sharp textural contact.
	A2	28′	Argillaceous siltstone.
			Sharp textural contact.
	A1	5′–0′	Sandstone.
			Sharp contact associated with .2′ to .6′ fractured zone. *Key bed.*
11	B	25′–30′	Calcareous, argillaceous sandstone.
			Very gradational.
	B_{co}	10′	"Upper Conglomerate." Basal Ss.-Cg. of Bed B.
			Angular unconformity and compositional sharp change. *Key bed.*
10	C_{co}	2′	"Upper Conglomerate" Top Tuff-Ss.-Cg. of Bed C.
			Very gradational.
9	C	48′–60′	"Blue-grey Sandstone." Tuff-sandstone, cross-bedded.
			No boundary, Completely gradational.
8	Cg-Du		Tuff-sandstone and Tuff-siltstone interbedded.
			Gradational.
7	Db	20′–12′	"Ash No. 1". Tuff-siltstone.
			.5′ white tuffbed. Sharp contact below it. *Key bed.*
6	Eu	4′	Sandstone-conglomerate.
			Slightly gradational. Changes in less than 1.0′.
5	Eb	38′	Sandstone.
			Sharp contact.
	Fu		Tuff-sandstone.
			Very gradational change.
4	Fm	110′	Tuff-sandstone and Tuff-siltstone interbedded.
			Very gradational change.
	Fb		"Ash No. 2". Conglomeratic tuff-siltstone.
			Ripple-marked disconformity, containing .1′ to .2′ Ss. *Key bed.*
3	G	70′	Echinoids, shark teeth, wood, nuts, in Sandstone.
			Very gradational. Pumice boulders in gradation.
2	H	6′	"Ash No. 3". Tuff-claystone.
			Ripple-marked disconformity containing .1′ to .2′ Ss. *Key bed.*
1	I	102.2′	Sandstone.
			Sharp contact containing 1′ Ss-clastic, coarse grained.
	J	27′	Sandstone.
			Sharp contact.
	K	5′	Sandstone.
Total		546′	

*Appendix 1 for detailed lithology.

assigned the Chagres formation and for the same reason its dip is thought to be in general gently northward toward the Caribbean Sea at a low angle as in the limestone below. No indication of bedding sufficiently well defined to determine dip and strike in this formation has ever been seen by the writer.

The formation resembles the Gatun formation but is much more massive, does not contain the tuff or conglomeratic beds of the Gatun formation and is less fossiliferous. The weathered rock and overburden over the Chagres sandstone average less than 10 feet thick. The overburden is red sandy clay.

Atlantic Muck.—The Atlantic Muck is a Pleistocene and Recent formation consisting of swamp deposits, both alluvial and marine, largely composed of clays, silts, and fine sands irregularly intermixed, uniformly soft and weak, and having a very high moisture content.

Thompson (1943, p. 23) divides the muck into four phases. The lower phase, adjacent to its contact with older formations, consists of grey to blue-grey silty clay. The phase deposited in brackish marine waters contains abundant mollusc shells in an organic, black-silt matrix. The littoral swamp deposit is composed of semi-decayed wood and other organic vegetable matter, intermixed with silt and is characteristically dark brown to black. A soft, light-grey, weak, plastic clay overlies the organic phase. The four phases intergrade, with sand lenses locally present. The muck was deposited upon a stream-eroded topography of considerable relief. Old core borings reveal depths of over 200 feet for this deposit. Hills of the Gatun formation protrude thru the black muck and in the area south of Gatun these hills form islands that are completely surrounded by the swamp muck deposits.

Observation of drill cores throughout the Gatun Lake area indicates that these four phases of the Muck are present in all thick muck deposits. In addition, the top and bottom phases appear to be thinnest and most widespread; the two middle phases are much the thickest, form the bulk of the formation, and interfinger so extensively that individual drill holes may show interbedding of these two phases. The brackish marine phase is north, or downstream from the littoral swamp phase and inter-fingers seaward with extensive beds of unconsolidated finger- and brain-coral fragments north of Gatun.

Chagres Alluvium.—These are Recent and Pleistocene alluvial deposits of interbedded clays, silts, sands, and gravels, variably loose to well compacted. The cobbles and pebbles composing the gravel are very hard and range from basalt to granite. This deposit is found along the old Chagres River valley and its principal tributaries, the Rio Gatun and Rio Trinidad, and along other principal valleys. It intergrades locally with the Atlantic Muck and is included with the Atlantic Muck on Plate 2. Beneath Gatun Lake, the boundary of these surficial deposits and the underlying bedrock is generalized from old French maps showing the margins of the pre-Gatun Lake lowland. The basis of this generalization is the field observation that practically all flat land areas below elevation 25 feet A.T. and bounded by a break in slope are underlain by these surficial deposits.

Outlying Areas

General Statement.—Little known or only locally investigated formations previously mapped in remote areas adjacent to and extending only a short distance into the Gatun Lake area are here discussed. For detailed descriptions and paleontological dating and affinities see Coryell and Embich (1937), Woodring and Thompson (1949).

Gatuncillo and Tranquilla Formations.—The Tranquilla formation was described and named by Terry (Coryell and Embich, 1937, p. 289 and 291). Coryell and Embich (1937) assigned it to the U. Eocene series and correlated it homotaxially with the Jackson fauna of the coastal plain of the Gulf of Mexico.

Although the type locality (Tranquilla Town, 79°13′W., 10°15′N.) is now under the water of Madden Reservoir, the description (Coryell and Embich, 1937, p. 289–291) of the extent of this formation and of the stratigraphic sequence above and below it leaves no doubt as to its identity[6] with the Gatuncillo formation of

[6] Cooke (1948, p. 91) says of faunal collection U. S. G. S. 16889 (from north of Madden Airfield, R. de P., on the south edge of the Madden Basin): "—The echinoids occur in limestone that comprises part of the late Eocene formation bearing the foraminiferal faunas recorded by Vaughan (1926) and

Woodring and Thompson (1949, p. 227). Perhaps the term "Gatuncillo formation" should be retained, nonetheless, for the limier facies farther west, evidently on the periphery of the U. Eocene Tranquilla Basin.

The equivalent shales, fine-grained limestones and limy sandstones were described and mapped as Gatuncillo formation by Thompson (1944) for several miles up and down the Gatuncillo River Valley from the Trans-Isthmian Highway. Its distribution is generalized on Plate 2 from a field traverse and from topographic map and aerial photograph studies. Recent identification by Stewart (1947b) of Upper Eocene fossils (fossil locality #23, Pl. 2) from limestone samples taken at the head of Quebrado Chinilla in the Canal Zone prove that this area also is underlain by the Gatuncillo formation. This is the first sedimentary rock found in the Canal Zone of age established paleontologically as Eocene (Jones, 1947b, p. 41).

Quebrancha Formation.—This formation of Oligocene and Lower Miocene age has been described and mapped in detail by Thompson (1944, p. 17) for several miles around the Cemento Panama Plant in the Republic of Panama. It is distinguished only by letter symbol from the rest of the Caimito formation on Plate 2 because it is considered to be typical Caimito formation (Jones, 1947b, p. 26). Woodring and Thompson (1949, p. 234) now concur that this series is Caimitoan and restrict the term "Quebrancha" to the thick silty limestone and limy sandstone member which they designate the "Quebrancha limestone member." The lithologic sequence and thicknesses here as elsewhere in the Caimito formation throughout the lake area (Pl. 2, Table 2) make it obvious that the calcareous siltstone and the Quebrancha limestone "members" are respectively the upper and middle members of the Caimito formation (formerly upper and lower members, Jones, 1947b, p. 24 to 26). If the name "Quebrancha" is to be retained it should be as the "Quebrancha parvafacies"; there is no justification for renaming this entire member of the Caimito formation.

"Alhajuela Formation."—The "Alhajuela formation" is Lower Miocene in age. The author considered it to be the "Alhajuela Member of the Caimito formation" and has generalized the boundary of this series (Pl. 2) from the areal geologic map by Reeves and Ross (1930, Pl. 6) to show how it fits into the overall picture.

A further disagreement is found in the relegation of the marine (?) volcanic lower member of the Caimito formation (formerly basal phase, Jones, 1947b, p. 24) to the Bohio formation in the Quebrancha syncline (Woodring and Thompson, 1949, p. 246). Since this volcanic member has not been proven either marine or non-marine it might be designated alternatively "Las Cascadas formation" or "lower member of the Caimito formation", but certainly not "Bohio formation".

The "gritty sandstone member of the Bohio formation" in the Quebrancha syncline (Woodring and Thompson, 1949, p. 232, 246) bears no resemblance to the Bohio formation as mapped elsewhere (Pl. 2). Its faunal affinities also leave doubt as to its status. This member has been provisionally included with the rest of the Quebrancha formation (Pl. 2) because of its conformable relations thereto. Certainly this sandy mudstone, locally slightly conglomeratic, resembling some of the Gatun formation beds (App. 1, Beds A, B) rather than anything in the Bohio formation should not be considered part of the same mappable unit. Even if it is ultimately proven to be a facies of the Bohio formation it should be given a distinct formational name because it is a mappable unit of considerable extent and great thickness beyond the limits of Plate 2. In the absence of published evidence, the writer on the basis of careful traverses doubts that this unit attains a demonstrable thickness, within the Quebrancha syncline, approaching the 1500 feet cited by Woodring and Thompson (1949, p. 232).

Reeves and Ross (1930) mapped successive members of a massive sandstone sequence at Madden Reservoir as Emperador, Caimito and Gatun (?) formations. According to Olsson (1942, p. 234, 243) "... these different members form a stratigraphic unit which can be referred to broadly as the Alhajuela sandstones or the Caimito formation". Since the age of the Gatun (?) beds mapped by Reeves and Ross has been shown paleontologically to be Lower Miocene, the name "Gatun" does not

by Coryell and Embich (1937)." These beds, examined by the writer in the course of his unofficial investigations, revealed lithologic character identical to that of the limier phases of the Gatuncillo formation of Woodring and Thompson. They are rich in shallow-water limestone algae, and are considered to be peripheral deposits grading basinward into the shalier deep-water facies called "Tranquilla" by Terry, Coryell and Embich (1937).

apply. Since the name "Camito", is already adopted by the writer to include Las Cascadan and Culebran to Lower Miocene beds, the term, "Alhajuela (Alahuela), member" has been applied to the Gatun (?) beds of Reeves and Ross. This is in line with established usage of calling them the "Alahuela formation". The Emperador is not a true member of the Caimito formation since it represents neither a continuous bed nor a discontinuous horizon in either the Caimito or Culebra formations (App. 2, Physical Data, Evolution of the name Caimito formation).

"*Sabanitas Formation.*"—This is considered a Middle Miocene (?) continental facies of the basal part of the Gatun formation. It is typically a tuff-conglomerate uncomformably overlying the pre-Tertiary Basement Complex. Over wide areas, exposure has deeply altered it to a weathered ash and gravel. It is unsorted and massive in type exposure along the Boyd-Roosevelt Highway northeast of Sabanitas. The best exposure showing its relation to the Basement Complex, is at Station 324 on the Boyd-Roosevelt Highway. Here the matrix of the tuff-conglomerate is white siltstone or silt; the psephitic fragments range up to large pebbles and may be classified as: (1) angular chert (resistant vein remnants from Basement Complex), (2) subangular weathered basalt, and (3) subrounded, soft, weathered tuff-siltstone. Elsewhere, as along Puerto Pilon Road and to the end of the Army Road north of Puerto Pilon, it is interbedded with and gradational into the fossiliferous Gatun formation thick-bedded marly tuffs and clastic sandstones. The eastern edge of the "Sabanitas formation," where it is bedded, is a shallow-water deposit. Dips exposed along Trans-Isthmian Highway—Puerto Pilon Road rather uniformly conform with those of the Gatun formation in the area—about 10–12° N 30–45°W. The shallow-water facies forming the western border ranges from tuff-siltstones (locally shaley with carbonaceous partings) to coarse quartzose sandstones. The latter are conglomeratic with granules which are replicas in miniature of the gravels at the type locality northeast of Sabanitas.

Structure

General Statement

The structure of the Gatun Lake area is dominated by several systems of faults and associated fractures, ranging from pre-Tertiary to Quaternary. The fractures which became apparent through the present study are indicated on Plate 2.

Each fault shown represents the extension by map and photograph study of a fault observed in the field, or it is part of a fracture system that includes faults identified in the field. Associated fractures are shown on the map which are equally apparent on the photographs but could not be proven to be faults in the time available for field work.

The faults, as far as can be told from the several score exposures visible in bedrock, are all high-angle with dips greater than 60°; most of them show a normal but some reverse component of displacement. Slickensiding generally indicates a large horizontal component wherever observable (mostly in the d-series). Determination of vertical displacements is impossible without detailed study. The large displacement of vertical or steeply dipping dikes, such as that of the Juan Grande Peninsula, and the undetectable displacement of flat structures, such as the Caimito-Gatun contact along faults, indicate that most are tear faults. More specific details of the individual fractures and faults are given in the following section.

The present topography appears at least locally to be the direct result of Quaternary movement along parts of most fault zones. This is shown by such evidence as: the drowning and silting of the major drainage south and east of Lagarto and Pina and of the Trinidad, Chagres, and Gatun valleys; the youthful doming of Barro Colorado Island; and the numerous fault scarps such as those east-northeast from Nuevo Limon, eastward from Gatun, along the south edges of Tigres and Lion Hill Islands, and northward from Escobal.

Moreover, the older formations throughout the area show progressively more disturbed conditions, indicating that diastrophism has been practically continuous during all of Cenozoic time.

Details of Fractures

In view of the importance that attaches to the fracture pattern (Pl. 2), the evidence on which it is based will be illustrated with a few details. The fractures have been given numbered

letters (a-1 to 13; b-1 to 11; c-1 to 14; d-1 to 19; e-1 to 10; Pl. 2), to which the following paragraphs refer:

a-1

This fault manifests itself most prominently by a long, evenly and gently curved valley that is asymmetrically steep on its north side. Its north side forms the entire north bank of the Gatun Arm of Gatun Lake. About 5 miles and again 10 miles east-northeast of Nuevo Limon, groups of hills south of the fault suggest underlying Basement Complex. In the westernmost group, the presence of Basement Complex was confirmed by field observation. For the other, inaccessible to field checking in the time available, aerial photographs bear out its presence. Tertiary rock underlies the remainder of the south side of this fault, judging by the topography which was studied stereoscopically and by numerous field traverses from the Boyd-Roosevelt Highway.

The north side of the fault line depression is in early youthful dissection, the south side in late maturity. Obviously a large and variable component of down-throw south of the fault is indicated by topography and arrangement of formations. The actual trace of this important fault, as of many of the other large faults in this and other tropical areas, is a belt of rock particularly susceptible to weathering and erosion. Consequently no rock outcrops are available in the fault zone for direct observation. Nonetheless the circumstantial evidence indicates this to be one of the greatest faults in the entire region. Its extent and throw to the east continues strongly beyond the area covered by Plate 2. At Nuevo Limon and to the west the throw appears to be diminishing rapidly as it disappears under Gatun Lake. However, the trend is continued at a little distance to the north by another great fault zone (a-2).

a-2[7]

This fault is manifested only by a series of extremely youthful scarps that form the north shore of Gatun Lake for 2½ miles east-northeast of Gatun, and then the south shore of Zorra and adjacent islands to the east. Map and photograph studies show such a straight and regular line along each of these scarps and an *en echelon* arrangement such as to preclude their being merely simple erosion scarps developed on the monoclinally northward-dipping Gatun formation. A steeply southward-dipping normal accessory fault with throw of about 15 feet is exposed in the Panama Railroad cut through this fault scarp at Quebrancha (2½ miles east-northeast of Gatun). The backslope of this scarp descends continuously to the Caribbean Sea and is maturely dissected. The top of the scarp forms the Gatun Lake watershed divide. The scarp has been breached by the Chagres River which has carved through it the old meander valley whose breadth extends from the west side of Gatun for 1.2 miles to the youthful scarp of the fault numbered d-1. West of d-1, in the hills west of Gatun Dam, this same fault is traceable on aerial photographs as a straight line of deeply entrenched youthful streams. This fault is one of great, but not specifically determined, down-throw on the south side. Together with d-1 it decreased the accuracy of the writer's thickness determinations of the Gatun formation (based on average width of outcrop and average dips) and rendered that value a probable maximum.

a-3

This fault is inferred from aerial photographs which show another straight line of deeply entrenched youthful streams (including a tangent of the Rio Media). Also the relief is greater and the condition of dissection more youthful abruptly north of both faults a-2 and a-3.

a-4, 5

These two faults are inferred where shown crossing bedrock because their indicated course is marked by prominent stream beds perfectly aligned on opposite sides of a divide. Under the muck the course of a-5 is apparently continued parallel to the prominent scarp that marks the southeastern side of the hills west of Limon Bay. The existence of both faults is supported by substantial offset of the Toro-Gatun contact south of a-4 from its expected position north of a-5.

a-6

This is a group of six faults, four of which are exposed in the sea cliffs at the mouth of the Chagres River by Ft. San Lorenzo Park. These zones are deeply weathered, but slickensided fresh surfaces appear in the face of the cliff near the shoreline. These faults can be traced by alignment of stream tangents and tilted blocks. Different stages of dissection exist on alternate sides of these faults. The two southern faults in this group, though not directly observed, exhibit all other features described above.

a-7 to 9

These three have large components of throw, and are represented by great southeasterly facing scarps, the bases of which were formerly hidden by swamp deposits and are now further concealed

[7] The presence of this fault was first pointed out to the author on a field trip south of Gatun in August, 1941 by Dr. D. F. MacDonald.

by Gatun Lake. These are fault scarps, rather than cuestas developed by differential erosion of sloping beds, because the strike of bedding is at variance with the azimuths of the scarps, and the beds involved are notably weak and homogeneous in resistance to weathering. The course of a-9 actually transects Juan Gallegos Island as indicated by a deeply weathered valley with the scarp on its northwest side.

a-10

This fault is discernable on aerial photographs by a low break in slope, where it marks the east edge of the broad topographic dome of Barro Colorado. The fault zone has not been seen, but the distribution of formation contacts and bedding dips, indicated by abundant outcrops, proves its existence.

a-11 to-13

These three faults are all marked by a prominent alignment of tangents of successively encountered streams. Locally much greater evidence is apparent in the distribution of formations and topographic development on opposite sides of the faults. Faults a-11 and a-12 have waterfalls where crossed by streams for a couple of miles north and northwest of Gamboa. The traverse of Wuenschel (oral communication Feb. 1949) shows the steepest gravity anomaly gradient across the whole Isthmus where this traverse crosses fault a-13 in a short interval where the dense Basement Complex on the southeast is evidently deeply buried under the lighter Tertiary rocks. Existence of fault a-11 has been doubted because its course parallels an eastward-facing cuesta of a basal sandstone of the Quebrancha formation (Bohio of Woodring and Thompson, 1949, p. 231–232) overlying the Gatuncillo formation. The absence of an analogous scarp at the west side of the Quebrancha basin and the presence of the small depressions traced on the aerial photographs indicate that the fault exists, and that it may form the contact between the Quebrancha and Guatuncillo formations for part of its course.

b-1, 2

No bedrock exposures have been found along the course of either of these faults, and fault b-1 is entirely buried beneath the Atlantic Muck of the lower Chagres Valley. The depressions and ridges formed by such faults as a-6 end abruptly at the Chagres River Valley. The Chagres-Gatun contact is offset greatly by b-1, and an undetected amount by b-2. Topographic maps and aerial photographs show great difference in physiographic texture on opposite sides of both faults (abruptly more youthful north of each) and the sea-shore lines on opposite sides of the faults have had different histories. The northeast side of each has either moved northwest or has been upthrown.

b-3 to 11, and c-1 to 14

This group of fractures crosses the countryside with generally uniform expression. All were first noted and traced out on aerial photographs where they are manifested by remarkably straight and continuous lines of gullies, low scarps and ridges, lines of different types of vegetable growth, and other linear features. No bedrock esposure was found along the course of any of these fractures, so evidence is lacking that all are faults.

Faults b-3 and b-4 have displaced the seacoast so the opposite sides have had different histories. The drainage pattern and topography are very different on opposite sides of the faults, especially south of their intersection with a-3. b-3 has drowned the easternmost Pliocene tributary of the Rio Cano Quebrado.

One fracture of each of the clusters referred to collectively as b-5 and b-6 has likewise displaced the shoreline. Parts of the Rio Cano Quebrado and Rio Pina and their tributaries are consequent along fractures b-3, 4, 5, 6. Faults b-10 have offset the Chorerra Basalt-Caimito contact.

Faults c-7, 8, and 14 have had such recent apparent down-throw on the south side that they have drowned the Pliocene tributaries of the Rio Cano Quebrado. Prominent troughs mark nearly the entire course of faults c-7 and 8.

Faults c-1 have displaced the Caribbean shoreline, helped drown the Rio Cano Quebrado, and produced different textures on opposite sides of each fault near the coast. The drowned portions of the river valleys are filled to near sea-level by black muck and gravel, presumably Pleistocene and Recent.

The remaining fractures of this group may be joints genetically associated with the faults parallel to them.

d-1[8]

This fault forms the western edge of Gatun Lake from Escobal to Gatun Dam. Its associated scarp is very straight for short, discontinuous, but perfectly aligned intervals, such as for 1 mile and from 5.4 to 6.6 miles north of Escobal. The straight intervals have sheer cliffs undissected about 50 to 150 feet above the lake level. The

[8] Examination of R. A. Terry's Tectonic Map of the Panama Region as reproduced by Schuchert (1935, p. 565) indicates this may be one of five faults shown crossing the Gatun Lake area by Terry.

irregular intervals of the cliff have short streams with numerous waterfalls and excessively steep gradients. The waterfalls have not begun to recede noticeably from the lake edge. The back slope of this scarp ranges locally from late youth to late maturity in its stage of dissection. Between the latitudes of Escobal and the south end of Gatun Dam, along the scarp the total and local relief increase fairly uniformly, as they do also between these latitudes progressively from the Caribbean Sea toward the scarp. South of the latitude of Escobal (as far as the basalt flows) and along the Caribbean coast, dissection is late mature to old age (except where rejuvenated by faults intersecting the coast as noted previously). These observations indicate that most of the relief between the Caribbean Coast and the scarp is attributable to its upthrow by uniform uplift or north-westward tilting. This tilting was progressively greater toward the north and was abruptly terminated at fault b-2.

Fault d-1 is obscured by Gatun Lake south of Escobal and is tentatively associated with a fracture south of the lake, observed on photographs to be lined up with it, but exhibiting no evidence of throw.

d-2 to 4

These fractures are manifested by features identical to those of faults a-7, 8, and 9 but are smaller in size. They strike variably normal and subparallel to the latter and are adjudged to be smaller associated faults. The valleys and scarps, trending at variance to the strike of the beds, appear much straighter on photographs than on the published maps.

d-5 to 9, and 12 to 19

Each of these fractures or fracture-zones appears plainly on aerial photographs as a very distinct valley or depression. These troughs are very straight and many are asymmetrical or bordered on one side by a scarp.

These fractures typically are found in areas of sufficiently substantial local relief and rock resistance to weathering that fresh outcrops are more closely spaced than along or adjacent to faults mentioned heretofore. Slickensided breccia-zones and closely spaced slip planes are abundant above lake-shore outcrop and where stream courses are shown by detailed maps to follows the faults d-12, 13, 15, and 18. Outcrops are closely enough spaced to detect offset of intraformational contacts at intersections with faults d-6 to 9, and 12 to 19. Offset of contacts was strongly indicated by textural study, but not demonstrated by outcrops along faults d-17. The remaining fractures of this group may be prominent associated joint zones rather than faults.

Three peculiarities of this group are: failure of the pattern to transect the post-Caimito unconformity; relatively short intervals of appreciable normal throw; the universality of a large strike-slip component whereever indicated by slickensides, even where throw is large.

d-10, 11

These fractures appear identical to faults d-9 on aerial photographs of Basement Complex terrane. But over Tertiary rock their expression is much less apparent. They may be faults of great pre-Tertiary, but little Cenozoic motion.

e-1 to 9

These fractures are identical to fractures c-1, 2, 3 etc. in their degree of persistence and topographic expression on aerial photographs. No bedrock outcrops have been seen along any of these fractures, but most, e-4 to 9, have demonstrably offset formation contacts as shown on Plate 2, and are therefore considered to be faults.

e-10

"This is a group of faults of prominent topographic expression in the asymmetric trough of Quebrada La Chinilla and associated fault-line troughs, and of large formation offset as mapped in the field (Pl. 2). These faults appear by alignment and formation offset to be minor associates of fault a-1.

Distance between outcrops renders offset of formational contacts undetectable except where very large. No slickensiding was found to indicate the net slip direction of most faults. Therefore, that the structures most commonly offset far enough to be detected are those which are nearly vertical is evidence for the great preponderance of strike-slip among all faults, except possibly faults a-1 to 9, b-1 to 4, d-1 to 4.

Continuity of fractures is evident on aerial photographs wherever they are shown continous (Pl. 2), but the topographic manifestation of most of them is broken at hundreds of places such as through muck- or water-embayed low spots, across alluviated stream valleys, in areas of mantle disturbed by mass-wasting. Consequently at most fault intersections it is not possible to determine which fault offsets which, so offset is not indicated.

The Fracture Pattern

General Statement.—Examination of aerial photographs covering a greater area has con-

vinced the writer that the fracture pattern of the Gatun Lake area represents that of the entire central Panamanian Isthmus.

North-south grain of the pre-Tertiary area.—The fractures that produce this grain (Pl. 2), described under "Physical Data," may well be the tension fractures at right angles to the dominant Mesozoic fold axis which trend east-west in the central Isthmian region (Umbgrove, 1947, Pl. 3).

Permanency of the fracture pattern.—The latest movement on some of the faults antedates the pre-Gatun unconformity; but these faults, (d-2, 3, 5 to 19) do not differ in trend from the later ones, nor in general character except that they seem to be much shorter on the whole. This suggests that the over-all deformation pattern has remained the same throughout the region to the present.

Conclusion.—The fracture pattern (Pl. 2) suggests several mechanical interpretations, but the area covered is too small for such a venture. Any interpretation must connect the pattern with the broader regional deformation. As a guide to thinking along this line the main features of the latter are presented in the following paragraphs. Supplementary ideas have been presented by Bucher (1947).

Isthmian Regional Structure: Relations and Inferences

Tectonic Axis.—The Cordillera de San Blas represents a structural axis of pre-Tertiary rock that strikes nearly east-west through the central Panamanian Isthmus. It is now sunk below sea level and buried under Tertiary sedimentary rocks from the longitiude of Chorrera to the southwest side of Mosquito Gulf (Pl. 1) and possibly much farther west. The pre-Tertiary age attributed to the basic volcanic complex on Valiente Peninsula is in accord with evidence presented by Schuchert (1935, p. 562) who says the sedimentary column in Bocas del Toro Province (R. de P.) begins with ". . . an Eocene limestone-volcanic series. . .". During the writer's examination of this peninsula the basic volcanic complex was seen to be overlapped on the west by an undated volcanic tuff in turn overlapped by the (Miocene) Hospital limestone.

The course of the structural axis east of the Columbia-Panama border is concealed by recent sediment of the Rio Atrato lowland. The exposed part of the axis, from the Columbia border to 7 miles east of Colon, is the crest of a variably dissected and faulted, north-facing scarp observed during an aircraft flight from a few miles northwest of Cape Tiburon to a few miles west of San Blas Point. This scarp is close to the north coast, precipitous and very young, obviously the result of recent faulting along its base. The backslope is very gentle, merging gradually with the drowned southern half of eastern Panana.

Between the westernmost occurrence of the Basement Complex terrane in the Gatun Lake area (west end of the exposed tectonic axis) and a longitude possibly as far west as the Valiente Peninsula, the writer suspects a late Cretaceous graben. The presence of such a graben would explain the abrupt termination of the exposed part of the tectonic axis a few miles east of Colon, and the general narrow and low configuration of the Isthmus within this interval. Gravity measurements by Wuenschel (oral communication, Feb., 1949) along the Trans-Isthmian Highway indicate that a zone of moderate positive Bouguer anomalies (+50 to +60 milligals, taking Balboa and Colon as approximate zero datum) exists at all gravity stations located on the Basement Complex terrane outcrop area (Pl. 2). Furthermore the total gravity anomaly gradient in the region covered is steepest at two intervals: the interval across the contact of the Basement Complex where that contact is formed by fault a-13; and the interval from about ½ to 1½ miles northwest of the northernmost contact of the Basement Complex along the highway. The latter gradient is much the longer and both are to be expected at the borders between high and low blocks of Basement Complex terrane.

Volcanic Axis.—The series of volcanoes (many active) that extends from southern Guatemala through western to central Panama marks a Cenozoic axis of volcanism now in its waning stages. The youngest volcanoes along this system vary in age from modern in Guatemala, El Salvador, and Nicaragua to pre-Upper Miocene (El Valle) in central Panama.

The pre-Upper Miocene age determination of El Valle is based on the following facts:

FIGURE 2.—MAJOR CRUSTAL SETTING

1. The Gatun formation, the youngest formation definitely datable (Middle Miocene on paleontologic basis by Keen, Woodring and others), contains syngenetic tuff beds (Table 2, beds, Db, Fb and H).

2. These tuff beds are foreset and bottomset marine delta beds the attitude of which indicates a southerly source.

3. The essentially syngenetic character of these tuffs (though their constituent particles may be reworked in entirely or in part from very slightly earlier ash beds) is based on thin-section examination of numerous samples. All specimens showed the tuffs to be composed predominantly of glass shards completely fresh and unaltered. Even the finest particles visible (× 325) showed the sharp angular outline and the index of refraction of silica glass; no clay or bentonite is present in these beds.

Schuchert (1935, p. 567, 568) interprets the El Valle crater as no older than Pleistocene and probably younger. The writer has examined the San Carlos formation in detail from Chame to Rio Hato, R. de P., and agrees with Hershey (1901, p. 260) that it is pre-Upper Pleistocene (provisionally, Middle Pleistocene). The studies indicate such a high permeability of the San Carlos formation as to suggest that even a greater age might justifiably be assigned the erosion features cited by Hershey on the surface of this formation (San Carlos Plain). Large proportions of runoff go underground instead of eroding the surface. Furthermore El Valle's eruptive period certainly antedates these Middle Pleistocene (?) beds for which its peripheral slopes furnished the sediment. In Schuchert's description, a much greater time interval than that since the Pleistocene is certainly required to breach a crater of interbedded tuffs and rhyolite flows from a rim over 3,000 feet high to the present exit stream level of 1900 feet A. T.

This Cenozoic volcanic axis is about 30 miles south of and parallel to the pre-Tertiary structural axis (Pl. 1). Recent major volcanic activity along this axis appears to be youngest from Mexico to Nicaragua and to increase in age through Costa Rica to Central Panama (Schuchert, 1935, p. 568). East of the longitude of Chorrera this Cenozoic axis apparently lies beneath Panama Bay and its adjoining coastal swamp deposits. The volcanic islands of Toboga, Urava, Otoque and others show that this axis continues beneath Panama Bay (unpublished reports of investigations by the writer in 1942-43). The pre-Tertiary and Cenozoic axes are roughly parallel to the edge of the continental shelf and may therefore be genetically related to it.

Basins and ridges adjoining the southern continental shelf.—Maps (American Geographical Society, 1944, Sheets 1A & 1B, and Int. Maps of the World; Sapper, 1916, 17; U. S. Hydrographic Office Charts, 1176, 5486, & 5487) of the Isthmian and adjacent region show (Fig. 2, Pl. 1) that the southern edge of the continental shelf south of Panama is the northern edge of a topographic and structural province of generally northeast-trending parallel ridges and troughs of very great relief (up to 15,000 feet). The writer has contoured these submarine ridges, troughs, and basins south of the continental shelf on Plate 1 to render them more apparent than they are from casual observation of the abundant soundings on H.O. Chart 1176. The western and southern border of this province, covered by H.O. Chart 5486, extends from the continental slope south of the Peninsula de Osa, Costa Rica, southwestward along the submarine Cocos Ridge, to the west end of the Galapagos Islands, and thence eastward along the submarine Galapagos-Guayaquil Ridge to and beyond Guayaquil, Ecuador. Cocos Ridge separates the province from the Albatross Plateau. The submarine part of this province is separated by the north-south trending submarine Coiba-Malpelo Ridge into a western part, here designated as the Galapagos-Panama Basin, and an eastern Ecuador Basin.

The eastern limit of the subaerial part of this province is some undetermined distance east of the longitude of Medellin, Colombia. The eastward extension of the latitude of the east-west trending continental slope south of Panama, from topographic consideration, forms the northern border of the province at least as far as the Rio Magdalena; for this latitude marks the northward termination of the cordilleras Occidental and Central of the Andes.

The deep along the southwest coast of Central America, the Guatemala Trench (Fig. 2), terminates southeastward and the one along the

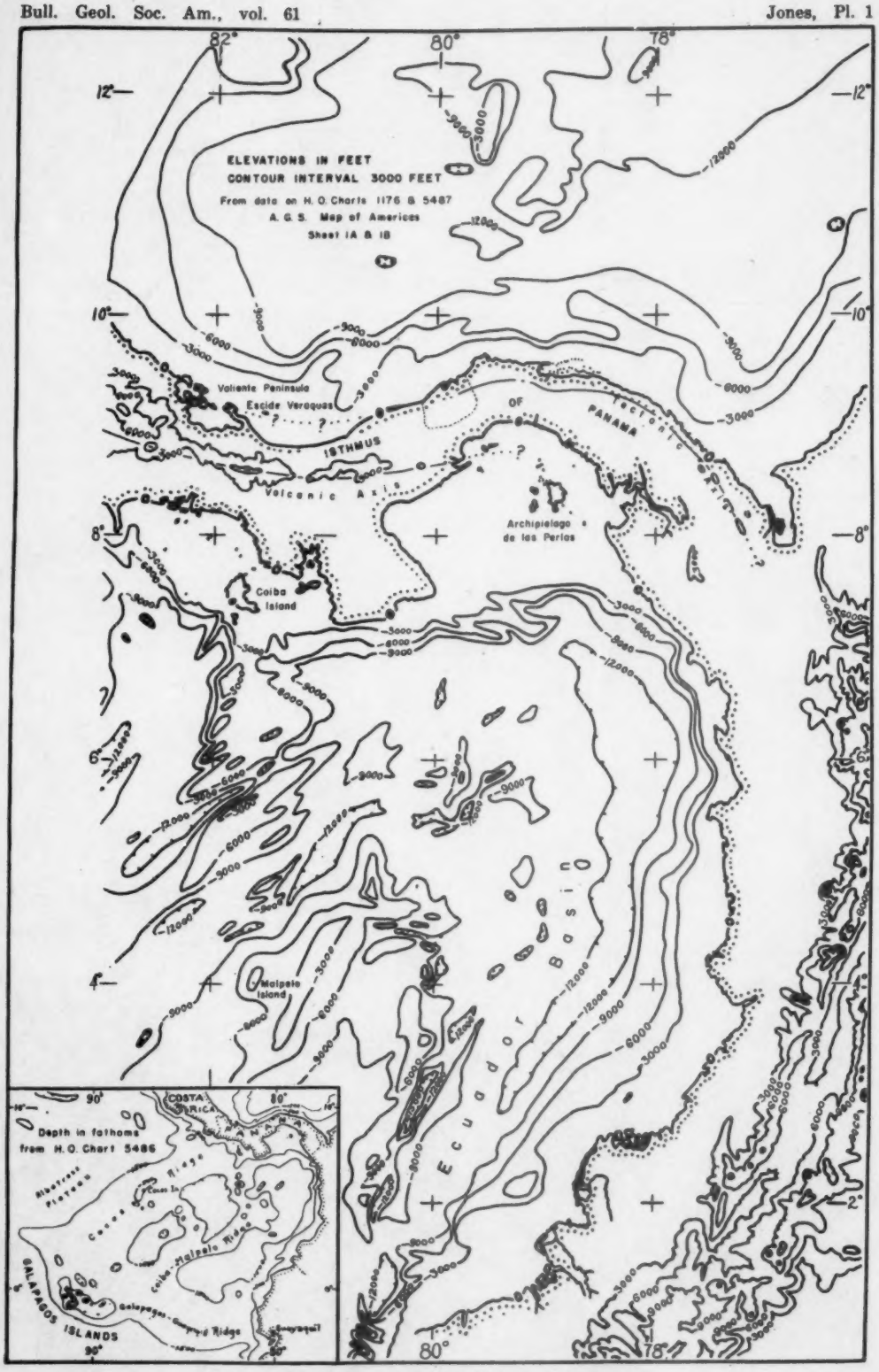

REGIONAL PHYSIOGRAPHY

west coast of South America, the Atacama Trench, terminates northward, both just short of this ridge and trough province.

The physiographic pattern and what is known of the Cenozoic geologic structure (Schuchert, 1935, p. 642, 643) indicate that the province is one of faulting on a large scale with great components of normal throw.

Soundings are too scattered to determine the topographic pattern of the Galapagos-Panama Basin and the Cocos Ridge; but not so the Coiba-Malpelo Ridge and the Ecuador Basin. The latter are long, broad, low features that trend northerly and are interrupted by numerous abrupt, short, narrow, and deep basins alternating with high ridges. Obviously the Coiba-Malpelo Ridge and the Ecuador Basin, whatever their origin, antedate the numerous sharper features that intersect them with a northeast trend. The latter may therefore be ascribed to Cenozoic faulting, the pattern of which resembles basin and range topography, and the province may be one of crustal extension at right angles to the trend of these numerous ridges and troughs (or of compression parallel to them).

Uniform outline of the Isthmus Ridge of Panama.—The present sigmoid outline (Schuchert, 1935, p. 556) of the Panamanian Isthmus is an ephemeral feature caused by embayment of the shelf under the Gulfs of Panama, Chiriqui, and the Mosquitos, the first of these, at least, of very recent origin (Rich, 1942, p. 280). The Isthmus Ridge separating the Caribbean and Ecuador basins is bounded by the edges of the shelves to the north and south. The slopes marking these edges extend from about 3000 to more than 9000 feet deep. It seems likely that the configuration of the subaerial isthmus, at least through Cenozoic time, has been limited only by these shelf edges, both of which trend nearly east-west and are parallel. Newell (personal communication, March, 1949) points out:

"The submerged part of the Isthmus is quite wide compared with the subaerial portion. Slight relative uplift would greatly increase the land area. If axis of uplift were along one or the other margin of the submerged shelf it would be theoretically possible for the Pacific (or Caribbean) to sweep clear across what is now exposed, without necessarily reaching or mingling with the Caribbean (or Pacific) waters. This may not be an important point, but it opens up the possibility that Pacific faunas might be found along the north side of the Isthmus or Caribbean faunas along the south shore".... (without the existence of an interoceanic strait).

Topographic and structural affinities of the western Caribbean and the Ecuador basins.—The slope that forms the edge of the northern shelf is less abrupt and regular than that of the southern shelf. This might mean that the Isthmus Ridge was, or now is, genetically closer to the southwestern edge of the Caribbean Basin than to the Ecuador Basin. However this may be, the symmetry observed in the mutual parallelism of the tectonic and volcanic axes and both north and south shelf edges is obvious; and its trend seems more in accord with Caribbean submarine topography than with that of the Ecuador Basin. If the Isthmus Ridge of Panama is the western end of the southern rim of the Caribbean Basin, we must turn to the borders of the Caribbean Sea, especially the east side with its volcanic arc, for structural comparisons. For the ridge and trough province, on the other hand, we must look to western Columbia and Ecuador, and counterparts in North America, such as the submarine topography off the coast of southern California (Shepard and Emery, 1941) and its counterparts on land.

Correlation with the Fracture Pattern.—The fault pattern of the Gatun Lake Area must be the result of the interplay of the forces that shaped the Isthmus Ridge between the two unlike sea basins. Before a satisfactory interpretation can be achieved, the mapping must be extended far beyond the Gatun Lake Area. Only one comment may be made at this time:

"Broad elongated upwarps exhibit quite generally a rectangular system of longitudinal and transverse tension fractures. In such cases, the major fault zones are apt to swerve from the typical direction over considerable distances" (Bucher, 1949).

In the Gatun Lake Area, north-south and east-west trending faults are conspicuous, and some of them swerve in this customary manner. The conclusion seems justified that they are the inevitable consequence of the uparching of the Panama Isthmus Ridge. The evidence of a

strong horizontal component in the movements along some of the faults does not contradict such an interpretation:

"What movements take place along fractures once they have come into existence depends on the progress of the over-all deformation of the rock body of which they are a part and not at all on the conditions of strain that produced them" (Bucher, 1949).

How the other faults and joints of the region fit into the picture must remain undecided at present.

Physiography

General Character

The Gatun Lake Area is a lowland basin covered with Tertiary and Quaternary sediments (Fig. 1). It opens northwestward into the Caribbean Sea and is flanked by high hills of the pre-Tertiary Basement Complex on the northeast, by the upfaulted Tertiary rocks of the Continental Divide on the southeast, and by the very high El Valle crater and associated late Tertiary and Quaternary rocks of volcanic origin on the southwest.

The physiography of the Gatun Lake Area is the expression of the humid cycle of stream erosion developed to varying degrees on a semi-drowned peneplane which has been rejuvenated locally to variable degrees by uplift. The area can be divided into two major topographic types: mountain and intermontane areas.

Mountain Areas

The mountain areas are generally of late youthful topography dissected in old resistant rocks of the pre-Tertiary Basement Complex. This topography may have been developing for a much longer time than the intermontane topography, but has remained in an early erosional stage because of the greater initial relief. The soil cover is much thicker on the average than in the intermontane areas, because the closer jointing allows deeper weathering. The dense vegetation tenaciously protects this soft mantle from erosion on even the steepest slopes, preserving the rugged surface. Total relief is about 1650 feet with local slopes reaching a maximum of 1300 feet per mile in the north, and averaging under 50 feet per mile in the south.

Intermontane Areas

The intermontane areas are of early youthful to extreme old age topography variably developed on young soft Tertiary rocks and Quaternary sediments. This topography is subdivided into four physiographic subtypes which may be characterized as follows:

(1) *Swamp and lowland areas* of the Chagres, Trinidad, Gatun and other Pliocene (?)[9] river valleys with associated inland and coasalt swamp areas. These are virtually flat areas of aggradation on former land surfaces now below sea level. They are all less than 25 feet above sea level and most are underlain by Quaternary muck and alluvium.

(2) *Interlowland areas* such as that represented by the Gigante-Agua Clara Peninsula, the unrejuvenated portions of an old peneplane standing generally between 100 and 200 feet A.T. (above sea level), with a few monadnocks of harder rock, such as Cerro Gigante (520 feet A.T.) and some outliers of basalt locally rising above 300 feet A.T.

(3) *Dissected highland areas* represented by the land between Gatun Lake and the Caribbean Sea, the Bohio Peninsula, Barro Colorado, and Juan Gallegos Island. In part these are areas of the former peneplane which have been rejuvenated by up-faulting and tilting. Where soft rocks are present, the resulting landforms are narrow valleys, steep hillsides, and rounded hilltops; where hard rocks underlie the surface, they form hogbacks, dike ridges and dome-shaped hills with small, steep-profiled streams. Relief ranges from 5 to 10 feet per mile at the Caribbean shore up to over 700 feet per mile near Gatun Lake and on Barro Colorado Island.

(4) *The hills region* with relief up to 1100 feet per mile in the south-eastern border of the area is the north edge of a province of fault blocks bounded by closely spaced major shear faults with much tilting and vertical displacement of the fault blocks. Many basic dikes and flows in the area transect softer Caimito and Las Cascadas rocks and the present relief is attributed to the resulting differential sculptur-

ing after disruption of the initial structure by complicated faulting. Balboa High southwest of Gamboa is a typical peak in this area.

Geologic History

The oldest rocks in the Gatun Lake Area, the Basement Complex, form a structurally and stratigraphically heterogenous mass. The common features which unite them under the heading "pre-Tertiary" are:

(1) a major unconformity between their collective upper surface and all younger rock systems;

(2) a major diastrophic hiatus between them and all other rock systems, a hiatus of such magnitude that the structure within the Basement Complex appears utterly chaotic, whereas the oldest known overlying series, Upper Eocene, is thought to be structurally decipherable in as much detail as may be desired.

The known history of the Gatun Lake Area, therefore, opens with the existence of a land mass of unknown shape and extent, formed at an unknown date during one or more of the first four eras of geologic time. This land mass had been subjected variably to much diastrophism, plutonism, and sedimentation prior to late Eocene time. During Paleocene or Early Eocene time (Olsson, 1942, p. 231), it was eroded to a relief of several hundreds or thousands of feet. In late Eocene time the area was submerged in part or in entirety. Some of the low areas resulting from Paleocene or Early Eocene erosion are the sites of the sediments now comprising the Upper Eocene Tranquilla-Gatuncillo formation.

How much more extensive the Late Eocene inundation was than its deposits now remaining is not known; but the sedimentaries of the Upper Eocene, just as those of the rest of the Cenozoic Era, have not yet been found outside the intermontane areas.

Between the topmost known Upper Eocene (Tranquilla-Gatuncillo formation) beds and the lowermost observed Oligocene (presumably Bohio formation) beds is an unobserved section which leaves a gap in the early Tertiary record.

The history is resumed in beds of the Bohio formation which indicate that in at least part of Early and probably in part of Late Oligocene time considerable sections of the Gatun Lake area were submerged and were receiving great quantities of basic clastic sands and gravels from a near-by terrestrial source of high relief. Great regional relief must have been produced near the end of Late Eocene or in Early Oligocene time, or both, probably by uplift. Large areas of Late Eocene deposition may then have been stripped by erosion. During this erosion interval slow submergence would have favored formation of a marine deposit like the Bohio formation of very coarse terrestrial sediments such as are usually found on the flanks of mountains.

Early in Late Oligocene time (end of Bohio-Obispo time), much tension and tear faulting occurred and some basaltic dikes and sills were intruded. The activity was greatest in the southeast, increasing in intensity toward the axis of the Continental Divide. The result within the Gatun Lake area was partial emergence of a variably faulted land surface. During the emergence, the land portions were maturely dissected to considerable relief. Then the area slowly sank again. During sinking, explosive vulcanism began, inception of which marked the beginning of Lower Caimito–Las Cascadas time. This vulcanism, centered a short distance southeast of the Gatun Lake Area, was most violent during its earliest (Las Cascadas) phase, and continued intermittently through early Quaternary time. This is evident by rock texture and distribution within the Gatun Lake—El Valle area. Las Cascadas time ends with the cessation of violent vulcanism, and continuation of faulting, of igneous intrusion, and of erosion of emergent areas.

After the outbursts of Las Cascadas time the entire area subsided approximately to sea level and comparative quiet ensued during those parts of the Late Oligocene and Early Miocene ages represented by Middle and Upper Caimito series. Different parts of the area were slightly above and below sea level during different intervals of these two epochs, but the break between the Middle Caimito and Upper Caimito Series is represented by a geographically more extensive local unconformity than any other break within these two series. Upper Caimito sedimentation was more extensive and uniform than that of Middle Caimito, probably because of a continuing slight subsidence and

of the progress of erosion in lowering relief. Upper Caimito sedimentation was ended during Early Miocene time by uplift accompanying much additional faulting, emplacement of many basaltic dikes, plugs, and flows, and by much erosion before, during, and after the igneous activity. Southeast of the southern margin of the Gatun formation no later rock record in the Lake area exists, and here the second greatest unconformity, that between the Gatun formation and the Caimito formation, forms the present erosion surface. Continuing southeastward, this erosion surface splits into the Caimito formation-Chorrera Basalt unconformity and the present erosion surface over the Chorrera basalts.

During the Middle Miocene time the northwest margin of the area was part of a continental submarine shelf receiving sediments eroded from the Caimito-Chorrera land surface and from contemporaneous intermittent vulcanism in the southwest. The numerous local unconformities and variations in texture within the Gatun formation indicate considerable unimportant diastrophism through Gatunian time. Toward the close of this time the ocean receded permanently from much of the land now underlain by the Gatun formation, but fluctuated back and forth over the extreme northwest margin (site of Toro limestone) during Toroan time, reworking and depositing a thick beach sand. Later, in Chargres sandstone time, the land subsided very gradually and smoothly an unknown amount.

Following Chagres time the entire Isthmus was elevated during Pliocene (?)[9] time to more than 300 feet above its present level with respect to the ocean. During this time the major drainage lines of today were established. Such rivers as the Chagres, Gatun, Trinidad, Cano Quebrado, Salud, Pina, and Lagarto carved in some places very wide valleys, all to depths below sea level at their mouths and to very low gradients. Because of continuing fault movements, uplift was uneven and some short courses of the valleys cut during these Pliocene (?) times are very narrow and deep instead of broad.

[9] Pliocene (?) because the valleys are cut in the Chagres formation and are filled with Atlantic muck.

During Pleistocene and early Recent time, the Isthmus subsided gradually and uniformly to about 25 or 30 feet below its present level with respect to the ocean; and the major Pliocene (?) valleys were drowned and gradually filled with sediments. The drowning and alluviation was accentuated locally by Quaternary faulting, such as that which now locally blocks the valley of the Cano Quebrado southeast of Lagarto.

In late Recent time continuing to the present, the area has emerged to the total extent of about 25 feet with respect to sea level. This emergence has been scarcely enough to do more to the topography than convert large areas of marine, brackish, and fluvial lagoons to mangrove swamps.

Appendix 1—Description of Beds in Excavation for Third Locks at Gatun

Bed A4 Silty Sandstone: Massively bedded; local .1-foot thick conglomeratic lenses contain .05 to .1-foot diameter round pebbles of lava and other materials of basic igneous origin; some fossil molds present; non-calcareous; some excellent carbonaceous leaf impressions (elm); grades laterally into beds A3 and A2.

Bed A3 Siltstone: Composed predominantly of clay and silt particles with fragments of rock material similar to the grains in A4.

Bed A2 Argillaceous Siltstone: Ranges from siltstone at the top to claystone at the base; non-calcareous; few fossils well preserved, and plant remains.

Bed A1 Sandstone: Lens of sandstone having identical outward appearance of Bed B with the fossils missing; resulted from submarine erosion of the southern upthrown block of a pre-A2 intraformational fault now obscured by compaction.

Bed B Calcareous Argillaceous Sandstone: Massively bedded; calcareous shells, foraminifera, and carbonized wood fragments abundant, especially calcareous shells in zones usually concordant with the bedding; irregular pockets of masses of shells, whole and broken. Lack of orientation of fossil fragments with respect to bedding suggests disturbed conditions of sedimentation. The basal 10–12 feet of this bed are increasingly comglomeratic and fossiliferous downward; the base contains .2-foot sub-rounded basalt pebbles, and thick-shelled fossils characteristic of near-shore faunas.

Bed C Tuff-sandstone: Even-grained, coarse-grained, angular-grained, cross-bedded; blue-gray

to lavender when unweathered; commonly weathered to yellow-green or buff; constitution is chiefly of reworked basic volcanic rock grains, angular quartz, pyraboles, pumice, and other tuffaceous material; fossils sparsely present only as empty molds; top 1 to 2 feet is conglomeratic, (C_{oo}), decreasingly so downward. Local thin conglomeratic lenses of a few feet lateral extent occur throughout. All conglomeratic pebbles in Bed C are identical to those in the base of Bed B, although the matrices of the pebbles in these two divisions are separated by a sharp contact which is an angular unconformity. This continuity of pebbles through the unconformity suggests that the basal conglomerate of Bed B is reworked from the top of Bed C.

Bed Cg-Du Tuff-sandstone and tuff-siltstone: Grades to fine grained downward with increase in quantity of .025-foot pumice inclusions; and disappearance of lavender rock grains with consequent color change to light buff; non-calcareous; fossil molds sparse.

Bed Db Tuff-siltstone: Angular grained, and even grained except for .025-foot abundant pumice fragments; composed chiefly of volcanic glass shards with a few angular quartz grains, clay grains, and indeterminable opaque grains; few scattered lumps of pumice, up to .2-foot in diameter are present; Db is the Ash #1 of Third Locks investigations.

Beds Eu and Eb Sandstone: Massively bedded; conglomeratic top portion, Bed Eu, about 4 feet thick, grades sharply into lower portion, Bed Eb; bed Eu is coarse-grained, even-grained, grains average .6-mm. in diameter. Bed Eb poorly sorted in grain size, ranging from silt size to .5-mm. in diameter; a few scattered rounded basalt pebbles present throughout; ashy and slightly marly; lignitized wood chips, fossil molds and calcareous, poorly preserved fossils all common.

Bed F Tuff-sandstone and Tuff-siltstone: This sequence of reworked volcanic material is coarse at the top (Fu), and grows finer-grained downward, with minor fluctuations from coarse to fine and back to coarse-grained throughout; pumice is prominent. Bed F is identical in physical properties and composition to the sequence C_{oo} to Db described in the preceding pages. In the sequence C_{oo} to Db, Fu corresponds to C_{oo} and C; Fm corresponds to Cg-Du; Fb corresponds to Db. Fb is the Ash #2 of Third Locks investigations. Fb differs from Db in that Db consists of a single massive bed, whereas Fb consists of alternating beds .5-3 feet thick, of fine-grained tuff with included pumice pebbles and cobbles and coarse-grained pumice rock with tuffaceous matrix. The fine-grained beds become more prominent downward.

Bed G Sandstone: Bedding massive; uneven-grained, fine to medium-grained; lignitized wood, calcified vegetable fibers, and calcareous shell fragments common, but abundant echinoids are the distinguishing fossil; perfectly preserved shark teeth frequently found. Quartz and calcite grains, opaque rock grains, altered ferromagnesian minerals and glass are all sparingly present. The bed is slightly marly and ashy and of uniform texture to within about 10 feet of the base where the marl gradually disappears, ash increases in quantity, and the grains approach the clay size of Bed H below, into which Bed G grades. This gradation zone between G and H is distinguished by its content of scattered pumice cobbles averaging .4-foot in diameter.

Bed H Tuff-claystone: No organic remains are present; grain size is so fine (about clay size) that constitution is not determinable megascopically; bed H is Ash #3 of Third Locks investigations.

Bed I Sandstone: Bedding massive; medium- to fine-grained; silty and marly; calcareous shell fragments are abundant but in a chalky, poorly preserved condition. Orientation of fossils is lacking. Shark teeth are found perfectly preserved. The texture of this bed is uniform.

Bed J Sandstone: Bedding massive; tuffaceous; limy with calcareous fossils abundant; medium fine-grained. (Seen in drill cores but not exposed by excavation.)

Appendix 2—Physical Data

General Statement

Previous attempts at mapping this area were subject to greater limitations than the present work; even though earlier maps were accomplished on a much smaller scale, considerable differences exist between them and the present map. Portions of it may be further refined as more detailed work is completed in the future. Some of the physical features and other pertinent data that form the basis of the inferred contacts (Pl. 2) are set forth as a guide to future workers in making these refinements.

Formations and Contacts

Basement Complex Terrane and its Bounding Unconformity.—The unconformity that marks the contact between the Basement Complex and the Tertiary formations is the most striking feature of the physiography east of Gatun Lake between the Caribbean Sea and the Chagres Arm of Gatun Lake. It is marked by a line of division between high mountainous country and country of low or broken hills. This line was traced out on topographic maps and aerial photographs and was

of the progress of erosion in lowering relief. Upper Caimito sedimentation was ended during Early Miocene time by uplift accompanying much additional faulting, emplacement of many basaltic dikes, plugs, and flows, and by much erosion before, during, and after the igneous activity. Southeast of the southern margin of the Gatun formation no later rock record in the Lake area exists, and here the second greatest unconformity, that between the Gatun formation and the Caimito formation, forms the present erosion surface. Continuing southeastward, this erosion surface splits into the Caimito formation-Chorrera Basalt unconformity and the present erosion surface over the Chorrera basalts.

During the Middle Miocene time the northwest margin of the area was part of a continental submarine shelf receiving sediments eroded from the Caimito-Chorrera land surface and from contemporaneous intermittent vulcanism in the southwest. The numerous local unconformities and variations in texture within the Gatun formation indicate considerable unimportant diastrophism through Gatunian time. Toward the close of this time the ocean receded permanently from much of the land now underlain by the Gatun formation, but fluctuated back and forth over the extreme northwest margin (site of Toro limestone) during Toroan time, reworking and depositing a thick beach sand. Later, in Chargres sandstone time, the land subsided very gradually and smoothly an unknown amount.

Following Chagres time the entire Isthmus was elevated during Pliocene (?)[9] time to more than 300 feet above its present level with respect to the ocean. During this time the major drainage lines of today were established. Such rivers as the Chagres, Gatun, Trinidad, Cano Quebrado, Salud, Pina, and Lagarto carved in some places very wide valleys, all to depths below sea level at their mouths and to very low gradients. Because of continuing fault movements, uplift was uneven and some short courses of the valleys cut during these Pliocene (?) times are very narrow and deep instead of broad.

During Pleistocene and early Recent time, the Isthmus subsided gradually and uniformly to about 25 or 30 feet below its present level with respect to the ocean; and the major Pliocene (?) valleys were drowned and gradually filled with sediments. The drowning and alluviation was accentuated locally by Quaternary faulting, such as that which now locally blocks the valley of the Cano Quebrado southeast of Lagarto.

In late Recent time continuing to the present, the area has emerged to the total extent of about 25 feet with respect to sea level. This emergence has been scarcely enough to do more to the topography than convert large areas of marine, brackish, and fluvial lagoons to mangrove swamps.

Appendix 1—Description of Beds in Excavation for Third Locks at Gatun

Bed A4 Silty Sandstone: Massively bedded; local .1-foot thick conglomeratic lenses contain .05 to .1-foot diameter round pebbles of lava and other materials of basic igneous origin; some fossil molds present; non-calcareous; some excellent carbonaceous leaf impressions (elm); grades laterally into beds A3 and A2.

Bed A3 Siltstone: Composed predominantly of clay and silt particles with fragments of rock material similar to the grains in A4.

Bed A2 Argillaceous Siltstone: Ranges from siltstone at the top to claystone at the base; non-calcareous; few fossils well preserved, and plant remains.

Bed A1 Sandstone: Lens of sandstone having identical outward appearance of Bed B with the fossils missing; resulted from submarine erosion of the southern upthrown block of a pre-A2 intraformational fault now obscured by compaction.

Bed B Calcareous Argillaceous Sandstone: Massively bedded; calcareous shells, foraminifera, and carbonized wood fragments abundant, especially calcareous shells in zones usually concordant with the bedding; irregular pockets of masses of shells, whole and broken. Lack of orientation of fossil fragments with respect to bedding suggests disturbed conditions of sedimentation. The basal 10–12 feet of this bed are increasingly conglomeratic and fossiliferous downward; the base contains .2-foot sub-rounded basalt pebbles, and thick-shelled fossils characteristic of near-shore faunas.

Bed C Tuff-sandstone: Even-grained, coarse-grained, angular-grained, cross-bedded; blue-gray

[9] Pliocene (?) because the valleys are cut in the Chagres formation and are filled with Atlantic muck.

to lavender when unweathered; commonly weathered to yellow-green or buff; constitution is chiefly of reworked basic volcanic rock grains, angular quartz, pyraboles, pumice, and other tuffaceous material; fossils sparsely present only as empty molds; top 1 to 2 feet is conglomeratic, (C_{co}), decreasingly so downward. Local thin conglomeratic lenses of a few feet lateral extent occur throughout. All conglomeratic pebbles in Bed C are identical to those in the base of Bed B, although the matrices of the pebbles in these two divisions are separated by a sharp contact which is an angular unconformity. This continuity of pebbles through the unconformity suggests that the basal conglomerate of Bed B is reworked from the top of Bed C.

Bed Cg-Du Tuff-sandstone and tuff-siltstone: Grades to fine grained downward with increase in quantity of .025-foot pumice inclusions; and disappearance of lavender rock grains with consequent color change to light buff; non-calcareous; fossil molds sparse.

Bed Db Tuff-siltstone: Angular grained, and even grained except for .025-foot abundant pumice fragments; composed chiefly of volcanic glass shards with a few angular quartz grains, clay grains, and indeterminable opaque grains; few scattered lumps of pumice, up to .2-foot in diameter are present; Db is the Ash #1 of Third Locks investigations.

Beds Eu and Eb Sandstone: Massively bedded; conglomeratic top portion, Bed Eu, about 4 feet thick, grades sharply into lower portion, Bed Eb; bed Eu is coarse-grained, even-grained, grains average .6-mm. in diameter. Bed Eb poorly sorted in grain size, ranging from silt size to .5-mm. in diameter; a few scattered rounded basalt pebbles present throughout; ashy and slightly marly; lignitized wood chips, fossil molds and calcareous, poorly preserved fossils all common.

Bed F Tuff-sandstone and Tuff-siltstone: This sequence of reworked volcanic material is coarse at the top (Fu), and grows finer-grained downward, with minor fluctuations from coarse to fine and back to coarse-grained throughout; pumice is prominent. Bed F is identical in physical properties and composition to the sequence C_{co} to Db described in the preceding pages. In the sequence C_{co} to Db, Fu corresponds to C_{co} and C; Fm corresponds to Cg-Du; Fb corresponds to Db. Fb is the Ash #2 of Third Locks investigations. Fb differs from Db in that Db consists of a single massive bed, whereas Fb consists of alternating beds .5-3 feet thick, of fine-grained tuff with included pumice pebbles and cobbles and coarse-grained pumice rock with tuffaceous matrix. The fine-grained beds become more prominent downward.

Bed G Sandstone: Bedding massive; uneven-grained, fine to medium-grained; lignitized wood, calcified vegetable fibers, and calcareous shell fragments common, but abundant echinoids are the distinguishing fossil; perfectly preserved shark teeth frequently found. Quartz and calcite grains, opaque rock grains, altered ferromagnesian minerals and glass are all sparingly present. The bed is slightly marly and ashy and of uniform texture to within about 10 feet of the base where the marl gradually disappears, ash increases in quantity, and the grains approach the clay size of Bed H below, into which Bed G grades. This gradation zone between G and H is distinguished by its content of scattered pumice cobbles averaging .4-foot in diameter.

Bed H Tuff-claystone: No organic remains are present; grain size is so fine (about clay size) that constitution is not determinable megascopically; bed H is Ash #3 of Third Locks investigations.

Bed I Sandstone: Bedding massive; medium- to fine-grained; silty and marly; calcareous shell fragments are abundant but in a chalky, poorly preserved condition. Orientation of fossils is lacking. Shark teeth are found perfectly preserved. The texture of this bed is uniform.

Bed J Sandstone: Bedding massive; tuffaceous; limy with calcareous fossils abundant; medium fine-grained. (Seen in drill cores but not exposed by excavation.)

Appendix 2—Physical Data

General Statement

Previous attempts at mapping this area were subject to greater limitations than the present work; even though earlier maps were accomplished on a much smaller scale, considerable differences exist between them and the present map. Portions of it may be further refined as more detailed work is completed in the future. Some of the physical features and other pertinent data that form the basis of the inferred contacts (Pl. 2) are set forth as a guide to future workers in making these refinements.

Formations and Contacts

Basement Complex Terrane and its Bounding Unconformity.—The unconformity that marks the contact between the Basement Complex and the Tertiary formations is the most striking feature of the physiography east of Gatun Lake between the Caribbean Sea and the Chagres Arm of Gatun Lake. It is marked by a line of division between high mountainous country and country of low or broken hills. This line was traced out on topographic maps and aerial photographs and was

found to enclose two areas of Basement Complex terrane: the small spur extending southeast of the Gatuncillo Valley from the east edge of the map and the huge lobate area extending southward from the northeast corner. Both areas are referred to as "mountain areas" and are seen on smaller scale maps to form the western limit of the Sierra de San Blas (Sierra de Chepo) on the east where they coalesce.

Numerous short traverses have been made across portions of the Basement Complex, upon which the description is based, and by which its extent was confirmed.

The distribution of the Basement Complex as shown is based in part on the theory that the Isthmus has been undergoing erosion since early Pliocene time and that the thickest, densest, most weather-resisting rock mass on the Isthmus is the Basement Complex. This theory is partially substantiated by gravity measurments made in January, 1949, on the Isthmus of Panama by Mr. Paul Wuenschel (Oral communication, Feb., 1949) who found the highest positive Bouguer anomalies at all gravity stations located on the area mapped as Basement Complex by the writer. Mr. Wuenschel's findings of much smaller anomalies near the canal and increasing negative anomalies toward Chorrera on the southeast of it support the contention that these areas are underlain predominantly by the lighter Tertiary rocks and that the so-called "basement complex" volcanics between Gamboa and Culebra Cut are part of the lighter Tertiary series. This evidence indicates that the Tertiary cover over the pre-Tertiary Basement Complex is thicker toward Chorrera. The isogals strike E-W, paralleling the volcanic and tectonic axes in their regional trend.

On aerial photographs the smallest physiographic features are seen whereas the best maps available show only the larger fluctuations of the ground. The writer's study of these photographs revealed a previously unsuspected north-south grain to the pre-Tertiary terrane. The grain is produced by nearly parallel arrangement in north-south direction of many thousands of minute ground features such as:

(a) Short, straight tangents along water courses of all size, especially the smaller ones.

(b) Short, straight discontinuous ridges and scarps of very small relief (many are falls where crossed by streams).

(c) Long, straight (some several miles) continuous and discontinuous very shallow and narrow depressions which line up on opposite sides or cross over large and small divides.

The writer attributes the north-south grain to a pre-Tertiary fracture direction which exerted control on the direction of subsequent minor readjustments to Tertiary and Cenozoic stresses. The Basement Complex differs from later formations in being thus closely fractured.

Contact Between Upper Eocene Rocks and Caimito Formation.—The rocks mapped as Caimito formation include the same lithological groups as are found in at least parts of the following Oligocene and Lower Miocene units distinguished elsewhere. The Las Cascadas, Culebra, "Emperador", Cucaracha, La Boca, "Panama" (at Diablo Heights), "Alahuela" and "Quebrancha" formations. The Caimito rocks also resemble in part some of the beds mapped as Gatuncillo formation. The only basis for distinguishing the Caimitoan formation from the older Eocene beds has been the fossils (Table 4). Fossil localities are so sparsely scattered in areas underlain by the Caimito formation that no serious attempt could be made to draw contacts between it and the Eocene beds. Therefore the same symbol is adopted on Plate 2 for Caimitoan and Eocene beds. Letter symbols indicate Eocene formations in the vicinity of Eocene fossil localities. The nature and course of the contact between the Eocene and the Caimitoan formations can be determined only approximately by additional careful stratigraphic and paleontologic studies where these formations are found outcropping in adjacent areas. It is likely that additional Eocene faunas will be found locally along the periphery of the Basement Complex terrane in areas mapped (Pl. 2) as Caimito.

Evolution of the Name "Caimito Formation".—MacDonald (1913, p. 709) described the Caimito formation as lying stratigraphically between the Emperador and Panama formations. In subsequent studies he realized that the "Emperador" represented a discontinuous series of limestone beds present locally through much of the Culebra and Cucaracha formations. Supposed localities of Caimito formation rocks (e.g. the sandstone quarry at Summit, C. Z.) later were found to be underlain by various Culebra and Cucaracha facies in the Continental Divide area. Areas mapped as Caimito formation by MacDonald (1915, Pl. IV) in the Gatun Lake area were extended by the writer to whom it soon became apparent that here too the Caimito formation was a series of rocks including the ranges of the Culebra-Cucaracha and possibly the La Boca series. In lieu of a valid basis of differentiating the Caimito formation in the low and deeply weathered Lake area, MacDonald's term was retained. This usage of the Caimito formation is justified by Olsson (1942, p. 233) who, speaking of the Canal Zone Tertiary section says:

"... Culebra beds, Emperador limestone and the Cucaracha formation are not recognizable units elsewhere in Panama; although doubtless represented by beds of equivalent age".

The writer would include the Gatun Lake area of the Canal Zone with the rest of Panama in the above statement because the fine Canal Zone Tertiary Section referred to by Olsson was described in the limited interval of the deep cuts in the Continental Divide area of the Canal Zone.

Contacts Above and Below the Bohio Formation.—The base of the Bohio formation is exposed, to the writer's knowledge, at only one place 3 miles N. 55°W. of Gamboa where it appears conformably to overlie tuffs typical of the Caimito series. A huge block of limestone float 10 feet high contained the only identifiable fossils in this patch. Field examination indicated the presence of *cf. Lep. canellei*. The block of limestone is well-preserved and rests on a flat slope so is assumed to be near its place of origin, necessarily beneath the Bohio conglomerate to the south. The nature of the contact is not conclusively determinable even here because of extensive weathering, so the possibility of a fault contact must be considered.

The upper contact of the Bohio conglomerate is not directly observable in bedrock exposure at any place yet seen by the writer. There are many places where this contact can be pointed out within a short interval. Many of the contacts between the Bohio formation and adjacent ones are suspected of being faults (Pl. 2).

Since the top of the Bohio formation is an irregular unconformity, there are many thin small patches of overlying Caimito (and Las Cascadas) present in areas mapped as Bohio formation and likewise small patches of Bohio conglomerate are occasionally seen protruding through where Caimito is indicated by the map. But the important areas of outcrop of the Bohio formation are those indicated on Plate 2.

The portions of the contact beneath the water of the lake were drawn on the map by "calculated guess" guided by the known distribution and attitude of the formation ashore.

Evolution of the Name "Bohio Formation."—The "Bohio formation", as originally proposed by Hill (1898, p. 183), who spelled it "Bujio", and later described by MacDonald (1915, p. 20), comprises essentially the rocks exposed in quarries at the former town of Bohio Soldado and in French excavations between Orchid and DeLesseps islands north of Barro Colorado Island and in other exposures now submerged in Gatun Lake. The rocks at the type localities not now submerged are essentially basaltic sandstones and sandstone-conglomerates of the series which are mapped herein as the Bohio formation.

Subsequent to Hill's work, MacDonald described beds containing Oligocene foraminifera and plants which he considered to be in the upper part of Hill's Bohio formation. These beds are included in the Caimito formation because there is a major unconformity at the top of the Bohio formation of Hill; that is, between the fossiliferous zone described and included in the Bohio formation by MacDonald and the Bohio formation as originally described by Hill.

Foraminifera collected by the writer from gritty basaltic sandstone interbeds of the Bohio sandstone-conglomerate 300 yards south of Rio Frijol were identified by Stewart as *Lepidocyclina canellei* Lemoine and Douville, which places this part of the Bohio formation as "late Lower or early Middle Oligocene" (Stewart, 1947a). It also eliminates the validity of *L. canellei* zones as a means of distinguishing the Caimito and Bohio formations. Indeed this discovery presents the possibility that beds mapped on a lithologic basis as Caimito formation, some containing locally *L. canellei* and other foraminifera heretofore believed characteristic of this formation, stratigraphically underlie the Bohio formation. If so the Bohio formation would be relegated to the status of a member or facies variant of the "Greater Caimito formation". At least this find presents the unusual situation of an angular unconformity of considerable topographic relief cutting across the range of a fossil as short-lived as *Lepidocyclina canellei*.

Unconformity and erosion surface over the Caimito Formation.—At different places the top of the Caimito formation is represented by an erosion surface forming the present land, an unconformity beneath basic lava flows, and an unconformity beneath the Gatun formation. North of New Providence the basal Gatun (Sabanitas formation) conglomerate rests directly on the Basement Complex terrane, hence the Caimito is believed to wedge out northward either because of erosional stripping or lack of original deposition or some of both. This doubtful region north of New Providence where the Caimito disappears is left blank on Plate 2 because the land is so low, densely jungled, and swampy, that no surface investigation was possible, and distinctive physiographic texture was not visible on maps or photographs. In the neighborhood of this blank area the supra-Caimito unconformity merges with that limiting the Basement Complex terrane.

The areas indicated as Caimito formation on the map are those believed to be underlain by rocks fitting the Caimito descriptions. Within these areas

abundant fresh and recognizable weathered Caimitoid rocks are very abundant in outcrop only on the northeastern half of Plate 2. In these portions, the field evidence is plentiful that Caimitoid rocks underly the mantle, and they are so mapped except where Eocene faunas have been found (Table 4).

In the remaining land areas indicated as Caimito on the southwestern half of Plate 2, the mapping was by examination of weathered mantle, highly weathered rock, and general topographic aspect. Extremely rare bedrock exposures are available of sufficient freshness to assure one that Caimitoid rocks are at least locally underlying. Fossils, if found in these low, deeply weathered areas would be unidentifiable clay casts. No trace of limy material remains. Steep slopes are absent and this area is an old erosion surface with one monadnock, Cerro Gigante (basalt neck), rising above the plain. A low broken line of southeastward facing scarps (Gatun fm) bounds the plain on the N.W. where the Caimito-Gatun unconformity begins. Another irregular line of northward facing scarps (Chorrera basalt flows) bounds it on the south where the Caimito-Chorrera basalt unconformity begins. Both sets of scarps are so low and have such flat slopes as not to be evident in the field except when seen in profile.

Contact between Gatun and Sabanitas formations.—This contact is gradational. A definite difference in fineness of texture of topography is plainly noted on aerial photographs on the opposite sides of the contact zone. This pattern is noticeably coarser and deeper where developed on the Gatun formation. This is attributed to the much more impermeable character of the fine-grained Gatun mudstones and tuffs and the overlying mantle clays. Nearly all the precipitation doubtless forms runoff which washes very deep gullies in the thick mantle over the quickly weathered Gatun bedrock. The Sabanitas tuff-conglomerate is more resistant to weathering, is permeable and is overlain by a highly permeable thin mantle of Ash and Basalt-Gravel. Hence much of the precipitation on it goes underground and the streams are shallower and closer together. The contact (Pl. 2) was located on aerial photographs as the approximate center of the zone separating these two topographic textures.

Contact between Sabanitas formation and Basement Complex.—This contact is part of that described earlier. If the writer's conception of the Sabanitas formation is correct, then its southern termination at Neuvo Limon is explained. South of this vicinity the Gatun formation overlaps the Caimito formation which would not provide hard material for pebbles as would the Basement Complex to the north.

Contact between Gatun formation and Toro Limestone.—This contact is described by Thompson (1943, p. 22) as a disconformity. All bedrock exposures of it seen by the writer confirm Thompson's opinion. The manner of mapping this contact is included in the following section.

TABLE 4—INDEX TO FOSSIL LOCALITIES ON PLATE 2[10]

Loc. No.	Formation or Age	Loc. No.	Formation or Age
1	Chagres Fm.	13	Caimito Fm.
2	Toro Ls.	14	" "
3	" "	15	" "
4	Gatun Fm.	16	" "
5	" "		Topotype locality for *Lepid. vaughani*
6	" "	17	Caimito Fm.
7	" "	18	" "
8	" "	19	" "
9	Caimito Fm.	20	" "
10	" "	21	" "
11	" "	22	" "
12	" "	23	Gatuncillo-Tranquilla Fm.
	Topotype locality for *Lepid. pancanalis*		

Contact between Toro Limestone and Chagres Formation.—This is a gradational and intertonguing contact. Owing to the excessively dense nature of the jungle and lack of continuous trails between the west side of Gatun Lake and the Caribbean Sea the field work in this area was confined to within a couple of hundred yards of existing roads. The contacts above and below the Toro limestone between the roads were interpolated by stereoscopic aerial photograph study, helped out by the knowledge of the regional structure west of the lake. Wherever measurable dips are found here, they are very gentle, fairly gradual and uniform in variation, and generally seaward. It should be emphasized that these contacts are located by no field check points west of the longitude of the mouth of the Chagres River. Field traverses along all roads west of this longitude however, do confirm most of the indicated extent of the Chagres formation. Field confirmation of these contacts in this western area would be an additional undertaking of several man-months' duration. The indicated thinning of the Toro formation in outcrop to the southwest is substantiated by two section measurements, the first already described, the second 4.6 miles N.35°W. of the small peninsula at Escoval. The features on the aerial

[10] Some identifications by W. P. Woodring (Jones, 1947a).

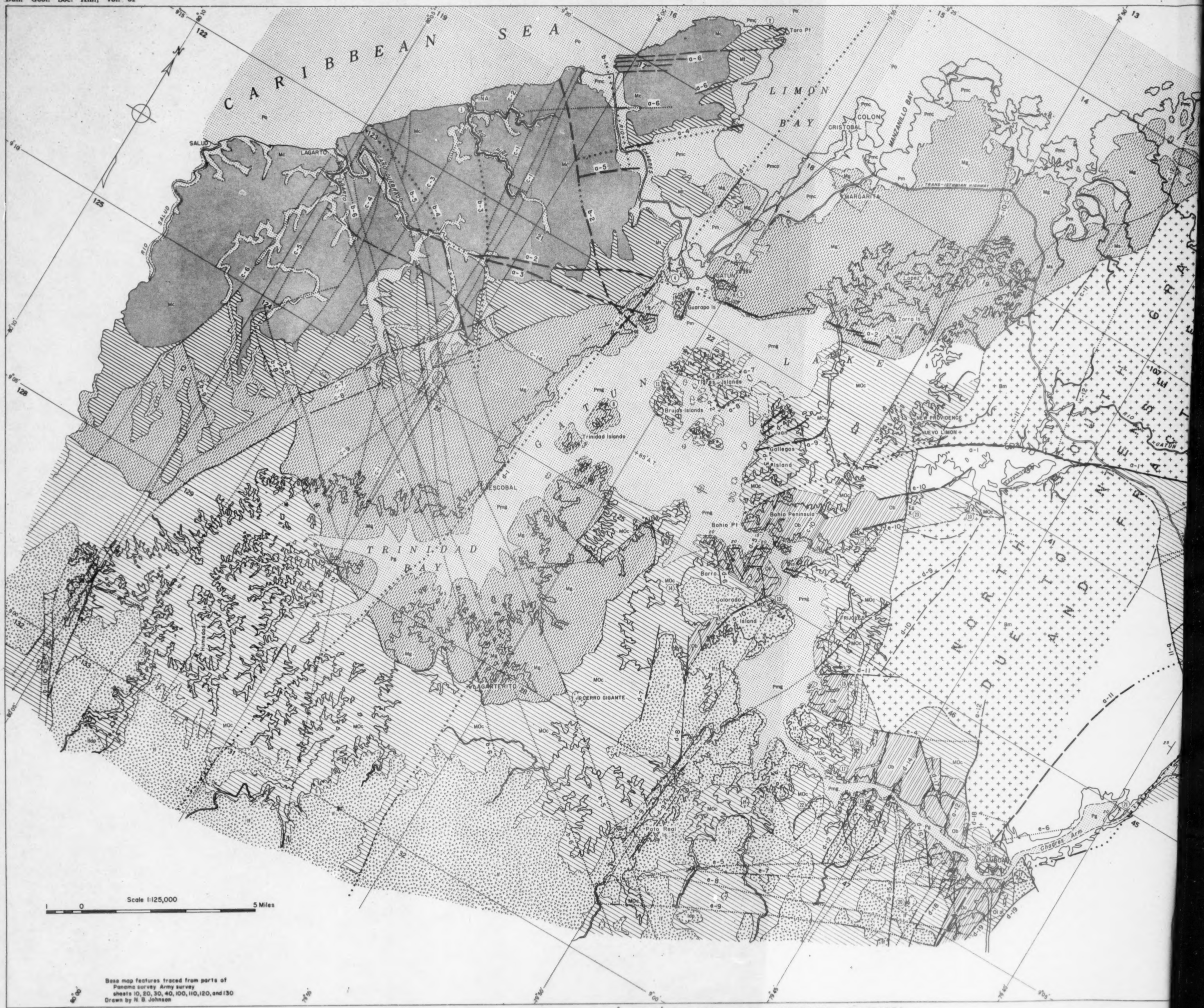

AREAL GEOLOGIC MAP, GATÚN LAKE AND VICINITY, PANAMA

abundant fresh and recognizable weathered Caimitoid rocks are very abundant in outcrop only on the northeastern half of Plate 2. In these portions, the field evidence is plentiful that Caimitoid rocks underly the mantle, and they are so mapped except where Eocene faunas have been found (Table 4).

In the remaining land areas indicated as Caimito on the southwestern half of Plate 2, the mapping was by examination of weathered mantle, highly weathered rock, and general topographic aspect. Extremely rare bedrock exposures are available of sufficient freshness to assure one that Caimitoid rocks are at least locally underlying. Fossils, if found in these low, deeply weathered areas would be unidentifiable clay casts. No trace of limy material remains. Steep slopes are absent and this area is an old erosion surface with one monadnock, Cerro Gigante (basalt neck), rising above the plain. A low broken line of southeastward facing scarps (Gatun fm) bounds the plain on the N.W. where the Caimito-Gatun unconformity begins. Another irregular line of northward facing scarps (Chorrera basalt flows) bounds it on the south where the Caimito-Chorrera basalt unconformity begins. Both sets of scarps are so low and have such flat slopes as not to be evident in the field except when seen in profile.

Contact between Gatun and Sabanitas formations.—This contact is gradational. A definite difference in fineness of texture of topography is plainly noted on aerial photographs on the opposite sides of the contact zone. This pattern is noticeably coarser and deeper where developed on the Gatun formation. This is attributed to the much more impermeable character of the fine-grained Gatun mudstones and tuffs and the overlying mantle clays. Nearly all the precipitation doubtless forms runoff which washes very deep gullies in the thick mantle over the quickly weathered Gatun bedrock. The Sabanitas tuff-conglomerate is more resistant to weathering, is permeable and is overlain by a highly permeable thin mantle of Ash and Basalt-Gravel. Hence much of the precipitation on it goes underground and the streams are shallower and closer together. The contact (Pl. 2) was located on aerial photographs as the approximate center of the zone separating these two topographic textures.

Contact between Sabanitas formation and Basement Complex.—This contact is part of that described earlier. If the writer's conception of the Sabanitas formation is correct, then its southern termination at Neuvo Limon is explained. South of this vicinity the Gatun formation overlaps the Caimito formation which would not provide hard material for pebbles as would the Basement Complex to the north.

Contact between Gatun formation and Toro Limestone.—This contact is described by Thompson (1943, p. 22) as a disconformity. All bedrock exposures of it seen by the writer confirm Thompson's opinion. The manner of mapping this contact is included in the following section.

TABLE 4—INDEX TO FOSSIL LOCALITIES ON PLATE 2[10]

Loc. No.	Formation or Age	Loc. No.	Formation or Age
1	Chagres Fm.	13	Caimito Fm.
2	Toro Ls.	14	" "
3	" "	15	" "
4	Gatun Fm.	16	" "
5	" "		Topotype locality for *Lepid. vaughani*
6	" "	17	Caimito Fm.
7	" "	18	" "
8	" "	19	" "
9	Caimito Fm.	20	" "
10	" "	21	" "
11	" "	22	" "
12	" "	23	Gatuncillo-Tranquilla Fm.
	Topotype locality for *Lepid. pancanalis*		

Contact between Toro Limestone and Chagres Formation.—This is a gradational and intertonguing contact. Owing to the excessively dense nature of the jungle and lack of continuous trails between the west side of Gatun Lake and the Caribbean Sea the field work in this area was confined to within a couple of hundred yards of existing roads. The contacts above and below the Toro limestone between the roads were interpolated by stereoscopic aerial photograph study, helped out by the knowledge of the regional structure west of the lake. Wherever measurable dips are found here, they are very gentle, fairly gradual and uniform in variation, and generally seaward. It should be emphasized that these contacts are located by no field check points west of the longitude of the mouth of the Chagres River. Field traverses along all roads west of this longitude however, do confirm most of the indicated extent of the Chagres formation. Field confirmation of these contacts in this western area would be an additional undertaking of several man-months' duration. The indicated thinning of the Toro formation in outcrop to the southwest is substantiated by two section measurements, the first already described, the second 4.6 miles N.35°W. of the small peninsula at Escoval. The features on the aerial

[10] Some identifications by W. P. Woodring (Jones, 1947a).

CARIBBEAN SEA
LIMON BAY
TRINIDAD BAY
GATUN LAKE
NORTH DUE LAND
SALUD
LAGARTO
PIÑA
CRISTOBAL
COLON
MANZANILLO BAY
MARGARITA
TRANS-ISTHMIAN HIGHWAY
GATUN
Toro Pt
Guarapo Is
Lopez Is
Zorra Is
Trinidad Islands
Brujas Islands
Flores Islands
Juan Gallegos Island
Bohio Peninsula
Bohio Pt
NEW PROVIDENCE
NUEVO LIMON
Barro Colorado Island
FRIJOLES
GAMBOA
Chagres Arm
RESCOBAL
VIGAGARTERITO
CERRO GIGANTE
Pato Real Is
Scale 1:125,000
0
5 Miles

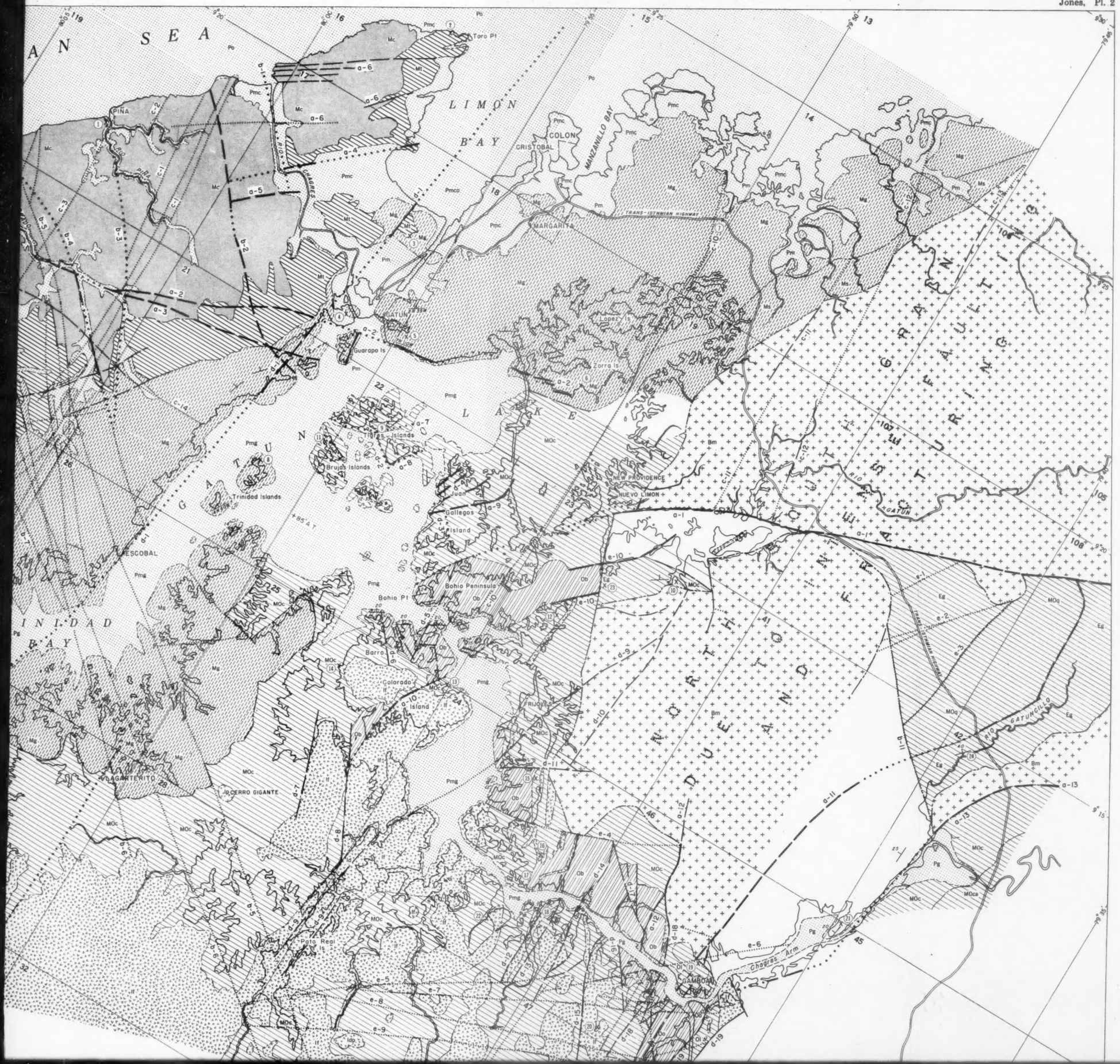

LEGEND

QUATERNARY

Pleistocene and Recent

Pm, Pg, Pc, Po — Unconsolidated deposits (Pm, atlantic muck; Pg, chagres gravel; Pc, coral and shells; Po, beach sand and ocean bottom silt)

Upper Miocene

Mc — Chagres sandstone

Mt — Toro limestone

TERTIARY

Middle Miocene

Mg, Ms — Middle Miocene (Mg, Gatun formation; Ms, Sabanitas formation)

Lower Miocene

Ip, Id, If — Bruja dolerite, Gigante basalt and related igneous rocks (Ip, intrusive plug or neck; Id, intrusive dike; If, extrusive flow)

Lower Miocene and upper Oligocene

MOc, MOca, MOq — Lower Miocene and Upper Oligocene (MOc, Caimito formation; MOca, Alahuela member of Caimito formation, (Gatun formation of Roas and Reeves); MOq, Quebrancha formation)

Upper Oligocene

Ol — Las Cascadas formation

Lower and upper Oligocene

Ob, Oo — Lower and Upper Oligocene (Ob, Bohio formation; Oo, Bas Obispo formation)

Eocene

Eg — Eocene (Eg, Gatuncillo formation

PRE-TERTIARY

Pre-Tertiary

+ Bm + — Pre-Tertiary complex (Metavolcanics, metaintrusives, hornfels, and basic to acidic intrusives)

Inferred contact

Inferred underwater contact

Contact representing a major unconformity

Average strike and dip of beds

45 — Army survey numbers assigned to five minute rectangles

x (24) — Fossil locality

Designation of fractures

Faults of major movement

Implied extension of faults of major movement

Faults of undetermined motion

Implied extension of faults of undetermined motion or fractures of unknown nature

AREAL GEOLOGIC MAP, GATUN LAKE AND VICINITY, PANAMA

Toro limestone

Middle Miocene (Mg, Gatun formation; Ms, Sabanitas formation)

Lower Miocene — Bruja dolerite, Gigante basalt and related igneous rocks (Ip, intrusive plug or neck; Id, intrusive dike; If, extrusive flow)

Lower Miocene and upper Oligocene — Lower Miocene and Upper Oligocene (MOc, Caimito formation; MOca, Alahuela member of Caimito formation, (Gatun formation of Ross and Reeves); MOq, Quebrancha formation)

Upper Oligocene — Las Cascadas formation

Lower and upper Oligocene — Lower and Upper Oligocene (Ob, Bohio formation; Oo, Las Obispo formation)

Eocene — Eocene (Eg, Gatuncillo formation

Pre-Tertiary — Pre-Tertiary complex (Metavolcanics, metaintrusives, hornfels, and basic to acidic intrusives)

TERTIARY

PRE-TERTIARY

Inferred contact

Inferred underwater contact

Contact representing a major unconformity

Average strike and dip of beds

45

Army survey numbers assigned to five minute rectangles

x (24)

Fossil locality

Designation of fractures

Faults of major movement

Implied extension of faults of major movement

Faults of undetermined motion

Implied extension of faults of undetermined motion or fractures of unknown nature

AREAL GEOLOGIC MAP, GATÚN LAKE AND VICINITY, PANAMA

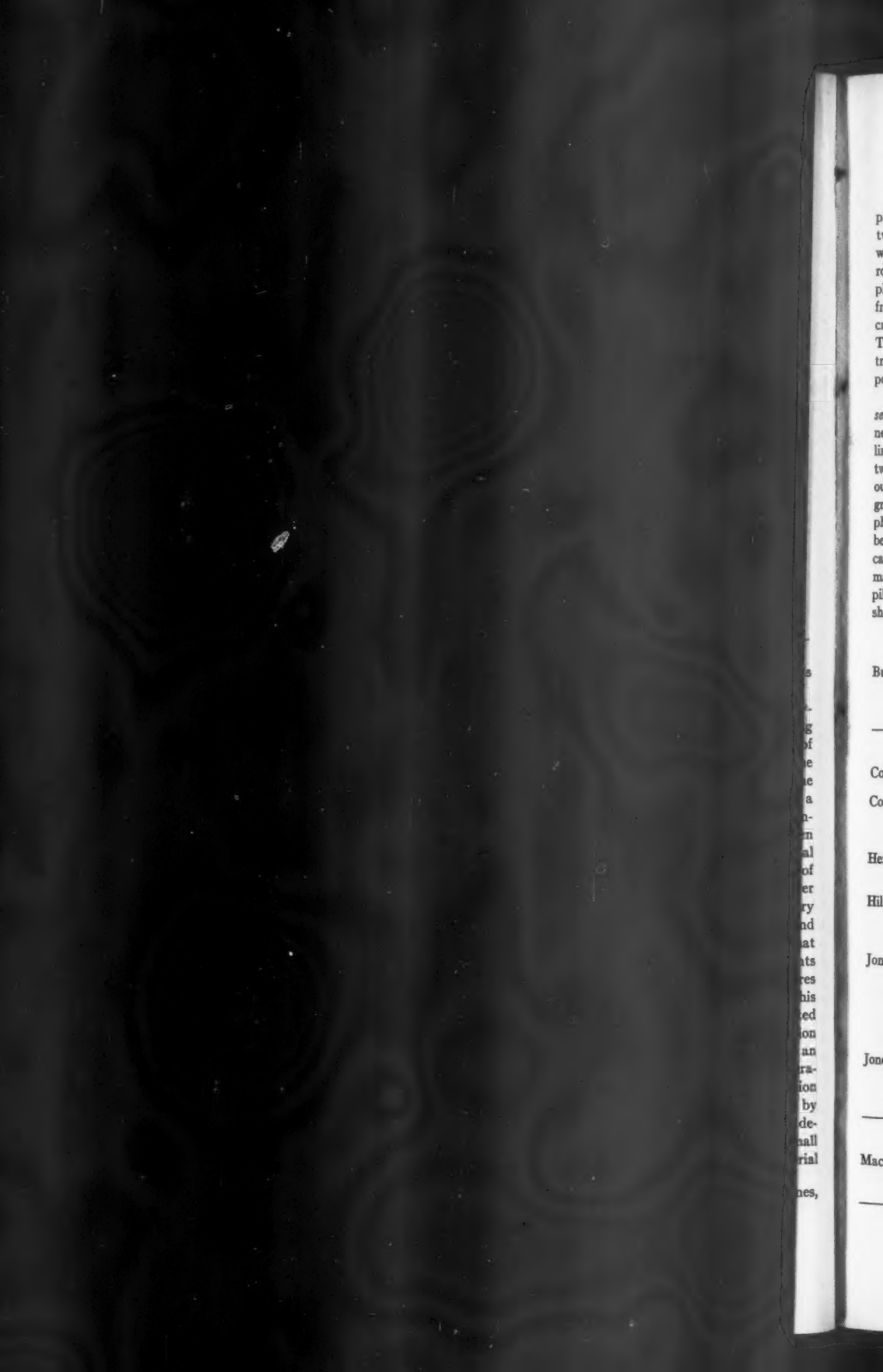

photographs, used to interpolate the contacts between the roads and to extrapolate beyond the westernmost crossing by roads, were a zone of rough, somewhat karst-like topography. In some places, this zone may have been indistinguishable from the jagged areas of scarps where many faults criss-cross the area. The indicated boundaries of the Toro limestone are the best approximation of its true extent that can be obtained without disproportionately great expenditure of time and effort.

Limits of unconsolidated Pleistocene and Recent sediment.—Those sediments of appreciable thickness beneath the waters of Gatun Lake were outlined on the basis of old French maps. Those between Gatun Lake and the Caribbean Sea were outlined using much newer and more accurate topographic maps and by stereoscopic study of aerial photographs. This contact where drawn on land between the lake and the sea is very accurate because field check points were afforded by a great many roads, railroads, excavations and caisson pilings, etc., all of which agreed with the limits shown.

References Cited

Bucher, W. H. (1947) *Problems of earth deformation illustrated by the Caribbean Sea Basin*, New York Acad. Sci., Tr., ser. II, vol. 9, no. 3, p. 98–116.

——, March, 1949, *Fault patterns and Fault movements*, address delivered before the local branches of the A.A.P.G., to be published.

Cooke, C. W. (1948) *Eocene Echinoids from Panama*, Jour. Paleont., vol. 22, p. 91–93.

Coryell, H. N. and Embich, J. R. (1937) *The Tranquilla Shale (Upper Eocene) of Panama and its Foraminiferal Fauna*, Jour. Paleont., vol. 11, p. 289–305.

Hershey, O. H. (1901) *Geology of central portion of Isthmus of Panama*, Univ. Calif. Bull. Dept. Geol., vol. 2, p. 231–267.

Hill, R. T. (1898) *The geological history of the Isthmus of Panama and portions of Costa Rica*, Harvard College, Mus. Comp. Zool., Bull., vol. 28, 285 p., 19 pls.

Jones, S. M. and Bartholomew, S. K. (1946) *Preliminary report of geologic features of the Gatun Lake Area portions* of the #8 routes, Panama sea level channels, I.C.S. 1947, memorandum to the chief, geology section, Spec. Engr. Div., The Panama Canal, 17 p., 3 appends.

Jones, S. M. (1947a) *Caimito fossil field identifications made by Dr. Woodring*, memorandum to the chief, geology section, Spec. Engr. Div., The Panama Canal, 3 p., 1 map.

——, (1947b) *Geology of Gatun Lake and Vicinity*, Oregon State College, Unpublished Thesis, 47 p., 4 pl.

MacDonald, D. F. (1913) *Geologic section of the Panama Canal Zone* (Abstract), Geol. Soc. Am., Bull. 24, p. 707–711.

——, (1915) *Some engineering problems of the Panama Canal in their relation to geology and topography*, U. S. Bur. Mines, Bull. 86, 88 p.

Olsson, A. A. (1942) *Tertiary deposits of northwestern South America and Panama*, 8th Am. Sci. Cong. 1940, Pr., vol. IV, Geol. Sci., Washington, p. 231–287.

Pettijohn, F. J. (1949) *Sedimentary rocks*, Harper Bros., N. Y.

Reeves, F., and Ross, C. P. (1930) *A geologic study of the Madden Dam Project, Alhajuela, Canal Zone*, U. S. Geol. Survey, Bull. 821-B, 49 p.

Rich, J. L. (1942) *The face of South America, an aerial traverse*, Am. Geog. Soc., Spec. Pub. 26.

Sapper, K. (1916–1917) *Zeitschrift fur Vulkanologie*, vol. 3, Pl. 19, 20, 21 Germany.

Schuchert, C. (1935) *Historical geology of the Antillean Caribbean region*, John Wiley and Sons, Inc., N. Y.

Shepard, F. P., and Emery, K. O. (1941) *Submarine topography off the California Coast*, Geol. Soc. Am., Spec. Paper 31.

Stewart, R. H. (1947a) *New occurrence of Lepidocyclina canellei in the Bohio formation*, memorandum to chief, Geol. section, Spec. Engr. Div., Panama Canal.

——, (1947b) *First record of Canal Zone sediments containing an Eocene fauna*, memorandum to chief, Geol. section, Spec. Engr. Div., Panama Canal.

Thompson, T. F. (1943) *Final report on modified Third Locks Project*, Part II Design, Chap. 3 Geology, (Pub. for limited distribution by the Spec. Engr. Div., the Panama Canal) 33 p.

—— (1944) *Geological explorations in the vicinity of Rio Quebrancha for the Panama Cement Company*, Panama Canal, Spec. Engr. Div.

Umbgrove, J. H. F. (1947) *The Pulse of the Earth*, Martinus Nijhoff, The Hague.

Vaughan, T. W. (1926) *The stratigraphic horizon of the beds containing* Lepidocyclina chaperi *on Haut Chagres, Panama*, Nat. Acad. Sci., Pr., vol. 12, p. 519–522.

Wentworth, C. K. (1937) *Terminology of the fine-grained mechanical sediments*, Rept. Comm. Sed., 1936–1937, Nat. Research Council, mimeo. p. 81–104.

—— and Williams, Howell (1932) *The classification and terminology of the pyroclastic rocks*, Rept. Comm. Sed., 1930–1932, Nat. Res. Council, Bull. 89, p. 19–53.

Woodring, W. P., and Thompson, T. F. (1949) *Tertiary formations of the Panama Canal Zone and adjoining parts of Panama*, Am. Assoc. Petrol. Geol., Bull., vol. 33, p. 223–247.

Charts and Maps Cited

American Geographical Society, 1944, Map of the Americas, Sheets 1-A and 1-B, 1:5,000,000; Sheets Panama, Bogota, Barranquilla, Cali and Rio Mira-Islas Galapagos 1:1,000,000.

Panama Survey Army Survey Maps 10, 20, 30, 40, 100, 110, 120, 130: (latest sheets in 1946).

U. S. Hydrographic Office Charts 1176, 5486, 5487.

New Mexico School of Mines, Socorro, New Mexico

Manuscript Received by the Secretary of the Society, May 9, 1949

STRUCTURE MAP OF WISSAHICKON SCHIST NORTHWEST OF PHILADELPHIA

BY

C. S. CH'IH

GEOLOGIC BOUNDARIES AFTER A.W. POSTEL (1940) AND F. BASCOM (1909)

SCALE

1 ½ 0 1 2 MI.

- generalized boundary of granitized areas
- high angle fault
- I,II chemical analyses (see Tables)
- •29 fabric and modal analyses
- °125 locality referred to in the text
- × outcrop of orthoclase kyanite gneiss
- △ outcrop of Springfield microcline gneiss outside the mapped boundary

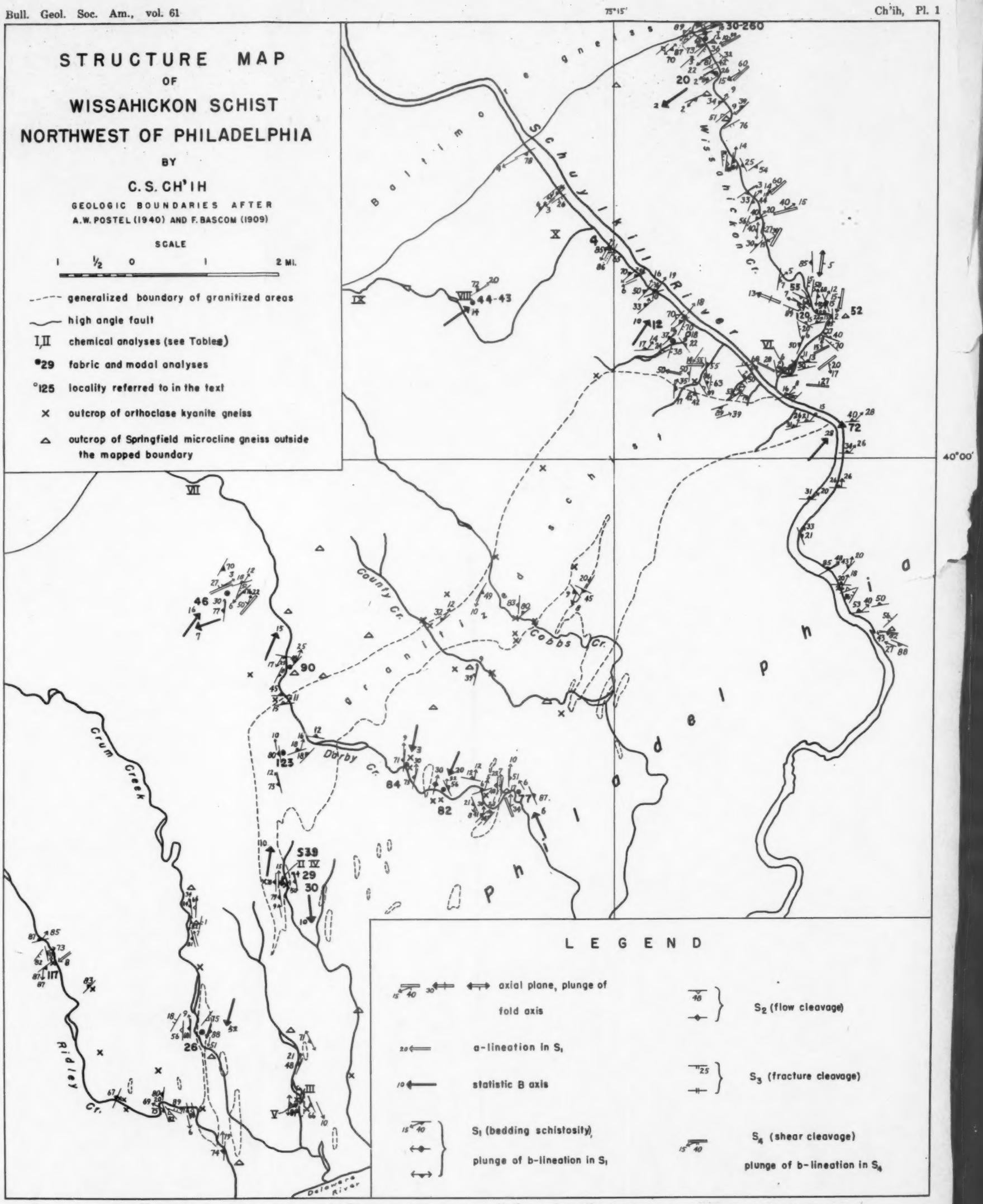

STRUCTURE MAP OF WISSAHICKON SCHIST NORTHWEST OF PHILADELPHIA

Ab
Int
Ac
Me
Ge
Gr
(
I
(
I
I
Me
I
S
A
Fig
1.
2.
3.
4.
5.
Pl
1
2
3
4
of
ne
du

BULLETIN OF THE GEOLOGICAL SOCIETY OF AMERICA
VOL. 61, PP. 923-956, 5 FIGS., 6 PLS. SEPTEMBER 1950

STRUCTURAL PETROLOGY OF THE WISSAHICKON SCHIST NEAR PHILADELPHIA, PENNSYLVANIA

With Special Reference to Granitization

By Chi-shang Ch'ih

CONTENTS

	Page
Abstract	923
Introduction	924
Acknowledgements	924
Methods of investigation	924
General geology	925
Granitization and hydrothermal metamorphism	926
General statement	926
Petrographic data	926
Springfield microcline gneiss	926
Orthoclase kyanite gneiss	927
Chemical data	927
Interpretation of granitization process	930
Hydrothermal (retrograde) metamorphism	933
Megascopic structure	933
Folds	933
S-surfaces and lineations	934
Analysis of field data	936
Petrofabric analysis	937
Preliminary statement	937
Fabrics of the Wissahickon schist	938
Mica fabric	938
Quartz fabric	944
Further notes on fabrics of Wissahickon schist	946
Fabrics of Springfield microcline gneiss	949
Mica fabric	949
Quartz fabric	950
Fabric of a typical porphyroblastic microcline gneiss	951
Fabric of a muscovite garnet type of microcline gneiss	951
Fabrics of orthoclase kyanite gneiss	951
Fabrics of crushed and sheared rock	953
Conclusions	954
References cited	948

ILLUSTRATIONS

Figure	Page
1. Triangular diagram showing chemical composition of Wissahickon schist	929
2. Triangular diagram showing changes in chemical composition during granitization of Wissahickon schist	929
3. Triangular diagram: comparison of chemical compositions of microcline gneisses and of average granodiorites and granites	929
4. Hypothetical reconstruction of the development of flexure-slip folds in Wissahickon schist	934
5. Relation between progressive folding (crenulations) and rotation of S-surfaces shown in mica fabrics (specimen 20)	943

Plate	Facing page
1. Structure map of Wissahickon schist northwest of Philadelphia	923
2. Wissahickon schist	926
3. Fabric diagrams	934
4. Fabric diagrams	942
5. Fabric diagrams	948
6. Fabric diagrams	956

Table	Page
1. Chemical analyses of granitized Wissahickon schists	928
2. Chemical analyses of Wissahickon schists	928
3. Chemical compositions, norms and calculated modes of average Wissahickon mica schist, average Springfield microcline gneiss and orthoclase-kyanite gneiss	931
4. Development of S-surfaces and lineations in different rock types of Wissahickon formation	937
5. Mica paragenesis in Wissahickon schist	939
6. Length and width of mica girdles and height of maxima	941
7. Correlation of quartz and mica fabrics (specimen 20)	945
8. Correlation of quartz maxima (Wissahickon schists and granitized equivalents)	947
9. Modes of granitized and ungranitized schist with fabric analyses	948

ABSTRACT

This paper is a comparative study of the fabrics of granitized and ungranitized Wissahickon schists near Philadelphia.

Granitization was effected chiefly by the introduction of alkalis and some lime, probably carried in hydrothermal solutions. The mica schists were reconstituted, becoming coarser in grain, with relative increase in feldspars and decrease in micas. A complementary enrichment of less-granitized patches and narrow border zones in iron and magnesia has produced biotite-rich rocks. Hydrothermal

activity following the main period of granitization has produced some retrograde metamorphism.

Folding in the ungranitized schist is of the flexural slip type. The development of folds can be traced in both mica and quartz fabrics, and the rotation of S-surfaces in the fabrics can be correlated with the overturned folds observed in the field. The same features can be identified in the granitized rocks, but less distinctly, since the physical properties of the latter made them react differently from the ungranitized schists during regional metamorphism. Granitization was syntectonic.

Late movements, occurring after the main period of granitization, are recorded locally in the sheared or crushed rocks.

Introduction

The Wisahickon formation in the Philadelphia area includes mica schists, quartz schists, plagioclase gneisses, amphibolites, and others, all of which have undergone intense folding accompanied by regional metamorphism. Granitization and subsequent hydrothermal alteration have also affected the rocks on a regional scale, probably during the latter part of the main period of deformation.

The present study, using chiefly the methods of structural petrology, was undertaken in the hope of clarifying the effects of granitization on the fabric of the mica schists, the period of granitization, and the chemistry of the granitization process. The area chosen (Pl. 1), namely, the whole exposed width of the formation approximately at right angles to the trend of folding, covers both the highly granitized area west of Philadelphia and the type section of the ungranitized schist on Wissahickon Creek from which the formation was named. To the north, the schist is cut off by the Cream Valley fault which brings it into contact with Baltimore gneiss; to the south near the Delaware River, the schist and gneiss disappear beneath a cover of Pleistocene and Recent deposits.

Earlier studies on this area have been published by H. D. Rogers (1858), J. P. Lesley (1883, 1892), T. D. Rand (1900), F. Bascom (1905, 1909), E. Armstrong (1941), and J. Weiss (1949). Two contributions, to which the present paper is directly related, are those of A. W. Postel (1940) and E. Cloos and A. Hietanen (1941, Part III).

Postel (1940) using petrographic criteria and field evidence, demonstrated the process of granitization in the mica schists. Cloos and Hietanen (1941, pt. III), in dealing with the "Martic Overthrust" problem in Pennsylvania, made fabric analyses of eight specimens of ungranitized Wissahickon schist from near Bryn Mawr, and showed that the S-planes of these rocks had been rotated during deformation. It was a great advantage to have their diagrams for comparison with those made by the writer.

Acknowledgments

The writer is deeply indebted to Professor Dorothy Wyckoff of Bryn Mawr College for her direction throughout the whole course of this work; to Professor Edward Watson of Bryn Mawr College, for his constant interest and stimulating criticisms and for checking some of the optical data; and to Professor Lincoln Drydon for his critical reading of the manuscript. Dr. A. Williams Postel, of the U. S. Geological Survey generously contributed all his collections of thin sections and specimens from this area and also accompanied the writer in the field pointing out many outcrops discovered by him. Professor Francis J. Turner of University of California made valuable suggestions as to the revision of the manuscript. Mr. Abraham Rosenzweig kindly made all the photographs.

Finally, the writer wishes to express gratitude to Bryn Mawr College and especially to the Chinese Scholarship Committee for the grants and scholarships that made this work possible.

Methods of Investigation

About 400 thin sections already available at Bryn Mawr College were studied. These included the collections of Bascom, Postel, Hietanen, and other previous workers in the Philadelphia region. This preliminary work served as a guide in collecting material for further study.

Since areal mapping of the region is largely complete, field work was directed toward observation of general and detailed structures in each of the principal rock types of the Wissahickon schist. Field readings on all observable structural elements were taken at abou

150 localities; these, plotted on the map (Pl. I), provide the regional framework with which the fabric data have been correlated. About 130 oriented specimens, well distributed over the area, were collected and re-oriented in the laboratory, using the apparatus designed by E. Ingerson (1937), to remeasure certain structural elements such as flow cleavage (S_2), which are difficult to observe precisely in the field. Constructions were made on a stereographic net, when necessary. One hundred and seven rock slices were sawed by the writer for sectioning, in most cases perpendicular to the main lineation on the principal schistosity (bedding schistosity S_1). Thin sections of representative rock types and illustrating common types of structures were then selected for fabric analysis.

Modal analyses of the mineral assemblages in these same specimens were made with an integrating stage. Where precise determinations of optical properties of individual minerals were necessary, separations were made with heavy liquids and the materials were studied in immersion oils or on the universal stage.

General Geology

The Appalachian Piedmont belt at Philadelphia is a region of intense folding. Within the area covered by the present study, the rocks affected by the folding may be divided into 3 groups: ungranitized rocks, granitized rocks, and hydrothermally altered rocks.

Among the ungranitized rocks, here jointly called the Wissahickon schist and not differentiated on the map, are mica schists, quartz schists, plagioclase gneisses, and the amphibolites, not discussed in this paper. The mica and quartz schists, originally pelitic to psammitic sediments, are mica-plagioclase-quartz rocks. The plagioclase gneisses, composed of the same minerals as the schists but much more feldspathic, occur as intricate pegmatite-like veins and lenticles or as separate layers in the schists, and are possibly metamorphic differentiates or products of anatexis.

The granitized group includes granitized equivalents of most members of the Wissahickon schist group. However, this paper is concerned only with the granitized mica schists, which are further subdivided into a highly granitized Springfield microcline gneiss and less granitized orthoclase-kyanite gneiss. The Springfield microcline gneiss was called granite gneiss by Bascom (1905) and Springfield porphyroblastic granodiorite by Postel (1940), who further distinguished a fine-grained type which he called aplite, and a muscovite-garnet type, which he called Ridley Park granodiorite. The orthoclase-kyanite gneiss is equivalent to the kyanite- and orthoclase-bearing types that Postel included in his medium-grained gneiss and purple schist. The granitized schists grade into ordinary schists. The boundary shown on the map (Pl. I), based on the work of Postel (1940), is somewhat arbitrary, for the contacts are gradational; it merely delimits the area within which granitized predominate over ungranitized rocks. Away from this transitional boundary, granitized patches decrease in number and eventually disappear. The main area of granitized rocks is about 10 miles long by 2 miles wide, and has a lenticular shape conforming to the changing regional trend. Minor granitized areas occur sporadically north and east of Philadelphia.

A third group comprises various hydrothermally altered rocks, among which the muscovite-quartz gneiss (the hydrothermally metamorphosed equivalent of the kyanite-orthoclase gneiss) is discussed.

Within the area, the main overturning of the folded belt is to the southeast. The trend of folding along Wissahickon Creek and Schuylkill River is north-northeast and gradually changes to nearly north-south as one proceeds southwestward. In the highly granitized southwestern part, the overturning is predominantly eastward while fold axes remain about horizontal (Pl. I).

Two major zones of cataclastic rocks have been mapped—one along the northern boundary fault (Armstrong 1941), the other along the northwestern edge of the area of intense granitization (Postel, 1940). Local crush zones are believed to be widely distributed in the area, probably representing late movements, after the period of granitization and recrystallization. Local shear zones, without cataclasis but marked by recrystallization effects, were observed at a few localities along the northern part of Darby Creek. Steep-axis fold-

ing was observed at only one locality (117) within the map, but is somewhat commoner in the schist west of the granitized area (P. A. Dike, personal communication).

Granitization and Hydrothermal Metamorphism

General Statement

The Wissahickon schist comprises metamorphic derivatives of pelitic to psammitic sediments. A relatively low ratio of K_2O to Al_2O_3 is expressed by the absence of potash feldspar (microcline) and the presence of muscovite and such alumino-silicates as almandine, staurolite, kyanite, and sillimanite. Typical rocks consist of muscovite, biotite, oligoclase, quartz, and a few accessories, with or without any of these aluminosilicates. The schist thus belongs to the amphibolite facies (Eskola, 1920; Eskola *et al.*, 1939). Most of the rocks represent the kyanite-staurolite subfacies, but the sillimanite - almandine subfacies, probably formed at somewhat higher temperatures (Turner, 1948, p. 81–87), is also locally developed.

Granitization of varying degrees, involving introduction of alkalis and possibly some lime, is expressed mainly by appearance of microcline, never present in the ungranitized schist. At the same time, some FeO-MgO seems to have been expelled, so that the schists bordering the highly granitized rocks have been enriched in these oxides with possibly also some addition of alkalis (chiefly soda). Orthoclase, instead of microcline, is a stable mineral phase in these border schists. The rocks with potash feldspars thus fall into two distinct categories: the microcline-bearing Springfield gneiss and the orthoclase-bearing kyanite gneiss.

The Springfield microcline gneiss exhibits a constant mineral assemblage: microcline, oligoclase, quartz, and green biotite, with epidote, sphene, and apatite as accessories; muscovite is generally present. This assemblage apparently belongs to the staurolite-kyanite subfacies.

The orthoclase-kyanite gneiss shows the mineral assemblage orthoclase, oligoclase, quartz, almandine, brown or reddish biotite, and usually muscovite; microcline occurs with orthoclase in some specimens. Kyanite also is commonly present, and its association with orthoclase instead of microcline suggests a higher temperature of metamorphism than that of the associated rocks. Accordingly the orthoclase-kyanite gneiss is provisionally assigned to the sillimanite-almandine subfacies, even though sillimanite itself is seldom present.

Petrographic Data

Springfield microcline gneiss.—Postel (1940), summarizing the field and petrographic evidence of granitization of the Wissahickon schist, stresses the transitional character of contacts between the schist and Springfield microcline gneiss, and records a series of replacement textures in the latter—as shown by feldspar porphyroblasts, myrmekites, perthites, antiperthites, and corroded quartz.

The petrographically demonstrated replacement is that between plagioclase and microcline. Other petrographic data indicating mineralogical rearrangement in the granitized rocks

---

Plate 2.—WISSAHICKON SCHIST

Figure 1.—Needle Kyanite Penetrating Myrmekite Rim Between Oligoclase and Orthoclase, under Plane Polarized Light

Figure 2.—Same as Figure 1, under Crossed Nicols

Figure 3.—Granitized Stringer in Orthoclate-Kyanite Gneiss

Cross-cutting S_1; small ones parallel to S_1.

Figure 4.—Sillimanite Replaced by Muscovite

Unaltered sillimanite core enclosed by porphyroblastic muscovite.

Figure 5.—Gently Dipping Shear Cleavage (S_4) Transgressing Steeply Dipping Bedding (S_1)

Figure 6.—Shear Cleavage (S_4) in Wissahickon schist, Transgressing S_1

Trends of mica arches of S_1 and of S_4 are nearly perpendicular to each other. S_4 represents later shearing and recrystallization along former S_3 (fracture cleavage). See diagrams of specimen 46.

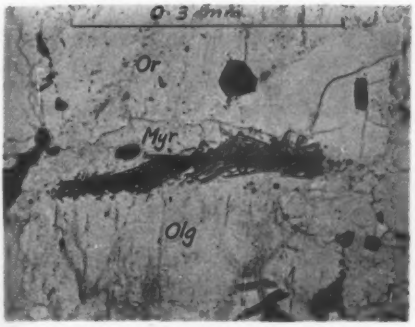

FIGURE 1

FIGURE 2

FIGURE 3

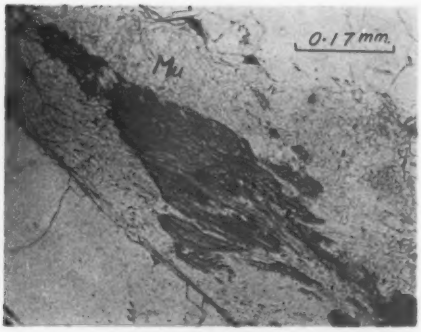

FIGURE 4

FIGURE 5

FIGURE 6

WISSAHICKON SCHIST

are: (1) the nearly complete elimination of muscovite, accompanied by appearance of microcline and increase in amount of plagioclase; (2) green biotite instead of greenish-brown to reddish as in the schist; (3) appearance of epidote and sphene, intergrown with biotite; (4) formation of mica-quartz and epidote-quartz symplectites in contact with microcline and quartz; (5) disappearance of almandine (usually present in the schist) in equilibrium rocks; and (6) general decrease in quartz content.

The respective mineral assemblages observed in the schist and in the Springfield gneiss can be equated (either for equal volumes or for equal weights) to express granitization process only if addition or subtraction of appropriate substances is assumed. This question can be considered further only in conjunction with chemical data.

Orthoclase-kyanite gneiss.—This rock type, believed to represent a somewhat higher grade of metamorphism, occurs (Pl. 1) as patches within the main area of nearly completely granitized Springfield gneiss, as zones bordering the latter, and west of the area studied as local patches probably associated with intrusive gabbro.

The most conspicuous mineralogical features are: (1) abundance of brownish-green to red biotites, sometimes in form of biotite-quartz symplectites pseudomorphous after kyanites; (2) presence of kyanite either as long blades oriented parallel to the main schistosities (S_1 and S_2) and uniformly distributed throughout the rock or as fine accicular aggregates margining plagioclase and orthoclase or penetrating myrmekites (Pl. 2, figs. 1, 2). The bladed type is perhaps a product of regional metamorphism, the accicular type of granitization. (3) abundance of orthoclase, partially inverted to microcline in marginal parts; and (4) the occasional occurrence of sillimanite.

The orthoclase-kyanite gneiss probably represents granitization involving introduction of mainly FeO—MgO and some Na_2O—K_2O.

Lack of equilibrium is indicated by local occurrence of sillimanite with kyanite and of orthoclase with microcline. Kyanite with orthoclase is the commonest association. The stability relations of these minerals require further consideration. The optical properties of orthoclase[1] are within the range of plutonic perthitic orthoclases as described by Spencer (1937, 1938). Microcline presumably crystallized at a lower temperature than orthoclase. It is usually assumed that crystallization of kyanite rather than sillimanite is favored by somewhat lower temperature or by higher stress. An alternative possibility (J. Verhoogen, personal communication) is that sillimanite, having lower solubility than kyanite in hydrochloric acid, is the stable phase over a wide range of temperatures (low temperatures included), but that its velocity of crystallization allows it to appear only at high temperatures; at lower temperatures the less stable (metastable) kyanite crystallizes instead. If this interpretation is correct, appearance of stable sillimanite at relatively low temperatures in these rocks could perhaps be correlated with some such special condition as accelerated chemical activity under the influence of granitizing solutions. If stress is also a controlling factor, possibly Al_2O_3 is more sensitive to stress than $KAlSi_3O_8$ and kyanite usually forms instead of sillimanite under stress conditions which produce only an incipient twinning in orthoclase.

The writer tentatively favors the view that microcline has here developed with falling temperature (retrogressive metamorphism) by inversion of orthoclase. Whether kyanite has at the same time partially inverted to sillimanite, or whether sillimanite is a relict from an even earlier (higher temperature) stage of metamorphism remains an open question, owing to lack of knowledge of the stability relations of kyanite and sillimanite.

Chemical Data

The chemical changes attending granitization are brought out by comparing ten available

[1] $\alpha = 1.517$ $\beta = 1.522$–1.523 $\gamma = 1.524$ (in sodium light)
(−) 2V (calculated from indices) = 44°–65°
(−) 2V (determined on U-stage) = 54°–68°, mostly near 60°–62°
plane of optic axes ⊥ (010), plane of optic axes ∧ (001) = 5°
X′ ∧ (010) on (001) = 0°, (010) ∧ (001) = 90°

chemical analyses (Tables 1, 2). This comparison is facilitated by plotting the analyses on two triangular diagrams (Figs. 1, 2).

In Figure 1, the analyses fall into two groups: quartz schists (IX and X) representing psammitic sediments (Clarke, 1924, p. 547), and mica schists (I–VIII) approximating pelitic sediments in composition (Clarke, 1924, p. 552, 554). Points respectively representing granitized schists (I–V) and mica schists (VI–VIII) fall within the same restricted area. This implies that granitization has not greatly affected the content of SiO_2, Al_2O_3, and the remaining less abundant constituents (K_2O, Na_2O, CaO, MgO, FeO etc.) as a whole. Its main chemical result has been to change the relative proportions of these less abundant constituents as shown in Figure 2.

Figure 2 shows the relations between K_2O, CaO, and (FeO + MgO + MnO) after recalculation to 100. It is evident that the change from mica schist to microcline gneiss involves addition of both K_2O and CaO. Within the group of granitized rocks (I–IV) K_2O and (FeO + MgO) are inversely related, while CaO is approximately constant. High K_2O content is interpreted as due to more advanced granitization. The diminished FeO and MgO content of the more potassic schists (I, II) seems to be related to enrichment of the border schist (V) in these oxides. This is in keeping with the basic front hypothesis of certain European geologists.

As compared with the mica schists, the granitized schists (I–V) are enriched notably in Na_2O as well as in K_2O, so that the distribution of points in Figure 2 remains much the same if Na_2O or (Na_2O + K_2O)—instead of K_2O—is plotted against CaO and (FeO + MgO + MnO).

TABLE 1.—CHEMICAL ANALYSES OF GRANITIZED SCHISTS
(Localities shown Pl. 1)

	I	II	III	IV	V
SiO_2	70.48	72.07	69.70	66.65	68.01
Al_2O_3	17.84	15.13	15.33	15.66	13.86
Fe_2O_3	0.99	0.71	0.91	1.01	0.63
FeO	0.68	1.69	2.29	3.44	5.28
MgO	0.28	0.55	0.90	1.31	2.22
CaO	1.89	1.89	2.48	3.05	1.03
Na_2O	3.58	2.59	3.28	3.43	3.77
K_2O	3.89	4.93	3.58	3.61	2.65
H_2O^+	0.48	0.20	0.61	0.62	0.91
H_2O^-	0.04	0.05	0.11	0.08	0.08
TiO_2	0.28	0.26	0.61	0.78	1.19
P_2O_5	—	—	0.10	0.21	0.19
MnO	0.03	0.04	0.04	0.07	0.06
Total	100.46	100.11	99.94	99.92	99.98

I. (52–46) Microcline gneiss, porphyroblastic type. Analyst, P. Vipond, Bryn Mawr College (J. Weiss, 1949).
II. (28–230) Microcline gneiss, fine-grained type. Analyst, P. Vipond, Bryn Mawr College.
III. (23–22) Microcline gneiss, intermediate type. Analyst, E. H. Oslund, University of Minnesota.
IV. (28–231) Microcline gneiss, porphyroblastic type. Analyst, E. H. Oslund, University of Minnesota.
V. (23–125) Orthoclase-kyanite gneiss. Analyst, E. H. Oslund, University of Minnesota.

TABLE 2.—CHEMICAL ANALYSES OF WISSAHICKON SCHISTS
(Localities shown Pl. 1)

	VI	VII	VIII	IX	X
SiO_2	69.94	69.85	67.40	78.48	81.90
Al_2O_3	14.12	13.74	16.61	11.56	8.59
Fe_2O_3	1.28	1.82	3.76	2.57	0.47
FeO	4.10	3.08	3.58	0.69	2.10
MgO	1.61	2.34	1.36	0.12	0.13
CaO	1.29	0.78	0.58	0.40	1.67
Na_2O	2.31	2.34	0.87	1.41	2.98
K_2O	3.66	2.57	3.25	2.26	1.16
H_2O^+	1.32	1.24	1.72	1.80	0.51
H_2O^-	0.14	0.12	0.12	0.17	0.11
TiO_2	0.75	1.46	0.75	0.61	0.60
P_2O_5	—	0.11	—	—	—
MnO	0.08	0.08	0.11	0.03	0.03
Total	100.60	99.53	100.11	100.10	100.25

VI. (52–15) Almandine mica schist. Analyst, P. Quinn, Bryn Mawr College (J. Weiss, 1949).
VII. (44–9) Mica schist. Analyst, O. C. Bates, Bryn Mawr College (Cloos and Hietanen, 1941, I. p. 142).
VIII. (44–42) Staurolite almandine mica schist. Analyst, R. Stoddard, Bryn Mawr College (Cloos and Hietanen, 1941, II, p. 142).
IX. (52–100) Quartz schist. Analyst, P. Vipond, Bryn Mawr College (J. Weiss, 1949).
X. (44–48a) Almandine quartz schist. Analyst, E. M. Hardy, Bryn Mawr College (Cloos and Hietanen, 1941, 1, p. 142).

FIGURE 1.—TRIANGULAR DIAGRAM SHOWING CHEMICAL COMPOSITION OF WISSAHICKON SCHIST (weight %)

Roman numerals indicate chemical analyses shown in Tables 1, 2, 3. Triangles indicate quartz schists; Open circles, ungranitized mica schists; Open circles, ungranitized mica schists; Solid circles, microcline gneisses; Cross-in-circle, orthoclase kyanite gneiss. Bulk composition of granitized and ungranitized mica schists is very similar.

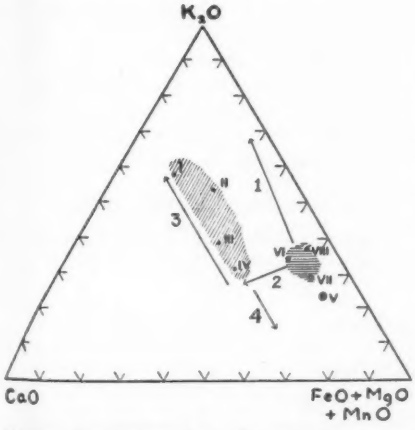

FIGURE 2.—TRIANGULAR DIAGRAM SHOWING CHANGES IN CHEMICAL COMPOSITION DURING GRANITIZATION OF WISSAHICKON SCHIST (weight %).

Roman numerals indicate chemical analyses shown in Table 1. Open circles, ungranitized mica schists; Solid circles, microcline gneisses; Cross-in-circle, orthoclase kyanite gneiss. Arrows: 1. Direction of change of composition with addition of K_2O during granitization. 2. Direction of change of composition with addition of CaO during granitization. 3, 4. Directions of changes of composition with addition of K_2O and complementary removal of (FeO, MgO), with CaO remaining constant.

Chemical similarity of the granitized Wissahickon schist to typical acid plutonic rocks is brought out in Figure 3. Seven representative analyses (A–G) of granodiorites, granodiorite aplite, quartz monzonite and granites (Johannsen, 1932; Daly, 1933) fall within a restricted (shaded) area, which is largely overlapped by the field (from Figure 2, also shaded) of the granitized rocks. However, in the igneous series, as K_2O varies over a wide range, the ratio CaO: (FeO + MgO + MnO) remains constant. But in the granitized schists CaO maintains a constant value while K_2O and (FeO + MgO + MnO) vary inversely.

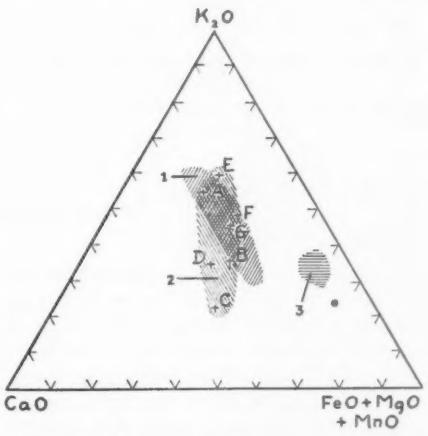

FIGURE 3.—TRIANGULAR DIAGRAM: COMPARISON OF CHEMICAL COMPOSITIONS OF MICROCLINE GNEISSES AND OF AVERAGE GRANODIORITES AND GRANITES (weight %).

A. Leucogranodiorite (average of 4), Johannsen (1932), p. 318. B. Granodiorite (average of 24), Johannsen (1932), p. 331. C. Granodiorite (average of 40), Daly (1933), p. 457 (5). D. Quartz monzonite (average of 20), Daly (1933), p. 457 (3). E. Granodiorite aplite (average of 3), Johannsen (1932), p. 365. F. Granite (average of 23), Johannsen (1932), p. 193, table 97. G. Granite (average of 546), Daly (1933), p. 457 (2). 1. Microcline gneisses, area from Fig. 2. 2. Igneous rocks. 3. Mica schists, area from Fig. 2. Cross-in-circle, orthoclase kyanite gneiss from Fig. 2.

In the light of the chemical data, the change from the Wissahickon schist to the Springfield microcline gneiss can be expressed by the following equation on the basis of equal weights (namely 100 gr. of the schist gives 100 gr. of the gneiss):

$$\underset{\text{quartz}}{73.7\ SiO_2} + \left\{\begin{matrix}\underset{\text{oligoclase } (An_{22})}{2.7\ Na_2Al_2Si_2O_{16}} \\ 1.5\ CaAl_2Si_2O_8\end{matrix}\right. + \left\{\begin{matrix}\underset{\text{biotite}}{.87\ H_4K_2(Fe,\ Mg)_3Al_4Si_6O_{24}} \\ .3\ H_4Na_2(Fe,\ Mg)_3Al_4Si_6O_{24}\end{matrix}\right. +$$

$$\underset{\text{muscovite}}{2.53\ H_4K_2Al_6Si_6O_{24}} + \underset{\text{almandine}}{.35\ Fe_3Al_2Si_3O_{12}} + \underset{\text{magnetite}}{1.4\ Fe_3O_4} + \underset{\text{ilmenite}}{1.2\ FeTiO_3} + .86\ K_2O + 2.19\ Na_2O +$$

$$2.48\ CaO + 1.28\ SiO_2 + 1.21\ Al_2O_3 - .83\ Fe_2O_3 - 4.33\ (FeO,\ MgO) - .6\ TiO_2 - 4.08\ H_2O \rightarrow$$

$$\underset{\text{quartz}}{52.66\ SiO_2} + \left\{\begin{matrix}\underset{\text{microcl. perthite (olg. 10)}}{2.97\ K_2Al_2Si_6O_{16}} \\ .19\ Na_2Al_2Si_6O_{16} \\ .11\ CaAl_2Si_2O_8\end{matrix}\right. + \left\{\begin{matrix}\underset{\text{oligoclase } (An_{22})}{4.17\ Na_2Al_2Si_6O_{16}} \\ 2.35\ CaAl_2Si_2O_8\end{matrix}\right. +$$

$$\left\{\begin{matrix}\underset{\text{biotite}}{.32\ H_2K_2(Fe,\ Mg)_4Al_4Si_6O_{24}} \\ .83\ H_2Na_2(Fe,\ Mg)_4Al_4Si_6O_{24}\end{matrix}\right. + \underset{\text{muscovite}}{.97\ H_4K_2Al_6Si_6O_{24}} + \underset{\text{zoisite}}{.23\ H_2Ca_4Al_6Si_6O_{26}} + \underset{\text{sphene}}{.6\ CaTiSiO_5} + \underset{\text{magnetite}}{.57\ Fe_3O_4}$$

Minerals (in molecular proportions) on the left side of the equation correspond to the calculated mode of the average of three chemical analyses (VI–VIII) of mica schists, and those on the right the calculated mode of the average of four analyses (I–IV) of microcline gneisses (Table 3). To the schist, though each constituent must be added or subtracted as required by the chemical data, addition of Na_2O, K_2O and CaO and subtraction of FeO, MgO and H_2O are regarded as much more important. The average microcline gneiss chosen for this equation does not serve as a typical example of advanced granitization, for a considerable amount of mucsovite appears in the mode (Table 3). Accordingly the addition of K_2O is comparatively low.

Similarly an equation representing chemical relation between the schist and the orthoclase-kyanite gneiss can be written as follows:

$$\underset{\text{quartz}}{73.7\ SiO_2} + \left\{\begin{matrix}\underset{\text{oligoclase } (An_{22})}{2.7\ Na_2Al_2Si_2O_{16}} \\ 1.5\ CaAl_2Si_2O_8\end{matrix}\right. + \left\{\begin{matrix}\underset{\text{biotite}}{.87\ H_4K_2(Fe,\ Mg)_3Al_4Si_6O_{24}} \\ .3\ H_4Na_2(Fe,\ Mg)_3Al_4Si_6O_{24}\end{matrix}\right. +$$

$$\underset{\text{muscovite}}{2.53\ H_4K_2Al_6Si_6O_{24}} + \underset{\text{almandine}}{.35\ Fe_3Al_2Si_3O_{12}} + \underset{\text{magnetite}}{1.4\ Fe_3O_4} + \underset{\text{ilmenite}}{1.2\ FeTiO_3} + 3.08\ Na_2O + 3.46(FeO,\ MgO) +$$

$$.29\ TiO_2 - .58\ K_2O - .05\ CaO - .89\ Al_2O_3 - 1.01\ Fe_2O_3 - 1.68\ SiO_2 - 4.63\ H_2O \rightarrow$$

$$\underset{\text{quartz}}{56.53\ SiO_2} + \left\{\begin{matrix}\underset{\text{oligoclase}(An_{21})}{2.73\ Na_2Al_2Si_6O_{16}} \\ 1.45\ CaAl_2Si_2O_8\end{matrix}\right. + \left\{\begin{matrix}\underset{\text{orthoclase}(Ab_{20})}{2.72\ K_2Al_2Si_6O_{16}} \\ .68\ Na_2Al_2Si_6O_{16}\end{matrix}\right. +$$

$$\left\{\begin{matrix}\underset{\text{biotite}}{.1\ H_2K_2(Fe,\ Mg)_4Al_4Si_6O_{24}} \\ 2.67\ H_2Na_2(Fe,\ Mg)_4Al_4Si_6O_{24}\end{matrix}\right. + \underset{\text{kyanite}}{.47\ Al_2SiO_5} + \underset{\text{magnetite}}{.39\ Fe_3O_4} + \underset{\text{ilmenite}}{1.49\ FeTiO_3}$$

It is obvious that conversion of the schist into orthoclase-kyanite gneiss necessitates mostly addition of (FeO, MgO) and Na_2O and removal of H_2O.

Assuming exchange of FeO and MgO between the microcline gneiss and the orthoclase-kyanite gneiss, granitization of the schist involves chiefly addition of Na_2O (+CaO) from outside sources with complementary removal of H_2O. (Compare the above two equations or columns 4 and 5 in Table 3.) The compositions of the plagioclases and potash feldspars used in the above equations are based on petrographic data; the biotite fromulae are arbitrarily chosen from those of commonly occurring biotites observed by Berman (1937).

Interpretation of Granitization Process

Regarding source of the granitizing solutions attention is drawn to Eskola's (1949, p. 470)

TABLE 3.—CHEMICAL COMPOSITIONS, NORMS AND CALCULATED MODES OF AVERAGE WISSAHICKON MICA SCHIST, AVERAGE SPRINGFIELD MICROCLINE GNEISS AND ORTHOCLASE-KYANITE GNEISS

		Mica schist (aver. of VI–VIII from Table 2, wt. %)	Microcline gneiss (aver. of I–IV from Table 1, wt. %)	Orthoclase-kyanite gneiss (V of Table 1, wt. %)	Relative change from mica sch. to microcline gneiss		Relative change from mica sch. to orth.-kyanite gneiss	
					wt. %	mol. % × 100	wt. %	mol. % × 100
Chemical Composition	SiO_2	69.06	69.73	68.01	+0.67	+1.20	−1.05	−1.70
	Al_2O_3	14.82	15.99	13.86	+1.17	+1.17	−0.96	−0.91
	Fe_2O_3	2.29	0.91	0.63	−1.38	−0.83	−1.66	−1.01
	FeO, MgO, MnO	5.45	2.84	7.56	−2.61	−4.30	+2.11	+3.50
	CaO	0.88	2.33	1.03	+1.45	+2.60	+0.15	+0.24
	Na_2O	1.84	3.22	3.77	+1.38	+2.20	+1.93	+3.08
	K_2O	3.16	4.00	2.65	+0.84	+0.85	−0.51	−0.58
	H_2O	1.43	0.48	0.91	−0.95	−5.30	−0.52	−2.88
	TiO_2	0.99	0.48	1.19	−0.51	−0.60	+0.20	+0.29
	P_2O_5	0.04	0.08	0.19	+0.04	—	+0.15	—
Norm	Quartz	40.00	29.00	28.00				
	Orthoclase	19.00	24.00	16.00				
	Albite	16.00	27.00	32.00				
	Anorthite	4.00	11.00	4.00				
	Hypersthene	7.00	5.00	13.00				
	Corundum	7.00	2.00	3.00				
	Magnetite	3.00	1.00	1.00				
	Ilmenite	2.00	1.00	2.00				
	Apatite	—	—	—				
Calculated Mode	Quartz	44.00	31.00	34.00				
	Microcline		17.00					
	Orthoclase			15.00 (1)				
	Albite			4.00 (1)				
	Albite	14.00 (2)	23.00 (3)	14.00 (4)				
	Anorthite	4.00 (2)	7.00 (3)	4.00 (4)				
	Biotite	11.00 (5)	10.00 (6)	24.00 (7)				
	Muscovite	20.00	8.00					
	Almandine	2.00						
	Zoisite		2.00					
	Sphene		1.00					
	Kyanite			1.00				
	Magnetite	3.00	1.00	1.00				
	Ilmenite	2.00		3.00				
	Apatite							

(1) Sodic orthoclase (Orth. 80 Ab. 20)
(2) Oligoclase (Ab. 78 An. 22)
(3) Oligoclase (Ab. 78 An. 22)
(4) Oligoclase (Ab. 79 An. 21)
(5) Biotite $74H_4K_2(Fe,Mg)_5Al_4Si_6O_{24}\cdot 26H_4Na_2(Fe,Mg)_5Al_4Si_6O_{24}$
(6) Biotite $28H_2K_2(Fe,Mg)_4Al_4Si_6O_{24}\cdot 72H_2Na_2(Fe,Mg)_4Al_4Si_6O_{24}$
(7) Biotite $4H_2K_2(Fe,Mg)_4Al_4Si_6O_{24}\cdot 96H_2Na_2(Fe,Mg)_4Al_4Si_6O_{24}$.

latest discussion on the mantled gneiss domes (Cloos and Broedel, 1937) in Maryland, Pennsylvania. Granitization of the Wissahickon schist (the mantle) may be attributed to the juices expelled from the underlying Baltimore gneisses (the domes), undergoing granitization and migmatization themselves during the period of doming which was also the period of

deformation of the Wissahickon schist. The microcline gneisses occurring both in the schist and in the gneiss are petrographically indistinguishable.

The chemical character of the border zone rocks has already been noted. This border zone can be observed at several places in the field. As one goes from the ordinary schists into the granitized rocks, there appears first a narrow zone rich in iron-magnesia (biotite) and, second, the main zone rich in alkali and lime (feldspars). This is strikingly similar to the upper migmatite zones observed in certain other metamorphic terrains (Read, 1948b, p. 197, Fig. 2, p. 178, Fig. 5, p. 180). The idea of "basic front" has been put forward by numerous recent writers (Wegmann and Kranck, 1931; Wegmann, 1935 a; 1935 b; Backlund, 1936; Jung and Roques, 1938; Perrin and Roubault, 1941; Bugge, 1943; Reynolds, 1943; 1944; 1946; 1947a; 1947b; 1947c; Read, 1943; 1944; 1946; 1948a; 1948b); and is by some regarded as an inseparable part of granitization process. The migration, in whatever form—ionic or as oxides, in solid state, or in solution—is supposed to be passive, since it is controlled by the introduction of Na, K, and Ca. In the region here described, there is no evidence that any large bodies of basic or ultrabasic rock have been formed by this process. The "basic front" of small scale, if the biotite-rich rocks of the border zone may be so regarded, may be connected with the fact that the actual amount of alkalis and lime introduced into the granitized rocks is also small.

The present scattered distribution of the orthoclase-kyanite gneisses suggests that either they formed only locally, possibly in the neighborhood of pre-granitization gabbroic intrusives of temperatures high enough for rocks of the sillimanite-almandine subfacies to be formed; or else they are remnants of a zone of more intense heating which preceded the introduction of large amounts of granitizing solutions at somewhat lower temperatures. The former possibility seems more likely because to the west outside the granitized area, rocks of the sillimanite-almandine subfacies showing exceptionally large sillimanite crystals are associated with gabbroic intrusives (D. Wyckoff, personal communication); and in the main granitized area, numerous pre-granitization gabbroic intrusives do occur (Postel, 1940). In either case, the orthoclase-kyanite gneiss survived only where the introduction of granitizing solutions occurred on a comparatively small scale.

There is also the question whether granitization has produced all microcline-bearing rocks in the region, or whether some were formed directly from intrusive igneous magmas. Postel (1940, p. 131, 134, 143), although considering most of the rocks in this area to be formed by granitization, distinguished the Springfield aplite and the Ridley Park granodiorite as true magmatic rocks, corresponding to the fine-grained type of microcline gneiss and the muscovite-garnet gneiss, respectively, of this paper. He based his opinion upon the cross-cutting relationship which they show locally toward the enclosing microcline gneiss. The writer has re-examined the type locality at Springfield Quarry (locality 29), where the "aplites" cross-cut the microcline gneiss. The schistosity (S_1) within the "aplite dikes", as marked by biotite flakes, parallels that of the adjacent enclosing microcline gneiss rather than the walls of the "dikes". This is confirmed under the microscope in a small "dike" (Pl. 2, fig. 3) as well as by its fabric. Replacement by the granitizing solutions has changed the mineralogical composition, but has not obliterated the foliation of the original schist. The writer interprets the fine-grained type (Postel's "aplite", represented by chemical analysis II, Table 1) as a fairly advanced granitized schist and suggests that these "aplites" may represent beds having mineral composition and perhaps also texture which rendered them unusually susceptible to attack by granitizing solutions. The muscovite-garnet gneiss (Postel's "Ridley Park granodiorite"), described by Postel (1940, p. 134, 149) as having "predominance of muscovite over biotite" (which is "brown"), lacking "the pronounced replacement textures", and containing "accessory garnet which occurs in small but constant amounts", is interpreted as a less granitized portion of the mica schist. Disequilibrium is indicated by the occurrence of almandine in presence of microcline.

Granitization apparently was taking place

during the main period of deformation. (See section on fabric analyses.) Significance of cross-cutting relationships in such rocks is uncertain. Many recent investigators have pointed out the ability of migmatites to flow and the deceptive similarity in appearance between some replacement and intrusive dikes (Jung and Roques, 1938; Roques, 1941; Holmes, 1946; Read, 1948b; Goodspeed, 1948; Ramberg, 1949). It is also now generally accepted that pegmatites and allied dike rocks are commonly formed by replacement at temperatures below the range of liquid magmas.

Hydrothermal (Retrograde) Metamorphism

Hydrothermal activity has played a considerable part in metamorphism in the Philadelphia region. Among the most conspicuous instances are some sporadic chloritization of the Wissahickon schists, and serpentinization and steatitization of the ultrabasic intrusives associated with the schists. Of the same nature, and possibly of the same period, is muscovitization of the orthoclase-kyanite gneiss.

These late muscovites, though perhaps nearly simultaneous, appear to be of two generations: an earlier porphyroblastic one, and a later one composed of confused, felted fibers growing around and into the former, in a fashion strikingly similar to that of kyanite needles penetrating feldspars. This relation suggests that the earlier porphyroblastic muscovites are perhaps pseudomorphs after orthoclase and the later felted ones pseudomorphs after "needle" kyanite. According to Goldschmidt (1921), hydrolysis of K_2O-feldspar leads to formation of muscovite and releases K_2O. In the presence of water, the K_2O so released could react with kyanite present in the immediate neighborhood and again lead to formation of a later muscovite (Billings, 1937 p. 299). Muscovite replacing sillimanite and kyanite (blade-type) is also common (Pl. 2, fig. 4). Muscovite-quartz gneiss is the ultimate result of this reaction.

There has been the question of source of water for hydrothermal metamorphism in general. Granitization, involving conversion of micas into feldspars, sets free considerable amount of molecular water. (See the equations and Table 3.) Thus hydrothermal activity has been observed as allied phenomenon of granitization in numerous places.

Megascopic Structure

Folds

The major regional structure is thought to be a syncline, exposed width of about 10 miles.

Apart from some small-scale flow folds (ptygmatic folds), the complex folds of the region are entirely of the flexure-slip type. They range from large folds measuring 100 feet or more from crest to crest down to crenulations of half an inch apart, which are superposed on minor folds of intermediate size. In most cases, the folds are open and asymmetric or slightly overturned, with axial planes dipping at about 55° NNW to W. A series of such folds can be seen along the railroad cut north of Roseglen Quarry (half a mile north of locality 4) and in a good many places along Wissahickon Creek. Where minor folds are developed on the more gently inclined limbs, the axial planes of both minor and main folds are parallel or subparallel. On the vertical limbs, the minor folds appear to be recumbent, with axial planes nearly horizontal (Pl. 1, locs. 52, 54, 55, 120).

The smallest crenulations are drag folds developed in micaceous layers lying between quartzose or amphibolitic layers. They obey the competency law and can be used to determine direction of overturning. The attitudes of the axial planes of the crenulations are determined by the amount of relative slipping between the layer in which they lie and the adjacent competent layer, and therefore differ in different parts of the fold. In the case of folds as complicated as those in this area, the attitudes of the axial planes of the crenulations and minor folds are in many cases only indirectly related to the axial planes of the major folds. The fine crenulations record deformation extending into ruptural stage, for the micas show not only bending but also breaking; this results in a fracture cleavage (S_3) discussed later.

Flow folds (ptygmatic folds) are generally developed only on a small scale. Throughout the region as a whole, folded quartzose or

amphibolitic layers commonly maintain a nearly uniform thickness in different parts of a fold, and even the incompetent micaceous layers lying between them do not show appreciable amounts of thickening near axes and thinning on limbs. Transport of material within any fold has evidently been limited. This fact, together with the lack of true flow folding on a large scale, may indicate that the rocks have never attained a highly plastic stage of deformation. Flow folds are perhaps connected with local concentration of percolating hydrothermal or granitizing solutions which would tend to increase plasticity. Flow folding thus has no regional structural significance in the present area and has not been investigated petrofabrically.

Throughout most of the area, the folds are all overturned to the southeast or east, with axial planes dipping northwest or west. But in a narrow zone, less than half a mile wide, to the north, schistosity regularly dips steeply southeast (70° to nearly vertical); axial planes of folds are rarely seen. This anomalous zone of apparent northward overturning could be perhaps interpreted as the result of beds being pushed northward against and over the rigid block of Baltimore gneiss as indicated by the fault (a reverse fault, with extensive mylonitization) along the northern boundary (Pl. 1). Alternatively (Weiss, 1949), a major synclinal structure might be inferred. This would also be asymmetric—with folds on the southern flank overturned comparatively gently toward the southeast (axial planes largely dipping about 55° NW) and beds on northern flank steeply (perhaps isoclinally) folded and overturned toward the northwest (Fig. 4). All flexure-slip folds in the area can thus be attributed to one simple mechanism: crustal shortening in combination with a horizontal couple, under high temperature and high confining pressure.

S-Surfaces and Lineations

Field measurements of various structural elements, respectively designated as S-surfaces (S_1, S_2, S_3 and S_4), lineations (*a* and *b*), and axial planes and axes of folds, are plotted both on the structural map (Pl. 1) and on a series of orientation diagrams (Pl. 6, Diagrams 88-94).

All workers in the Philadelphia area think that the most conspicuous foliation in the Wissahickon schist represents the original bed-

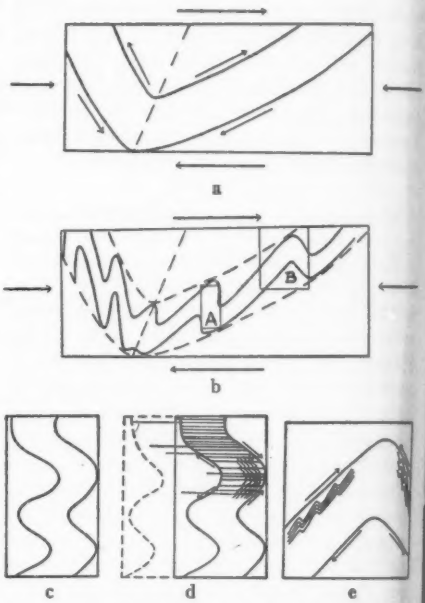

FIGURE 4. HYPOTHETICAL RECONSTRUCTION OF THE DEVELOPMENT OF THE FLEXURE-SLIP FOLDS IN WISSAHICKON SCHIST.

a. First stage. Inferred asymmetric major syncline with axial plane dipping toward NW. b. Second stage. Development of folds on both flanks, showing overturning both toward NW and SE. c. Section A of Fig. b. Second stage. Vertical limbs thrown into minor recumbent folds. d. Section A of b. Third stage. Development of crenulations and fracture cleavage. Note that fracture cleavage extends into the adjacent quartz schist. e. Section B of Fig. b. Third stage. Development of crenulations and fracture cleavage on both limbs of open fold.

ding. One evidence of this is perhaps that the anorthite content of plagioclase in the mica schist layer is usually higher (e.g. specimen 12, Table 9) than that in the adjacent quartz schist layer separated from the former by S_3. In rocks with foliation otherwise originated (e.g. segregation banding), feldspars in different compositional bands have uniform composition (Turner, 1941). Though chemical equa-

EXPLANATION OF DIAGRAM

Diagram Number	Specimen and Locality	No. of Readings	Mineral or Structure	Contour in Per Cent	Rock Type
1	20	87 (all available)	large muscovite	0-1-7-13-18-26-40 (47)	Mica Schist
2	20	204	medium muscovite	0-1-3-6-12-19 (20)	Mica Schist
3	20	204	small muscovite	0-1-2-4-6-8-9 (10)	Mica Schist
4	20	327	collective muscovite	0-1-3-5-9-12-13-16 (18)	Mica Schist
5	20	175	medium biotite	0-1-2-3-6-10-18-23 (25)	Mica Schist
6	20	208	small biotite	0-1-2-3-6-10-15 (19)	Mica Schist
7	20	292	collective biotite	0-1-2-3-7-9-12-19 (20)	Mica Schist
8	20	288	quartz	0-1-2-3-4	Mica Schist
9	20	Synoptic diagram of 1-7			Mica Schist
10	20	Correlation of quartz maxima			Mica Schist
11	12	176	large biotite	0-1-3-6-10-12-16-19 (20)	Mica Schist
12	12	116	medium biotite	0-1-3-4-5-9-10-11 (12)	Mica Schist
13	12	199	small biotite	0-1-2-3-4-6-8	Mica Schist
14	12	350	collective biotite	0-1-2-3-4-7-8 (9)	Mica Schist
15	12	212	quartz	0-1-2-3-4-5 (6)	Mica Schist
16	12	198	medium biotite	0-1-3-5-9-14 (18)	Quartz Schist
17	12	198	small biotite	0-1-2-3-4-5-7-8-9 (10)	Quartz Schist
18	12	365	collective biotite	0-1-2-3-6-10 (11)	Quartz Schist
19	12	204	quartz	0-1-2-3-5	Quartz Schist
20	12	Synoptic diagram of 11-13, correlation of quartz and mica fabrics			Quartz Schist
21	12	Synoptic diagram of 16, 17, correlation of quartz and mica fabrics			Quartz Schist
22	90	204	muscovite	0-1-2-3-4-5-8 (10)	Mica Schist
23	90	204	biotite	0-1-2-3-4-6-8 (10)	Mica Schist
24	90	204	quartz	0-1-2-3-4-6	Mica Schist

M = muscovite, Bi = biotite, Ml = large muscovite, Mm = medium muscovite
Ms = small muscovite, Bl = large biotite, Bm = medium biotite, Bs = small biotite
Q = quartz, Qdef. = deformed quartz, Qcor. = corroded quartz, Qa, b, = quartz maximum a or b
Hb = hornblende.
g = gneiss.
d = "dike".

——————— megascopic S_1, S_2, S_3
——————— Slip plane corresponding to main maximum of micas
– – – – – – – Slip plane corresponding to sub-maximum of micas
– – – – – – – – Slip plane corresponding to small submaximum of micas
——————— Slip plane corresponding to quartz maximum
– – – – – – – – Slip plane corresponding to maximum of deformed quartz
– – – – – – – – Slip plane corresponding to (100) of hornblende
– · – · – · – · Slip plane corresponding to (110) of hornblende

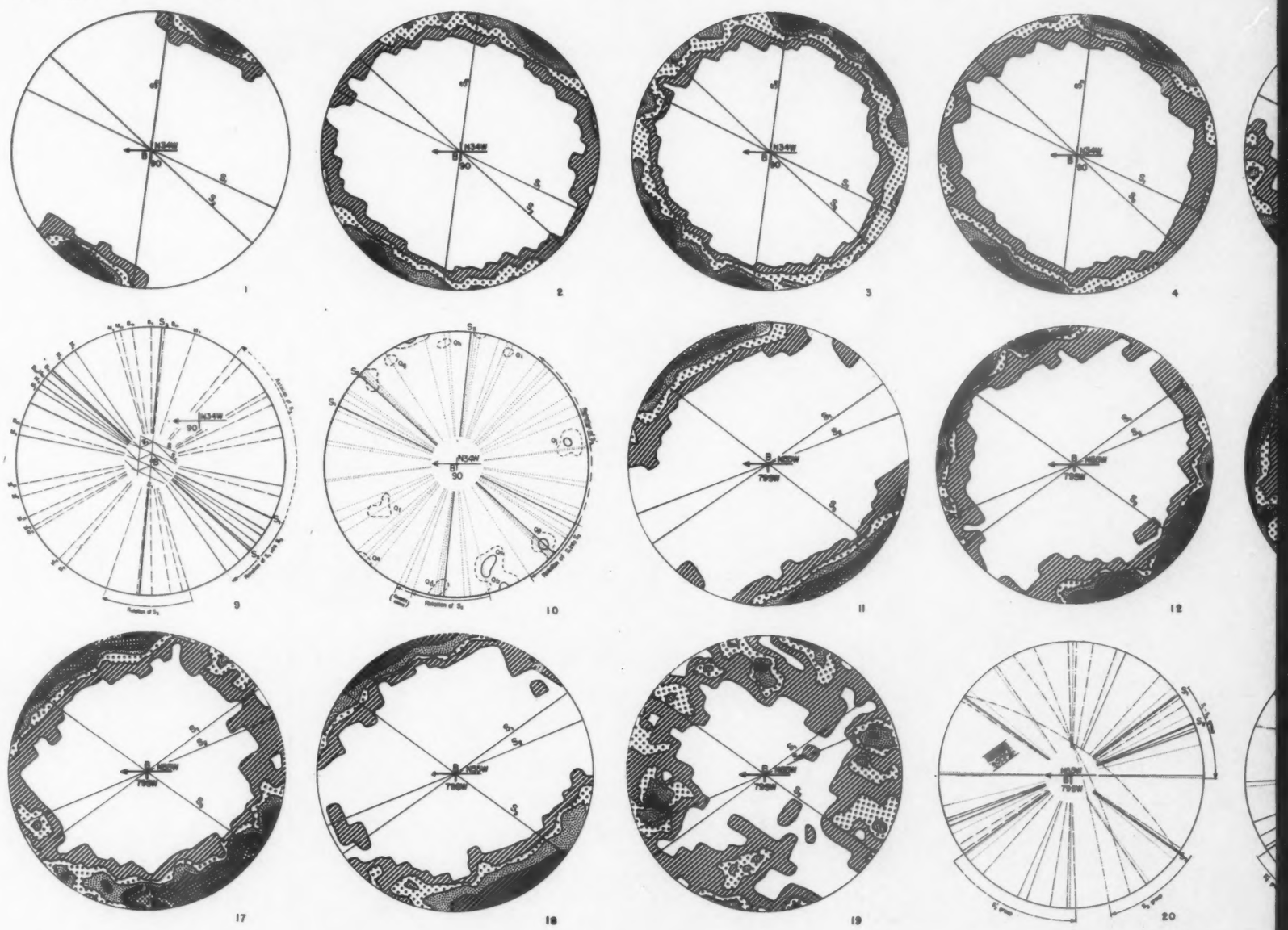

FABRIC DIA

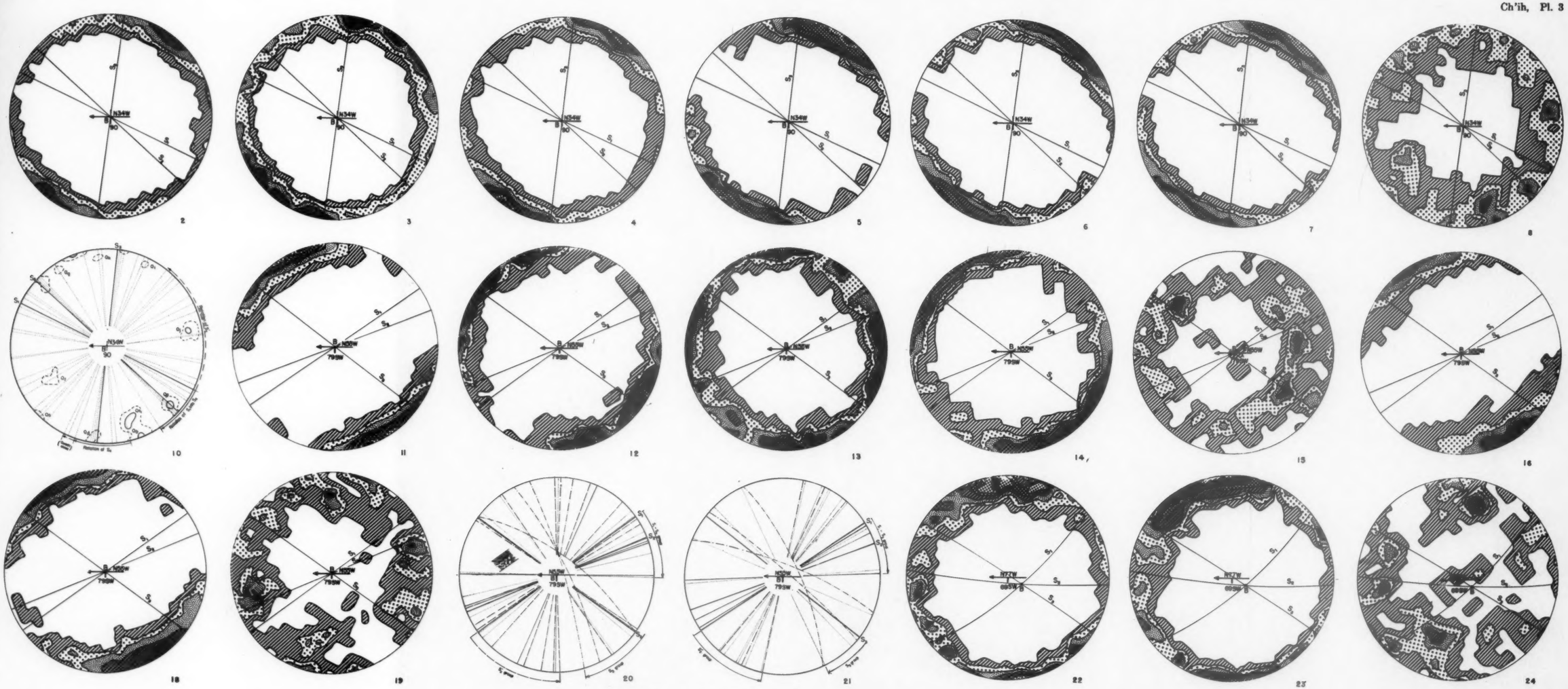

FABRIC DIAGRAMS

li
in
c
t
A
p
(
n
b
b
f
c
i
a
s
a
c
d
v
a
n
a
c
f
o
t
s
t
f
t
c
t
h
l
i
h
a
t
h
t
c
s
o
s
C
c
S
d

librium has been nearly reached in each individual bed during rock metamorphism, exchange of materials between beds is thought to have been extremely slow and insignificant. Also, the structures of the region confirm the principle, which was first emphasized by Sander (1930), that there is a tendency for slip movements (accompanied by recrystallization) to begin along mechanically weak surfaces such as bedding already present in the rock. S_1 therefore represents a type of bedding schistosity.

Cloos and Hietanen described S_2 as flow cleavage or axial plane cleavage, and succeeded in distinguishing in the field a faint flow cleavage making an angle of 10°–20° with the bedding schistosity (S_1), but their interpretation of this as axial plane cleavage does not seem applicable to the Wissahickon schist of the Philadelphia region. As a result of the present investigation, including field observation as well as fabric analyses, the writer believes that the mineral orientation in S_2 is a result of slipping and recrystallization along one set of limbs of crenulations (drag folds). Since these drag folds, like the large folds, are asymmetric, one limb commonly makes a smaller angle with the bedding (S_1) than the other does, and these surfaces of mechanical weakness, subparallel to S_1, have served to localize movements during folding of the S_1 surfaces. S_2 thus represents a type of flow cleavage, but not an axial plane cleavage.

In micaceous layers in which the crenulations are well-developed, S_2 can be traced throughout the crenulations. In the psammitic layers on the other hand, crenulations are lacking, and S_2 is a weak megascopic cleavage, which however is sharply revealed by fabric analysis as the best developed S-surface of mica orientation.

Development of the S_2 cleavage in the Wissahickon schist near Philadelphia is to be contrasted with the appearance of axial plane cleavage (also termed S_2) at a corresponding stage of deformation in the Octoraro phyllite of Pennsylvania and equivalent Wissahickon schist in the region in Maryland described by Cloos and Hietanen (1941). Perhaps the deciding factor of the mode of development of S_2 is the difference in mechanical response to deformation of the coarse-grained, laminated micaceous rock (in present area) and the finer-grained, relatively homogeneous rock investigated by Cloos and Hietanen.

S_3 is a planar structure parallel to the axial planes of the small crenulations, showing no evidence of recrystallization. Instead, the micas are broken at the axial part of the crenulations, so that S_3 may be regarded as a fracture cleavage. S_3 is especially conspicuous in the micaceous layers associated with recumbent minor folds on vertical limbs of larger folds; here closely packed S_3-surfaces extend into adjacent psammitic layers (Fig. 4d).

S_4 occurs at a few localities as a gently inclined structure parallel to the axial planes of the crenulations in micaceous layers. In some hand specimens, it forms the only schistosity; in the field, it can be seen to transgress bedding marked by lithological change. S_4 appears to have been formed by extensive recrystallization along S_2 (fracture cleavage), and so may be described as a flow cleavage. This recrystallization was probably initiated by sub-horizontal shearing movements along the closely spaced parallel surfaces (S_3); in this sense S_4 represents shear cleavage. Displacements however are on a microscopic scale and no recognizable shear folds have been formed (Pl. 2, figs. 5, 6).

What is perhaps another kind of shear cleavage is developed in the mylonite zone along the northern boundary fault. If the steeply dipping beds were isoclinally folded, the shear cleavages would be developed along axial planes of the folds as well as parallel to bedding schistosity (S_1). Under microscope the limbs of the crenulations are seen to be actually sheared off along the schistosity. This fault zone deserves a special study but is outside the scope of this paper.

Axial planes and fold axes: The axial planes of the folds dip on the average about 55° NW. Fold axes of minor folds are parallel to those of the larger folds with which they are associated; it is unnecessary to postulate more than one main period of deformation. The folds plunge toward both ends; in any given fold the axis plunges gently in the middle part, more steeply and in opposite directions near the ends (Cloos and Hietanen, 1941, p. 157). However, the steeper plunges are toward the Northeast ends of most folds, indicating that the regional

structure as a whole plunges in that direction (Pl. 6, Diagram 88).

Lineations: The main lineation (*b*-lineation) on bedding schistosity (S_1), is defined by Cloos and Hietanen (1941) as crinkling and intersection of cleavages and bedding parallel to B, the axis of rotation and folding of contemporary folds. In the micaceous layers the mica crenulations (from which S_2 and S_3 are derived) are commonly curved surfaces (as where they are bent around porphyroblasts), so that these lineations are not straight lines. E. M. Anderson (1948) has lately called lineation of this kind the Tummel type and claims that it is parallel to *a*, the direction of slip movements during deformation. However, there is every reason to believe that the lineation here, though it has all the characteristics of the Tummel type, is parallel to *b* (B), and therefore perpendicular to *a*. The *a* lineations in the present area are most common in highly crushed zones.

In Table 4 the respective degrees of development of the recognizable S-surfaces and lineations in various rocks of the Wissahickon formation in the present area are summarized.

Analysis of Field Data

In Diagram 88, fold axes and *b*-lineations for the whole area are plotted into an equal area net (projection is on the lower hemisphere) and contoured. The number of readings is perhaps too small to warrant definite detailed conclusions, but the diagram suggests some general relationships. That the trend of folding swings from N50°E to NS is indicated by a continuous elongated belt of 4%–6% concentration, containing one main maximum (14%) and two sub-maxima (7%). The main maximum brings out the predominant trend of fold axes (about N38°E). As a whole, the northward plunges average 16° and southward ones 4° (as shown by the positions of the maxima). This bears out the earlier observation that though the folds plunge toward both ends (as shown by the incomplete girdle pattern), the steeper plunge is generally northward. The appearance of only two isolated areas (1% and 2%) in the center of the diagram shows that steep lineations and fold axes are of only minor importance in this area.

The linear structures of the granitized southern area and the ungranitized northern area, are plotted separately for comparison (Pl. 6, Diagrams 89, 90). The diagrams suggest that the changing regional trend from the northern area to the southern area is continuous. In Diagram 89, steep lineations still appear unimportant.

The poles of all recorded S_1 planes are plotted in Diagram 91 (Pl. 6). The three maxima, I (10%), II (6%), and III (6%), designate three groups of folds. Maximum II appears to represent the comparatively gently inclined limbs (dipping 40° NW) of a series of asymmetric to slightly overturned folds. The second limb, vertical to slightly overturned, is indicated by the 3% area which encloses maximum II and extends to the margin of the diagram. This group demonstrates the major southward overturning and the attitude of the folds in the northern part of the area under discussion. The group of folds represented by maximum concentrations (4% and 6%) near the margin of the diagram correspond to folds with one limb dipping about 76° W; the poles corresponding to the other limb are rather scattered and fail to show as a maximum in the diagram. This group of folds commonly occurs in the southwestern part of the area. The remaining group indicated by the main maximum (I), represents very gently dipping limbs probably mostly those of recumbent minor folds. The apparent high concentration is perhaps due to the fact that the recumbent minor folds are commonly associated with both of the other two groups of folds and also that both limbs of the recumbent folds give similar field readings.

S_1 planes of the granitized and ungranitized areas respectively, plotted separately for comparison (Pl. 6, Diagrams 92, 93), show that the folding in the granitized area conforms to the general regional pattern, with perhaps a greater concentration of poles corresponding to maximum III on Diagram 91. This probably reflects the fact that folds trending NS (Diagram 89) and overturned to the east are more common in the southwestern part of the region.

In Diagram 94 (Pl. 6) poles of S_2 and S_3 are plotted with different symbols. Readings are too scanty to bring out any strong preferred orientation, but S_2 and S_3 strike generally

TABLE 4.—DEVELOPMENT OF S-SURFACES AND LINEATIONS IN DIFFERENT ROCK TYPES OF WISSAHICKON FORMATION

Types of Rocks		S_1	S_2	S_3	S_4	*b*-lineation	*a*-lineation	Remarks
Wissahickon Schist	Mica Schists	good	fairly good to poor	good		good		
	Quartz Schists	good	fairly good to poor			good		
	Plagioclase gneisses	fairly good to poor						
Springfield Microcline gneisses		good	wanting or very poor			wanting or very poor		gradations to those of mica schists represented
Kyanite orthoclase gneisses		good				wanting or very poor		S_1 being segregation banding
Sheared mica schist		good			good	good	?	S_1 marked by lithologic changes
Crushed rocks		good		poor		poor	good	*a*-lineation in addition to other structural elements of corresponding rock types

Northeast. More poles of S_3 fall in the NW sector of the diagram; this may indicate that S_3-surfaces commonly dip in the opposite direction from the axial planes of major folds.

A hitherto unpublished diagram (Pl. 6, 95) made by A. Postel and kindly contributed to this study shows the poles of 253 joint surfaces measured in the granitized area which he investigated (1940). The combined two main maxima (4%) suggest that the predominant joints are cross joints normal to fold axes (NS in the granitized area), and also indicate that these fold axes statistically are about horizontal.

This statistical analysis confirms the generalizations as to attitude of folds (Figure 4) based on observation on discontinuous outcrops.

PETROFABRIC ANALYSIS

Preliminary Statement

The objects of fabric study were to reconstruct the general movement picture of deformation affecting the Wissahickon schists; to analyze the rock fabrics modified by granitization; to date the periods of granitization and

of late hydrothermal activity; and to recognize the nature of late local tectonic disturbances subsequent to granitization.

Five specimens of Wissahickon schists, five of microcline gneisses, three of orthoclase-kyanite gneisses, and two representing special structures (i.e. one with S_4, and the other highly crushed) were analyzed. Mica and quartz were measured in all specimens; hornblende—(110) cleavage—in one specimen only.

All diagrams represent the lower half of the sphere of projection. The plane of projection is in every case nearly normal to *b* (the principal lineation); synoptic diagrams, in which quartz and mica fabrics are correlated, represent a combination of several partial diagrams each of which has first been rotated into the plane normal to *b*. The geographic orientation of each diagram is shown by a strike and dip symbol at the center; the bearing of strike given by an arrow (a symbol $\left[\begin{smallmatrix}\leftarrow\text{N60W}\\ |\\ \text{80N}\end{smallmatrix}\right]$ indicates that N60W is toward the left). The concentration-percentage per unit area was counted at every centimeter intersection, and near a maximum at every half-centimeter intersection. The mica diagrams show the distribution of poles of (001) cleavages; the acute bisectrices were directly plotted for those micas with (001) making less than 35° angles with the plane of thin section. The quartz diagrams show the distribution of c-axes, and the hornblende diagram, of poles of (110) cleavages.

Three distinct types of fabric were recognized: (1) R-tectonite fabrics (the main type) shown by all typical schists and granitized schists; (2) S-tectonite fabrics, representing the highly crushed equivalents of the above rocks; (3) $B_1 \wedge B_2$-tectonite fabrics in sheared schists having S_4.

In the R-tectonites, the fabric diagrams for different mineral constituents of one specimen have a common fabric axis *b* (B) which is also the axis of folds in the locality where the specimen was taken (homotactic fabric, Sander 1930, p. 144–145). B axes statistically determined from the fabric diagrams are plotted on Plate 1. There is petrofabric evidence that during deformation planar structures, correlated with the megascopically visible S-surfaces (S_1, S_2 and S_3), have been rotated to various degrees around the *b* (B) axes of the fabric. The rotations are evident in mica, quartz, and probably also hornblende orientations. The orientation diagrams of R-tectonites also show another group of planar structures, here denoted as S_2', which like S_2 is related to the fine crenulations observed in the field. S_2 represents the direction of the longer, normal limbs of these crenulations; S_2' corresponds to the direction of the shorter, perhaps overturned, limbs (inset sketch, Pl. 3, Diagram 9). In the field, the position of S_2' can be recognized in some cases, but recrystallization has not been sufficient to produce a flow cleavage parallel to this plane.

The S-tectonite type represents laminar slip upon one set of parallel S-planes. The $B_1 \wedge B_2$-tectonite type perhaps depicts superposition of two unrelated movements.

Fabrics of the Wissahickon Schist

Mica Fabric.—Interpretation of mica fabric is possible only if the sequence of crystallization of mica is established.

Sequence of Crystallization of Mica: Two fundamental rules seem to govern crystallization of micas in the Wissahickon schists: (1) Mica tends to be oriented parallel to the S-surfaces in the rock, (2) Mica tends to decrease in size as recrystallization continues.

In conformity with the first rule, micas oriented along S_1 are usually cut across by those oriented along S_2 or S_2'; and trains of mica oriented along S_3 usually transgress all other micas oriented along S_1, S_2, or S_2'. In conformity with the second rule, micas of the S_1 group are usually large and bent, those of the S_2' group are of medium size, and those of the S_3 group are small. Since S_2 served continuously as the most efficient slip surfaces throughout the period of deformation and recrystallization, large, medium, and small micas, believed to represent successive stages of crystallization, are all found parallel or subparallel to S_2.

Two exceptions to the rules complicate interpretation of the time sequence of crystallization of micas: (1) S_1, being the oldest slip surface, still remained active in some rocks when rotation of S-surfaces was already greatly ad-

TABLE 5.—MICA PARAGENESIS OF WISSAHICKON SCHISTS

Relative abundance	S group	Size	Mica1	Mica2	Mica3
predominant mica	S_1	large medium small	bent or not		
	S_2	large medium small	rotated into S_2	X X	 X
	S_2'	large medium small		X	
	S_3	large medium small			 X
subordinate mica	S_1	large medium small	 X X	X X X	rare X X
	S_2	large medium small		 X	rare X
	S_2'	large medium small		X X	rare X X
	S_3	large medium small			rare X
period of crystallization	pre-deformation para-deformation post-deformation		X X	X	X ?

vanced; or in other cases S_1-surfaces became intensified by mimetic crystallization of micas parallel to S_1 after movement upon S_1 had completely died out. Thus micas oriented parallel or subparallel to S_1 may occasionally be found to cut across those parallel or subparallel to S_2, S_2', or even S_3. Similar exceptions are found in the cases where mica has continued to crystallize in S_2 and S_2' after development of S_3; (2) Although the oldest micas (S_1 group) are usually large and bent, some medium-sized and small undeformed flakes may also be of the same age. Similarly some late micas of the S_3 group are very large. Such modifications also occur in the S_2 and S_2' groups.

Reconstruction of the history of crystallization of mica in the various S-surfaces of the Wissahickon schist must therefore be based on statistical analysis of the relative frequency of large, medium, and small, and of bent or undeformed flakes in each group of S-surfaces (Table 5). The actual sizes of large, medium, and small micas are recorded in Table 9.

In many rocks muscovite and biotite have crystallized alternately. Consistently however, the earliest mica of the S_1 group and the latest one of the S_3 group are both muscovite, as

pointed out by Cloos and Hietanen (1941, p. 151). It therefore seems that the recrystallization of muscovite generally started earlier and lasted longer than that of biotite.

The relation between the period of crystallization and the period of deformation can be tentatively determined on the basis of petrographic criteria (Table 5). Large, bent (cataclastic) micas are pre-deformational, but syntectonic micas are difficult to distinguish from those of post-deformational mimetic growth. Microscopic observation of mica arches and rolled garnets indicating syntectonic crystallization may help in some cases (Knopf, 1933), but it is not certain that micas ($mica_{s\ and\ 2}$) located elsewhere beyond such an arch have the same age as the critical syntectonic flakes on and under the arch. There is evidence that some micas ($mica_3$) are later than these, and therefore may be post-deformation. Similarly, there is no proof that all $mica_3$ (or even $mica_2$) had ceased to crystallize before garnet appeared. Therefore paracrystalline garnets cannot be used to date micas.

PROCEDURE: Separate partial diagrams have been prepared for large, medium, and small muscovite and biotite, and have also been combined as collective diagrams. Planes corresponding to main maxima, submaxima, and small submaxima in the partial diagrams for each specimen analyzed have been grouped into S_1, S_2, S_2', and S_3 and plotted with different symbols in a separate diagram (synoptic diagram) to be correlated with the quartz fabric. Data on length and width of girdles and height of maxima are listed in Table 6.

Length of girdle is measured in degrees, 360° representing a complete girdle. The width of girdle is also measured in degrees and represents the difference between the radius of the projection circle and the average radius of the area of zero concentration. The degree of preferred orientation is thus inversely proportional to the width of girdle. Cloos and Hietanen (1941, p. 41) use width where the present writer uses length. Although it is regrettable to introduce confusion into the terminology, the change seems desirable, for the girdle (as projected upon a sphere) is actually an elongated area, its maximum length being that of a great circle (360°) in the case of a complete girdle; its dimension at right angles to the length should then logically be designated as width.

ANALYSIS OF A TYPICAL MICA FABRIC: Specimen 20 (Pl. 3, Diagrams 1–10) was taken from the normal limb of a minor fold overturned toward the north. Measurements made in the field were: S_1, strike N 64°E, dip 26°SE; S_2, strike N 61°E, dip 42°SE; S_3, strike N 58°E, dip 84°NW; and *b*-lineation, trend N 58°E, plunge 2°SW.

Strictly speaking, there is not really any mica maximum on S_1. Movement began by slipping on S_1, as shown by the large muscovites, but most of these large muscovites have already been slightly rotated out of the S_1 plane by incipient crenulation, as shown (Diagram 1) by the somewhat elongated character of the fabric pattern, and by the fact that the center of the maximum is not exactly at right angles to S_1. This rotation (deviation from the normal to S_1) amounts to about 6° (clockwise). Similar small rotations appear consistently in many other specimens analyzed, and thus cannot be regarded as the result of accumulated errors from various possible sources.

S_2 and S_2' arose by continued bending of the original S_1 surfaces, together with recrystallization promoted by further slipping movements on the limbs of the crenulations so formed. This is shown (Diagram 2, prepared for medium muscovites) by the elongation of fabric pattern into a continuous girdle of 1% to 2% with several submaxima. The main maximum shows a further rotation of S_1 into what is now more correctly described as S_2—a rotation (clockwise) of about 8° from the position of the main maximum in Diagram 1, or 14° from the original position of S_1. The submaxima are weaker; but it appears that two of them (6% and 7%) are associated with S_2'. If more grains had been measured, these two submaxima would probably have coalesced into one. It is to be expected that the maximum of S_2' should be less well defined and more rotated (in the opposite sense) than that of S_2 at the same stage of crenulation. It appears that S_2' has been rotated (counter-clockwise) about 33°–49° from the original position of S_1, or 41° if these represent a single submaximum. The remaining sub-

TABLE 6.—LENGTH AND WIDTH OF MICA GIRDLES AND HEIGHT OF MAXIMA (WISSAHICKON SCHISTS AND THE GRANITIZED EQUIVALENTS)

Rock type	Specimen number	Diagram number	Mineral	Length of girdle (degrees)				Average width of girdle (degrees)	Height of main maxima (per cent)
				1%		3%			
				continuous girdle	discontinuous girdle	continuous girdle	discontinuous girdle		
Mica Schist	20	1	Ml	104		104			47
		2	Mm	352		208	234	14	20
		3	Ms	360		360		19	10, 8
		4	Collective muscovite	360		212	260	19	18
		5	Bm	290		152		16	25
		6	Bs	328		168	190	19	19
		7	Collective biotite	336		182		19	20
Mica schist layer		11	Bl	212	237	156	168	26	20
		12	Bm	347		228	240	26	12
		13	Bs	360		146	306	25	8
	12	14	Collective biotite	360		240	252	25	9
Quartz schist layer		16	Blm	258		158	172	27	17
		17	Bs	360		172	290	27	10
		18	Collective biotite	280	324	164		24	11
Mica Schist	90	22	M	360		178	238	24	10
		23	Bi	360		174	250	24	10
Mica Schist	44-43	26	M	352		250	262	19	14
		27	Bi	356		304		24	9
Plagioclase Gneiss	77	31	M	360		140	252	38	7
Microcline Gneiss Porphyroblastic Type	29	35	Bl	348		64	203	30	7
		36	Bs	356		106	198	30	6
		37	Collective biotite	360		62	228	31	5
Microcline Gneiss Intermediate Type	26	40	M	286	318	144		28	14
		41	Bi	360		172	198	27	9
Microcline Gneiss fine-grained type	30	45	Bi	360		144	292	28	9
Microcline Gneiss	72	50	Bl	212		160		20	25
		51	Bms	336		134	146	29	12
		52	Collective biotite	336		156	168	29	13
Microcline Gneiss muscovite garnet type	123	56	M	360		128	310	22	8
		57	Bi	360		184	284	27	7

TABLE 6.—*Continued*

Rock type	Specimen number	Diagram number	Mineral	Length of girdle (degrees)				Average width of girdle (degrees)	Height of brain maxima (per cent)
				1%		3%			
				continuous girdle	discontinuous girdle	continuous girdle	discontinuous girdle		
Orthoclase kyanite gneiss	84	60	Ml	276	324	170		37	8
		61	Ms	348		192	224	37	8
		62	Collective muscovite	348		180		37	8
		63	Bl	352		152		38	8
		64	Bs	338		132	178	28	8
		65	Collective biotite	350		156	184	28	8
Orthoclase kyanite gneiss	82	69	Bi	360		108	130	43	8
Orthoclase kyanite gneiss	S-39	72*	M, Bi	264	328	140		19	10
		73†	M, Bi	216	288	132	132	36	6

* gneiss portion.
† "dike" portion.
M—muscovite
Ml—large muscovite
Mm—medium muscovite
Ms—small muscovite
Bi—biotite
Bl—large biotite
Bm—medium biotite
Bs—small biotite

maximum is very weak (only 3%), but its position (consistent in all specimens analyzed) indicates that it is significant and probably reflects incipient recrystallization on S_3. The tendency for S_3 to develop into a flow cleavage shown in fabric has also been noted by Cloos and Hietanen (1941, p. 165).

Continued rotation of all these planes is shown by small muscovite (Diagram 3). The small muscovite has a more complete girdle, with the main maximum split into two or perhaps three parts, and several submaxima. The height (9% to 10%) of the main maxima is much reduced as compared with that in diagrams of large or medium muscovites. By the time the latest of the small muscovites crystallized, S_2 had apparently rotated (clockwise) about 30° from the original position of S_1; S_2' had rotated about 70° (counter-clockwise); and S_3 had rotated about 35° (clockwise) from the position it had when it first appeared. The fabric relations of the muscovites are summarized in Figure 5.

The biotite diagrams 5 and 6 agree with the movement plan illustrated by muscovite diagrams. Large muscovite seems to be the earliest; medium biotite appeared at about the same time as medium muscovite, and was followed by small biotite; and probably small muscovite continued to crystallize latest of all (Diagram 9). The collective diagrams (4 and 7) give all essential characters of the partial diagrams, though many small submaxima fail to show.

INTERPRETATION OF MICA FABRIC: The maxima in all the mica diagrams fall into four fairly well marked groups corresponding to S_1, S_2, S_3, and S_2'. The angular relations between these elements, i.e., $(S_2 \wedge S_1) < (S_2' \wedge S_1)$ and $(S_2 \wedge S_3) < (S_2' \wedge S_3)$, and their directions of rotation shown in the fabrics are what would be expected in the asymmetric crenulations (drag folds) with reference to the larger folds with which they are associated in the field. Each one of these groups of S-surfaces in the fabric was rotated as the crenulations became progressively sharper (Figure 5). This is interpreted as reflecting progressive overturning of the minor folds, and presumably the major folds also. Obviously the rotation of the S-surfaces on the two limbs of a fold must occur in opposite directions. The direction of rotation on the normal limb of an overturned

	Height of brain maxima (per cent)
	8
	8
	8
	8
	8
	8
	8
	10
	6

the same
followed
nuscovite
(Diagram
) give a
diagrams,
o show.
RIC: The
into four
ing to S_1
s between
$\wedge S_1$) and
rections of
hat would
enulations
rger folds
the field.
ces in the
ns became
is is inter-
turning of
the major
n of the
fold must
irection of
overturned

EXPLANATION OF DIAGRAM

Diagram Number	Specimen and Locality	No. of Readings	Mineral or Structure	Contour in Per Cent	Rock Type
25	90	Synoptic diagram of 22, 23, correlation of quartz and mica fabrics			Mica Schist
26	44-43	250	muscovite	0-2-4-6-8-9-10 (14)	Mica Schist
27	44-43	200	biotite	0-1-2-3-5-8-9	Mica Schist
28	44-43	300	hornblende	0-1-2-3-4-5-6 (7)	Mica Schist
29	44-43	250	quartz	0-1-2-3-4-5 (6)	Mica Schist
30		Synoptic diagram of 26, 27, correlation of quartz, hornblende and mica fabrics			Mica Schist
31	77	198	muscovite	0-1-2-3-5-6 (7)	Plagioclase gneiss
32	77	204	quartz	0-1-2-3-4 (5)	Plagioclase gneiss
33	77	148 (all available)	large quartz	0-1-2-3-5 (6)	Plagioclase gneiss
34	77	Correlation of quartz and mica fabrics			Plagioclase gneiss
35	29	204	large biotite	0-1-2-3-5-7	Microcline gneiss, porphyroblastic type
36	29	204	small biotite	0-1-2-3-4-5-6	Microcline gneiss, porphyroblastic type
37	29	273	collective biotite	0-1-2-3-4-5	Microcline gneiss, porphyroblastic type
38	29	198	quartz	0-1-2-3-4-5 (7)	Microcline gneiss, porphyroblastic type
39		Synoptic diagram of 35, 36, correlation of quartz and mica fabrics			Microcline gneiss, porphyroblastic type
40	26	204	muscovite	0-1-2-3-4-5-8-12 (14)	Microcline gneiss, intermediate type
41	26	204	biotite	0-1-2-3-4-6-8 (9)	Microcline gneiss, intermediate type
42	26	204	undeformed quartz	0-1-2-3-5 (7)	Microcline gneiss, intermediate type
43	26	80 (all available)	deformed quartz	0-1-3-4-6 (9)	Microcline gneiss, intermediate type
44	26	238	collective quartz	0-1-2-3-4-5 (7)	Microcline gneiss, intermediate type
45	26	Synoptic diagram of 40, 41, correlation of quartz and mica fabrics			Microcline gneiss, intermediate type
46	30	204	biotite	0-1-2-3-4-6-8 (9)	Microcline gneiss, fine grained type
47	30	224	quartz	0-1-2-3-4	Microcline gneiss, fine grained type
48	30	115 (all available)	deformed quartz	0-1-2-5-6 (7)	Microcline gneiss, fine grained type

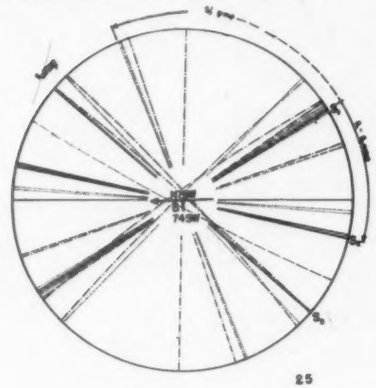

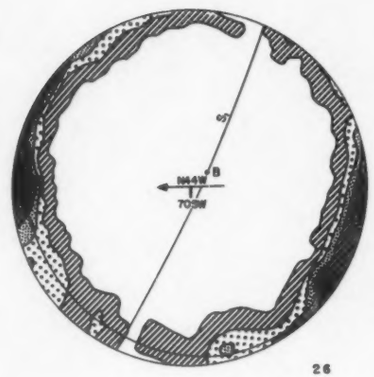

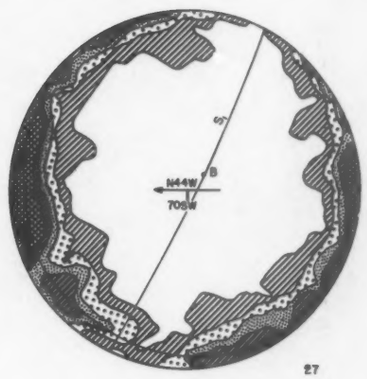

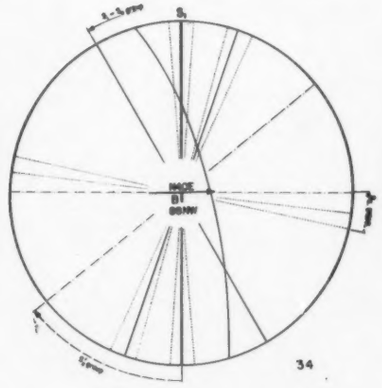

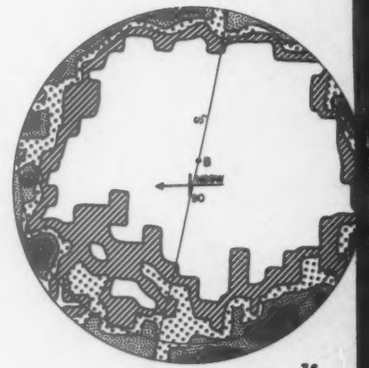

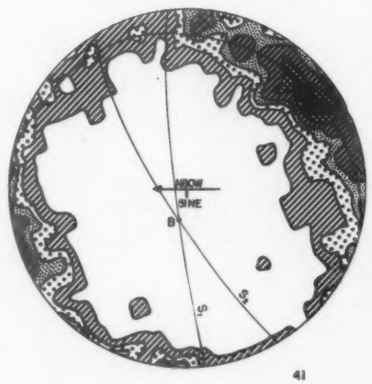

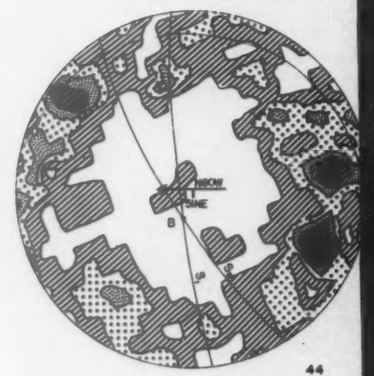

FABRIC

See Plate 3

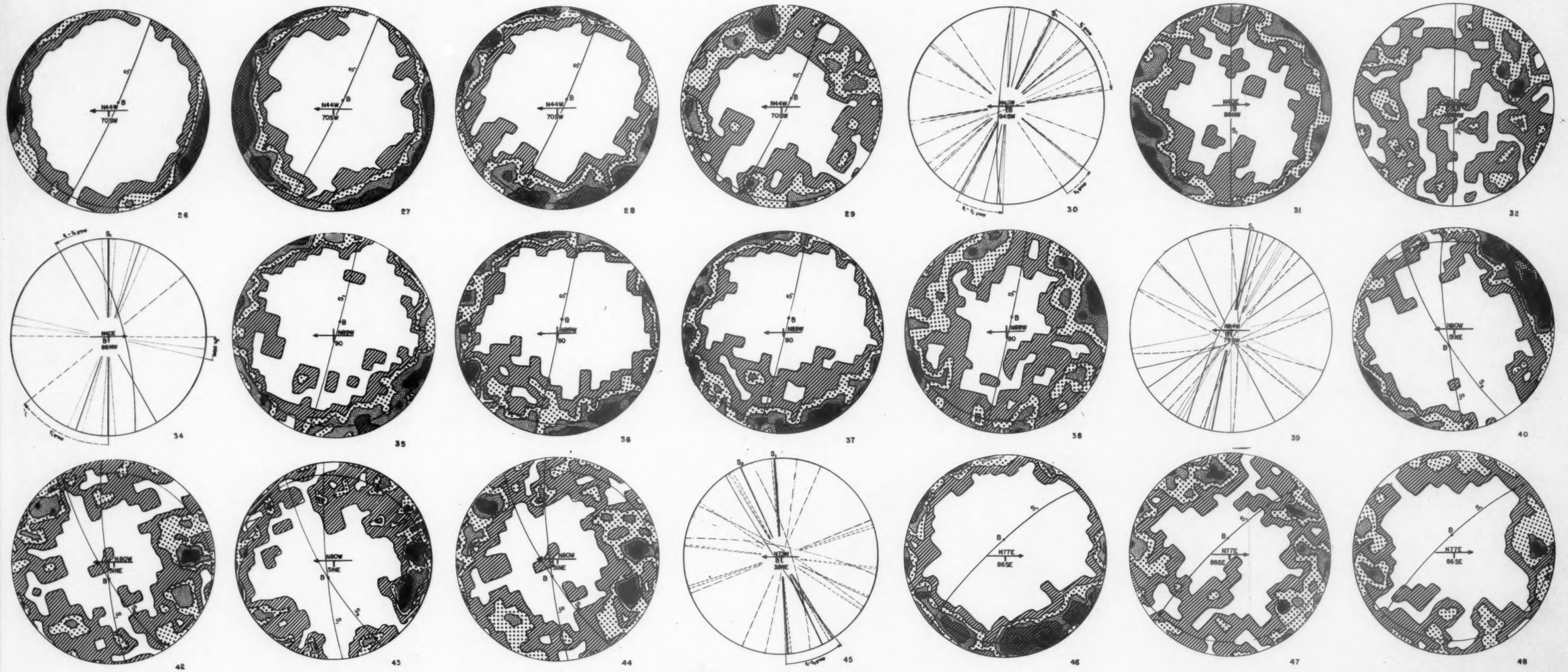

FABRIC DIAGRAMS

See Plate 3 for abbreviations

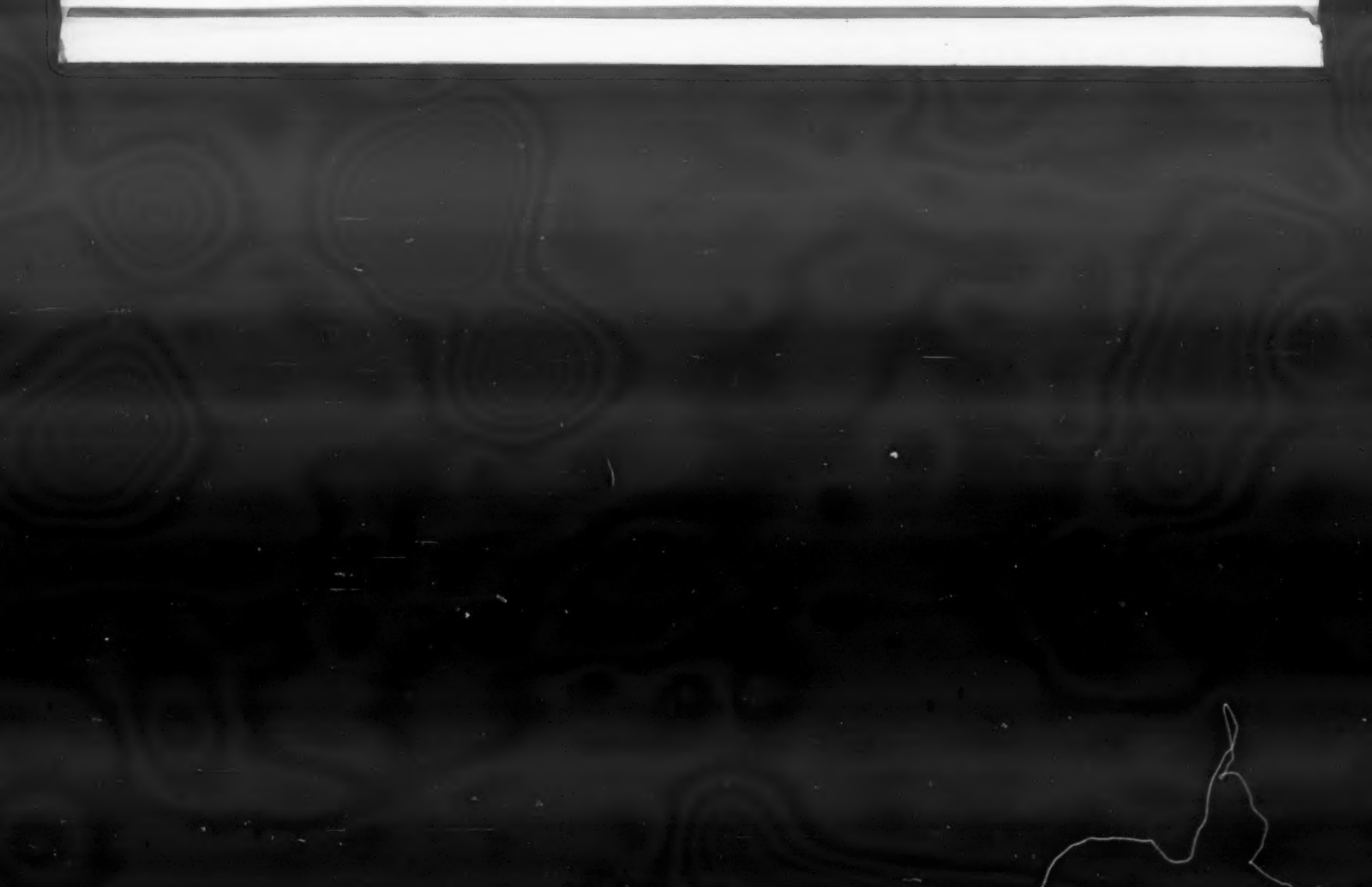

fold is the same as the direction of rotation on the inverted limb of a fold overturned in the opposite direction, as may be seen by comparing Diagram 9, which represents the rotation on the normal limb of a northward-overturned fold, and Diagram 21, which represents the rotation on the inverted limb of a southward-overturned fold. Therefore, direction of regional overturning cannot be deduced from direction of rotation observed in the fabric without considering the attitude of the bed from which the specimen came.

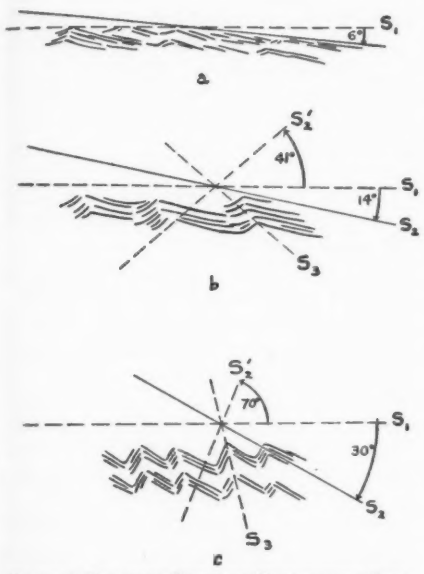

FIGURE 5. RELATION BETWEEN PROGRESSIVE FOLDING (CRENULATIONS) AND ROTATION OF S-SURFACES SHOWN IN MICA FABRICS (SPECIMEN 20).

a. Slight bending of original S_1-surfaces; recorded in fabric diagram of large muscovite. b. Development of bent S_1-surfaces into asymmetrical microfolds, the limbs of which form new surfaces of slip, S_2 and S_2'; recorded in fabric diagram of medium muscovite. S_3 represents the axial plane of folds, but no true cle...age is yet developed on S_3. c. Sharp folding of crenulations, with further rotation, in opposite directions, of S_2 and S_2'; recorded in fabric diagram of small muscovite. S_3 now appears as incipient axial plane cleavage.

The movement picture is easy to reconstruct in the case of mica schist in which the fabric can be correlated with S_1, S_2 and S_3 observed in the field. As shown in the next section, the picture in quartz schist is essentially the same. S_2 is not visible in every outcrop. In the microscopic fabric, S_2 (like S_2' and S_3) is found to be a group of obliquely intersecting S surfaces, not a single well defined plane. The S_2 surface measurable in the field is usually that formed during the period of biotite crystallization and therefore megascopically more conspicuous.

The mica fabrics of all the schists studied show that maxima on the poles of S_1 surfaces are rare; that almost all main maxima are related to S_2; that submaxima predominate in the S_2' group; and that small submaxima form the S_3 group. This indicates that slipping movements on S_2 surfaces (in preference to S_2') were the most effective and have controlled development of the main flow cleavage. S_3 is in some cases very conspicuous in the field as a fracture cleavage. This is consistently associated, in the fabric, with weak submaxima (3% to 4%) and may be interpreted as an incipient flow cleavage, which is in keeping with the results obtained from quartz fabrics. Cloos and Hietanen (1941, p. 165) reached a similar conclusion.

The maxima of large mica show the least rotation away from S_1 and are the earlier members of the S_2 group. The number of maxima of medium mica corresponding to S_2 or S_2' is greater than that corresponding to S_3, but the maxima of small mica are more numerous in S_3. The S_2 group is characterized by maxima of micas of all three sizes. Also connected with this size-age relation of micas is the completeness of girdle and the height of main maxima. Large micas form only an incipient girdle and the maxima are high; medium micas form a good girdle, with maxima of medium height; small ones form a perfect girdle with low maxima (Table 6). These facts are interpreted to mean that, as deformation proceeded, the rock was provided with increasing numbers of slip surfaces for the later micas. Possibly, too, many late micas oriented along earlier S-surfaces grew by mimetic crystallization.

The mica fabric of the Wissahickon schist shows a single B-girdle (R-tectonite, probably representing one act of deformation). The fabric has monoclinic symmetry for it possesses a single plane of symmetry (*ac*-deformation plane) normal to the *b*-axis of the fabric. Of the samples of mica and quartz schists analyzed,

each one was taken on a limb of a fold. Therefore, within the field of investigation, each fabric appears homogeneous. The fabric of the plagioclase gneiss (specimen 77) with large feldspars shows inhomogeneity, apparently influenced by the mineralogic environment in the rock.

Quartz fabric.—Quartz occurs in the schists (1) as inclusions in plagioclase, garnet, and micas; (2) as veins in many cases parallel to one of the S-surfaces in the rock; and (3) as metamorphically recrystallized quartz, which far predominates over the other two types. The *Si* fabric of the quartz inclusions has not been studied. Cloos and Hietanen (1941, p. 173–174) have made a special study on the syntectonic and post-tectonic quartz veins in the schists.

The predominant type of quartz has been completely recrystallized over a long period, which outlasted even that of the latest type of mica ($mica_3$). Cloos and Hietanen (1941, p. 178 and Table 20) have also noted this. As (Table 5) $mica_3$ may have recrystallized by mimetic growth after deformation, recrystallization of some of the latest quartz may also be post-tectonic. Unfortunately, it is impossible to distinguish such quartz from early quartz for the purpose of making partial diagrams.

In mica schists, quartz grains are dimensionally oriented along S_1, S_2, S_2', or S_3, though always to a less degree than in the crushed rocks. The relative proportion of deformed quartz grains showing undulose extinction as compared with undeformed grains is much lower in the schists than in the granitized rocks. Also the number of undulous bands in individual grains from schists seldom exceeds three, whereas in the granitized rocks it reaches 7 or 8. The bands in any one grain are approximately parallel to the *c*-axis of the quartz, but commonly are inclined to the length of the elongated grains.

General Nature of Quartz Diagrams: The diagrams depicting preferred orientation of quartz in selected rocks are all similar, showing *ac* girdles each with several maxima—some on the periphery of the girdle, others on small circles (cleft-girdle type). No obvious symmetry can be detected between individual maxima and individual S-planes or fabric axes. The symmetry of the quartz fabric as a whole is monoclinic, with a single symmetry plane parallel to *ac*. The heights of main maxima range between 4% and 6%.

Methods of Correlation of Quartz and Mica Fabrics: Quartz and mica fabrics of each analyzed specimen can be correlated satisfactorily if two assumptions are made: (1) Orientation of quartz was controlled by the same rotating S-surfaces as controlled development of the mica fabric. (2) Quartz oriented with respect to a given S-surface may show concentration of optic axes in one or more of the eight possible positions (Pl. 6, Diagram 96) summarized by Fairbairn (1939, p. 1478, Fig. 4) on the basis of the fracture hypothesis of Griggs and Bell (1938).

The quartz diagram, rotated if necessary so that *b* is in the center, is superposed concentrically on the key diagram (Diagram 96). The quartz diagram is then rotated around the common center until one quartz maximum lies over one of the maxima of the key diagram; the line of *ab* plane of the key diagram is now traced, representing a possible S-plane associated with that quartz maximum. For instance, four possible S-planes—one corresponding to maximum I, one to V and two to II of the key diagram—can be drawn for any maximum which lies on the periphery of the quartz diagram. Whenever the position of the possible S-plane so determined coincides with an actual S-plane revealed by the synoptic mica diagram of the same rock, it is assumed that this particular plane has actually functioned in controlling the orientation of the quartz. For the sake of clarity, S-planes corresponding to mica and quartz maxima are shown separately for specimen 20 (Diagrams 9, 10). For each of all other specimens these two sets of S-planes appear in one synoptic diagram.

This procedure is similar in principle to that used by Cloos and Hietanen (1941, p. 168–169).

Analysis and Correlation of a Typical Quartz Fabric: The quartz diagram for specimen 20 (Pl. 3, Diagram 8) is typical of quartz diagrams for the schists in general. Diagram 10 (Pl. 1) contains all possible S-planes indicated by the quartz fabric, using the procedure described. Table 7 sets out the possible correlation of observed quartz maxima (Q_a, Q_b etc.) of Diagram 10, with observed mica maxima

TABLE 7.—CORRELATION OF QUARTZ AND MICA FABRICS
(Specimen 20. Data from diagrams 9 and 10)

S-planes from mica maxima (Diagram 9)	Theoretical (Fairbairn, 1939) and observed quartz maxima (Diagram 10)									
	I	II	III	IV	V	VI	VII	VIII	Total	%
S_1-S_2 group, proceeding in direction of rotation										
S_1 (original posit.)					XQi					
M_1		X*Qb*		X*Qj*					12	24
Ms				X*Qc*						
Mm = Bm	?	?		?	?					
Bs (=S_2)	X*Qa*				XQe					
Ms					XQe					
Ms	XQg									
S_2-group, in direction of rotation										
Ms		XQi		XQi						
Mm	?	?		?	?					
Bm	XQh	X*Qa*		X*Qa*					18	36
Bs		?		?						
Bm (=S_2)	XQd	XQe				XQf				
		XQg								
Ms	XQi	X*Qb*		X*Qc*						
S_2'-group, in direction of rotation										
Bm		XQg		XQg		XQf				
Ms		X*Qa*			XQd					
Mm		XQe			XQh					
Ms	?				X				20	40
Mm					X*Qb*					
Ms		XQi		XQi						
Bs					?Qg		XQf			
Ms	XQe	XQd			X*Qa*					
Bs	XQe			XQj	X*Qa*					
Using all maxima — Total	10	14	0	11	12	2	1	0	50	100%
Using all maxima — %	20	28	0	22	24	4	2	0	100%	
Using only good correlations — Total	7	11	0	8	9	2	1	0	38	
Using only good correlations — %	18	29	0	21	24	5	3	0	100%	
Using only 4% maxima — Total	1	4	0	5	3	0	0	0	13	
Using only 4% maxima — %	8	31	0	38	23	0	0	0	100%	

Note: Symbol (X) indicates a really good correlation.
Symbol (?) indicates the nearest possible correlation.
Symbols (Qa), (Qb) etc. refer to maxima shown on Diagram 10; *italicized* ones represent 4% maxima.

(Ms_1, Mm_2 etc.) and observed S-surfaces (S_1, S_2 etc.) in the same rock, assuming identification of the quartz maxima as belonging to types I–VIII of Fairbairn. Comparing Diagram

10 with the synoptic Diagram 9 of mica, and with Table 7, shows correlation of quartz and mica fabrics to be satisfactory. Twenty-one S-planes are indicated by mica maxima, among which only three cannot be correlated with quartz (Table 7). Table 7 also shows that one slip plane in the rock may cause simultaneous orientation of quartz by several different mechanisms (e.g. in the bottom horizontal row, Bs is correlated with three maxima Qa, Qe and Qj). On the other hand, one quartz maximum may be the result of orientation, simultaneously or successively, by one or more mechanisms related to several S-planes within the rock, e.g. Qb (II) is related to both Ml and Ms; or Qb (II, V) to Ml, Ms and Mm of different S-groups. This may illustrate in some cases how a main quartz maximum (e.g. Qb) has been formed. It also could account for the tendency for a number of maxima, all of relatively low concentration, to be present in quartz diagrams of B-tectonites in general. Diagram 10 reveals several S-planes (indicated by the quartz fabric), which are later than the latest one indicated by the mica fabric; perhaps because quartz records the latest deformation in the rock.

This correlation although compatible with Griggs and Bells' hypothesis of quartz orientation dependent on alinement of fractured splinters in S-planes of slip—does not depend on acceptance of any hypothesis of a quartz-orienting mechanism. Sander, Fairbairn, and others have noted the tendency for quartz to be oriented in various ways (maxima I–VIII) in relation to observed S-surfaces. In the present case, the S-surfaces presumed to have been effective in controlling quartz orientation have been reconstructed on the assumption that they may be any of types I–VIII. All the prominent maxima and the great majority of submaxima can be correlated with types I, II, IV and V, which incidentally are the maxima most commonly recorded in S-tectonites. This strengthens the case for this correlation.

Conclusions: Of the five specimens studied, the highest, also the commonest, maximum observed is of 6% concentration. Except maxima III and VIII, all other theoretical ones occur, IV being the commonest. Deformation of quartz apparently may be related to any of the S-groups, perhaps more frequently to later ones. Though S_2' is not a megascopic cleavage, and maxima representing this group are generally small and scattered in mica fabric, it appears important in quartz fabric. This suggests that quartz is more strongly deformed in layers which contain less mica. The correlation of quartz with mica is so good that in the majority of cases, all the quartz maxima present can be satisfactorily correlated. It is notable that the data in Table 8 on plagioclase gneiss differ appreciably from the rest. In fact the fabric of the plagioclase gneiss is similar to those of microcline gneisses. It is believed that this is due to the similar mineralogical environment of these two last-mentioned rock types, in which quartz is deformed in a matrix relatively poor in micas.

Further notes on fabrics of Wissahickon.—The remaining specimens of mica schist analyzed are in general similar to specimen 20, as regards preferred orientation of mica and quartz, and will therefore be discussed much more briefly. Data on these are given in Tables 6 and 8.

Mica Schist and Quartz Schist (Specimen 12, Pl. 3, Diagrams 11–21): The specimen was taken on the inverted limb of a southward overturned fold, with megascopically recognizable S_1, S_2, and S_3 (Pl. 1). The rotation of the corresponding S-groups in the microfabric is clockwise. The specimen includes a layer of mica schist in contact with one of quartz schist, both being represented in the thin section. Although the quartz schist appears nearly massive, S-groups may be recognized in the microfabric and correspond closely with megascopically visible S-surfaces in the mica schist from which the field readings were taken (Diagrams 20, 21). S-surfaces of the S_1–S_2 group expressed by the main maxima in mica diagrams for quartz schist, are closer to S_1 (original position) than in the mica schists. It would appear that rotation of S-surfaces in the quartz schist may have been relatively retarded because of comparative deficiency of mica. The size-age relationship reflected in the change in length of girdle and height of maxima (Table 6) conforms to that proposed for specimen 20. S_2' appears to have influenced strongly the orientation of quartz in the quartz schist (Table 8).

TABLE 8.—CORRELATION OF QUARTZ MAXIMA
(Wissahickon schists and the granitized equivalents)

Rock type	Specimen number	Diagram number	Height of main maximum	Quartz maxima							Most related slip surfaces	Total no. of quartz maxima	Quartz maxima which cannot be correlated	
				I	II	III	IV	V	VI	VII			No.	Per cent
Mica schist	20	8, 10	4	x	x		x	x	x	x	S_1, S_2	9	0	0
Mica schist	12	15, 20	6	x	x		x	x	x	x	equally all	8	1	12
Quartz schist	12	19, 21	5	x	x		x	x	x	x	S_2'	10	1	10
Mica schist	90	24, 25	6	x	x		x		x	x	S_1, S_2	4	0	0
Mica schist	44-43	29, 30	6		x		x	x			S_2, S_3	4	0	0
Plagioclase gneiss	77	32, 33, 34	6						x		S_1, S_2', S_3	6	2	33
Microcline gneiss (Porphyroblastic type)	29	38, 39	7				x		x		S_2	5	0	0
Microcline gneiss (Intermediate type)	26	42, 45	7				x				S_3 ?	3	1	33
		43*, 45	9		x		x	x			S_3 ?	10	3	30
Microcline gneiss (Fine-grained type)	30	47, 49	4		x		x		x	x	S_3	7	2	29
		48*, 49	7		x		x				S_3	4	0	0
Microcline gneiss stringer	72	53, 55	5		x		x		x		?	3	1	33
		54*, 55	6	x	x		x				?	9	2	22
Microcline gneiss (Muscovite-garnet type)	123	58, 59	5				x	x	x	x	S_2, S_2'	6	0	0
Orthoclase-kyanite gneiss	84	66, 68	7	x	x		x	x			S_2, S_3	5	0	0
		67†, 68	7		x		x		x		S_2, S_3	3	0	0
Orthoclase-kyanite gneiss	82	70, 71	4				x		x	x	?	2	0	0
Orthoclase-kyanite gneiss	S-39	74‡, 76	6				x		x		S_2	3	0	0
		75§, 76	7		x		x		x		S_2	3	0	0

* Quartz with multiple undulatory extinction bands.
† Corroded quartz associated with myrmekite.
‡ Fabric made for the gneiss portion.
§ Fabric made for the "dike" portion.
x Indication of the presence of a maximum.
x Indication of the presence of the commonest maximum.

MICA SCHIST (SPECIMEN 90, PLS. 3, 4, DIAGRAMS 22–25): In the field this specimen shows only S_1 and a faint *b*-lineation on S_1 (readings shown on Pl. 1). S_2 and S_3, as shown on the diagrams, are microscopically visible, and make rather large angles with S_1 (i.e. are sharply micro-folded). The orientation diagrams indicate S_1, S_2, and S_3 groups rather closely packed

TABLE 9.—MODES OF GRANITIZED AND UNGRANITIZED SCHIST WITH FABRIC ANALYSES

Rock type		Mica schist	Mica schist layer	Quartz schist layer	Mica schist	Mica schist	Plagioclase gneiss	Microcline gneiss, porphyroblastic type	Microcline gneiss, intermediate type	Microcline gneiss, fine-grained type	Microcline gneiss	Microcline gneiss, muscovite-garnet type	Orthoclase-kyanite gneiss	Orthoclase-kyanite gneiss	Orthoclase-kyanite gneiss		Crushed mica schist	Mica schist with S_4
															Gneiss portion	"Dike" portion		
Specimen and Locality No.		20	12	12	90	44–43	77	29	26	30	72	123	84	82	S-39	S-39	30–260	46
Quartz		46	13	28	37	58	70	13	44	30	35	32	38	46	45	33	44	41
Orthoclase													13	9	3	21		
Microcline								16	12	20	29	18	1			tr.		
Plagioclase		18	4	47	27	25	8	52	24	36	22	31	29	15	31	38	30	4
Anorthite Content		An_{28}	An_{14}	An_{28}	An_{22}	An_{30} An_{28}*	An_{15}	An_{22}	An_{28}	An_{22}	An_{23}	An_{22}	An_{22}	An_{24}	An_{21}	An_{21}	An_{21}	An_{19}
Myrmekite								6	1	3	7	2		tr.				
Muscovite		17		tr.	22	tr.	21	tr.	11	tr.	tr.	10	5		1	3	4	29
Biotite		18	80	24	13	4	tr.	11	7	10	6	6	12	23	17	4	20	25
Almandine		tr.				3	tr.		tr.			0.5		tr.	2		1	tr.
Kyanite													tr.	7	tr.	tr.		
Hornblende						6												
Epidote					1	1		1	tr.	tr.	tr.	tr.						
Sphene			tr.			1		1		tr.	tr.	tr.	tr.		tr.			
Apatite		tr.	1	tr.	tr.	tr.	tr.	tr.	tr.	tr.	tr.	tr.	tr.	tr.	tr.		tr.	tr.
Zircon		tr.		tr.	tr.	tr.	tr.	tr.	tr.			tr.			tr.	tr.	tr.	tr.
Chlorite						tr.											tr.	tr.
Tourmaline															tr.	tr.		tr.
Sericite						tr.	tr.									tr.		
Allanite					tr.													
Ore			2	tr.	tr.	1	tr.	tr.		tr.		tr.	1	tr.	tr.	tr.	tr.	1
Grain size (mm.)		.44	1.40	.63	.54	1.55 .29	.44 3.46	3.0	1.86	.57	1.05	.79	.45	.52	.19	.32	.19	.92
		.15	.38	.27	.25	.64† .19	.22 1.89‡	0.4	0.40	.31	0.59	.46	.26	.31	.10	.18	.08	.26
Size of Micas appearing in Fabric Analyses (mm.)	Large	.74	1.57					1.89			1.62		.68					
		.16	.42					0.39			0.44		.45					
	Medium	.42	.75	.71														
		.07	.17	.22														
	Small	.15	.27	.20				0.58			0.42		.15					
		.03	.06	.04				0.13			0.10		.03					

* Plagioclase in amphibolite layer.
† Almandine and hornblende porphyroblasts.
‡ Large quartz occurring as stringers.

together (Diagram 25). S_1 dips 48°NW; and the microfabric shows clockwise rotation in the direction S_1 to S_1 to S_2. Therefore the attitude of the bed may be inferred to represent the inverted limb of a southward overturned fold. The correlation of quartz maxima is good (Table 8).

MICA SCHIST (SPECIMEN 44–43, PL. 4, DIAGRAMS 26–30): The specimen shows faint asymmetric crenulations, but S_2 and S_3 were not measurable in the field. In the fabric diagrams, the positions of main maxima of both micas clearly indicate the presence of S_2', and the grouping shown in Diagram 30 is convincing. This corresponds to the normal limb of a fold overturned toward the south, as rotation from S_1 to S_2 to S_3 groups in the diagram is counterclockwise, and S_1 dips 72°NW in the field. The specimen contains a thin layer ($\frac{3}{4}$ inch) of amphibolite also represented in the thin section, Diagram 28 is prepared from poles of (110) cleavages of hornblende crystals, and these can be seen from microscopic inspection alone to be dimensionally oriented with the crystallographic c-axes (elongation) parallel to b (B) of the fabric. In Diagram 28 the maxima (three of 7% and one of 5%) form two pairs; the angle between the two maxima of each pair is about 56°. The

EXPLANATION OF DIAGRAM

Diagram Number	Specimen and Locality	No. of Readings	Mineral or Structure	Per Cent Contour in	Rock Type
49	30	Correlation of quartz and mica fabrics			Microcline gneiss, fine grained type
50	72	76 (all available)	large biotite	0-1-4-9-18-22 (25)	Microcline gneiss
51	72	164	medium and small biotite	0-1-2-3-4-8-11 (12)	Microcline gneiss
52	72	198	collective biotite	0-1-2-3-4-7-12 (13)	Microcline gneiss
53	72	204	quartz	0-1-2-3-4 (5)	Microcline gneiss
54	72	140 (all available)	deformed quartz	0-1-2-3-4-6	Microcline gneiss
55	72	Synoptic diagram of 50, 51, correlation of quartz and mica fabrics			Microcline gneiss
56	123	204	muscovite	0-1-2-3-5-7 (8)	Microcline gneiss Muscovite garnet type
57	123	204	biotite	0-1-2-3-5 (7)	Microcline gneiss Muscovite garnet type
58	123	204	quartz	0-1-2-3-4-5	Microcline gneiss Muscovite garnet type
59	123	Synoptic diagram of 56, 57, correlation of quartz and mica fabrics			Microcline gneiss Muscovite garnet type
60	84	174 (all available)	large muscovite	0-1-2-3-5-7-8	Orthoclase kyanite gneiss
61	84	170	small muscovite	0-1-3-4-7 (8)	Orthoclase kyanite gneiss
62	84	198	collective muscovite	0-1-2-3-4-5-7-8	Orthoclase kyanite gneiss
63	84	198	large biotite	0-1-2-3-4-5-6-8	Orthoclase kyanite gneiss
64	84	152	small biotite	0-1-2-3-5-7 (8)	Orthoclase kyanite gneiss
65	84	217	collective biotite	0-1-2-3-4-5-6-7 (8)	Orthoclase kyanite gneiss
66	84	234	quartz	0-1-2-3-4-6-7	Orthoclase kyanite gneiss
67	84	198	corroded quartz	0-1-2-3-5-7	Orthoclase kyanite gneiss
68	84	Synoptic diagram of 56, 57, 59, 60, correlation of quartz and mica fabrics			Orthoclase kyanite gneiss
69	82	198	biotite	0-1-2-3-6-7 (8)	Orthoclase kyanite gneiss
70	82	204	quartz	0-1-2-3-4	Orthoclase kyanite gneiss
71	82	Correlation of quartz and mica fabrics			Orthoclase kyanite gneiss
72	S-39	204	Mica (gneiss portion)	0-1-2-3-7-8 (10)	Orthoclase kyanite gneiss showing cross-cutting relationship

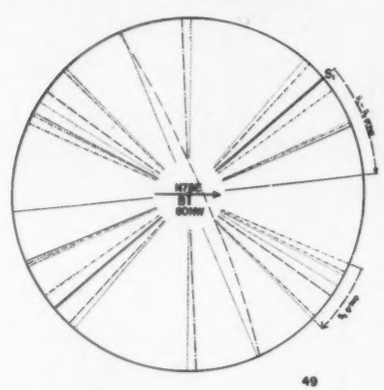

49

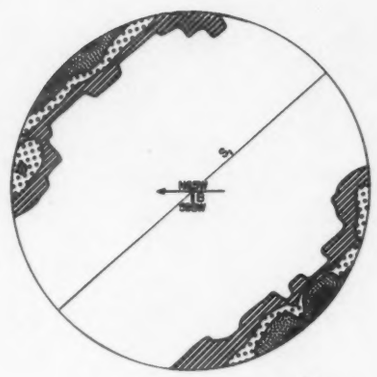

50

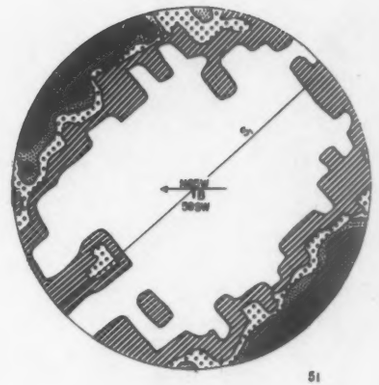

51

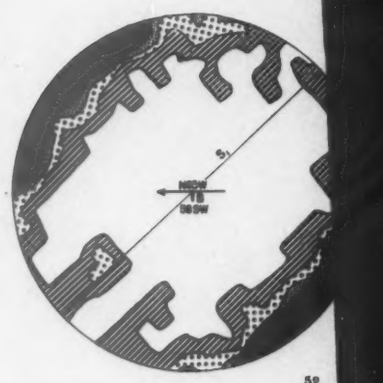

52

57

58

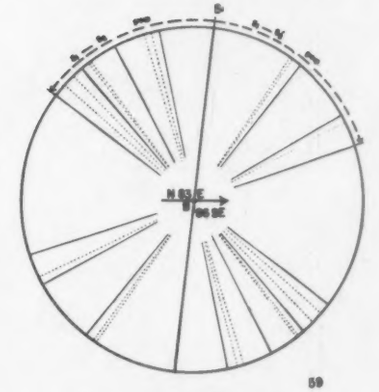

59

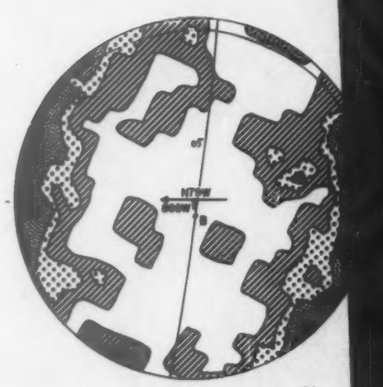

60

65

66

67

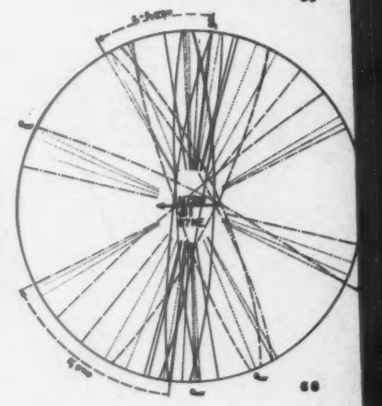

68

FABRI

See Plat

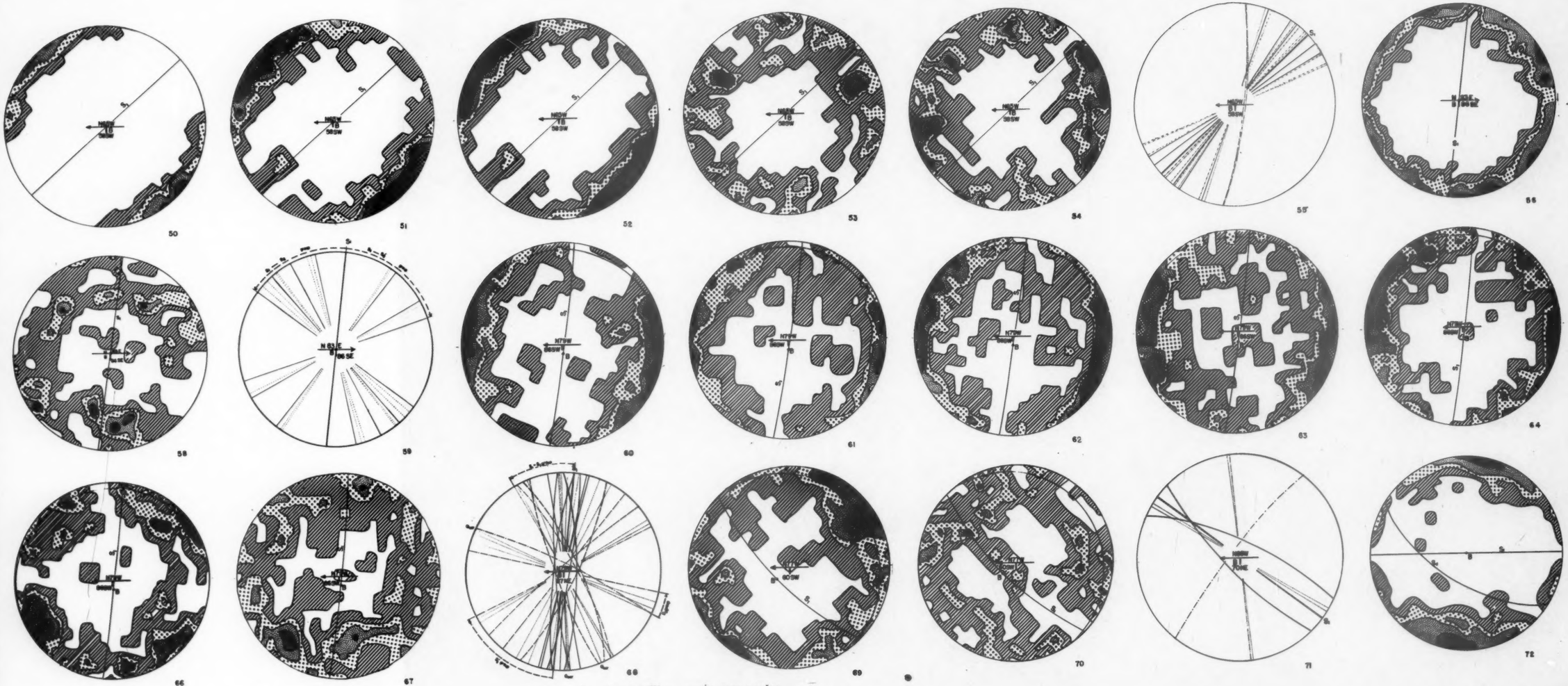

50 51 52 53 54 55 56

58 59 60 61 62 63 64

66 67 68 69 70 71 72

FABRIC DIAGRAMS

See Plate 3 for abbreviations

two bisectors of the obtuse angles between the maxima of each pair represent (100) of hornblende. Plotted on Diagram 30, these fall well within the range of S_2' group, and can be correlated with two S-planes in the rock, deduced respectively from a muscovite submaximum (cf. Diagram 26) and a quartz maximum (cf. Diagram 29). This correlation is based on the assumption that hornblende would tend to be dimensionally oriented with *c* (elongation) in the direction of *b* (B) of the fabric and at the same time with the (100) direction (flattening) in a S-plane of the rock (Sander, 1930). The alternative correlation based upon lattice orientation, assuming that hornblende slips on (110) cleavages (with *c*-axis parallel to b (B) of the fabric), seems equally possible. This would put two maxima in the group of S_1–S_2 (one coincides with S_1), one in the groups of S_2', and possibly one in S_2 group (Diagram 30). It is possible that hornblende has been oriented both dimensionally and according to space lattice, for the two slip planes deduced from the first hypothesis as being parallel to (100) almost coincide with two of the four slip planes inferred from orientation of (110). In either case, rotation of S-planes in the rock is indicated by hornblende orientation as well as by quartz and mica fabrics. The correlation of quartz maxima is excellent (Diagram 30, Table 8).

Plagioclase Gneiss (Specimen 77, Pl. 4, Diagrams 31–34): The plagioclase gneiss is a coarse-grained rock of pegmatitic appearance and possessing poor schistosity (S_1); lineation and other S-structures are hardly visible. The thin section was cut normal to *b* (B), as determined in the adjacent schist. Diagram 34 gives a possible grouping of S-planes, though the relative positions of the S_2 and S_2' groups are uncertain. The apparent increase in width of girdle (Table 6) resembles that shown by mica girdles of the granitized rocks. Occurrence of a single quartz maximum and the less satisfactory correlation of quartz are fabric characters also found in some microcline gneisses. Two separate Diagrams (32 and 33) prepared for the large (comparatively later) recrystallized quartz grains and the small grains respectively are similar.

Fabrics of Springfield Microcline Gneiss

Mica Fabric.—The microcline gneiss is typically rich in biotite but deficient in muscovite. Reconstitution and recrystallization of both micas are so complete that no relict mica referable to the original mica schist is recognizable, and it is therefore difficult to date recrystallization in terms of the various stages of deformation. However, even the largest biotites (on the average coarser than the largest in the schist) are rarely bent, and are not oriented along S_1, as are the bent $mica_1$ of the schist. Therefore, the biotite in the microcline gneiss is interpreted as having formed later than $mica_1$ of the schist. On the other hand, as discussed later, granitization was probably syntectonic, so that most of the biotites could not have crystallized later than $mica_2$ of the schist.

The rules used to determine the sequence of crystallization of mica in the schists cannot be applied here since there is no consistent age-size relationship, and S_1 in most cases is the only directly observable S-surface. In the microfabrics, the distinctness of the various S-groups varies in degree, and some uncertainty enters nto their interpretation.

Comparison of Mica Fabrics of Microcline Gneiss and Wissahickon Schist: Partial diagrams were prepared for micas of different sizes, when possible, to facilitate comparison with the partial diagrams made for the schists. The corresponding data on mica fabrics, together with those for the schists, are summarized in Table 6.

All the diagrams—like those for schist fabrics—show B-girdles and monoclinic symmetry. The asymmetric drag-fold pattern of the S-surfaces as described for the fabrics of the Wissahickon schists has been partially destroyed, most in the porphyroblastic type, less in the intermediate type, and least in the fine-grained and garnet-muscovite types. Principal differences in fabric, attributed to conversion of schist to gneiss are (Pls. 4, 5; Diagrams 35–59, Table 6): (1) The maxima do not always appear on the periphery of the projection circle. When planes corresponding to these maxima are used in synoptic diagrams, the intersections of the planes are scattered around *b* (B) instead of falling exactly on *b* (B). (2) The

rock cleavages—S_1 and S_2—are less distinct, as shown by the lowered heights of the main maxima. (3) The girdles are generally wider than those of the schists, and isolated areas within the zero girdle (the vacant field in the central part of the diagram) may appear. (4) Though lengths of girdle are comparable with schist, the rule that smaller micas make more complete girdles no longer holds true. In some rocks the micas are of rather uniform size, so that partial diagrams cannot be made on this basis. (5) The grouping of S-surfaces is very doubtful in the extreme case (porphyroblastic type). (6) Where such grouping seems clear, it is impossible to discern the angular relationships among the S-surfaces as in the schist fabrics.

Quartz Fabric.—Quartz occurs in microcline gneiss as (1) inclusions in the feldspar porphyroblasts; (2) small, round, corroded grains in close association with myrmekites; and (3), most abundant of all, large recrystallized grains, on the average much coarser than in the schist. Sometimes the coarse recrystallized quartz seems to have been formed by welding together several small grains, with boundaries detectable only under crossed nicols. It often shows multiple undulatory extinction bands (up to six or seven per grain) resulting from deformation evidently after recrystallization. The ratio of deformed to undeformed quartz is much higher in the porphyroblastic and intermediate types of microcline gneiss than in the schist. Large quartz apparently recrystallized after most of the biotites, perhaps also after all other minerals in the rock. Where these two minerals are in contact, quartz penetrates crystals of biotite, the margins of which typically have the appearance of worm-eaten leaves. Dimensional orientation of quartz in the microcline gneiss is poor.

Quartz Fabric and Its Interpretation: The quartz diagrams show B-girdles and monoclinic symmetry much as in the schists. Correlation of quartz fabric with the corresponding mica fabric, though less satisfactory than in the case of the schists (Table 8), suggests convincingly that the quartz fabric conforms to the movement plan indicated by the mica fabric (homotactic fabric) (Diagrams 39, 45, 49, 55, 59). In general quartz orientation seems best referred to S-surfaces of the S_3 group. In the commonest types of microcline gneisses—the porphyroblastic and the intermediate types—the height (7%) of main quartz maxima exceeds that of the highest observed in the schists; that (9%) of the deformed quartz with multiple undulatory extinction bands is still higher (Table 8). The deformed quartz can be correlated with the same set of S-surfaces in the rock as may be deduced from diagrams for undeformed quartz and for mica (See fabric of Specimen 26, Diagrams 40–45). These facts, as well as petrographic indications that quartz recrystallized late, suggest that granitization occurred during the main period of deformation, perhaps near its close.

Quartz grains having multiple bands of undulatory extinction parallel to the *c*-axis apparently show more pronounced orientation than unstrained quartz. However, the lattice orientation concerned appears to be unrelated to the direction of these bands; if the quartz had been oriented by slipping in the direction of the prism faces in any active S-plane in the rock, maxima of types I, VII or VIII would occur. In fact, maxima I and VII are extremely rare in diagrams for this kind of quartz and maximum VIII never occurs; maximum IV is consistently predominant (Table 8). It is possible that the lattice orientation developed first and that the undulatory extinction bands represent a later ruptural stage, when recrystallization declined.

In quartz fabrics of the microcline gneiss, as well as in those of the schist, maximum IV consistently occurs as the commonest maximum. In the microcline gneisses, however, this maximum tends to be the only important one and hence has greater height; in the schists, several other maxima may occur together in one quartz fabric (Table 8). This difference is interpreted as reflecting difference in respective mineralogical environments of these two types of rock, rather than difference in intensities of deformation, for other minerals do not show any greater amount of strain in the microcline gneiss than in the schist.

In quartz diagrams representing the fine-grained type, the muscovite-garnet type and a granitized stringer in the schist, maxima have lower heights. Maximum IV predominates only

in diagrams for deformed quartz. Here, as in corresponding mica diagrams, are points of resemblance to schist fabrics.

Fabric of a typical porphyroblastic microcline gneiss.—This sample represents the predominant type of microcline gneiss and illustrates the extreme of fabric evolution accompanying granitization of schist. Field readings are obtainable only on S_1 and *b*-lineation in S_1 (Pl. 1). Muscovite occurs only as a scanty accessory, so no partial diagrams for muscovite were made. The girdles defined by the large biotites (Diagram 35) and the small biotites (Diagram 36) are similar in character. Small biotites show a complete girdle of 1%, large ones an almost complete girdle (348°); the widths of both girdles are the same, and wider than in any of the schists except the plagioclase gneiss (Table 6). Isolated areas of 1%–2% within the zero girdle, perhaps indicating more or less random orientation of micas, appear only in the diagram of the large biotite. The heights of main maxima in all biotite diagrams (35, 36, and 37) are low—on the average lower than the quartz maxima of the same rock (Diagram 38, Table 8). In Diagram 39, S-plane intersections around the *b* (B) axis are somewhat scattered, and the position of S_2 seems to be at about 10°–20° (clockwise) from S_1, where slip planes corresponding to one main maximum of large biotite, one of small biotite, and three of quartz are concentrated. Grouping of all S-surfaces however is difficult to interpret. Correlation of the quartz maxima with the mica fabric is satisfactory (Table 8). Maximum IV is the commonest, maximum VI occurs twice, and no other maxima are represented. All the diagrams show B-girdles and monoclinic symmetry.

Fabric of a muscovite-garnet type of microcline gneiss (Specimen 123, Diagrams 56–59).—The specimen shows well marked S_1 and *b*-lineation. (Pl. 1) Both the muscovite and biotite diagrams show perfect B-girdles with several maxima and sub-maxima presumably of the S_2 and S_2' groups (Diagrams 56, 57, 59). The position of S_2 is probably indicated by the 3% area located at nearly 90° to the pole of S_1 in the biotite diagram (Diagram 57). In general, the fabrics suggest sharp micro-foldings, analogous to that of specimen 90 (Diagrams 22–25)—an ungranitized schist. The widths of mica girdles, the vacant field inside the zero-girdles of the mica diagrams, the peripheral location of mica maxima, and the character and height of main quartz maxima further bring out the resemblance of this fabric to that of the ungranitized schist (Tables 6, 8 and Diagram 58). Fabric evidence on the whole supports the view that the muscovite-garnet type of gneiss is a product of granitization of schist rather than a rock of magmatic origin.

For the remaining types of microcline gneisses, data are summarized in Tables 6 and 8 from fabric Diagrams 40–45 (Specimen 26, intermediate type), 46–49 (Specimen 30, fine-grained type) and 50–55 (Specimen 72, granitized stringer in the schist) for inspection.

Fabrics of Orthoclase-Kyanite Gneiss

Under the microscope, muscovite of three generations can be distinguished in the orthoclase-kyanite gneiss: $muscovite_1$, variable in size but mainly coarse, probably recrystallized mica of the parent schist; $muscovite_2$, large porphyroblasts, pseudomorphous after orthoclase, sillimanite or kyanite (blade-type); $muscovite_3$, small fibers, pseudomorphous after kyanite of the "needle" type. The last two types of muscovite discussed in the section on granitization, indicate granitization into the hydrothermal stage. As biotite is intergrown chiefly with $muscovites_{1,2}$, its period of recrystallization is interpreted as having also been continued into the hydrothermal stage but perhaps not as late as $muscovite_3$.

The occurrence of quartz is comparable to that in the microcline gneisses—as inclusions in feldspars, as corroded grains in association with myrmekites, and as large recrystallized grains segregated into stringers. Recrystallization of the last quartz continued longer than that of all other minerals in the rock. Quartz eats into margins of grains of other minerals, and itself contains small, rounded oligoclase inclusions. In many orthoclase-kyanite gneisses 50% or more of the large recrystallized quartz shows multiple undulatory extinction bands.

Orthoclase-Kyanite Gneiss (Specimen 84, Pls. 5, 6, Diagrams 60–68): The thin section was cut normal to the strike of S_1, the only structure observed in the field (Pl. 1). Partial

diagrams were made for micas of different sizes and for the corroded quartz associated with myrmekite.

All diagrams prepared for micas and quartz show very wide B-girdles, with average width greater than in any of the microcline gneisses. This, along with the appearance of numerous isolated areas within the zero-girdle, indicates that more micas have a somewhat random orientation than in schist and microcline gniess. Only in the diagram for small biotite is the degree of orientation (indicated by the narrower girdle) comparable with that for the schist. The large muscovite and biotite with random orientation appear as porphyroblasts. Their orientation was perhaps controlled by the shape and the lattice structure of the minerals they replace, rather than by the movement plan. The small muscovites (Diagram 61) show preferred orientation, perhaps similarly inherited from a dimensional orientation of the needles of kyanite.

Possible slip planes corresponding to the maxima in all partial diagrams of micas, as well as such submaxima as show good correlation with quartz maxima, are represented in the synoptic Diagram 68. Numerous planes corresponding to the main maxima are concentrated near S_1, though the group as a whole makes a small angle (rotated counterclockwise) with S_1. This mean position is assumed to be that of S_2, corresponding to a main maximum of large biotite, and at an angular distance of 6° from it, three possible S-planes inferred from quartz maxima. On this basis of grouping, S_1, S_2, S_1', and S_3 seem to conform to the pattern of the schist. S_3, as usual, is insignificant in mica fabrics, but its position is indicated by the quartz maxima. The age-size relation of micas is entirely different from that of the schists, because a large number of the micas is in the form of pseudomorphs. Scattering of *b* (B) axis is similar to that of microcline gneisses. The pertinent data are listed in Table 6.

Quartz maxima are high, and their correlation is satisfactory. The large recrystallized quartz, the latest of all the minerals in the rock, is related to the same set of slip planes as is the small corroded quartz associated with myrmekites, though the maxima for these two types of quartz are somewhat different in character (Table 8).

Muscovite$_2$ and muscovite$_3$, as well as some recrystallized quartz are products of hydrothermal metamorphism. The fabric data indicate that this hydrothermal activity occurred during the main period of deformation (perhaps near its close), when stress was waning. On this account the fabric of the mica pseudomorphs was preserved almost intact, but quartz, being more sensitive to stress, continued to record the deformation plan until the very end of its period of crystallization.

Orthoclase-Kyanite Gneiss (Specimen S-39, Pls. 5, 6, Diagrams 72–76): In hand specimen (Pl. 2, Fig. 3), the gneiss is penetrated by several aplite-like stringers, the biggest of which is discordant to the main foliation (S_1) of the gneiss. The field orientation of this specimen is not known. As shown on the diagrams, the walls of the "dike" (S_d) make an angle of 40° with S_1, the line of intersection being inclined at 44° to *b* (B). S_d, which apparently guided the granitizing solutions, must represent some earlier rock opening (fracture) not related to regional rock cleavages (which invariably intersect in *b*).

Diagram 72 shows the orientation of micas in the host gneiss, and Diagram 73 that of micas in the cross-cutting "dike". These two diagrams have their main maxima in nearly identical positions, related to S_1, or more likely to S_2, quite unrelated to S_d, the trend of the "dike". There are, however, some differences. Diagram 72 (gneiss) shows narrower B-girdle and higher concentration of the main maxima, and Diagram 73 ("dike") is characterized by its more pronounced isolated areas within the zero-girdle, and by more pronounced scattering of slip surfaces (referred from sub-maxima) from sharp intersection in B. The similarity in mica fabrics eliminates the possibility of any recognizable primary flow structure in the "dike", while the minor differences in fabrics are attributed to the greater degree of granitization experienced by the "dike" portion of the rock. This conclusion is confirmed by quartz diagrams (Diagram 74 for the gneiss and Diagram 75 for the "dike"), which are closely similar, in general pattern and in the positions

of main maxima and sub-maxima, except that Diagram 75 ("dike") shows higher concentration of maxima and sub-maxima, and a tendency for more maxima to be developed. The correlation between quartz and mica fabrics (Diagram 76; Table 8) is good; all quartz maxima can be so correlated. The slip surfaces, deduced from mica and quartz maxima on all diagrams prepared for both the "dike" and the gneiss portions, do not form separable groups (Diagram 76). Possible slip surfaces of the S_3 group, not shown on the diagram, are perhaps represented on the mica diagrams by areas below 3% concentration.

Fabrics of Crushed and Sheared Rocks

Crushing and shearing are late phenomena in this region, extensively but locally effected all rock types studied.

CRUSHED WISSAHICKON SCHIST (SPECIMEN 30-260, PL. 6, DIAGRAMS 77, 78): The sample was taken in the zone of the northern boundary fault, and the thin section was cut normal to the strike (N70°E) of vertically dipping S_1. The fabric of quartz or mica is that of S-tectonite, with a single set of S- planes (S_1), and orthorhombic symmetry with respect to three axial planes of the fabric. In the mica Diagram 77, the main maximum (22%) corresponds well with the pole of S_1. In the quartz Diagram 78, a sharp maximum (7%) and the mid-point of an almost equally clear divided maximum (7%) both coincide exactly with the theoretical positions of maxima II of the key diagram. There is also a submaximum of 3% at the position of maximum I.

This type of orthorhombic, or nearly orthorhombic, symmetry has also been found in the fabrics of three specimens of the Baltimore gneiss from the northern boundary fault. The same pattern has been recorded in mylonitized quartzites and gneisses from other regions (Fairbairn 1941; Ingerson and Tuttle, 1945).

WISSAHICKON SCHIST WITH S_4 (SPECIMEN 46, PL. 6, DIAGRAMS 79–87): Field readings on this specimen are:

S_1: strike N28°E, dip 70°SE

S_4: strike N67°E, dip 27°NW

b lineation on S_4: trend N60°E, plunge 3°NE

In a thin section cut nearly normal to the *b*-lineation on S_4, the micas which belong to the S_4 generation show nearly vertical cleavage cracks; those which belong to the earlier S_1 generation show cleavage cracks much tilted from the vertical. Also, in this particular section biotites of the first generation can readily be distinguished by their slight change in pleochroism (Bx_a nearly perpendicular to thin section). Besides, the trends of the respective arches of the micas of these two generations are nearly perpendicular to each other; that for mica of the second generation transgresses that for mica of the first (see inset sketch on Diagram 87; Pl. 2, Fig. 6).

Orientation diagrams for muscovites and biotites of the first generation show single girdles, the axes of which coincide and are denoted as B_1 (Diagrams 79, 82). Those for micas of the second generation show another single girdle with axis denoted as B_2 (Diagrams 80, 83). The angle between B_1 and B_2 is 27° in the two collective Diagrams (81, 84) prepared for muscovites and biotites respectively. The B_2 girdle is less complete than the B_1 girdle. A synoptic diagram (86, rotated with B_1 in center) of planes which correspond to maxima of the partial diagrams prepared for micas of the first generation indicates that symmetrical crenulations (S_2 and S_2') have been developed on S_1, and that the position of S_3 coincides with that of what is now S_4. These mica crenulations are relict structures with reference to the deformation responsible for S_4; the maxima therefore are low (6%–7%). A synoptic diagram (87, B_2 in center) similarly constructed from partial diagrams prepared for micas of the second generation shows that the original S_3 surface (now S_4) has been microfolded, and several new slip surfaces have formed about a new axis B_2 markedly inclined to B_1. The position of S_1 indicates that S_4 makes a high angle (82°) with S_1 as measured in the section normal to B_2.

The quartz fabric is represented by Diagram 85. In Diagram 87, all four quartz maxima can be correlated with the slip planes recognizable from mica fabric, and each group of slip planes can be correlated with one or two quartz maxima, of types II, III, V or VI. On Diagram 86, the same four quartz maxima can all be

correlated, but only with S_1. This may be due to the fact that quartz grains initially oriented in S_1 (maxima II, IV or VII) were already favorably oriented with respect to S_4 (maxima II, III, V or VI) when this became active.

The fabrics thus indicate two unrelated acts of deformation, with their respective rotation-axes B_1 and B_2 independent and mutually inclined at 27°. Development of S_4, as a shear cleavage, is likely later than evolution of all other structures in the rock.

Conclusions

Both the Wissahickon schist and its partially and more completely granitized equivalents are classified as R-tectonites, with a single B-girdle, representing one deformation.

Where megascopic, fine crenulations (drag folds) have been developed in the rock (as in mica schist), these are clearly reflected in the preferred orientation patterns of mica and quartz. Where crenulations are not directly visible (as in quartz schist), the main features of the orientation patterns identify their presence. One orienting mechanism (flexure-slip folding) has been responsible for evolution of the schistose structure. Orientation diagrams for mica, quartz, and hornblende all indicate that rotation of S-planes played an important role in deformation of the rock. Direction of overturning of a fold can usually be determined from this rotation, if the attitude of the specimen in relation to the fold is also known. When separate diagrams are prepared for micas of different sizes, the successive stages of development of the regional folding can be reconstructed from the fabrics. Correlation of respective maxima of quartz with mica diagrams for the same rock by the method described is generally satisfactory. For this reason it is suggested as working hypothesis that the S-planes which determined the mica orientation also functioned to varying degrees in orienting the quartz. Of the eight standard types of quartz maxima recognized by Fairbairn (following Sander) in S-tectonites, maximum IV occurs most frequently, while all the others except III and VIII are represented.

Orientation diagrams for mica of the microcline gneiss conform to the same general pattern as for the schist. Deviations from the pattern of schist fabrics scattering of *b* (B) axes, lower heights of main maxima, increased widths of girdles, etc.) are attributed to modifying influence of grain size, texture, and mineral composition upon rock deformation of one general type. In details of orientation, the fine-grained type of microcline gneiss resembles the schist more closely than does the porphyroblastic type, probably because it also resembles the schist in grain size and even texture. Quartz orientation in the gneiss can be correlated with the mica orientation much as in the schist. However, the main quartz maxima increase in height as the number of theoretically possible types of maxima (I–VIII) decreases. Maximum IV occurs alone in typical cases.

The orthoclase-kyanite gneiss is petrofabrically similar in a number of respects to both the schist and the microcline gneiss. However, higher temperatures of crystallization, later hydrothermal activity, and waning stress toward the end of crystallization of the orthoclase-kyanite gneiss perhaps have influenced the mica fabrics of these rocks, which generally show a lower degree of preferred orientation than in the other two groups of rocks.

The period of granitization, including the final phase of hydrothermal activity, is dated as syntectonic. Regional metamorphism (deformation) had probably begun before granitization, as is shown by the presence of relict garnet, kyanite, sillimanite, or biotite in some of the granitized rocks. However, the general similarity between the fabric orientation patterns of quartz and mica of the schist to those of the granitized rocks shows that deformation on the same plan controlled orientation of micas in both types of rocks. This conclusion is confirmed by the quartz fabrics. Recrystallization of quartz has lasted longer than that of most other minerals in both granitized and non-granitized rocks, and the quartz fabrics can be correlated with the same movement picture, as is shown by the mica fabrics in both cases. The higher maxima shown in quartz diagrams for granitized rocks are probably attributable to more intense deformation of quartz in a matrix deficient in mica. Recrystallization of quartz in the later stages of granitization was still going

on when S_3 (fracture cleavage) was developing; and this latest quartz shows an even more pronounced orientation than quartz formed at earlier stages. Quartz, being very sensitive to stress, probably records the very latest movements in the region.

Postel (1940) distinguished true igneous dikes on the basis of their cross-cutting relation to granitized rocks in the field. Fabric study of one such case (S-39) reveals almost identical orientation patterns for mica and quartz in host rock and in the "dike" rock (both represented in one thin section). Moreover, these patterns conform to the regional deformation plan, and are unrelated to trend of the "dike" walls. If there had been either pre-tectonic or syntectonic flow of magma along the "dike", its walls should have functioned as slip surfaces during regional deformation, and these slipping movements should then have left some imprint on the fabric. The "dike" is interpreted as a product of nearly complete granitization by solutions moving along a fracture parallel to the present trend of the "dike". But orientation of the grains with which the solution reacted was already determined by S-surfaces of the S_1–S_2 group common to the rock as a whole.

Late deformation, after the period of granitization, has produced S-tectonites with orthorhombic symmetry in crushed rocks along the fault zones. There are also locally sheared rocks with $B_1 \wedge B_2$ girdles and a well defined new cleavage (S_4). These also are attributed to superposition of late local deformation (B_2) upon a normal schist fabric (B_1).

References Cited

Anderson, E. M. (1948) *On lineation and petrofabric structure and the shearing movement by which they have been produced*, Geol. Soc. London, Quart. Jour., vol. CIV, pt. 1, p. 99–125

Armstrong, Elizabeth (1941) *Mylonitization on hybrid rocks near Philadelphia, Pennsylvania*, Geol. Soc. Am., Bull., vol. 52, p. 667–694.

Backlund, H. (1936) *Der Magmaaufsteig in Faltengebirgen*, Comm. geol. Finlande, Bull., no. 115, p. 293–347.

Bascom, F. (1905) *Piedmont district of Pennsylvania*, Geol. Soc. Am., Bull., vol. 16, p. 289–328.

——— (1909) *Philadelphia District*, Geol. Soc. U. S., folio, no. 167.

Berman, H. (1937) *Constitution and classification of the natural silicates*, Am. Mineral., vol. 22, no. 5, p. 342–408.

Billings, M. P. (1937) *Introduction of potash during regional metamorphism in western New Hampshire*, Geol. Soc. Am., Bull., vol. 49, p. 289–302.

Bugge, J. A. W. (1943) *Geological and petrographical investigations in the Kongsberg-Bamble formation*, Norges Geol., no. 160.

Clarke, F. W. (1924) *The data of geochemistry*, U. S. Geol. Survey, Bull., no. 770.

Cloos, E. and Broedel, C. H. (1937) *The structure of the Gneiss Domes near Baltimore, Maryland*, Maryland Geol. Survey, vol. XIII, Pt. III, p. 149–188.

Cloos, E. and Hietanen, A. (1941) *Geology of the "Martic Overthrust" and the Glenarm series in Pennsylvania and Maryland*, Geol. Soc. Ann., Spec. Paper, no. 35.

Daly, R. A. (1933) *Igneous rocks and the depths of the earth*, McGraw-Hill, New York.

Eskola, P. (1920) *The mineral facies of rocks*, Norsk. Geol. Tidsskr., vol. 6, p. 143–194.

———, Barth, T. F. W., and Correns, C. W. (1939) *Die Entstehung* der Gesteine, Teil III, Springer, Berlin.

——— (1949) *The problem of mantled gneiss domes*, Geol. Soc. London, Quart. Jour., vol. CIV, p. 461–476.

Fairbairn, H. W. (1939) *Hypotheses of quartz orientation in tectonites*, Geol. Soc. Am. Bull., vol. 50, p. 1475–1492.

——— (1941) *Deformation lamellae in quartz from the Ajibik formation, Michigan*, Geol. Soc. Am., Bull., vol. 52, p. 1265–1278.

——— (1942) *Structural petrology of deformed rocks*, Addison-Wesley, Cambridge, Mass.

Goldschmidt, V. M. (1921) *Die Injektionsmetamorphose im Stavanger-Gebiete*, Vidensk. Skr., Mat.-Naturv. Kl., no. 10.

Griggs, D. and Bell, J. F. (1938) *Experiments bearing on the orientation of quartz in deformed rocks*, Geol. Soc. Am., Bull., vol. 49, p. 1723–1746.

Goodspeed, G. E. (1948) *Origin of granites*, Geol. Soc. Am., Mem., no. 28, p. 55–78.

Holmes, A. (1946) *Principles of physical geology*, T. Nelsons and Sons, London.

Ingerson, E. (1937) *Accurate orientation of thin ssctions*, Am. Mineral., vol. 22, p. 760–772.

——— and Tuttle, O. F. (1945) *Relations of lamellae and crystallography of quartz and fabric directions in some deformed rocks*, Am. Geophys. Union, Tr., vol. 26, p. 95–105.

Johannsen, A. (1932) *A descriptive petrography of the igneous rocks*, vol. II. 2nd ed., University of Chicago Press.

Jung, J. and Roques, M. (1938) *Les schistes cristallins du Massif central*, Bull. Services Carte géol., France, vol. XXXIX, p. 284–312.

Knopf, E. B. (1933) *Petrotectonics*, Am. Jour. Sci., 5th ser., vol. 25, p. 460–467.

Lesley, J. P., Roger, H. D., Frazer, P., and Hall, C. E. (1883) *The geology of Chester County, Pennsylvania*, Penna. Geol. Surv., 2nd vol., C4.

——— (1892) *A summary description of the geology of Pennsylvania*, Penna. Geol. Surv., Final report, 3 vols.

Perrin, R. and Roubault, M. (1941) *Observation d'un "front" de metamorphisme regional*, Bull. Soc. Geol. France, 5th ser., XI, p. 183.

Postel, A. W. (1940) *Hydrothermal emplacement of granodiorite near Philadelphia*, Acad. Natur. Sci. Phila., Pr., vol. XCII, p. 123–152.

Ramberg, H. (1949) *The facies classification of rocks: A clue to the origin of quartzofeldspathic massifs and veins*, Jour. Geol., vol. 57, p. 18–54.

Rand, T. D. (1900) *Notes on the geology of Southeastern Pennsylvania*, Acad. Natur. Sci. Phila., Pr. p. 160–338.

Read, H. H. (1943) *Meditations on granites*, Part I, Geol. Assoc. London, Pr., vol. 54, p. 64–85.

——— (1944) *Meditations on granites*, Part II, Geol. Assoc. London, Pr., vol. 55, p. 45–93.

——— (1946) *This subject of granite*, Science Progress, vol. 34, p. 659–669.

——— (1948a) *Granites and granites*, Geol. Soc. Am., Mem. 28.

——— (1948b) *A commentary on place in plutonism*, Geol. Soc. London, Quart. Jour., vol. CIV, pt. 1, pp. 193–196.

Reynolds, D. L. (1943) *Granitization of hornfelsed sediments in the Newry granodiorite of Goraghwood Quarry, Co. Armagh.*, Geol. Soc. London, Quart. Jour., vol. XLVIII, sect. B., p. 231.

——— (1944) *The south-western end of the Newry igneous complex*, Geol. Soc. London, Quart. Jour., vol. XCIX, p. 205.

——— (1946) *The sequence of geochemical changes leading to granitization*, Geol. Soc. London, Quart. Jour., vol. CII, pp. 389–446.

——— (1947a) *The granite controversy*, Geol. Mag., vol. lxxxiv, p. 209.

——— (1947b) *The association of basic "fronts" with granitization*, Science Progress, vol. xxxv, p. 205.

——— (1947c) *Hercynian Fe-Mg metasomatism in Cornwall: a reinterpretation*, Geol. Mag., vol. lxxxix, p. 61.

Rogers, H. D. (1858) *The geology of Pennsylvania*, government survey, 2 vols.

Roques, M. (1941) *Les schistes cristallins de la partie sudouest du Massif central francais*, Mem. pour servir à l' explication de la carte geol. d étaillé de la France, Paris.

Sander, B. (1930) *Gefügekunde der gesteine*, Vienna.

——— (1934) *Fortschritte der Gefugekunde der gesteine*, Fort. Min. Krist. Petr., vol. 18, p. 111–170.

Spencer, E. (1937) *The potash-soda-feldspars. I. Thermal stability*, Mineral. Mag., vol. 24, p. 453–494.

——— (1938) *The potash-soda-feldspars. II. Some applications to petrogenesis*, Mineral. Mag., Vol. 25, p. 87–118.

Turner, F. J. (1941) *The development of Pseudostratification by metamorphic differentiation in the schists of Otago, New Zealand*, Am. Jour. Sci., vol. 239, p. 1–16.

——— (1948) *Evolution of the metamorphic rocks*, Geol. Soc. Am., Mem. 30.

Wegmann, C. E. and Kranck, E. H. (1931) *Beitrage zur Kenntnis der Svecofenniden in Finnland*, Comm. géol. Finlande, Bull., no. 89, p. 73-102.

——— (1935a) *Zur Deutung der Migmatite*, Geol. Rundsch., vol. xxvi, p. 305–350.

——— (1935b) *Preliminary report on the Canadian orogeny in Christian X's land, Northeastern Greenland*, Medd. om. Grönland, vol. 103, no. 3.

Weiss, J. (1949) *The Wissahickon schist at Philadelphia*, Geol. Soc. Am., Bull., vol. 60, p. 1689–1726.

UNIVERSITY OF CALIFORNIA, BERKELEY, CALIF.

MANUSCRIPT RECEIVED BY THE SECRETARY OF THE SOCIETY, JULY 22, 1949

EXPLANATION OF DIAGRAM

Diagram Number	Specimen and Locality	No. of Readings	Mineral or Structure	Contour in Per Cent	Rock Type
73	S-39	204	Mica ("dike" portion)	0-1-2-3-4-6	Orthoclase kyanite gneiss showing cross-cutting relationship
74	S-39	204	Quartz (gneiss portion)	0-1-2-3-4-5 (6)	Orthoclase kyanite gneiss showing cross-cutting relationship
75	S-39	204	Quartz ("dike" portion)	0-1-2-3-5-6 (7)	Orthoclase kyanite gneiss showing cross-cutting relationship
76	S-39		Correlation of quartz and mica fabrics		Orthoclase kyanite gneiss showing cross-cutting relationship
77	30-260	200	mica	0-1-3-12-19 (22)	Crushed mica schist
78	30-260	200	quartz	0-1-2-3-5-6 (7)	Crushed mica schist
79	46	204	muscovite related to B_1	0-1-2-4-5 (6)	Mica Schist with S_1
80	46	110	muscovite related to B_2	0-1-3-6-8-13-15 (18)	Mica Schist with S_1
81	46	204	collective muscovite	0-1-2-3-4-5-8-9 (10)	Mica Schist with S_1
82	46	204	biotite related to B_1	0-1-2-3-5 (7)	Mica Schist with S_1
83	46	121	biotite related to B_2	0-1-3-6-12 (13)	Mica Schist with S_1
84	46	204	collective biotite	0-1-2-4-6-8-9 (11)	Mica Schist with S_1
85	46	204	quartz	0-1-2-3-4-5	Mica Schist with S_1
86	46		Synoptic diagram of 70, 73, correlation of quartz and mica fabrics		Mica Schist with S_1
87	46		Synoptic diagram of 71, 74, correlation of quartz and mica fabrics		Mica Schist with S_1
88		123	Fold axes and b-lineations	0-1-2-4-7-10 (14)	
89		50	b-lineations and fold axes in granitized area		
90		73	b-lineations and fold axes in ungranitized area		
91		146	S_1	0-1-2-3-4-6-8 (10)	
92		50	S_1 in granitized area		
93		96	S_1 in ungranitized area		
94		50	S_2 and S_3	poles of S_2 in circles, poles of S_3 in dots	
95		253	joints in granitized area	0-1-2-3-4	
96			key diagram of quartz maxima (after Fairbairn)		

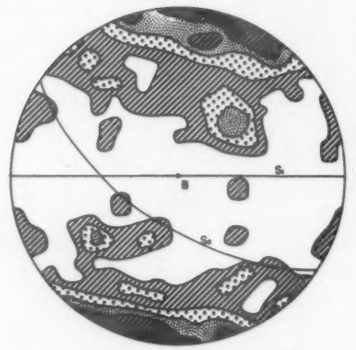

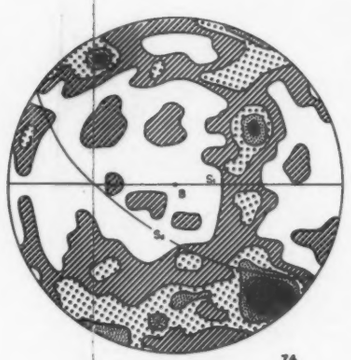

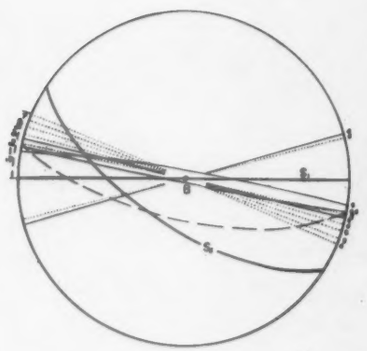

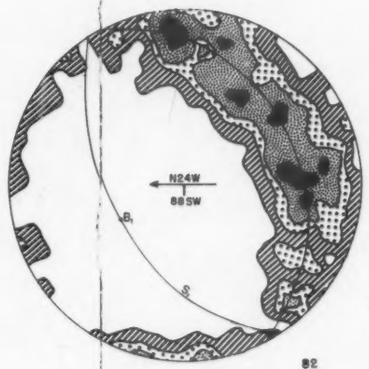

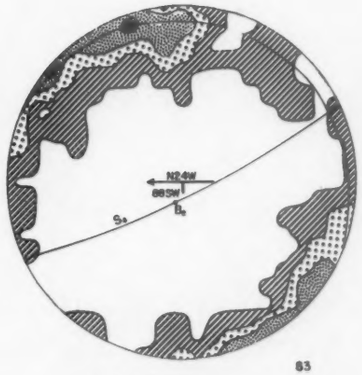

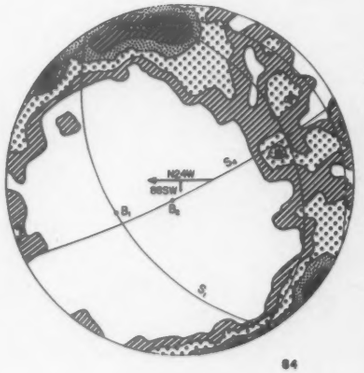

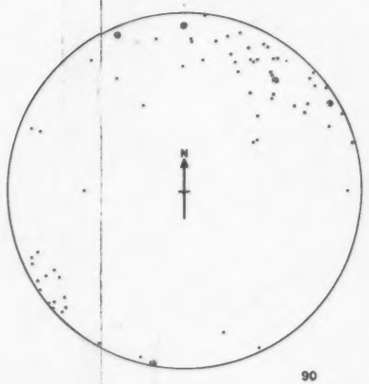

FABRIC DIA

See Plate 3 for abb

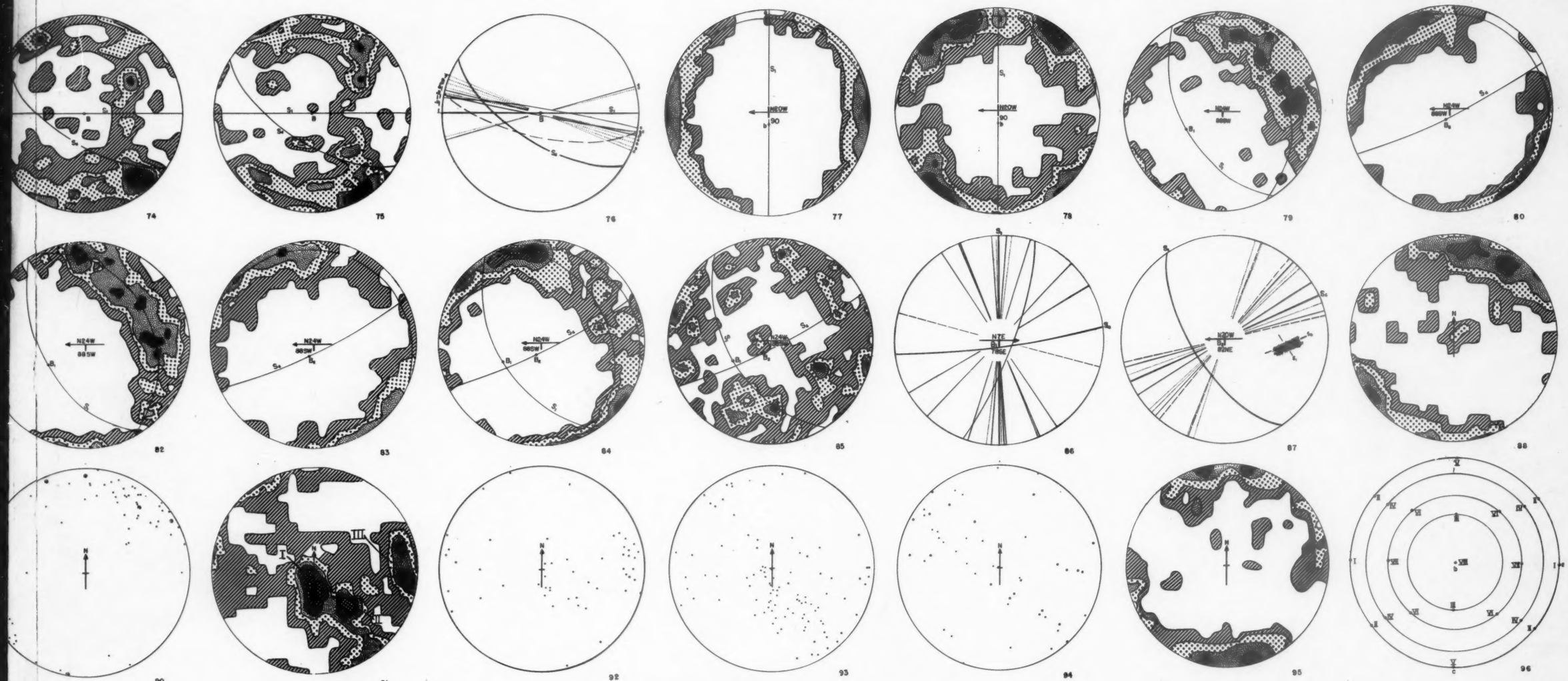

74 75 76 77 78 79 80

82 83 84 85 86 87 88

90 91 92 93 94 95 96

FABRIC DIAGRAMS

See Plate 3 for abbreviations

Al
In
Ac
Su
M

M

Or

Fig
1.
2.
3.
4.
5.
6.
7.
8.
9.
10.
11.
12.
13.
14.
15.

BULLETIN OF THE GEOLOGICAL SOCIETY OF AMERICA
VOL. 61, PP. 957-1020, 32 FIGS., 6 PLS. SEPTEMBER 1950

PETROLOGY OF HAKONE VOLCANO AND THE ADJACENT AREAS, JAPAN

By Hisashi Kuno

CONTENTS

	Page
Abstract	958
Introduction	958
Acknowledgments	959
Summary of geologic history	959
Minerals	963
Plagioclase and alkali-feldspar	963
Silica minerals	968
Olivines	969
Monoclinic pyroxenes	972
Orthorhombic pyroxenes	977
Amphiboles	979
Accessory minerals	982
Mineral assemblage	983
Method of representation	983
Nature of the various types of assemblage	986
Order of crystallization of the minerals and reaction series	988
Continuous reaction series	988
Discontinuous reaction series	990
Order of crystallization	991
Comparison with artificial systems	992
Origin of the rock series	992
Distinction of the two rock series	992
Evolution of the ferromagnesian components	993
Origin of the two rock series	994
Crystallization of pyroxenes	996
Evidences of contamination in the hypersthenic rock series in other regions of Japan	999
Chemical compositions of the rocks	999
Bulk compositions and modes	999
Compositions of aphyric rocks and those of groundmasses	1003
Relations between the bulk and the groundmass compositions	1007
Comparison with rocks of other regions	1008
Comparison with basalts and dolerities of the tholeiitic magma-type	1008
Comparison with rocks of other volcanoes of Japan and adjacent regions	1010
Problem of the parental magma	1012
References cited	1012

ILLUSTRATIONS

Figure	Page
1. Distribution of chief volcanoes in the southern part of the Fossa Magna	960
2. Distribution of the older Miocene rocks, the middle Miocene to Pliocene rocks, and the Quaternary rocks	960
3. Stereographic projection of the optic orientations of plagioclases and anorthoclase	966
4. Various stages of the development of the groundmass inclusions in plagioclase	967
5. Dust inclusions in plagioclase	968
6. Honey-combed structure in plagioclase	968
7. Crystal habit of some groundmass olivine	970
8. Various stages of development of olivine crystals	971
9. Olivine crystals surrounded by hypersthene and vermicular magnetite	971
10. Double rims of groundmass pyroxenes around olivine	971
11. Grouped phenocrysts of plagioclase, magnetite, and hypersthene, the last surrounded by fayalite and tridymite	972
12. Diagram showing chemical compositions of various pyroxenes	973
13. Augite phenocrysts rimmed with quasi-uniaxial pigeonite	974
14. Augite phenocrysts surrounded by groundmass hypersthene	974
15. Corona of augite and olivine around a xenocryst of hypersthene	978
16. Zonal structure of colorless cummingtonitic hornblende and common green hornblende	981
17. Common green hornblende with core of fibrous hypersthene	981
18. Spinel and picotite inclusions in olivine	983
19. Order of crystallization of the principal minerals and reaction relations	989
20. Diagram showing the chemical compositions of the groundmass pyroxenes of the two rock groups	992
21. Evolution of the principal rock types	993
22. Evolution of pyroxenic components of the two rock series	994
23. Stability fields of clino- and orthopyroxenes and the average temperatures of crystallization of pyroxenes in natural magmas	996
24. Relations between the clino- and orthopyroxene inversion curves and the liquidus and solidus curves for the crystallization of pyroxenes from magmas	997
25. Hypothetical equilibrium diagrams for pyroxenes	998
26. Variation diagrams for the oxide compositions of the rocks of Izu and Hakone	1007
27. Compositions of the normative feldspars of the rocks of Izu and Hakone	1008
28. Compositions of the normative pyroxenes of the rocks of Izu and Hakone	1008

Figure Page
29. Ratio normative quartz: normative femic minerals: normative feldspars of the rocks of Izu and Hakone....1008
30. Compositions of the normative feldspars of the basalts and dolerites of the tholeiitic magma-type....1010
31. Compositions of the normative pyroxenes of the basalts and dolerites of the tholeiitic magma-type....1010
32. Ratio normative quartz: normative femic minerals: normative feldspars of the basalts and dolerites of the tholeiitic magma-type....1010

Plate Facing page
1. Photomicrographs of the rocks of Izu and Hakone....1014
2. Photomicrographs of the rocks of Izu and Hakone....1015
3. Photomicrographs of the rocks of Izu and Hakone....1016
4. Photomicrographs of the rocks of Izu and Hakone....1017
5. Photomicrographs of the rocks of Izu and Hakone....1018
6. Photomicrographs of the rocks of Izu and Hakone....1019

Abstract

Rocks of Hakone volcano and adjacent areas cover a wide range from basalt to dacite approximate to soda-rhyolite. They were erupted from various different centers during the period from older Miocene to Recent.

Two different rock series are recognized, one characterized by the occurrence of monoclinic-pyroxene (a solid solution series from augite to iron-rich pigeonite) as the only pyroxenic phase of the groundmass; the other by the presence of hypersthene (sometimes together with augite) in the groundmass. They are designated as "pigeonitic rock series" and "hypersthenic rock series" respectively. The pigeonitic rock series was derived from a parental olivine-basalt magma through simple fractional crystallization; the hypersthenic rock series was formed from the same magma through contamination of acid igneous rocks (probably granitic).

In the pigeonitic rock series, the crystallization of the groundmass pyroxenes took place over the clino- and orthopyroxene inversion temperatures, resulting in pigeonite. In the hypersthenic rock series, the crystallization temperatures were lowered by concentration of volatile substances due to the contamination; its crystallization took place always below the inversion temperature, resulting in hypersthene. Porphyritic hornblende appeared in the later stage of the crystallization of the latter series.

The chemical compositions of the groundmasses of these rocks resemble those of basalts and dolerites of the tholeiitic magma-type of the world.

Introduction

Hakone and its vicinity represent probably one of the most remarkable volcanic fields in Japanese islands. Many different types of volcanic phenomena occurred here since older Miocene time, and rocks of varying compositions were erupted from a number of vents.

The present region has been studied by the writer since 1931 under the auspices of the Geological Institute and the Earthquake Research Institute, Tokyo University. This paper presents the results of the petrological study of the region. A detailed description of the geology of the region, only briefly stated here, will be published in another paper with two sheets of geologic maps.

The rocks of this region show a close consanguinity to one another; quite similar types are encountered repeatedly among the rocks erupted from different centers. Thus they constitute a distinct petrographic province. Reference is often made in this paper to the rocks of the adjoining regions which appear to belong to the same province.

The rocks are classified according to the color index of the groundmass, namely, the sum of the normative femic minerals Wo + En + Fs + Mt + Il + Hm as calculated from the groundmass composition. This is based on the idea that the bulk compositions of porphyritic rocks may be affected by crystal sorting, while the groundmass compositions represent those of possible magmatic liquids (Tsuboi, 1925, p. 70; Bowen, 1928, p. 93). Thus, "basalt" is distinguished from "andesite" by a color index higher than 37, whereas "dacite" is distinguished from "andesite" by a color index lower than 10. The "basalts" thus defined show normative feldspars of the groundmass generally more calcic than An_{50} while the "andesites" show normative feldspars of the groundmass generally more sodic than that composition. Where no chemical analysis or volumetry is available, as is often the case, the content of the colored minerals is roughly estimated by comparing with the rocks of known composition. Subdivisions of the rocks are further made according to the mafic minera

phenocrysts (except magnetite) contained. Thus, for example, andesites are divided into hypersthene-andesite (where hypersthene is the only mafic mineral phenocrysts), olivine-augite-hypersthene-andesite (where there are phenocrysts of olivine, augite, and hypersthene in the order of increasing amount), and hypersthene-bearing olivine-andesite (where there are phenocrysts of olivine together with those of a few hypersthene), and so on. Again, "quartz-dacite" is distinguished from simple "dacite" according to the presence or absence of quartz phenocrysts.

The common rock types occurring as lava flows and minor intrusives are olivine-pyroxene-basalt, pyroxene-andesite (carrying, in most cases, both augite and hypersthene), and pyroxene-dacite, of which pyroxene-andesite is the most predominant.

Rocks carrying phenocrysts of hornblende are comparatively rare, confined largely to the Tertiary andesites and dacites that occur in the northern part of the region; those with biotite phenocrysts are entirely absent.

These rocks constitute probably the most calcic suite of the world. They are characterized by the presence of extremely calcic plagioclase phenocrysts in the basic end of the suite, and by the universal occurrence of silica minerals in the groundmass. A peculiar type of basalt carrying phenocrysts of anorthite and olivine in a melanocratic groundmass with about 5 per cent cristobalite is not uncommon.

The basic and intermediate rocks make up the bulk of the flows, pyroclastics, and dikes. The acid ones tend to occur either as minor extrusives and intrusives, or as wide-spread pyroclastic layers (tuffs and pumice).

Rocks with plutonic or hypabyssal texture are encountered as plug-like intrusives (quartz-gabbro and quartz-diorite) and also as ejecta (either cognate or accidental) embedded in tuffs (olivine-eucrite, allivalite, quartz-diorite, etc.).

In the present study, the refractive indices of minerals were determined by the immersion method. Especially for olivine and pyroxene, Sueno's (1933, p. 421) standard glass powders were used, and for plagioclase, Tsuboi's (1934, p. 325) dispersion method. The optic axial angles were measured by the universal stage and the modes of rocks by the integrating stage.

The separation of the constituent minerals from the rocks for chemical analyses was made by hand picking, with the aid of the electromagnetic mineral separator, and by means of the heavy solutions (bromoform, methylene iodide, and Clerici's solution).

The chemical compositions of the minerals, either determined by the actual analyses or inferred optically, are always expressed in weight per cent of the principal components.

The present study is based on the microscopical examination of about 1800 thin sections cut from the rock specimens, on 6 chemical analyses of the minerals, and 23 rock analyses. This study is yet far from completion, and it is hoped that this paper presents a basis for further investigation.

Acknowledgments

The writer offers his cordial thanks to Professor Seitarô Tsuboi of the Geological Institute, Tokyo University for many courtesies received throughout this study. He is greatly indebted to Dr. W. F. Foshag of the Smithsonian Institution, to Dr. H. H. Hess of the Princeton University, and to Dr. F. Walker of the University of Cape Town for helpful criticisms and advice. The writer greatly appreciates the receipt of many facilities from the Geological Institute and the Earthquake Research Institute, Tokyo University, and acknowledges a grant from the Scientific Research Expenditure of the Department of Education which was used for some of the apparatus and instruments.

Summary of Geologic History

The Hakone region includes numbers of Tertiary volcanic units and a few sedimentary formations, and also Quaternary volcanics belonging to five major cones: Usami, Taga, Yugawara, Hakone, and Huzi (Fuji), which constitute a part of the Huzi volcanic zone (Fig. 1). We are not concerned here with the rocks of the Huzi volcano except where particularly mentioned.

The succession of the principal volcanic and

sedimentary units are shown in Table 1 in which the arrows indicate the age relationships between the units. Pyroclastic rocks are classified according to the scheme proposed by Wentworth and Williams (1932).

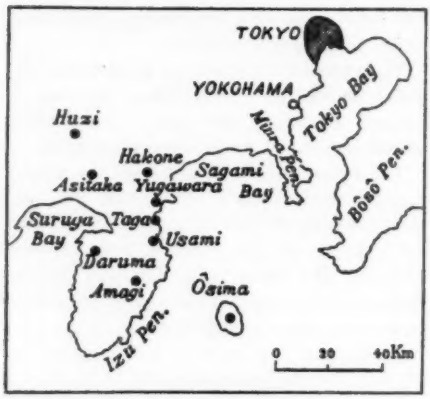

FIGURE 1.—DISTRIBUTION OF CHIEF VOLCANOES IN THE SOUTHERN PART OF THE FOSSA MAGNA

OLDER MIOCENE VOLCANISM: The oldest volcanic rocks in this region known to us constitute a massive complex, possibly more than a few thousand meters thick, consisting of pyroxene-andesites and basalts associated with pyroclastics Fig. 2). They are products of submarine eruptions of older Miocene age. The rocks are altered by hydrothermal solutions, resulting in the precipitation of zeolite, calcite, and chlorite in the forms of amygdules and veinlets. The strata, where visible, are much dislocated and faulted, as a result of Miocene crustal movement. The older Miocene complex exposed near the northern border of the mapped area (Fig. 2) is known as the Misaka Series, which extends to the Tanzawa Mountainland lying to the north. In the central part of this mountainland, various metamorphic rocks originated from the basic volcanics of the complex (Sugi, 1931, p. 87). The southern extension of the complex, which is exposed at the base of the younger volcanics of the mapped area, is referred to here as the Yugasima Series.

MIDDLE TO YOUNGER MIOCENE AND PLIOCENE VOLCANISM: The Tertiary volcanic formations of post-older Miocene age (Fig. 2) overlie the erosion surface which cuts the Yugasima Series. They are preserved in less altered and less disturbed conditions, their aggregate thickness being several hundred meters.

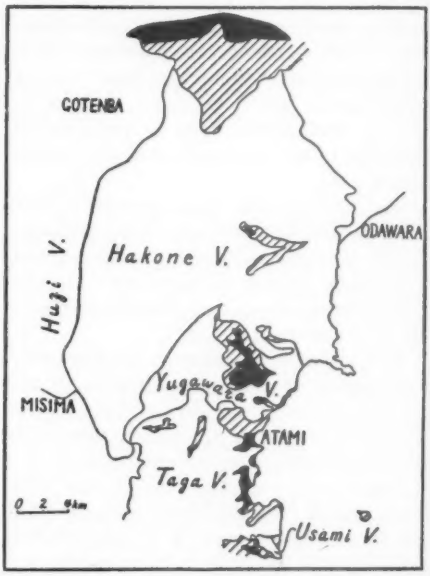

FIGURE 2.—DISTRIBUTION OF THE OLDER MIOCENE ROCKS (black areas), THE MIDDLE MIOCENE TO PLIOCENE ROCKS (shaded area), AND THE QUATERNARY ROCKS (white areas)

During younger Miocene (or older Pliocene?) time, an eruption caused by an acid magma gave rise to extensive series of shallow sea deposits, consisting largely of pumice tuffs and tuff breccias of pyroxene-quartz-dacites and pyroxene-hornblende-quartz-dacites (Atami Tuffs and Haya-kawa Tuff Breccias). This eruption was succeeded by an outpouring of blocky lavas of glassy pyroxene-andesites (Sukumo-gawa Andesite Group. Haya-kawa Tuff Breccias and the last-named andesites are now exposed along the deep gorges which traverse the Hakone volcano, forming the foundation of this body.

During Pliocene, alternate eruptions of basic to intermediate lavas and pyroclastics took place over the southern part of the region, accompanied by intervening periods of quiescence and denudation. A thick series of lavas

TABLE 1.—STRATIGRAPHIC SUCCESSION

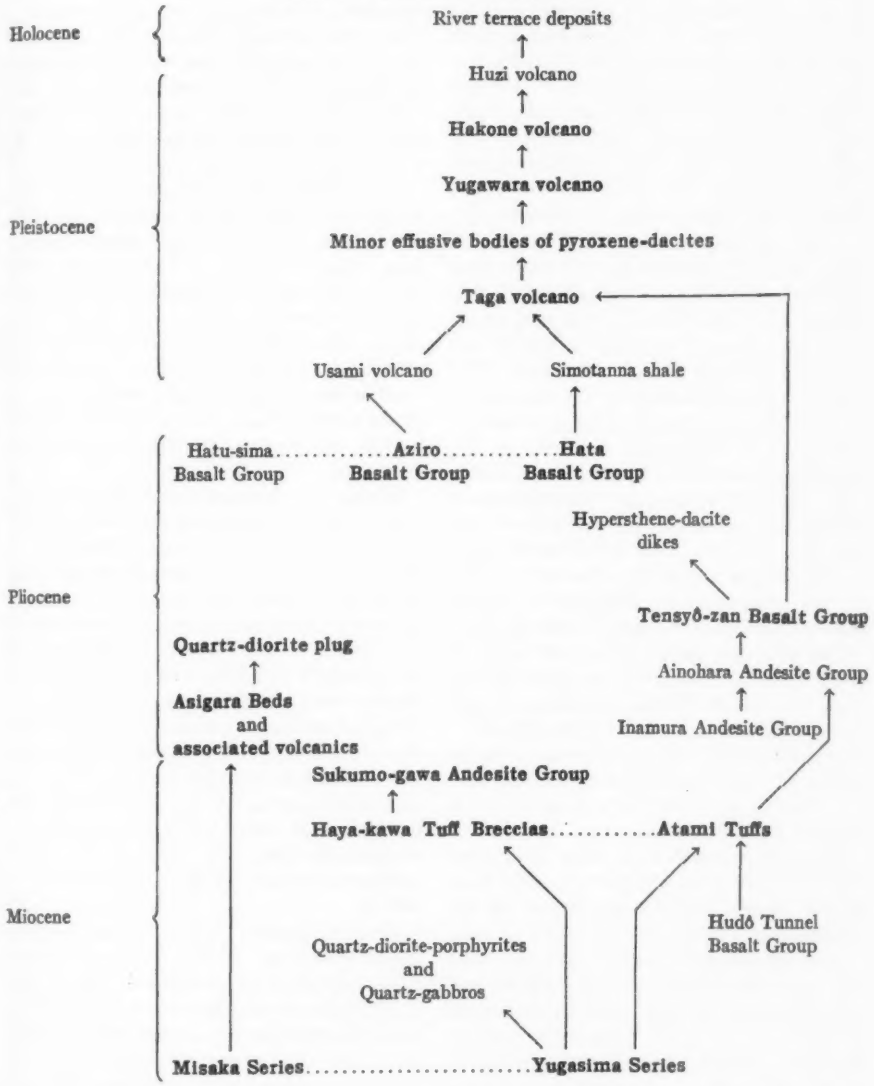

and pyroclastics of basalts and pyroxene-andesites, interbedded with a flow of hornblende-pyroxene-quartz-dacite, was laid down over the area extending from the present site of Atami City to the northern limit of the present Yugawara volcano (Tensyô-zan Basalt Group). At the close of Pliocene (or the beginning of Pleistocene?), basaltic magmas with a high fluidity were erupted in the forms of lavas, scoriae, and spindle-shaped bombs, which accumulated over the area later covered by the Taga volcano (Aziro Basalt Group, and Hata Basalt Group).

In the southern part of the region, a subaerial

condition seems to have prevailed during the Pliocene volcanic episode, whereas near the northern border of the mapped area, a local geosynclinse existed during older Pliocene time. Here, a series of marine sediments (conglomerates, sandstones, and fossiliferous mudstones) at least 4000 m. thick was deposited (Asigara Beds). Contemporaneous eruptions gave rise to flows and pyroclastic deposits of andesites and dacites which were interbedded with the sediments. Intrusion of a plug of augite-bearing hypersthene-quartz-diorite took place after the sediments had suffered folding (middle or younger Pliocene). This rock grades to hornblende-augite-hypersthene-andesite toward the contact with the sediments. The volcanic rocks erupted during this geosynclinal subsidence are characterized by the common occurrence of hornblende; the rocks of the southern area are almost devoid of this mineral.

QUATERNARY VOLCANISM: The eruptions of this age built up cone-shaped and dome-shaped volcanos. However, some of the older cones have suffered such dissection that the locations of their eruptive centers can only be inferred from their ill-defined topography and structure.

The lithologic characters of the rocks of these cones and domes do not differ greatly from those of the Tertiary volcanics. Basalts and pyroxene-andesites are the most predominant; some dacites are also represented. Rocks with hornblende phenocrysts are extremely rare. The rocks are markedly fresh as compared with those of the Tertiary age.

Usami is a stratovolcano made up of lavas and pyroclastics, chiefly of andesites, lying largely outside the southern border of the mapped area (Fig. 2) (Tsuya, 1937, p. 264).

Taga volcano, whose eruptive products have the aggregate thickness of about 500 m. was built up around the main center situated south of the present site of Atami. The earliest explosive eruption deposited tuff breccias of wide lateral extension, interbedded with flows of basic andesites. This activity was succeeded by alternate eruptions of andesite agglomerates and lavas in the area west of the main center and by gentle outpouring of andesite lavas in the north. The next event was the construction of the main body made up of lavas of andesites and basalts, associated with some pyroclastics. The lavas of the main body show a regular succession, in ascending order, from augite-hypersthene-andesites, through olivine-hypersthene-augite-andesites and -basalts, to augite-olivine-basalts. The activity of this volcano came to an end when an explosion at the central crater spread out extensive layers of volcanic breccias over the slope of the cone.

Minor effusive bodies of augite-hypersthene-dacites and -quartz-dacite appeared near the northern border of the Taga volcano (Izusan dacite, Higane dacite, and Karuisawa dacite), and a like body of hypersthene-hornblende-quartz-dacite within the breached crater of the volcano (Kamitaga dacite). All are probably older than the Yugawara volcano, but another small domical mass of augite-bearing hypersthene-dacite (Kaziya dacite) protruded through the northeastern slope of the last-named cone.

Yugawara is a rather simple stratovolcano, with an eruptive center near the present site of Yugawara, about 5 km north of Atami. The main part of the cone is made up of alternate layers of andesitic and basaltic lavas and pyroclastics, with an aggregate thickness of a few hundred meters. A part of the slope of this volcano is covered by thin beds of volcanic breccias erupted at the close of its activity.

Hakone is a triple volcano, consisting of an old somma of about 1000 m. in average height, which encircles a caldera about 12 km. in maximum diameter, a young somma about 900 to 800 m. high, which lies in the eastern part of the caldera just mentioned, and seven central cones, the highest peak of which attains to 1439 m.

The oldest cone was constructed by alternate eruptions of lavas and pyroclastics, now well exposed on the inner, precipitous wall of the old somma, with an aggregate thickness of at least 700 meters (the old somma lavas). Basaltic lavas occur chiefly near the base of the old somma succession, closely associated with agglomerates of the same material. The other part of the old somma is made up of andesitic lavas and pyroclastics, interbedded with a few lavas of pyroxene-dacites. At some intermediate stage of this eruptive period, a dislocation occurred along a line that traversed the cone through its center in NW-SE direction. Two

remarkable parasitic volcanoes were then formed upon this line of dislocation. One is a dome on the southeastern flank of the main cone (Maku-yama lava dome), the rock of which shows alternating bands of pyroxene-andesite and pyroxene-quartz-dacite, and another a stratovolcano of olivine-hypersthene-andesites on the northwestern (Kintoki-san volcano). At some later stage of this period of activity, several parasitic lava domes protruded through the northwestern flank of the main cone.

A cauldron subsidence then occurred in the center of the main cone, succeeded by a period of denudation. The old somma then appeared.

The next activity was chiefly gentle outpourings of fluid lavas of acid augite-hypersthene-andesites and -dacite (the young somma lavas), which gave rise to a gentle-sloped shield volcano within the now formed caldera. A great mass of hypersthene-augite-dacite pumice was then erupted from the central crater of the shield, which, in the course of descending the slope in the form of pumice flows, overflowed the old somma through its lower points, and finally spread over the skirts of the oldest cone.

A cauldron subsidence occurred again in the area extending over the greater part of the older caldera. The western part of the shield volcano was down-faulted, resulting in the young somma along the eastern margin of the new caldera.

After a short period of denudation, the central cones were built up successively by renewed activity occurring within the caldera. The vents were opened along the NW-SE line of dislocation already mentioned, through which six lava domes (Daigatake, Kozuka-yama, an unnamed mountain 1325 m. high, Komaga-take, and Kami- and Simo-hutago-yama) and a steep-sided stratovolcano (Kami-yama) were erupted. At the beginning of this activity, a mass of pumice was ejected from one of the vents, which spread extensively over the eastern and southwestern areas. Again, the fragmentary materials erupted from Kami-yama moved eastward along the gorge of Haya-kawa, partly in the form of nuée ardente, and partly as mud flows. The rocks of these central cones are quite similar to one another, differing only in the crystallinity and texture of the groundmass. They are hypersthene-augite-andesite with or without phenocrysts of olivine.

The last phase of activity of this period was a destructive explosion, comparable to that of Bandai-san in 1887, by which the western part of Kami-yama was blown off, resulting in a fan-shaped deposit of avalanche debris at the western foot of the mountain.

Only a part of the gentle-sloped skirt of the famous volcano Huzi (Fuji), made up of basalt lavas and mud flows, is included within the mapped area. However the brownish basalt lapilli and ash, ejected from the volcano, covers the whole of the region.

Minerals

Plagioclase and alkali-feldspar

Plagioclase varies from pure anorthite to oligoclase, which passes into potash-oligoclase and anorthoclase. Pure potash-feldspar (orthoclase or sanidine) has not yet been detected. Albite occurs only as a secondary mineral in hydrothermally altered rocks.

Plagioclase: Plagioclase is the commonest mineral both as phenocrysts and as a groundmass constituent. There are few rocks that do not contain plagioclase phenocrysts.

Whether phenocrysts or a groundmass constituent, plagioclase usually forms zoned crystals. The zonal structure tends to be more pronounced, and also more complicated, in the intermediate members of the solid solution series than in the more sodic and more calcic ones. Thus, almost unzoned crystals of anorthite are not uncommon, whereas it is almost impossible to find comparatively homogeneous crystals of labradorite. In strongly zoned crystals of intermediate plagioclase, oscillatory zoning is a quite common feature. The commonest mode of zoning of porphyritic plagioclase in basalts and andesites is such that a broad homogeneous core of anorthite or bytownite is surrounded by narrow zones that become successively more sodic toward the margin. The composition range of plagioclase phenocrysts within a single rock often exceeds 40 per cent of An content.

In many basalts and andesites, cores of larger phenocrysts, when carefully examined,

TABLE 2.—CHEMICAL ANALYSES OF SOME ROCK-FORMING MINERALS FROM IZU, HAKONE, AND ADJACENT REGION

	Anorthite				Olivine		Monoclinic pyroxene			Hypersthene		
	1	2	3	4	5	6	7	8	9	10	11	12
SiO_2	43.54	43.91	44.03	44.49	38.82	39.75	49.86	50.57	50.28	52.83	53.24	52.07
Al_2O_3	35.66	35.98	36.80	36.00	0.20	0.60	5.48	1.47	2.03	2.42	1.38	1.70
Fe_2O_3	0.58	0.15	n.d.	0.08	1.65	0.20	2.42	1.53	2.33	1.53	1.05	none
FeO	none	0.18	n.d.		14.93	17.60	4.23	4.42	21.70	18.05	18.70	22.65
MgO	0.06	0.14	0.20	0.04	42.51	41.80	15.02	17.20	14.77	23.05	23.34	21.13
CaO	19.53	19.58	19.29	19.49	0.40	n.d.	22.34	21.68	8.02	1.45	1.23	1.55
Na_2O	0.26	0.48	0.23	0.59	n.d.	n.d.	none	0.04	n.d.	n.d.	tr.	n.d.
K_2O	tr.	0.03	n.d.	0.03	n.d.	n.d.	none	0.53	n.d.	n.d.		n.d.
H_2O+	0.20	0.20	n.d.	n.d.	0.90	n.d.	0.20	0.99	neglig.	n.d.	0.10	n.d.
H_2O-	0.10	0.18	n.d.	n.d.	n.d.	n.d.	0.11	0.03		n.d.		n.d.
TiO_2	tr.	n.d.	n.d.	n.d.	none	n.d.	0.41	0.57	0.59	0.29	0.23	0.47
P_2O_5	tr.	n.d.	n.d.	n.d.	n.d.	n.d.	none	0.40	0.00	n.d.	tr.	n.d.
MnO	tr.	n.d.	n.d.	n.d.	0.23	0.99	0.15	0.06	0.38	0.36	0.85	0.48
Total.....	99.93	100.83	100.55	100.72	99.64	100.94	100.22	99.49	100.10	99.98	100.12	100.05
Composition (wt. %)	$Ab_{97}An_{98}$	$Ab_{97}An_{96}$	$Ab_{97}An_{98}$	$Ab_{97}An_{95}$	$Fo_{79}Fa_{22}$	$Fo_{71}Fa_{28}$	$Wo_{50}En_{41}Fs_9$	$Wo_{47}En_{48}Fs_6$	$Wo_{48}En_{39}Fs_{13}$	$Wo_2En_{63}Fs_{35}$	$Wo_2En_{60}Fs_{37}$	$Wo_2En_{54}Fs_{43}$

1. Anorthite from olivine-eucrite (H.K. 33010901e), an ejected block of cognate origin in tuff of the Taga volcano. Southwest of Wadaki, north Izu. Analyst, S. Tanaka. According to the spectroscopic analysis by Eiichi Minami of the Chemical Institute of this University, BaO is absent from this anorthite. Professor E. Minami kindly undertook the spectroscopic analysis.

2. Anorthite (phenocrysts) from olivine-basalt, occurring as isolated crystals in beach sand. Borawazawa, Hatizyô-zima volcano, Seven Izu Islands (Harada, 1933, p. 343). Analyst, T. Nemoto.

3. Anorthite (phenocrysts) from basalt, occurring as crystal lapilli. Miyake-zima volcano, Seven Izu Islands (Kikuchi, 1889, p. 43). Analyst, Kitamura.

4. Same as the above (Kôzu, 1914, p. 23). Analyst, H. S. Washington.

5. Olivine included in anorthite crystals ejected in 1874. Miyake-zima volcano, Seven Izu Islands (Seto, 1929, p. 23). Analyst, K. Seto.

6. Olivine (phenocrysts) from olivine-basalt (?). Borawa-zawa, Hatizyô-zima volcano, Seven Izu Islands (Harada, 1936, p. 294). Analyst, A. Kannari.

7. Augite (phenocrysts) from hypersthene-bearing olivine-augite-basalt, occurring as isolated crystals in tuff of the Taga volcano. Southwest of Wadaki, north Izu (Kuno and Sawatari, 1934, p. 328). Analyst, S. Tanaka.

8. Diopside (phenocrysts) from diopside-porphyrite, a dike through Miocene conglomerate. Sano, Yamanasi Prefecture, west of the Huzi volcano (Kôzu, Seto, and Ueda, 1928, p. 406). Analyst, K. Seto.

9. Pigeonite (groundmass) from aphyric andesite (H.K. 33081909a), a lava of the old somma of the Hakone volcano. Saru-sawa, south of Yumoto (Kuno, 1940 c, p. 347). Analyst, I. Iwasaki.

10. Hypersthene (phenocrysts) from augite- and olivine-bearing hypersthene-andesite (H.K. 34090901), a lava of the old somma of the Hakone volcano. West of Tôno-mine, north of Yumoto (Kuno, 1941a, p. 206). Analysts, K. Tada and M. Huzimoto.

11. Hypersthene (phenocrysts) from hypersthene-augite-dacite (H.K. 36082106), forming the pumice flow deposit of the Hakone volcano. West of Odawara (Kuno, 1938a, p. 218). Analyst, S. Tanaka.

12. Hypersthene (phenocrysts) from quartz-bearing augite-pigeonite-hypersthene-andesite (H.K. 330 22001), a lava of the old somma of the Hakone volcano. Near Hakone-tôge, south of Hakone-mati. Analyts, K. Tada and M. Huzimoto. The writer's thanks are due to these analysts of the Research Institute of Tokyo-Sibaura Electric Company, and also to Dr. Inuzuka of the same Institute, through whose courtesy the analysis was undertaken.

are found to have a composition approximate to An_{100} (n_1 on cleavage flakes = 1.582). The outermost narrow zones of phenocrysts in basalts are rarely more sodic than bytownite; in andesites, such narrow zones vary greatly in composition, depending not only on the com-

position of the groundmass, but also on its granularity. They tend to be more sodic (labradorite to andesine) as the surrounding groundmass is coarser in granularity. Andesites with fine-grained groundmass sometimes carry phenocrysts of anorthite surrounded by narrow rims which are as calcic as bytownite.

One of the outstanding features of the basic lavas of this region and adjacent areas is the occasional occurrence of well-shaped, large crystals (up to 3 cm.) of anorthite. Twinning on pericline law is characteristic. Such crystals often include grains of olivine and rarely grains of pyroxenes. In a basaltic andesite occurring as a dike immediately east of Miyanosita, Hakone, rounded grains of olivine included in anorthite phenocrysts are arranged radially from the centers of the host crystals. These anorthite crystals invariably have compositions approximate to An_{100}-An_{98}, sometimes surrounded by narrow rims of more sodic anorthite. Crystals (0.5–1.5 cm) from basaltic tuff of the Taga volcano, 2 km. southwest of Wadaki, near Aziro, have the following properties:

Core: $\alpha = 1.577$ (min.), $\beta = 1.584$ (min.) – 1.585 (max.), $\gamma = 1.590$ (max.) (all ± 0.0005)
$(-)2V = 75°$
X′∧010 on 001 = 37° – 40°
Composition: An_{100}–An_{98}
Margin: $\alpha = 1.574$, X′∧010 on 001 = 34°
Composition: An_{95}

Chemical analyses of quite similar crystals from the Hatizyô-zima volcano, and those from the Miyake-zima volcano, both of the Seven Izu Islands, are cited in Table 2 (columns 2, 3, 4). They are invariably calcic anorthite containing negligible amount of K_2O.

Optical properties of the Miyake-zima anorthite, as determined by Kôzu (1914, p. 23), are: $\alpha = 1.5747$, $\beta = 1.5827$, $\gamma = 1.5880$, $2V = 77°16'$.

Homogeneous crystals of anorthite also occur as a constituent of olivine-eucrite and allivalite (olivine-augite-anorthite rock and olivine-anorthite rock respectively, both with a little interstitial groundmass, Pl. 2, figs. 1, 2). These rocks, which occur as cognate ejecta, represent early segregations in basaltic magmas. The analysed anorthite from olivine-eucrite (H.K. 33010901e) contained in the tuff of the Taga volcano just mentioned (Table 2, column 1) is glass clear and entirely free from inclusions except a negligible amount of fine dust so that the appreciable amount of Fe_2O_3 in the analysis cannot be attributed to impurities. In other respects, its composition is quite similar to the anorthites from Hatizyô-zima and Miyake-zima. Calculation of the anorthite and albite molecules from the analysis does not yield any notable amounts of excess or deficient SiO_2 and Al_2O_3 (+ Fe_2O_3); the analysis agrees closely with the formula of pure feldspar. The optical properties of this anorthite, compared with those of pure anorthite (An_{100}), are:

	Wadaki anorthite An_{98}	
Min.	*Max.*	*Aver.*
$\alpha = 1.575$*	?	1.576
$\beta = 1.583$	1.585	1.584
$\gamma =$?	1.589	1.588
$(-)2V = 76°$	80°	78°

Inclined dispersion very weak with $\rho < v$.

Pure anorthite An_{100}**

$\alpha = 1.5755$
$\beta = 1.5832$
$\gamma = 1.5885$
$(-)2V = 77°$

Inclined dispersion weak with $\rho < v$.

* All ±0.0005.
** After Winchell (1933, p. 332, 333).

Alkali-feldspar: Andesine and oligoclase often pass into a peculiar feldspar showing a microcline-like appearance. A typical example is the feldspar in hypersthene-bearing augite-pigeonite-quartz-diorite (Kuno, 1940a, p. 176), a partially remelted rock-fragment ejected with the pumice of the Hakone volcano. The core of each feldspar crystal shows all the appearances of the ordinary plagioclase, with lamellar twinning both on the albite and pericline laws. These twinning lamellae become finer and more plentiful toward the margin until the outermost zone exhibits a kind of

lattice structure due to two sets of fine twinning lamellae, one parallel to 010 and the other parallel to 001 (Pl. 1, figs. 1 and 2). Where the lamellae become submicroscopic, the feldspar shows mottled extinction. A complete gradation is seen between the core and the margin, not only in the coarseness of the twinning lamellae but also in the optical properties:

Core	*Intermediate zone*	*Marginal zone*
1) (−)2V = 88°→	(−)2V = 68°→	(−)2V = 45°
2) (+)2V = 89°——	gradual ——	(−)2V = 52°
3) ?	?	(−)2V = 44°
4) ?	?	(−)2V = 61°

The optical orientation of one of the crystals (1) is plotted in Figure 3. The optical properties show that the core is a member of the ordinary plagioclase series (about An_{44}), while the marginal zone deviates from this series. This zone has α (min) = 1.530. β (min) = 1.535, and appears to be potash-oligoclase or lime-rich anorthoclase. Gradual passage from andesine to potash-oligoclase, or further to anorthoclase, is also noted in feldspar crystals in some quartz-dioritic or granodioritic ejecta embedded in pumice deposit of the Hakone volcano exposed near Asinoyu, and also in the Tertiary tuffs near Atami. In these rocks, however, the marginal zones of the crystals do not show mottled extinction, or show it quite indistinctly. They have $\beta \doteqdot 1.540$, $(-)2V \doteqdot 60°$, and $\beta \doteqdot 1.530$, $(-)2V \doteqdot 40°$, the optic angle 2V about X tending to decrease with the refractive indices.

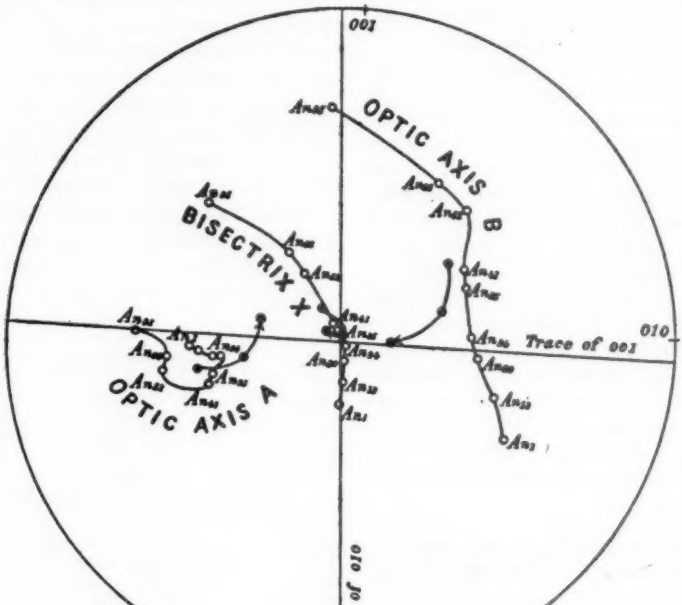

FIGURE 3. -STEREOGRAPHIC PROJECTION OF THE OPTIC ORIENTATIONS OF PLAGIOCLASES AND ORTHOCLASE
On a plane normal to a-axis. Open circles: normal plagioclase series. Solid circles: zoned plagioclase-anorthoclase in pigeonite-quartz-diorite from Hakone (H.K. 37090503), showing the optic orientations of the core, intermediate zone, and marginal zone.

Furthermore, anorthoclase (α = 1.524, γ = 1.529, $(-)2V \doteqdot 40°$) occurs commonly in holocrystalline groundmass of andesites and

dacites, especially in coarsely crystalline patches, forming narrow rims around andesine crystals (about An_{40} in most cases) in crystallographic continuity (Pl. 1, fig. 6) and also isolated prisms. Anorthoclase crystals are usually embedded poikilitically in coarser grains of interstitial quartz. Although the transitional zone between the anorthoclase and the andesine is difficult to recognize due to fineness of the grains, the sequence of crystallization is essentially the same as in the more slowly crystallized quartz-dioritic rocks. Andesine, potash-oligoclase, and anorthoclase constitute a simple solid solution series, which forms either a continuous zoning or an apparently discontinuous one without the intermediate member, depending largely on the rate of cooling.

The feldspar of this region forms a rather simple continuous reaction series, from anorthite (An_{100}) to anorthoclase. There is no indication that pure potash-feldspar (orthoclase or sanidine) appears as a separate phase throughout the history of the magma.

Inclusions in Plagioclase: Phenocrysts of plagioclase often show peculiar textures due to inclusions. Three types are to be distinguished: irregular-shaped inclusions of the groundmass, right and below); this arrangement and outlines give an impression of having been developed from independent grains.

Some rocks enclose small fragments of argillaceous sediments completely recrystallized into exceedingly minute grains of plagioclase, pyroxene, graphite, and iron ore. Around such xenoliths are developed mosaic aggregates of short prismatic or granular plagioclase, with interstices infilled with the groundmass material. Toward the margin of the aggregates, the plagioclase crystals show distinct tendency to become coarser and to rearrange themselves to a common orientation (Fig. 4, below). In a more advanced stage of rearrangement, these dust-like inclusions, and those giving rise to a honey-combed structure in the host.

Typical examples of the groundmass inclusions are shown in Figure 4 and Plate 1, figure 3. The crystallinity of the included material runs parallel to that of the groundmass in which the plagioclase is embedded. The inclusions are so often connected with one another through narrow channels that the interior of each plagioclase crystal is divided into numerous sectors with roughly prismatic or granular outline (Fig. 4, left), usually uniformly

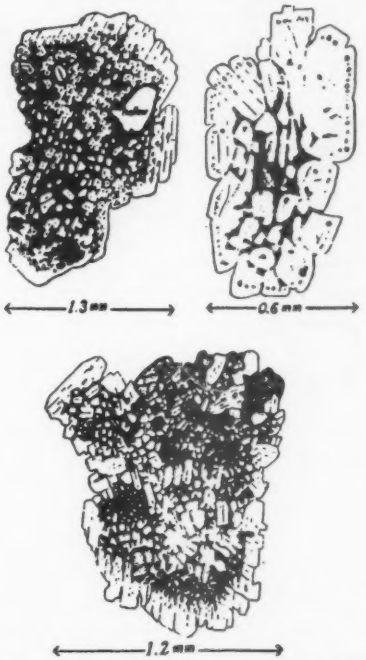

Figure 4.—Various Stages of the Development of the Groundmass Inclusions in Plagioclase

oriented throughout. In some instances, they show slightly different orientations (Fig. 4, crystals coalesce to form a single crystal comparable in size to the ordinary phenocrysts; the interstitial groundmass between the former mosaic grains is preserved as irregular-shaped inclusions. Thus, a complete passage can be traced from the mosaic aggregates of plagioclase around the xenoliths to the phenocrysts with the groundmass inclusions.

The dust inclusions in plagioclase consist of finely divided particles of pyroxene and iron ore, with or without glass, often elongated parallel to the cleavage traces of the enclosing plagioclase (Fig. 5). The inclusions are crowded either in the core of the host crystal (Pl. 5, figs. 4, 5; Pl. 6, fig. 3) or in a definite zone in the

condition seems to have prevailed during the Pliocene volcanic episode, whereas near the northern border of the mapped area, a local geosynclinse existed during older Pliocene time. Here, a series of marine sediments (conglomerates, sandstones, and fossiliferous mudstones) at least 4000 m. thick was deposited (Asigara Beds). Contemporaneous eruptions gave rise to flows and pyroclastic deposits of andesites and dacites which were interbedded with the sediments. Intrusion of a plug of augite-bearing hypersthene-quartz-diorite took place after the sediments had suffered folding (middle or younger Pliocene). This rock grades to hornblende-augite-hypersthene-andesite toward the contact with the sediments. The volcanic rocks erupted during this geosynclinal subsidence are characterized by the common occurrence of hornblende; the rocks of the southern area are almost devoid of this mineral.

QUATERNARY VOLCANISM: The eruptions of this age built up cone-shaped and dome-shaped volcanos. However, some of the older cones have suffered such dissection that the locations of their eruptive centers can only be inferred from their ill-defined topography and structure.

The lithologic characters of the rocks of these cones and domes do not differ greatly from those of the Tertiary volcanics. Basalts and pyroxene-andesites are the most predominant; some dacites are also represented. Rocks with hornblende phenocrysts are extremely rare. The rocks are markedly fresh as compared with those of the Tertiary age.

Usami is a stratovolcano made up of lavas and pyroclastics, chiefly of andesites, lying largely outside the southern border of the mapped area (Fig. 2) (Tsuya, 1937, p. 264).

Taga volcano, whose eruptive products have the aggregate thickness of about 500 m. was built up around the main center situated south of the present site of Atami. The earliest explosive eruption deposited tuff breccias of wide lateral extension, interbedded with flows of basic andesites. This activity was succeeded by alternate eruptions of andesite agglomerates and lavas in the area west of the main center and by gentle outpouring of andesite lavas in the north. The next event was the construction of the main body made up of lavas of andesites and basalts, associated with some pyroclastics. The lavas of the main body show a regular succession, in ascending order, from augite-hypersthene-andesites, through olivine-hypersthene-augite-andesites and -basalts, to augite-olivine-basalts. The activity of this volcano came to an end when an explosion at the central crater spread out extensive layers of volcanic breccias over the slope of the cone.

Minor effusive bodies of augite-hypersthene-dacites and -quartz-dacite appeared near the northern border of the Taga volcano (Izusan dacite, Higane dacite, and Karuisawa dacite), and a like body of hypersthene-hornblende-quartz-dacite within the breached crater of the volcano (Kamitaga dacite). All are probably older than the Yugawara volcano, but another small domical mass of augite-bearing hypersthene-dacite (Kaziya dacite) protruded through the northeastern slope of the last-named cone.

Yugawara is a rather simple stratovolcano, with an eruptive center near the present site of Yugawara, about 5 km north of Atami. The main part of the cone is made up of alternate layers of andesitic and basaltic lavas and pyroclastics, with an aggregate thickness of a few hundred meters. A part of the slope of this volcano is covered by thin beds of volcanic breccias erupted at the close of its activity.

Hakone is a triple volcano, consisting of an old somma of about 1000 m. in average height, which encircles a caldera about 12 km. in maximum diameter, a young somma about 900 to 800 m. high, which lies in the eastern part of the caldera just mentioned, and seven central cones, the highest peak of which attains to 1439 m.

The oldest cone was constructed by alternate eruptions of lavas and pyroclastics, now well exposed on the inner, precipitous wall of the old somma, with an aggregate thickness of at least 700 meters (the old somma lavas). Basaltic lavas occur chiefly near the base of the old somma succession, closely associated with agglomerates of the same material. The other part of the old somma is made up of andesitic lavas and pyroclastics, interbedded with a few lavas of pyroxene-dacites. At some intermediate stage of this eruptive period, a dislocation occurred along a line that traversed the cone through its center in NW-SE direction. Two

remarkable parasitic volcanoes were then formed upon this line of dislocation. One is a dome on the southeastern flank of the main cone (Maku-yama lava dome), the rock of which shows alternating bands of pyroxene-andesite and pyroxene-quartz-dacite, and another a stratovolcano of olivine-hypersthene-andesites on the northwestern (Kintoki-san volcano). At some later stage of this period of activity, several parasitic lava domes protruded through the northwestern flank of the main cone.

A cauldron subsidence then occurred in the center of the main cone, succeeded by a period of denudation. The old somma then appeared.

The next activity was chiefly gentle outpourings of fluid lavas of acid augite-hypersthene-andesites and -dacite (the young somma lavas), which gave rise to a gentle-sloped shield volcano within the now formed caldera. A great mass of hypersthene-augite-dacite pumice was then erupted from the central crater of the shield, which, in the course of descending the slope in the form of pumice flows, overflowed the old somma through its lower points, and finally spread over the skirts of the oldest cone.

A cauldron subsidence occurred again in the area extending over the greater part of the older caldera. The western part of the shield volcano was down-faulted, resulting in the young somma along the eastern margin of the new caldera.

After a short period of denudation, the central cones were built up successively by renewed activity occurring within the caldera. The vents were opened along the NW-SE line of dislocation already mentioned, through which six lava domes (Daigatake, Kozuka-yama, an unnamed mountain 1325 m. high, Komaga-take, and Kami- and Simo-hutago-yama) and a steep-sided stratovolcano (Kami-yama) were erupted. At the beginning of this activity, a mass of pumice was ejected from one of the vents, which spread extensively over the eastern and southwestern areas. Again, the fragmentary materials erupted from Kami-yama moved eastward along the gorge of Haya-kawa, partly in the form of nuée ardente, and partly as mud flows. The rocks of these central cones are quite similar to one another, differing only in the crystallinity and texture of the groundmass. They are hypersthene-augite-andesite with or without phenocrysts of olivine.

The last phase of activity of this period was a destructive explosion, comparable to that of Bandai-san in 1887, by which the western part of Kami-yama was blown off, resulting in a fan-shaped deposit of avalanche debris at the western foot of the mountain.

Only a part of the gentle-sloped skirt of the famous volcano Huzi (Fuji), made up of basalt lavas and mud flows, is included within the mapped area. However the brownish basalt lapilli and ash, ejected from the volcano, covers the whole of the region.

Minerals

Plagioclase and alkali-feldspar

Plagioclase varies from pure anorthite to oligoclase, which passes into potash-oligoclase and anorthoclase. Pure potash-feldspar (orthoclase or sanidine) has not yet been detected. Albite occurs only as a secondary mineral in hydrothermally altered rocks.

Plagioclase: Plagioclase is the commonest mineral both as phenocrysts and as a groundmass constituent. There are few rocks that do not contain plagioclase phenocrysts.

Whether phenocrysts or a groundmass constituent, plagioclase usually forms zoned crystals. The zonal structure tends to be more pronounced, and also more complicated, in the intermediate members of the solid solution series than in the more sodic and more calcic ones. Thus, almost unzoned crystals of anorthite are not uncommon, whereas it is almost impossible to find comparatively homogeneous crystals of labradorite. In strongly zoned crystals of intermediate plagioclase, oscillatory zoning is a quite common feature. The commonest mode of zoning of porphyritic plagioclase in basalts and andesites is such that a broad homogeneous core of anorthite or bytownite is surrounded by narrow zones that become successively more sodic toward the margin. The composition range of plagioclase phenocrysts within a single rock often exceeds 40 per cent of An content.

In many basalts and andesites, cores of larger phenocrysts, when carefully examined,

TABLE 2.—CHEMICAL ANALYSES OF SOME ROCK-FORMING MINERALS FROM IZU, HAKONE, AND ADJACENT REGION

	Anorthite				Olivine		Monoclinic pyroxene			Hypersthene		
	1	2	3	4	5	6	7	8	9	10	11	12
SiO_2	43.54	43.91	44.03	44.49	38.82	39.75	49.86	50.57	50.28	52.83	53.24	52.07
Al_2O_3	35.66	35.98	36.80	36.00	0.20	0.60	5.48	1.47	2.03	2.42	1.38	1.70
Fe_2O_3	0.58	0.15	n.d.	0.08	1.65	0.20	2.42	1.53	2.33	1.53	1.05	none
FeO	none	0.18	n.d.		14.93	17.60	4.23	4.42	21.70	18.05	18.70	22.65
MgO	0.06	0.14	0.20	0.04	42.51	41.80	15.02	17.20	14.77	23.05	23.34	21.13
CaO	19.53	19.58	19.29	19.49	0.40	n.d.	22.34	21.68	8.02	1.45	1.23	1.55
Na_2O	0.26	0.48	0.23	0.59	n.d.	n.d.	none	0.04	n.d.	n.d.	tr.	n.d.
K_2O	tr.	0.03	n.d.	0.03	n.d.	n.d.	none	0.53	n.d.	n.d.		n.d.
H_2O+	0.20	0.20	n.d.	n.d.	0.90	n.d.	0.20	0.99	neglig.	n.d.	0.10	n.d.
H_2O-	0.10	0.18	n.d.	n.d.	n.d.	n.d.	0.11	0.03		n.d.		n.d.
TiO_2	tr.	n.d.	n.d.	n.d.	none	n.d.	0.41	0.57	0.59	0.29	0.23	0.47
P_2O_5	tr.	n.d.	n.d.	n.d.	n.d.	n.d.	none	0.40	0.00	n.d.	tr.	n.d.
MnO	tr.	n.d.	n.d.	n.d.	0.23	0.99	0.15	0.06	0.38	0.36	0.85	0.48
Total.....	99.93	100.83	100.55	100.72	99.64	100.94	100.22	99.49	100.10	99.98	100.12	100.05
Composition (wt. %)	Ab_2An_{98}	Ab_4An_{96}	Ab_2An_{98}	Ab_5An_{95}	$Fo_{76}Fa_{24}$	$Fo_{74}Fa_{26}$	$Wo_{50}En_{41}Fs_9$	$Wo_{36}En_{43}Fs_{21}$	$Wo_{31}En_{38}Fs_{31}$	$Wo_3En_{67}Fs_{30}$	$Wo_3En_{60}Fs_{37}$	$Wo_4En_{42}Fs_{54}$

1. Anorthite from olivine-eucrite (H.K. 33010901e), an ejected block of cognate origin in tuff of the Taga volcano. Southwest of Wadaki, north Izu. Analyst, S. Tanaka. According to the spectroscopic analysis by Eiichi Minami of the Chemical Institute of this University, BaO is absent from this anorthite. Professor E. Minami kindly undertook the spectroscopic analysis.

2. Anorthite (phenocrysts) from olivine-basalt, occurring as isolated crystals in beach sand. Borawa-zawa, Hatizyô-zima volcano, Seven Izu Islands (Harada, 1933, p. 343). Analyst, T. Nemoto.

3. Anorthite (phenocrysts) from basalt, occurring as crystal lapilli. Miyake-zima volcano, Seven Izu Islands (Kikuchi, 1889, p. 43). Analyst, Kitamura.

4. Same as the above (Kôzu, 1914, p. 23). Analyst, H. S. Washington.

5. Olivine included in anorthite crystals ejected in 1874. Miyake-zima volcano, Seven Izu Islands (Seto, 1929, p. 23). Analyst, K. Seto.

6. Olivine (phenocrysts) from olivine-basalt (?). Borawa-zawa, Hatizyô-zima volcano, Seven Izu Islands (Harada, 1936, p. 294). Analyst, A. Kannari.

7. Augite (phenocrysts) from hypersthene-bearing olivine-augite-basalt, occurring as isolated crystals in tuff of the Taga volcano. Southwest of Wadaki, north Izu (Kuno and Sawatari, 1934, p. 328). Analyst, S. Tanaka.

8. Diopside (phenocrysts) from diopside-porphyrite, a dike through Miocene conglomerate. Sano, Yamanasi Prefecture, west of the Huzi volcano (Kôzu, Seto, and Ueda, 1928, p. 406). Analyst, K. Seto.

9. Pigeonite (groundmass) from aphyric andesite (H.K. 33081909a), a lava of the old somma of the Hakone volcano. Saru-sawa, south of Yumoto (Kuno, 1940 c, p. 347). Analyst, I. Iwasaki.

10. Hypersthene (phenocrysts) from augite- and olivine-bearing hypersthene-andesite (H.K. 34090901), a lava of the old somma of the Hakone volcano. West of Tôno-mine, north of Yumoto (Kuno, 1941a, p. 206). Analysts, K. Tada and M. Huzimoto.

11. Hypersthene (phenocrysts) from hypersthene-augite-dacite (H.K. 36082106), forming the pumice flow deposit of the Hakone volcano. West of Odawara (Kuno, 1938a, p. 218). Analyst, S. Tanaka.

12. Hypersthene (phenocrysts) from quartz-bearing augite-pigeonite-hypersthene-andesite (H.K. 330 22001), a lava of the old somma of the Hakone volcano. Near Hakone-tôge, south of Hakone-mati. Analysts, K. Tada and M. Huzimoto. The writer's thanks are due to these analysts of the Research Institute of Tokyo-Sibaura Electric Company, and also to Dr. Inuzuka of the same Institute, through whose courtesy the analysis was undertaken.

are found to have a composition approximate to An_{100} (n_1 on cleavage flakes = 1.582). The outermost narrow zones of phenocrysts in basalts are rarely more sodic than bytownite; in andesites, such narrow zones vary greatly in composition, depending not only on the com-

position of the groundmass, but also on its granularity. They tend to be more sodic (labradorite to andesine) as the surrounding groundmass is coarser in granularity. Andesites with fine-grained groundmass sometimes carry phenocrysts of anorthite surrounded by narrow rims which are as calcic as bytownite.

One of the outstanding features of the basic lavas of this region and adjacent areas is the occasional occurrence of well-shaped, large crystals (up to 3 cm.) of anorthite. Twinning on pericline law is characteristic. Such crystals often include grains of olivine and rarely grains of pyroxenes. In a basaltic andesite occurring as a dike immediately east of Miyanosita, Hakone, rounded grains of olivine included in anorthite phenocrysts are arranged radially from the centers of the host crystals. These anorthite crystals invariably have compositions approximate to An_{100}-An_{98}, sometimes surrounded by narrow rims of more sodic anorthite. Crystals (0.5–1.5 cm) from basaltic tuff of the Taga volcano, 2 km. southwest of Wadaki, near Aziro, have the following properties:

Core: $\alpha = 1.577$ (min.), $\beta = 1.584$ (min.) – 1.585 (max.), $\gamma = 1.590$ (max.) (all $\pm$ 0.0005)
$(-)2V = 75°$
X′∧010 on 001 = 37° – 40°
Composition: An_{100}–An_{98}
Margin: $\alpha = 1.574$, X′∧010 on 001 = 34°
Composition: An_{95}

Chemical analyses of quite similar crystals from the Hatizyô-zima volcano, and those from the Miyake-zima volcano, both of the Seven Izu Islands, are cited in Table 2 (columns 2, 3, 4). They are invariably calcic anorthite containing negligible amount of K_2O.

Optical properties of the Miyake-zima anorthite, as determined by Kôzu (1914, p. 23), are: $\alpha = 1.5747$, $\beta = 1.5827$, $\gamma = 1.5880$, $2V = 77°16'$.

Homogeneous crystals of anorthite also occur as a constituent of olivine-eucrite and allivalite (olivine-augite-anorthite rock and olivine-anorthite rock respectively, both with a little interstitial groundmass, Pl. 2, figs. 1, 2). These rocks, which occur as cognate ejecta, represent early segregations in basaltic magmas. The analysed anorthite from olivine-eucrite (H.K. 33010901e) contained in the tuff of the Taga volcano just mentioned (Table 2, column 1) is glass clear and entirely free from inclusions except a negligible amount of fine dust so that the appreciable amount of Fe_2O_3 in the analysis cannot be attributed to impurities. In other respects, its composition is quite similar to the anorthites from Hatizyô-zima and Miyake-zima. Calculation of the anorthite and albite molecules from the analysis does not yield any notable amounts of excess or deficient SiO_2 and Al_2O_3 (+ Fe_2O_3); the analysis agrees closely with the formula of pure feldspar. The optical properties of this anorthite, compared with those of pure anorthite (An_{100}), are:

	Wadaki anorthite An_{98}	
Min.	*Max.*	*Aver.*
$\alpha = 1.575$*	?	1.576
$\beta = 1.583$	1.585	1.584
$\gamma = ?$	1.589	1.588
$(-)2V = 76°$	80°	78°

Inclined dispersion very weak with $\rho < v$.

Pure anorthite An_{100}**

$\alpha = 1.5755$
$\beta = 1.5832$
$\gamma = 1.5885$
$(-)2V = 77°$
Inclined dispersion weak with $\rho < v$.

* All ± 0.0005.
** After Winchell (1933, p. 332, 333).

Alkali-feldspar: Andesine and oligoclase often pass into a peculiar feldspar showing a microcline-like appearance. A typical example is the feldspar in hypersthene-bearing augite-pigeonite-quartz-diorite (Kuno, 1940a, p. 176), a partially remelted rock-fragment ejected with the pumice of the Hakone volcano. The core of each feldspar crystal shows all the appearances of the ordinary plagioclase, with lamellar twinning both on the albite and pericline laws. These twinning lamellae become finer and more plentiful toward the margin until the outermost zone exhibits a kind of

lattice structure due to two sets of fine twinning lamellae, one parallel to 010 and the other parallel to 001 (Pl. 1, figs. 1 and 2). Where the lamellae become submicroscopic, the feldspar shows mottled extinction. A complete gradation is seen between the core and the margin, not only in the coarseness of the twinning lamellae but also in the optical properties:

Core	*Intermediate zone*	*Marginal zone*
1) (−)2V = 88°→	(−)2V = 68°→	(−)2V = 45°
2) (+)2V = 89°——	gradual——	(−)2V = 52°
3) ?	?	(−)2V = 44°
4) ?	?	(−)2V = 61°

The optical orientation of one of the crystals (1) is plotted in Figure 3. The optical properties show that the core is a member of the ordinary plagioclase series (about An_{48}), while the marginal zone deviates from this series. This zone has α (min) = 1.530. β (min) = 1.535, and appears to be potash-oligoclase or lime-rich anorthoclase. Gradual passage from andesine to potash-oligoclase, or further to anorthoclase, is also noted in feldspar crystals in some quartz-dioritic or granodioritic ejecta embedded in pumice deposit of the Hakone volcano exposed near Asinoyu, and also in the Tertiary fuffs near Atami. In these rocks, however, the marginal zones of the crystals do not show mottled extinction, or show it quite indistinctly. They have $\beta \doteqdot 1.540$, $(-)2V \doteqdot 60°$, and $\beta \doteqdot 1.530$, $(-)2V \doteqdot 40°$, the optic angle 2V about X tending to decrease with the refractive indices.

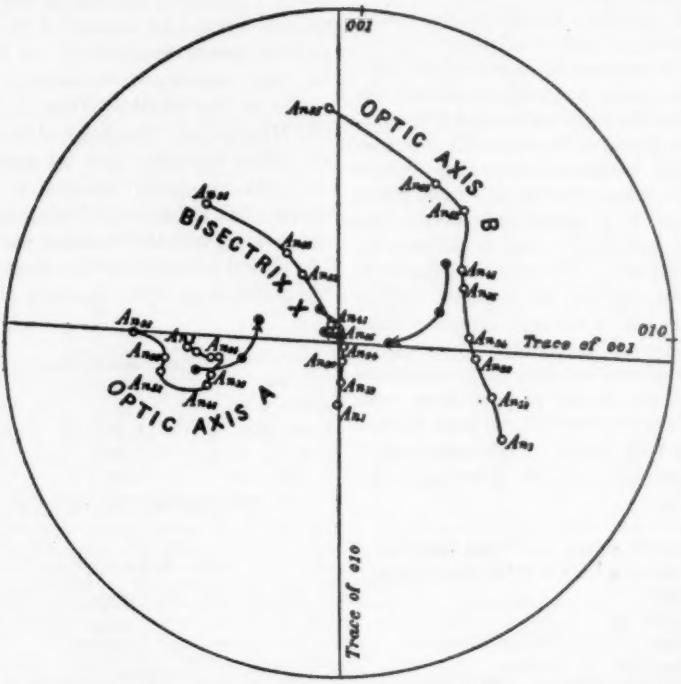

FIGURE 3. -STEREOGRAPHIC PROJECTION OF THE OPTIC ORIENTATIONS OF PLAGIOCLASES AND ORTHOCLASE
On a plane normal to a-axis. Open circles: normal plagioclase series. Solid circles: zoned plagioclase-anorthoclase in pigeonite-quartz-diorite from Hakone (H.K. 37090503), showing the optic orientations of the core, intermediate zone, and marginal zone.

Furthermore, anorthoclase (α = 1.524, γ = 1.529, $(-)2V \doteqdot 40°$) occurs commonly in holocrystalline groundmass of andesites and

dacites, especially in coarsely crystalline patches, forming narrow rims around andesine crystals (about An_{40} in most cases) in crystallographic continuity (Pl. 1, fig. 6) and also isolated prisms. Anorthoclase crystals are usually embedded poikilitically in coarser grains of interstitial quartz. Although the transitional zone between the anorthoclase and the andesine is difficult to recognize due to fineness of the grains, the sequence of crystallization is essentially the same as in the more slowly crystallized quartz-dioritic rocks. Andesine, potash-oligoclase, and anorthoclase constitute a simple solid solution series, which forms either a continuous zoning or an apparently discontinuous one without the intermediate member, depending largely on the rate of cooling.

The feldspar of this region forms a rather simple continuous reaction series, from anorthite (An_{100}) to anorthoclase. There is no indication that pure potash-feldspar (orthoclase or sanidine) appears as a separate phase throughout the history of the magma.

Inclusions in Plagioclase: Phenocrysts of plagioclase often show peculiar textures due to inclusions. Three types are to be distinguished: irregular-shaped inclusions of the groundmass, right and below); this arrangement and outlines give an impression of having been developed from independent grains.

Some rocks enclose small fragments of argillaceous sediments completely recrystallized into exceedingly minute grains of plagioclase, pyroxene, graphite, and iron ore. Around such xenoliths are developed mosaic aggregates of short prismatic or granular plagioclase, with interstices infilled with the groundmass material. Toward the margin of the aggregates, the plagioclase crystals show distinct tendency to become coarser and to rearrange themselves to a common orientation (Fig. 4, below). In a more advanced stage of rearrangement, these dust-like inclusions, and those giving rise to a honey-combed structure in the host.

Typical examples of the groundmass inclusions are shown in Figure 4 and Plate 1, figure 3. The crystallinity of the included material runs parallel to that of the groundmass in which the plagioclase is embedded. The inclusions are so often connected with one another through narrow channels that the interior of each plagioclase crystal is divided into numerous sectors with roughly prismatic or granular outline (Fig. 4, left), usually uniformly

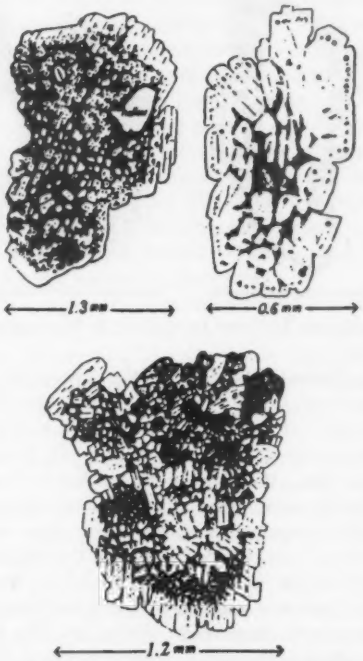

Figure 4.—Various Stages of the Development of the Groundmass Inclusions in Plagioclase

oriented throughout. In some instances, they show slightly different orientations (Fig. 4, crystals coalesce to form a single crystal comparable in size to the ordinary phenocrysts; the interstitial groundmass between the former mosaic grains is preserved as irregular-shaped inclusions. Thus, a complete passage can be traced from the mosaic aggregates of plagioclase around the xenoliths to the phenocrysts with the groundmass inclusions.

The dust inclusions in plagioclase consist of finely divided particles of pyroxene and iron ore, with or without glass, often elongated parallel to the cleavage traces of the enclosing plagioclase (Fig. 5). The inclusions are crowded either in the core of the host crystal (Pl. 5, figs. 4, 5; Pl. 6, fig. 3) or in a definite zone in the

outer part of the host (Fig. 5). In the latter case, the outher margin of the zone of the inclusions is parallel to the outline of the

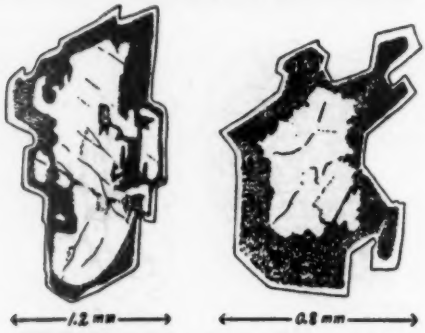

FIGURE 5.—DUST INCLUSIONS IN PLAGIOCLASE

plagioclase crystal, while the zone of the inclusions often sends small tongues toward the interior of the plagioclase crystal, truncating the zonal structure inside (Fig. 5). In some instances, the zone of the inclusions is distinctly more calcic than adjacent zones. In other instances, a narrow calcic zone is developed just outside the zone of the inclusions.

The dust inclusions are explained as formed in plagioclase enclosed by a magma in equilibrium with more calcic plagioclase. The dusts originated by partial crystallization of liquid particles formed by incipient melting of the xenocrystic plagioclase along its cleavages. A part of the materials of the liquid particles was introduced from the magma outside by diffusion.

Such xenocrysts may have represented either crystals suspended in another part of the magma differing in composition or detached crystals from inclusions of cognate origin (either plutonic or volcanic rock in texture). Crystals of purely accidental origin (such as those from deep-seated granitic rocks) appear to be quite rare, as judged from the absence of crystals with fractured outlines or the lack of associated minerals undoubtedly derived from granitic rocks.

Where the liquid particles from the remelting of xenocrystic plagioclase are coarser, they assume irregular or vermicular shapes and are often connected with one another by narrow channels, solidifying into a honey-combed structure in the host plagioclase (Fig. 6; Pl. 1, fig. 4).

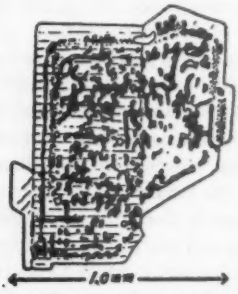

FIGURE 6.—HONEY-COMBED STRUCTURE IN PLAGIOCLASE

Inclusions are monoclinic pyroxene (finely dotted), clear glass, and dusts of pyroxene and iron ore.

Silica minerals

Nearly all the rocks of this region, except glassy lavas, contain at least one of cristobalite, tridymite, and quartz. Cristobalite and tridymite are confined to the groundmass. Quartz occurs as phenocrysts and as a groundmass constituent, and is the only silica mineral in medium-grained intrusive rocks and coarse-grained plutonic rocks.

The microscopical characters and mode of occurrence of these minerals in the groundmass, described in earlier publication (Kuno, 1933a, p. 382 and 1936a, p. 107), are briefly summarized here together with those features noted more recently.

Cristobalite occurs usually in basic to intermediate rocks, and sometimes in acid ones, whereas tridymite and quartz, commonly associated, are largely confined to intermediate and acid rocks, being especially predominant in those with higher crystallinity, though in some basalts they fill up microscopical cavities.

Cristobalite, usually with an appearance of roofing tiles due to multiple twinning but sometimes with irregular mosaic pattern, occurs interstitially or forms rounded or irregular-shaped patches (up to 0.2 mm) somewhat larger than the general grains of the groundmass. When the mineral grows in microscopical cavities, it shows hexagonal or rounded outline in cross section.

In some glassy andesites, however, slender needles of cristobalite are uniformly scattered throughout the groundmass, surrounded by the matrix of brown glass having refractions higher than that of cristobalite and nearly equal to or slightly lower than that of the balsam. The needles show ill-defined parallel arrangement, along with feldspar laths, due to flow of the magma[1] (Pl. 1, fig. 5). This fact strongly indicates that the mineral crystallized before the final solidification of the residual magma which resulted in the glassy matrix. In the same rocks, these crystals also project into microscopical cavities, forming a mesh of crystals due to interpenetration of the needles.

Tridymite fills up interstices of the groundmass and projects into cavities. The crystals are usually elongated or tabular, with characteristic wedge-shaped twinning. In some dacites, compact aggregates of wedge-shaped tridymite form rounded patches and ill-defined streaks where volatile substances seem to have been concentrated (Pl. 2, fig. 3; Pl. 3, fig. 4). Again, well-shaped tridymite crystals, often attaining 1 mm in length, are encountered commonly in coarsely textured, cognate inclusions (so-called autoliths) in some andesitic lavas (Pl. 1, fig. 6).

In the groundmass of lavas, quartz occurs either interstitially or as mosaic aggregates in coarsely crystalline patches and bands of pegmatitic composition, usually associated with anorthoclase and biotite.

In the groundmass of holocrystalline acid andesites, quartz forms more or less rounded patches with uniform extinction throughout relatively large areas (often 0.2–0.3 mm across), where it includes poikilitically numerous laths of andesine and anorthoclase and grains of pyroxene and magnetite. Its textural relation toward the included laths of feldspars resembles in some way that of ophitic pyroxene. In some cases, such patches of poikilitic quartz make up the bulk of the groundmass. In others, they are intermingled with areas of the same general texture but with interstitial filling of tridymite (or cristobalite?) instead of quartz (Pl. 5, fig. 1). In the former case, the groundmass shows uniformly smooth appearance; in the latter, the smooth areas interlock irregularly with those of shagreened appearance.

In the pegmatitic patches and bands, mosaic aggregates of quartz include prisms of anorthoclase, which tend to be concentrated toward the margin of the aggregates. Although the quartz usually exceeds the feldspar in amount, no definite ratio appears to exist. Again, in the groundmass of some dacites, quartz and tridymite form delicate intergrowth, often radiating from a common center (Pl. 6, fig. 6). Judging from its textural relation to the other minerals, quartz is probably the last mineral to separate during the groundmass formation.

Phenocrysts of quartz are comparatively rare in this region. In most cases, they are associated with phenocrysts of hornblende. Fractured xenocrysts of quartz are found in a few basalts and andesites, surrounded by corona of tridymite or pyroxene.

In hypabyssal and plutonic rocks, quartz occurs as subhedral to anhedral grains, and sometimes forms graphic intergrowth with oligoclase which grows radially from euhedral andesine.

The modes of occurrence of these silica minerals justify the conclusion that they are primary crystallization products of magmas and not introduced later by pneumatolitic or hydrothermal process (Kuno, 1933a, p. 388; Larsen et al., 1936, p. 692; MacGregor, 1938, p. 60–61).

In glassy rocks, however, these silica minerals are obviously occult in the glass base.

In many instances, tridymite and quartz seem to have formed where volatile substances have been concentrated at the final stage of solidification of magmas.

Olivines

This mineral occurs in two distinct groups, magnesium olivine and fayalite.

Magnesium olivine is found usually as phenocrysts in most basalts and some andesites, but sometimes as a groundmass constituent in some basalts and a few andesites.

The crystals, usually equant or slightly elongated parallel to c-axis, are sometimes euhedral but more often rounded in outline due to magmatic corrosion. Skeletal crystals or crystals

[1] The writer observed a quite similar phenomenon in needle-like or platy crystals of tridymite in the groundmass of dacite (a lava of 1934–35) from Ô-zima, south Kyûsyû (see Tanakadate, 1935, p. 371), and also in some glassy andesites from the western coast of north Izu.

with deep embayments are not uncommon. The groundmass olivine sometimes forms long prismatic or needle-like crystals elongated parallel to a-axes (elongation being always positive), with deep hollows at both ends of the needles (Fig. 7). A complete gradation is seen from these needles, through skeletal crystals, to those of the ordinary habit common to phenocrysts (Fig. 8).

Another feature of the groundmass olivine is an ill-defined ophitic growth with plagioclase laths.

The magnesium olivine in this region ranges from $Fo_{88}Fa_{12}$ to $Fo_{44}Fa_{56}$ (α(min.) = 1.662, β (max.) = 1.734), as estimated from the diagram by Bowen and Schairer (1935, p. 197). They are always optically negative.

Clear yellow crystals of olivine occurring in the olivine-eucrite (H.K. 33010901e) (p. 21) and those in allivalite (H.K. 35082604b) contained in a pumice bed of Hakone volcano, both of which represent the early formed members of the group, were examined optically with the following results:

Olivine from the eucrite

Min.	*Max.*	*Aver.*
α = 1.674	?	1.675
β = 1.694	1.696	1.695
γ = ?	1.715	1.714
(−)2V = 87°		$\rho > \upsilon$

Olivine from the allivalite

Min.	*Max.*	*Aver.*
α = 1.667	?	1.668
β = 1.685	1.687	1.686
γ = ?	1.706	1.705
(−)2V = 87°		$\rho > \upsilon$

Their estimated compositions are about $Fo_{71}Fa_{29}$ and $Fo_{76}Fa_{24}$ respectively.

Early formed olivines from volcanoes of Seven Izu Islands (Table 2, columns 5, 6) have compositions approximate to that of the olivine from this allivalite.

The composition of olivine often varies greatly in different grains within a single rock as well as in a single crystal. Four isolated phenocrysts in hypersthene-bearing augite-olivine-basalt from the Taga volcano (occurring as one of the cognate ejecta in the tuff bed southwest of Wadaki) were examined separately with the following result:

Crystal A α = 1.665 − 1.668 aver. $Fo_{77}Fa_{23}$
Crystal B α = 1.685 − 1.687 aver. $Fo_{33}Fa_{45}$
Crystal C α = 1.670 − 1.686 $Fo_{75}Fa_{25}$ − $Fo_{33}Fa_{45}$
Crystal D α = 1.672 − 1.674 aver. $Fo_{73}Fa_{27}$

The refractive indices were determined on 001 cleavage flakes.

The widest range of composition of olivine so far observed within a single rock is from $Fo_{76}Fa_{24}$ to $Fo_{44}Fa_{46}$ (basalt from Simotanna).

Olivine phenocrysts are often marginally zoned. The rim is always more ferriferous

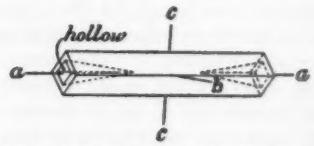

FIGURE 7.—CRYSTAL HABIT OF SOME GROUNDMASS OLIVINE

than the core, as indicated by higher double refraction (γ-α, β-α) and smaller optic angle. No instance of reverse zoning is known. It is evident that the magnesium olivine constitutes a continuous reaction series from about Fo_{88} to about Fo_{44}, the later-formed members being more ferriferous.

Olivine is frequently surrounded by a corona of porphyritic hypersthene, and rarely by one of porphyritic augite, only where there is no hypersthene in the rock. In the former case, the outline of each olivine crystal indicates resorption by the magma from which the hypersthene was separated to form the reaction rim; in the latter, the feature is less obvious. The hypersthene prisms are often tangentially disposed around the olivine crystals. In some instances, however, the hypersthene corona encloses vermicular magnetite arranged more or less radially from the resorbed olivine. In a more advanced stage of resportion, when the olivine disappears completely, the whole aggregate consists of dense stellate groupings of vermicular magnetite in the center and the corona of hypersthene in the margin (Fig. 9).

Every stage of resorption of porphyritic olivine and replacement by groundmass pyroxenes, and/or magnetite, is seen in comparatively

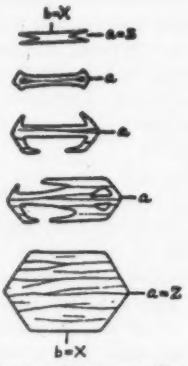

FIGURE 8.—VARIOUS STAGES OF DEVELOPMENT OF OLIVINE CRYSTALS

Uppermost figure is cross section of crystal shown in Figure 7; the lowermost one is that with the ordinary habit. Each section is perpendicular to c-axis.

FIGURE 9.—OLIVINE CRYSTALS SURROUNDED BY HYPERSTHENE AND VERMICULAR MAGNETITE

In the lowermost figure, olivine is almost completely resorbed. Each aggregate is about 1 mm. across.

coarse-grained basalts and andesites. The radial growth of vermicular magnetite around olivine is also to be found in these rocks (Pl. 4, fig. 3).

When the pyroxenic phase of the groundmass is simply monoclinic, the corona around olivine is usually made up of pigeonite (Pl. 4, figs. 1, 2, 3), in a few cases, of hypersthene alone or of hypersthene inside and pigeonite outside (Fig. 10). When both hypersthene and augite

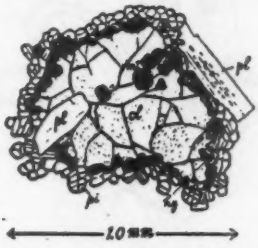

FIGURE 10.—DOUBLE RIMS OF GROUNDMASS PYROXENES AROUND OLIVINE

hy: hypersthene; pi: pigeonite; ol: olivine; mt: magnetite; pl: plagioclase.

occur in the groundmass, the corona consists almost invariably of hypersthene (Pl. 5, fig. 6). In a few cases, when the groundmass contains hypersthene, augite, and pigeonite, the corona is made up of the last-named pyroxene, sometimes attended with a few hypersthene.

Characteristic inclusions are small octahedrons of picotite, magnetite, and green spinel. Rounded grains of augite, hypersthene, and plagioclase are not entirely absent.

In the olivine-eucrite and allivalite (cognate ejecta) olivine is usually idiomorphic toward anorthite and augite (Pl. 2, figs. 1, 2) and rarely moulded upon anorthite. Rounded grains of olivine are often included in anorthite and augite crystals. Probably, therefore, olivine began to crystallize usually earlier than anorthite and augite.

Fayalite occurs as a druse mineral in coarsely crystalline facies of two dacites (hypersthene-oxyhornblende-quartz-dacite and hypersthene-dacite) (Kuno, 1940b, p. 228). It forms either well-shaped crystals projecting into cavities together with needles of pargasite, or interstitial grains between wedge-shaped tridymite crystals which grow inward from the walls of the druses or veins. The remaining spaces are completely infilled with fayalite (Pl. 2, fig. 3) The composition of fayalite from the dacite (H.K. 39010903b) south of Kaziya, is about

Fo_3Fa_{97}, as inferred from its optical properties: $\alpha = 1.802$, $(-)2V = 56°$, $\rho > \nu$, pale yellow in thin section, without pleochroism. In this dacite, the fayalite forms coronas around hypersthene phenocrysts of a composition about $En_{63}Fs_{37}$. (Fig. 11).

FIGURE 11.—GROUPED PHENOCRYSTS OF PLAGIOCLASE (pl), MAGNETITE (black), AND HYPERSTHENE (hy), THE LAST SURROUNDED BY FAYALITE (fa) AND TRIDYMITE (tr)

Fayalite is probably the last mineral to crystallize from the final residuum of magma consisting chiefly of silica and iron together with high proportion of volatiles. Thus there is a distinct gap between the crystallization stage of the magnesium olivine and that of fayalite.

Monoclinic pyroxenes

Macdonald's (1944a, p. 628–629) classification of monoclinic pyroxenes is found to be most useful for pyroxenes in volcanic rocks. Thus the name augite is given to pyroxenes with 2V larger than 45°, pigeonitic augite to those with 2V between 45° and 30° (Macdonald placed the limit at 32°), and pigeonite to those with 2V smaller than 30°.

The monoclinic pyroxenes of this region constitute a complete solid solution from augite (diopsidic), through pigeonitic augite, to iron-rich pigeonite, though there may be some gap in miscibility between pigeonitic augite and magnesian pigeonite. No alkali-pyroxene or titan-augite has been detected, except for aegirine-augite in xenoliths included in andesites.

Phenocrysts are usually augite, occasionally grading into pigeonitic augite in marginal zones. Augite phenocrysts occur in rocks of nearly all compositions. Groundmass grains are usually pigeonitic augite and/or pigeonite, the latter predominant in acid rocks, and less commonly augite associated either with hypersthene or olivine. Pigeonite occurs rarely as phenocrysts and as a constituent of a certain ejected block of plutonic texture.

AUGITE: Crystals are either as long as broad or slightly elongated parallel to c-axis. Twinning on 100 is common. Augite occurring most frequently as phenocrysts is pale green or pale brownish-green, often with a weak pleochroism, especially in more ferriferous members: X ≒ Z = pale green, sometimes with a slight brownish tinge, Y = pale greenish brown. The refractive index β ranges from about 1.685 to about 1.705, most frequently between 1.695 and 1.700. The angle $c \wedge Z$ varies from 40° to 45°, with a weak disperson: $c \wedge Z$ for red light $< c \wedge Z$ for blue light. The optic axial angle 2V about Z rarely exceeds 60°, clustered around 50°, with a weak dispersion $\rho > \nu$.

Chemical analysis of augite occurring as well-shaped crystals (3–10 mm.) in the basaltic tuff (hypersthene-bearing olivine-augite-basalt) of the Taga volcano, exposed at a point 2 km. southwest of Wadaki, is shown in Table 2 (column 7). Its optical properties (Kuno and Sawatari, 1934, p. 327) are as follows:

	Min.	*Max.*	*Aver.*
α	1.680	?	1.689
β	1.687	1.704	1.696
γ	?	1.723	1.715

(+)2V = 60.9° – 56.2°
Aver. 59°
$c \wedge Z$ = 40.5° – 44.5°
Aver. 43°
Dispersion in optic angle weak: $\rho > \nu$
Dispersion in extinction angle weak: $c \wedge Z$ for red light $< c \wedge Z$ for blue light.
Pleochroism:
X = pale green Y = pale greenish-brown
Z = pale brownish-green X > Z > Y

This augite is rich in diopside molecule, containing appreciable amount of Al_2O_3 and

Fe_2O_3 (Table 2). The absence of alkalies is in good agreement with the poverty of these components in the basic rocks of this region.

The analysed augite forms exceptionally large crystals; more common phenocrysts are samller (1–2 mm.) and appear richer in $FeSiO_3$, having generally higher refractive indices and smaller optic angles. For example, augite from pigeonite-bearing andesite (H.K. 33022001) from Hakone-tôge (an old somma lava of the Hakone volcano), apparently the most ferriferous member of the porphyritic augite group, has an approximate composition $Wo_{32}En_{37}Fs_{31}$, as inferred from its optical properties: $\alpha = 1.701$, $\beta = 1.706$, $\gamma = 1.729$, (+) $2V = 48° - 43°$, $c \wedge Z = 43°$ (Kuno, 1936a, p. 125).

The Wadaki augite (Fig. 12, A_1) represents the early-formed members of the group; that from Hakone-tôge (Fig. 12, A_2) represents the later members. Other augites of the region have compositions lying roughly within the elliptical area between these two augites as plotted in Fig. 12.

The augites in the ground mass have the same general characters (refractive indices and optic angle) as the porphyritic ones, and appear to have compositions well within the range indicated.

Diopside from Sano, west of the Huzi volcano (Table 2, column 8), forms large phenocrysts (up to 2 cm) in diopside-porphyrite (a dike related to the Misaka Series?). This colorless diopside is poorer in Al_2O_3 and Fe_2O_3 than the pale-green augite from Wadaki and distinctly lower in refraction and smaller in extinction angle, though similar in optic angle: $\alpha = 1.6729 - 1.6732$, $\beta = 1.6795$, $\gamma = 1.7005 - 1.7006$, $2V = 58°33'$, $c \wedge Z = 39°$ (Kôzu, Seto, and Veda, 1928, p. 406). Similar colorless, low-refracting augite or diopside characterizes the rocks of the Misaka Series exposed around the Huzi volcano, including the area near the northern limit of the geologic map (Fig. 2).

The porphyritic augite of Izu and Hakone are somewhat variable in composition within a single rock and also within a single crystal. The range in refractive indices rarely exceeds 0.01 within a single rock, being usually about 0.005; optic angle range 10°–5°, with a few exceptions to be noted just below.

Two types of zonal structure are noted in porphyritic augite.

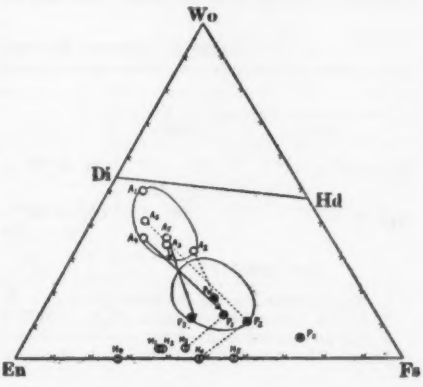

FIGURE 12.—DIAGRAM SHOWING CHEMICAL COMPOSITIONS OF VARIOUS PYROXENES

A_1: analyzed augite from Wadaki. A_2: porphyritic augite associated with pigeonite P_1. A_3: average composition of porphyritic augites (estimated from $\beta = 1.698$, $2V = 48°$ (core) $= 43°$ (margin)) showing the first type of zonal structure. A_4: porphyritic augite of Table 3 (2), showing the second type of zonal structure. A_5: porphyritic augite of Table 3 (3) showing the second type of zonal structure. In A_3, A_4, and A_5, the heads of arrows indicate the compositions of the marginal zones. A_6: augite associated with pigeonite P_2.

P_1: porphyritic pigeonite in pigeonite-bearing andesite from Hakone-tôge (H.K. 33022001). P_2: pigeonite in hypersthene-pigeonite-quartz-diorite, northeast of Yumoto-mati (H.K. 37090503). P_3: pigeonite occuring as microphenocrysts in hypersthene-andesite (H.K. 34041401a), south of Yumoto-mati. P_4: analyzed groundmass pigeonite in aphyric andesite from Saru-sawa, south of Yumoto-mati (H.K. 33081909a). P_5: pigeonite in druses of augite-hypersthene dacite, southeast of Byôbu-yama (H.K. 40040801a).

H_1: analyzed hypersthene from Tôno-mine (H.K. 34090901). H_2: analyzed hypersthene from Odawara City (H.K. 36082106). H_3: analyzed hypersthene from Hakone-tôge (H.K. 33022001) associated with A_2 and P_1. H_4: most Mg-rich hypersthene in olivine-bearing augite-hypersthene-andesite from Aziromati (H.K. 31041408). H_5: most Fe-rich hypersthene in fayalite-bearing hypersthene-dacite from Kaziya (H.K. 39010903b). H_6: hypersthene associated with P_2 and A_6.

In the first type, each crystal is surrounded by a narrow marginal zone showing somewhat smaller optic angle and extinction angle on 010, lower refractive indices, and paler color than the core (Kuno and Sawatari, 1934, p.

329). The optic angle of the core varies from about 50° to 45°, that of the margin from about 45° to 40°. The passage from the core to the margin is usually gradual, although distinct boundary is occasionally observed.

pyroxenic phase of the surrounding groundmass is made up either of hypersthene alone or of hypersthene and very little augite.

PIGEONITIC AUGITE AND PIGEONITE: Monoclinic pyroxene from pigeonitic augite to pigeonite is probably the commonest mineral next to plagioclase and silica minerals.

Pigeonite occurs (1) as true intratelluric crystals; (2) as microphenocrysts; and (3) as minute groundmass grains, closely associated with and grading into pigeonitic augite.

Pigeonite scarcely differs from augite in its

TABLE 3.—OPTICAL PROPERTIES OF ZONED AUGITE-PIGEONITE

1		2		3	
Core	Margin	Core	Margin	Core	Margin
2V = 47° – 45°	15° – 0° (rarely 37°)	2V = 53° – 47°	16°	2V = 54° – 45°	9° – 0° (in 010) 8° (⊥ to 010)
c∧Z = 44°	35°	c∧Z = 42° – 40°	38° – 35°	c∧Z = 45° – 41°	38°
		β = 1.692	1.699–1.705	β = 1.698–1.700	1.695
β=1.698–1.706		β(aver.)=1.700			

1. Hypersthene-bearing olivine-augite-basalt (H.K. 37112107b), a lava of the Hata Basalt Group.
2. Augite-hypersthene-andesite (H.K. 32090104), a lava of the Taga volcano.
3. Olivine-bearing augite-hypersthene-andesite (H.K. 37081502), a lava of the Yugawara volcano.

Note:—The measurements were made on several grains in each rock.

In the second type, no so frequent as compared with the preceding, the core of each crystal is augitic, and the rim is quasi-uniaxial pigeonite (Table 3). The rim, which may be distinctly bounded from the core or may rapidly grade into it, is traversed by numerous cracks and is given a spongy appearance by inclusions of minute pores (Fig. 13; Pl. 5, figs. 2, 3).

These two types of zoning are frequently observed in other volcanic rocks of Japan.

The compositions of some monoclinic pyroxenes showing different types of zoning are plotted in Figure 12 (A_2, A_4, A_5). Judged from the incomplete data at hand, the second type of zoning is confined to augite embedded in groundmass whose pyroxene (pigeonite) is especially rich in iron (Tables 12, 14, columns 3, 12, 23). The first type of zoning is encountered in augite embedded in groundmass of varying chemical and mineral compositions; the groundmass pyroxene may consist simply of monoclinic pyroxene or of augite and hypersthene.

In a few acidic rocks, porphyritic augite is surrounded by a thin corona of hypersthene (Fig. 14; Pl. 6, fig. 5). The outline of the augite crystal indicates that it has been redissolved by the magma from which the hypersthene was separated to form the reaction rim (Fig. 14, right). It is important to note here that the

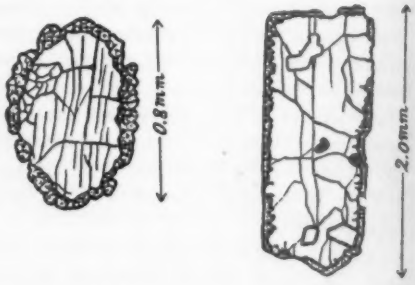

FIGURE 13.—AUGITE PHENOCRYSTS RIMMED WITH QUASI-UNIAXIAL PIGEONITE

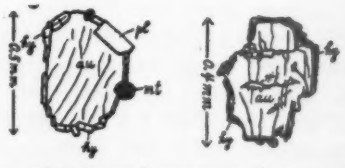

FIGURE 14.—AUGITE PHENOCRYSTS SURROUNDED BY GROUNDMASS HYPERSTHENE

crystal habit, axial colors, double refraction, and extinction angle, although it tends to be generally higher in refraction. While multiple twinning on 100 is characteristic of some crystals, simply twinned or untwinned grains are by an aggregate of fine granules of pigeonite, augite, and magnetite. As this aggregate approaches to the glass, the fine granules are successively rearranged to form a larger homogeneous crystal of pigeonite (Pl. 2, fig. 5).

TABLE 4.—OPTICAL PROPERTIES AND ESTIMATED CHEMICAL COMPOSITIONS OF INTRATELLURIC PIGEONITES

Pigeonite in andesite (H.K. 33022001	Pigeonite in quartz-diorite (H.K. 37090503)
$\alpha \wedge \beta = 1.704$, $\gamma = 1.728$	$\alpha \wedge \beta = 1.712$
$(+)2V = 17° - 10°$ in 010	$(+)2V = 19° - 11°$ (rarely 0°) in 010
Dispersion in optic angle insensible	Dispersion in optic angle distinct: $\rho < v$*
$c \wedge Z = 43°$	$c \wedge Z = 44°$
Pleochroism distinct:	Pleochroism weak:
X = pale brownish green	X = pale green
Y = pale greenish brown	Y = pale red
Z = pale green	Z = pale green
Absorption $X \wedge Z < Y$	
$Wo_{11}En_{39}Fs_{48}$	$Wo_{11}En_{34}Fs_{55}$

* This type of dispersion is the reverse to that of augite common in this region.

not uncommon among the groundmass pigeonite.

Large crystals of pigeonite, formed in all probability under deep-seated conditions, occur in quartz-bearing augite-pigeonite-hypersthene-andesite, and also in the partially remelted hypersthene-bearing augite-pigeonite-quartz-diorite (p. 23), both from the Hakone volcano (Table 4).

In the former rock (Kuno, 1936a, p. 107), pigeonite occurs as rounded crystals up to 3 mm. long (Pl. 20, fig. 4), associated with phenocrysts of augite (p. 38) and hypersthene (Table 2, column 12), both of which form parallel intergrowth with the pigeonite.

In the quartz-diorite, pigeonite occurs as deeply embayed crystals up to 1 mm across (Pl. 1, fig. 1; Pl. 2, fig. 5), associated with hypersthene (γ = 1.699–1.720, $En_{68}Fs_{32}$–$En_{52}Fs_{48}$) and augite (β = 1.695, $(+)2V = 55°$, $Wo_{41}En_{45}Fs_{14}$). The last two minerals are marginally changed to pigeonite. Relatively large crystals of pigeonite are found within pale-brown glass formed by the partial resolution of quartz and potash-oligoclase when the rock mass was captured by a magma.

Hornblende, supposed to have been formerly present in the rock, is now completely replaced

It may be inferred that, while quartz and acid feldspar were being dissolved, the pigeonite was growing in the liquid at the expense of the resorption products of hornblende. Probably, this process was carried out slowly in the throat of the volcano.

In Figure 12, the points representing estimated compositions of these pigeonites (p_1 and p_2) are located near the arrow heads representing the compositions of the marginal zones of the porphyritic augites, indicating that these pigeonites represent the later-formed members of the monoclinic pyroxene group.

Microphenocrysts of pigeonite are found in some andesites and a few basalts. They are almost confined to rocks in which phenocrysts of augite are either absent or quite subordinate, and especially predominant in olivine-hypersthene-andesite. The crystals are prismatic, usually about 0.2 mm. long (Pl. 4, fig. 6), sometimes attaining to 0.5 mm. in comparatively elongated crystals. Lamellar twinning on 100 is very common.

This pigeonite, which is weakly pleochroic, is either quasi-uniaxial or slightly biaxial with the optic plane more commonly perpendicular to 010 than parallel to it—strong contrast to the general optic orientation of the groundmass pigeonite. A typical example, pigeonite in hy-

persthene-andesite (H.K.34041401a) from the Hakone volcano, exposed at a point about 1 km. southwest of Yumoto), has the following optical properties: $\alpha \fallingdotseq \beta = 1.693$, $(+)2V = 8°$ (O.P. parallel to 010) $-11°$ (O.P. perpendicular to 010), $c \wedge Z = 40°–43°$, pleochroism weak with $X \fallingdotseq Z$ = pale green, Y = pale red; estimated composition $Wo_{12}En_{48}Fs_{40}$ (Fig. 12, P_3).

The microphenocrysts of pigeonite sometimes occur along with those of hypersthene; the two often form parallel intergrowth. The finer pyroxene grains in the matrix usually consist simply of monoclinic pyroxene, but rarely of augite and hypersthene. In the former case, the finer-grained pyroxene is nearly uniaxial or biaxial with larger optic angle in 010 (pigeonite or pigeonitic augite) than that of the microphenocrystic pigeonite. It is highly probable that these microphenocrysts were formed during or immediately before the effusive stage, at least prior to the crystallization of the finer pyroxene grains in the matrix.

Groundmass monoclinic pyroxenes are either granular or prismatic with somewhat rounded outline, and acicular in a few cases. In coarsely-crystalline basalts, they show ophitic relationship toward plagioclase laths.

An outstanding feature of the groundmass pyroxene is the remarkable variability of its optic angle, even in a single thin section. Thus pigeonitic augite with 2V about 40° and pigeonite with 2V less than 10° tend to occur side by side most frequently. Pyroxene with 2V between 40° and 10° does occur in the same section, though much less frequently. Even a single grain may consist of two distinct parts, pigeonitic augite and pigeonite. The two parts often show no zonal arrangement and appear to grade into one another very rapidly. So far as can be observed, the optic plane of the groundmass pigeonite is always parallel to 010.

The average value of optic angle of the groundmass grains tends to be larger in basic rocks (average 2V about 30° in basalts) than in acid ones (2V about 0° in acid andesites). Coarser grains in basaltic groundmass have optic angles larger than the finer ones in the same rock, and in grains with distinct zonal structure, the optic ang e is larger in the core than in the margin, although the reverse case is not entirely lacking.

These facts lead us to the conclusion that the early-formed pyroxene of the groundmass is richer in $CaSiO_3$ than the later-formed one. Strongly contrasted to this, in the groundmass pyroxenes of olivine-hypersthene-andesites and hypersthene-andesites, the early-formed grains (the microphenocrysts) are pigeonite extremely poor in $CaSiO_3$ (or hypersthene), while the later-formed ones (the grains in the matrix) are pigeonitic augite or pigeonite richer in $CaSiO_3$.

The refractive indices of groundmass pyroxene are also variable, but generally higher than those of the associated porphyritic augite.

Groundmass pyroxene, typical of the later-formed monoclinic pyroxenes, was separated from a coarsely-textured aphyric andesite (H.K. 33081909a, Pl. 2, fig. 6) from the Hakone volcano. The analysed material (Table 2, column 9) ranges from pigeonitic augite to pigeonite. The average composition is plotted in Figure 12 (P_4). The mineral occurs as even-grained, rounded or prismatic crystals, associated with andesine, anorthoclase, quartz, cristobalite, biotite, magnetite, ilmenite, and a little apatite.

This pyroxene is rich in FeO, and rather poor in Al_2O_3 and Fe_2O_3. The amount of TiO_2 is approximate to that of the Wadaki augite already mentioned. The optical properties (Kuno, 1940c, p. 347) are as follows:

Min.	*Max.*
$\alpha = 1.700$	?
$\beta = 1.705$	1.713
$\gamma = ?$	1.738

$(+)2V = 44° - 41°$ for 4 grains
ca. 0° for 5 grains
$36° - 0°$ for 1 grain
$c \wedge Z = 43°$

The most probable values:
$\alpha = 1.713, \beta = 1.713, \gamma = 1.738$
$2V \fallingdotseq 0°$
$\alpha = 1.700, \beta = 1.705, \gamma = 1.725$
$2V = 44° - 36°$

Pleochroism: $X \fallingdotseq Z$ = pale green
Y = pale brownish-green

The average composition of this pyroxene, as estimated from its optical properties, is $Wo_{39}En_{44}Fs_{16}$. The normative pyroxene calculated from the analysis of this andesite has the composition $Wo_{39}En_{16}Fs_{44}$ (Table 14, column 22). Both of these values show rather striking agreement with the result of the actual analysis of the mineral.

The approximate compositions of some of the other groundmass monoclinic pyroxenes are estimated either optically or from the norms of the rocks in which they occur. When plotted in Figure 12, they fall within the ovoid area lying in the lower part of the diagram.

Groundmass pigeonite often forms coronas around olivine and hypersthene. In both cases, the corona pigeonite is smaller in average optic angle ($2V \fallingdotseq 0°$ in most examples) than the monoclinic pyroxene scattered throughout the groundmass. In a coarsely crystalline augite-olivine-basalt, monoclinic pyroxene surrounding olivine has an optic angle approximate to 0° at the junction with the latter mineral, which opens up to about 40° toward the outer portion of the corona.

Pigeonite occurring in microscopical druses of augite-hypersthene-dacite (H.K.40040801a) from Hakone (an ejected block contained in the earliest dacite tuff of the young somma, southeast of Byôbu-yama) represents the last-formed member of the monoclinic pyroxene group. It forms prismatic or interstitial grains associated with tridymite which fills up the druses (Pl. 3, figs. 1, 2). The pigeonite sometimes fringes hypersthene phenocrysts. Its optical properties and estimated composition are as follows: $\alpha \fallingdotseq \beta = 1.730$ (max), $\gamma = 1.760$ (max); (+) $2V \fallingdotseq 0°$, rarely about 10°; $c \wedge Z \fallingdotseq 40°$; weakly pleochroic; composition: $Wo_4En_{25}Fs_{71}$. The composition of this pigeonite (Fig. 12, P_4) lies at the iron-rich end of the monoclinic pyroxene group.

In mode of occurrence and composition, this pigeonite is comparable to the clinoferrosilites found in lithophysae of rhyolites from Africa, North America, and Iceland (Bowen, 1935, p. 481), although it is more magnesian.

Figure 12 shows that, generally speaking, the course of crystallization is from diopsidic augite to iron-rich pigeonite, both under the intratelluric and effusive conditions.

Orthorhombic pyroxenes

Hypersthene is nearly always present as phenocrysts in andesites and dacites, but rather rare in basalts. It occurs also as a groundmass constituent, either alone or together with monoclinic pyroxene, chiefly in andesites and dacites. Again, minute needles of the mineral are found in microscopical cavities or coarsely crystalline acid patches of groundmasses of some basalts and andesites.

Hypersthene forms prismatic crystals bounded with broad pinacoidal and comparatively narrow prismatic faces, together with bipyramidal faces. When it occurs in the ground mass, needle-like crystals are not uncommon.

Hypersthene shows distinct pleochroism: X = pale red or brown, Y = pale greenish or yellowish brown, Z = pale green, with absorption $X > Z \geqslant Y$. The refractive index γ varies from 1.694 to 1.730, corresponding to the composition range from $En_{72}Fs_{27}$ to $EFs_{47}n_{43}$ (inferred from the diagram by Bowen and Schairer, 1935, p. 198). (Fig. 12, H_4, H_5). The mineral is always optically negative, with optic angle 2V varying from about 80° to about 50°, with distinct dispersion, usually $\rho > \nu$, but $\rho < \nu$ in the iron-rich variety (Kuno, 1941a, p. 204). Optic orientation is: a = Y, b = X, c = Z.

The most iron-rich hypersthene ($\gamma = 1.724$–1.730, (−) $2V = 56°$—$54°$, $\rho < \nu$) (Fig. 12, H_5) is associated with fayalite in the dacite (H.K. 39010903b) already mentioned, where the fayalite forms a corona around it.

Three chemical analyses of hypersthenes from the present region are available (Table 2, columns 10, 11, 12). Their compositions are plotted in Figure 12 (H_1, H_2, and H_3 respectively). The optical properties are given in Table 5.

The first two hypersthenes are almost identical to one another in chemical composition as well as in optical properties; the third is richer in iron and higher in refraction. The last hypersthene has stronger pleochroism than any hypersthenes so far observed by the writer.

Like olivine, composition of hypersthene varies greatly in different grains within a single rock as well as in a single crystal. The widest range found in a single rock is from $En_{68}Fs_{32}$ to

$En_{52}Fs_{48}$ (γ = 1.699–1.720, in hypersthene of the pigeonite-quartz-diorite (H.K.37090503) from Hakone.

Hypersthene is often marginally zoned, the outer zone being usually more ferriferous than the inner, as inferred from the difference of refractive index, double refraction, or optic angle, although reverse zoning is not rare.

It is evident that the hypersthene constitutes a continuous reaction series at least from about En_{70} to about En_{44}, the later-formed members being more ferriferous.

Parallel intergrowth of hypersthene and augite is quite common, the *c*- and *b*-axes of the former coinciding with the respective axes of the latter. In most cases, the augite grows outside the hypersthene, sometimes completely enveloping it. The junction between the two minerals indicates that there was no mutual reaction. This structure is seen both in phenocrysts and in groundmass grains.

In a few basalts, porphyritic hypersthene is surrounded by a dense aggregate, or a single crystal, of porphyritic augite, often attended by olivine. The augite and olivine sometimes show radial growth from the hypersthene. The outline of the enclosed hypersthene crystal indicates reactive resorption. Every stage of resorption can be traced until the hypersthene disappears completely and the whole aggregate consists of granular augite or augite plus olivine. In a typical example (Fig. 15) a resorbed crystal of hypersthene is surrounded by a single crystal of augite and radially grown crystals of olivine.

Such hypersthene is common in very basic basalts (olivine-augite-basalt with groundmass olivine), in which the mineral may be regarded as xenocrysts. Probably, the hypersthene, when included in a basic magma with which the mineral was not in equilibrium, was readily resorbed by the magma with concomitant precipitation of augite and olivine, viz., the phases with which the magma was then saturated. Dense aggregates of porphyritic augite, with or without hyperrsthene in the center, occasionally found in andesites, may be regarded also as relics of the hypersthene xenocrysts

TABLE 5.—OPTICAL PROPERTIES OF THE ANALYZED HYPERSTHENES

Hypersthene from Tôno-mine			Hypersthene from Odawara			Hypersthene from Hakone-tôge		
Min.	Max.	Aver.	Min.	Max.	Aver.	Min.	Max.	Aver.
α = 1.691	?	1.696	α = 1.686	?	1.691	α = 1.699	?	1.702
β = 1.698	1.708	1.703	β = 1.696	1.706	1.701	β = 1.709	1.714	1.712
γ = ?	1.713	1.708	γ = ?	1.710	1.705	γ = ?	1.717	1.715
(−)2V = 58°	66°	62°	(−)2V = 57°	64°	60°	(−)2V = 57°	62°	59°
Core is larger in 2V than margin.			Dispersion distinct with $\rho > v$.			Dispersion strong with $\rho > v$.		
Dispersion distinct with $\rho > v$.			Pleochroism distinct:			Pleochroism strong:		
Pleochroism distinct:			X = pale reddish-brown			X = pale reddish-brown		
X = pale reddish-brown			Y = pale brownish-yellow			Y = pale greenish-brown		
Y = greenish-yellow			Z = pale green			Z = pale smoky green		
Z = pale buff green			X > Y ≒ Z			X > Z > Y		
X > Y ≒ Z								

FIGURE 15.—CORONA OF AUGITE (au) AND OLIVINE (ol) AROUND A XENOCRYST OF HYPERSTHENE (hy)

either partly or completely resorbed by the basic magmas.

The structure (Fig. 15) resembles closely that of the "pseudo-hypersthene" described by Tomita (1931, p. 216, 416, 427, 463, 466; 1933, p. 3) from trachybasalts of the Circum Japan Sea Province. In his examples, the monoclinic pyroxene around the hypersthene is a pigeonitic variety which passes to augite toward the margin of the aggregate. According to Tomita's (1931, p. 214) description and also to the writer's own observation of numbers of Manchurian basalts, the "pseudo-hypersthene" is often associated with reversely zoned crystals of andesine. From this fact, the view of the xenocrystic origin of the "pseudo-hypersthene" is also justified.

Porphyritic hypersthene is often surrounded by coronas of groundmass pigeonite. Every stage of resorption of the hypersthene and marginal replacement by the pigeonite can be traced in rocks with relatively coarse-grained groundmass. In some instances, hypersthene is rimmed with closely packed aggregate of granular pigeonite (Pl. 5, fig. 1), with no definite crystallographic relationship between the two. In other instances, thin lamellae of pigeonite grow all around hypersthene prisms, forming parallel intergrowth (Pl. 3, fig. 3). The hypersthene crystals, especially at both ends of the prisms, are striated with numerous submicroscopic lamellae of pigeonite, which the latter passes outward into the mantle of polysynthetically twinned pgeonite around the hypersthene prisms. These structures are distinct from the simple intergrowth of hypersthene and augite (p. 51) and indicate some kind of reaction between the hypersthene and surrounding magma to form the pigeonite.

Thin lamellae of monoclinic pyroxene with small extinction angle are included near the centers of some hypersthene phenocrysts. In some instances, such parts of the crystals are also rich in inclusions of dust and fine augite granules. This structure is essentially similar to the so-called lamellar structure of orthorhombic pyroxene so common in plutonic rocks (orthopyroxene of the Bushveld type of Hess and Phillips, 1938, p. 450), although less conspicuous than in the latter case.

As already mentioned, hypersthene forms coronas around olivine. The difference of optical properties (Table 6) shows that the corona hypersthene is somewhat richer in MgO than the hypersthene occurring as isolated phenocrysts in the same rock. This fact, though more data are needed, indicates the reaction relation between olivine and hypersthene (Kuno, 1936a, p. 137; Taneda, 1943a, p. 32).

TABLE 6.—OPTICAL PROPERTIES OF CORONA HYPERSTHENES AROUND OLIVINE AND OF HYPERSTHENES OCCURRING AS ISOLATED PHENOCRYSTS

	No. 1 (H.K. 33022004)	No. 2 (H.K. 33010901a)	No. 3 (H.K. 33022002)	No. 4 (51227)	No. 5 (H.K. 31042804)
Corona hypersthene	Portion adjacent to olivine $(-)2V = 71°$ Portion adjacent to groundmass $(-)2V = 54°$	Portion adjacent to olivine $\gamma = 1.697$ Portion adjacent to groundmass $\gamma = 1.710$	$(-)2V = 74°$	$\gamma = 1.685$	$\gamma = 1.700$
Isolated phenocrysts of hypersthene	$(-)2V = 69° - 55°$	$\gamma = 1.699 - 1.710$	$(-)2V = 62° - 57°$	$\gamma = 1.696 - 1.704$	$\gamma = 1.708 - 1.719$

Nos. 1 and 3:—andesites from the Hakone volcano.
No. 2:—basalt from the Taga volcano.
Nos. 4 and 5:—basalt and andesite from the Aziro Basalt Group.

Amphiboles

Amphiboles are rather uncommon minerals in the present region. They are of three groups:

a solid solution series from cummingtonitic hornblende to common green hornblende, oxyhornblende, and pargasite.

CUMMINGTONITIC TO COMMON GREEN HORNBLENDE: Cummingtonitic hornblende (Kuno, 1938b, p. 221) is found in a few dacites (Fig. 16) and also in hypersthene-biotite-hornblende-quartz diorite, a cognate block ejected from Hakone.[2] It is always associated with common green hornblende within a single crystal; the green hornblende is either distinctly demarcated from it or grades into it within a narrow transitional zone. In the dacites, cummingtonitic hornblende occurs in the cores of green hornblende phenocrysts (Table 7).

TABLE 7.—OPTICAL PROPERTIES OF ZONED HORNBLENDE PHENOCRYSTS*

Cummingtonitic hornblende (core)	Green hornblende (margin)
$\beta = 1.649$—slightly higher	$\beta = 1.657$–1.673
$(+)2V = 88° - 86°$	$(-)2V = 81° - 79°$
Dispersion distinct: $\rho < v$ (about Z)	Dispersion distinct: $\rho > v$ (about X)
$c \wedge Z = 16°$	$c \wedge Z = 16°$
X = nearly colorless or pale yellow	X = straw yellow
Y = pale brown	Y = slightly brownish-green
Z = pale green	Z = green
Absorption: $X < Y \doteqdot Z$	Absorption: $X < Y \doteqdot Z$
Inferred composition about $(FeSiO_3)_{40}$ $(MgSiO_3)_{60}$ in mol.%	

* From hypersthene-hornblende-quartz-dacite (H.K. 36090501a), a dike in Asigara Beds, southeast of Hata.

In another dacite (H.K. 36082810), a lava intercalated between the Asigara Beds, 2 km. southeast of Oyama, a dense aggregate of fibrous hypersthene occurs in the center of green hornblende (Fig. 17). The hypersthene has a composition about $Fs_{32}En_{68}$ (in mol. %, $\gamma = 1.704$), approximate to that of the cummingtonitic hornblende. Possibly, the aggregate of hypersthene is a pseudomorph after cummingtonitic hornblende which formerly occupied the core of the green hornblende.

Green hornblende, the commonest amphibole of the region, occurs as phenocrysts in acid andesites and dacites. In most cases, its optical properties do not differ greatly from those of the green hornblende shown in Table 7, except that β attains sometimes to 1.679, while $2V(-)$ ranges from 85° to 77°. Zonal structure is very rarely observed.

In a cognate inclusion of plutonic texture (H.K. 36090501b) in the dacite dike, large hornblende crystals ($\alpha = 1.658$ (min.), $\beta = 1.671$–1.673, $\gamma = 1.683$ (max.), $(-)2V = 85°$, dispersion distinct with $\rho > v$, $c \wedge Z \doteqdot 16°$, color slightly brownish-green) are surrounded by extremely thin rims of deep-green variety. Interstices of these hornblende crystals, which make up the bulk of the inclusion together with those of anorthite, are filled with meshes of acicular crystals of andesine and deep-green hornblende and grains of iron ore, along with interstitial zeolite. The acicular hornblende is of the same nature as that forming the rims of the larger crystals. Its optical properties are as follows: $\beta = 1.672$–1.685, $(-)2V = 82°$ (pale-colored core),—79° (deep-colored margin), with distinct dispersion $\rho > v$, about X, pleochroism, X = pale brownish yellow, Y = slightly brownish smoky green, Z = deep smoky green, absorption $X < Y < Z$). Probably, the deep-green hornblende is the latest member of the solid solution series from cummingtonitic to common green hornblende, formed under a certain limited condition, such as the high concentration of soda and volatiles.

Phenocrysts of green hornblende are often

[2] The writer also found similar colorless hornblende (2V about 90°) in dacite tuff from Bôsô peninsula, southeast of Tokyo, and in a dacite from Sambe volcano, southwest Japan. Yamaguti (1938, p. 696) also described pale-colored hornblende in dacite pumice from South Kyûsyû. He kindly communicated to the writer that the mineral has quite similar characters to those described by the writer.

surrounded by an opacite margin (Pl. 6, fig. 3). In an advanced stage of opacitization, the mineral is completely replaced by minute grains of monoclinic pyroxene and magnetite, sometimes attended by hypersthene.

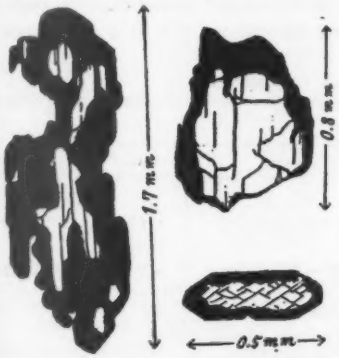

FIGURE 16.—ZONAL STRUCTURE OF COLORLESS CUMMINGTONITIC HORNBLENDE (core) AND COMMON GREEN HORNBLENDE (outer zone)

OXYHORNBLENDE: Deep-brown or reddish-brown hornblende with high birefringence and small extinction angle (about 0°) is found only in two extrusive masses of dacites, the dacite dome of Kamitaga and the flow in the Tensyô-zan Basalt Group. The mineral is associated with common green and brown hornblende. In the latter dacite, exposed 1.5 km. north of the town of Yugawara, reddish-brown oxyhornblende and brown hornblende (partially oxydized hornblende?) occur within several meters of the same exposure.

These two masses of dacites are subaerial flows, whereas many other rocks with green hornblende, which occur in the Asigara Beds and the Haya-kawa Tuff Breccias, form submarine flows or intrusive masses.

The same relation seems to hold more generally in the Cenozoic volcanic rocks of Japan. So far as known, oxyhornblende is mostly confined to lavas of Pleistocene and Recent cones which were erupted subaerially, whereas hornblende occurring in flows and dikes associated with Tertiary and Pleistocene sediments belongs usually to a greenish variety, although a brownish one may occasionally be found.

It may be suggested, though not conclusively in the absence of more extensive information, that the formation of oxyhornblende is favored by the subaerial condition.

Petrologists have recently come to a general agreement that oxyhornblende is produced

FIGURE 17.—COMMON GREEN HORNBLENDE WITH CORE OF FIBROUS HYPERSTHENE

A pseudomorph after cummingtonitic hornblende. Green hornblende is marginally opacitized.

through oxidation of ferrous iron in original green hornblende to ferric state, the oxygen necessary for this change being introduced from the mineral itself, as a result of liberation of hydrogen from H_2O in the green hornblende (Larsen et al., 1937, p. 898).

In laboratory experiment, the oxydation can be brought about by heating green hornblende at about 800°C. In natural rocks, however, oxyhornblende is often found where there is no indication of reheating. Such is the case in those dacite flows of this region and also in many flows of other regions of Japan. The oxidation may be brought about during the normal cooling of lavas, if the mineral is kept at an appropriate temperature for some time, under a condition which facilitates the escape of volatiles. It is likely that such a condition is encountered in subaerial flows rather than in submarine flows and intrusive masses.

PARGASITE: Tiny needles (2–3 mm.) of amphibole often grow in cavities of dacites and acid andesites, associated with crystals of phlogopitic biotite (Pl. 6, fig. 1), and rarely with those of fayalite. Under the microscope, the same mineral is found in druses lined with tridymite, and also in coarsely crystalline patches of groundmass (Pl. 3, fig. 4). It is scattered sporadically throughout the holocrystalline acid groundmass. The mineral often fringes both augite and hypersthene.

This amphibole is pale brown or brownish-

green, always optically positive with a weak dispersion $\rho > \nu$ about Z. From its optical properties (Table 8), combined with its mode of occurrence, it is described as pargasite.[3]

In its mode of occurrence and also in its optical properties, especially in type of dispersion of optic angles, this amphibole is distinct from the cummingtonitic to common green hornblende series which occurs always as phenocrysts but not in groundmass and in cavities. The two types of amphibole appear to be genetically independent. The pargasite was formed probably from a volatile-rich residuum of magma. From San Juan region, Colorado, a similar cavity amphibole has been described as soda-tremolite (Larsen et al., 1937, p. 896).

TABLE 8.—OPTICAL PROPERTIES OF PARGASITE

A			B		
Min.	Max.	Aver.	Min.	Max.	Aver.
$\alpha = 1.628$	?	1.629			
$\beta = 1.638$	1.641	1.639	$\beta = 1.660$	1.671	1.665
$\gamma = ?$	1.654	1.652			
$(+)2V = 83°$	$\rho > \upsilon$	$c \wedge Z = 20°$	$(+)2V = 83° - 71°$	$\rho > \upsilon$	$c \wedge Z = 23°$
Pleochroism:			Pleochroism:		
X = pale yellow			X = pale greenish-yellow		
Y = yellowish-brown			Y = pale brown		
Z = slightly greenish-yellow			Z = pale brownish-green		
Absorption $X < Y \doteqdot Z$			Absorption $X < Y \doteqdot Z$		

A. Pargasite from augite-hypersthene-andesite (H.K. 34081408), a lava of the old somma of the Hakone volcano. Loc., west of Kaziya, north of Yugawara station.

B. Pargasite from augite-bearing hypersthene-dacite (H.K. 40040801a), a lava of the young somma of the Hakone volcano. Loc., a cliff southeast of Byôbu-yama.

Accessory minerals

Biotite does not appear as phenocrysts, but shows a wide distribution throughout the intermediate to acid groundmass of high crystallinity, although in quite subordinate amount. It is the only mafic silicate mineral in the groundmass of the most acid dacites. Thin hexagonal plates (1–2 mm.) of biotite are found in cavities of a few dacites (Pl. 3, fig. 2). Biotite tends to associate with pargasite, quartz, tridymite, anorthoclase, and ilmenite, the minerals which appear to have been formed from low-temperature residual magmas enriched in volatile substances.

The biotite is a phlogopitic variety, having low refraction and moderate optic angle with strong dispersion $\rho < \nu$. It is always pale for brown. Phlogopitic biotites associated with the pargasite in the two rocks already referred to (A and B of Table 8), have the following optical properties: A, $\gamma = 1.587$, $(-)2V = 23°$, $\rho < \nu$, pleochroism strong, X = pale greenish yellow, Y = reddish brown, Z = yellowish brown, absorption $X < Z \leqslant Y$; B, $\gamma = 1.593$, $(-)\ 2V \doteqdot 20°$, $\rho < \nu$, pleochroism and absorption same as those of A.

Similar cavity biotite has been described from a few other localities (Kôzu and Yoshiki, 1933, p. 265; Kôzu and Tsurumi, 1933, p. 269; Larsen et al., 1937, p. 902; Macdonald, 1944b, p. 1340).

Biotite occurring in plutonic and hypabyssal rocks (quartz-diorites and porphyrites) is either dark brown or greenish-brown, and nearly uniaxial, approaching to the biotite so common in acid plutonic rocks.

Magnetite or *titano-magnetite* is present in nearly all the groundmasses from basic to acid. In some coarse-grained basalts, it shows ophitic relationship toward plagioclase laths (Pl. 4, fig. 2).

[3] After this manuscript was written, Sameshima (oral communication), completed a chemical analysis of this mineral associated with fayalite in the dacite from Kaziya. He showed that the mineral is an iron-rich pargasite with 0.68% F.

Porphyritic magnetite is rather rare in basalts but common in andesites and dacites, especially conspicuous in acid rocks. It is confined, with a few exceptions, to rocks with porphyritic hypersthene, with which it often forms grouped

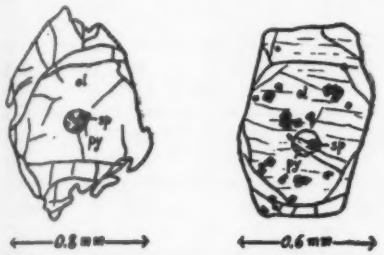

FIGURE 18.—SPINEL (sp) AND PICOTITE (black) INCLUSIONS IN OLIVINE (ol)

Spinel is closely associated with monoclinic pyroxene (py).

phenocrysts. As already stated, the resorption of olivine gives rise to separation of magnetite along its margin, which, upon complete disappearance of the olivine, tends to coalesce to form porphyritic grains (Fig. 9). Most, if not all, of magnetite phenocrysts appear to have been formed as the result of resorption of olivine with concomitant precipitation of hypersthene.

Phenocrysts of magnetite which are embedded in acid groundmass of high crystallinity are surrounded by thin rims of biotite.

Ilmenite (or an isomorphous mixture of hematite and ilmenite) forms irregular flakes in intermediate to acid groundmasses of high crystallinity. It varies, according to its thickness, from chestnut brown to almost opaque. In many slightly alkaline basalts from southwest Japan, Korea, Manchuria, and Alaid volcano, north Kurile, it is purplish brown.

Apatite, largely confined to intermediate and acid rocks, forms stout prismatic phenocrysts up to 0.3 mm. long (Pl. 6, fig. 4) and needle-like crystals in groundmass of high crystallinity (Pl. 2, fig. 6).

In a few instances, porphyritic apatite is sensibly biaxial, with n(mean) = 1.634 (augite-hypersthene-andesite (H.K. 34081408), an old somma lava of the Hakone volcano). It often includes numerous fine rods of a brownish, subtransparent mineral which is arranged parallel to *c*-axis of the apatite and is pleochroic from greenish to brownish.

Spinel and picotite occur as small grains included in olivine phenocrysts, but not as isolated crystals.

Green spinel (hercynite or ceylonite) is found within small patches of groundmass completely enveloped by olivine, where it is closely associated with monoclinic pyroxene (Fig. 18). Such enclosed patches of liquid magma were probably impoverished in silica, as there was no supply of liquid material from outside in the course of reaction with the olivine. This condition favoured the formation of the spinel.

Dark-brown picotite in small octahedral grains is rather common (Fig. 18, right). It is easily mistaken for magnetite; only high magnification reveals it to be subtransparent. A complete gradation seem to exist between picotite and magnetite. Picotite grains in individual olivine phenocrysts are often concentrated in certain areas or even clustered together.

From its mode of occurrence, picotite is the mineral which was separated prior to olivine.

Zircon occurs as small rounded grains in a few dacites.

Zeolite, probably of deuteric origin, fills up interstices of feldspar and quartz in some acid groundmass. It occurs also as an obviously secondary mineral in amygdaloidal cavities and veinlets.

Other secondary minerals are chlorite (partly serpentine?), calcite, albite, quartz, epidote, hematite, and a talc-like mineral. The last-named mineral replaces olivine and hypersthene, and in crystal habit and optical orientation, closely resembles talc or mica; its optical properties are as follows: $\alpha = 1.51\pm$, $\gamma = 1.57\pm$, $(-)2V \doteqdot 0°\text{–}30°$, pleochroic with X = pale yellow to almost colourless, Y $\doteqdot$ Z = pale green. Possibly, it is a hydrous silicate of MgO and FeO (a kind of chlorite?).

MINERAL ASSEMBLAGE

Method of representation

All possible types of assemblage of the ferromagnesian silicate minerals, excluding pargasite and phlogopitic biotite, in the porphyritic rocks of the regions, are represented in Tables 9 and 10.

TABLE 9.—TYPES OF ASSEMBLAGE OF THE CHIEF FERROMAGNESIAN SILICATE MINERALS IN THE TERTIARY ROCKS OF HAKONE AND THE ADJACENT AREAS*

Phenocrysts \ Groundmass	Olivine Mono. pyrox. Orth. pyrox.	Olivine Mono. pyrox.	Mono. pyrox.	Mono. pyrox. Orth. pyrox.	Orth. pyrox.
Orth. pyrox.	Ia	Ib	Ic <1?	Id <1?	Ie
Olivine Orth. pyrox.	IIa	IIb	IIc 2 1	IId	IIe
Olivine	IIIa	IIIb 1	IIIc 7	IIId	IIIe
Olivine Mono. pyrox.	IVa	IVb 3	IVc 19	IVd <1	IVe
±Olivine Mono. pyrox. Orth. Pyrox.	Va	Vb 1	Vc 34 8	Vd 13	Ve 2
±Olivine Mono. pyrox. Orth. Pyrox. Hornblende	VIa	VIb	VIc	VId 3	VIe 1
±Olivine Orth. pyrox. Hornblende	VIIa	VIIb	VIIc	VIId <1	VIIe 1
±Olivine Hornblende	VIIIa	VIIIb	VIIIc	VIIId	VIIIe <1
±Olivine Mono. pyrox. Hornblende	IXa	IXb	IXc	IXd	IXe
Mono. pyrox.	Xa	Xb	Xc	Xd	Xe

* Each figure represents the percentage of the specimens of rocks belonging to each type. Mark ? means that the assemblage of the porphyritic minerals cannot be known with certainty because of the scantiness of phenocrysts within available slices, 370 specimens were examined.

Since phenocrysts of olivine are extremely rare in hornblende-bearing rocks (types VI–IX) and occur somewhat haphazardly in rocks of type V, the olivine-bearing type was not distinguished from that without olivine in each of these types.

Groundmass with olivine alone or olivine + orthorhombic pyroxene, without appreciable glass, has not so far been found in nature, so that they are omitted in the tables.

The fifty types of assemblage obtained by the combination of the assemblage of phenocrysts and that of groundmass crystals are represented by the symbols Ia, IIb, etc.

Tables 9 and 10 show statistically how frequently the various types of assemblage occur among the specimens of rocks collected in the region.

Specimens in which glass occupies more than about 10 per cent of the groundmass are also

TABLE 10.—TYPES OF ASSEMBLAGE OF THE CHIEF FERROMAGNESIAN SILICATE MINERALS IN THE ROCKS OF USAMI, TAGA, YUGAWARA, AND HAKONE VOLCANOES*

Groundmass / Phenocrysts	Olivine Mono. pyrox. Orth. pyrox.	Olivine Mono. pyrox.	Mono. pyrox.	Mono. pyrox. Orth. pyrox.	Orth. pyrox.
Orth. pyrox.	Ia	Ib	Ic 3 <1	Id	Ie
Olivine Orth. pyrox.	IIa	IIb	IIc 6 1	IId <1	IIe
Olivine	IIIa	IIIb 1	IIIc 7 <1	IIId <1	IIIe
Olivine Mono. pyrox.	IVa	IVb 1	IVc 8 <1	IVd <1	IVe
±Olivine Mono. pyrox. Orth. pyrox.	Va	Vb <1	Vc 45 14	Vd 12	Ve
±Olivine Mono. pyrox. Orth. pyrox. Hornblende	VIa	VIb	VIc	VId	VIe
±Olivine Orth. pyrox. Hornblende	VIIa	VIIb	VIIc	VIId	VIIe
±Olivine Hornblende	VIIIa	VIIIb	VIIIc	VIIId	VIIIe
±Olivine Mono. pyrox. Hornblende	IXa	IXb	IXc	IXd	IXe
Mono. pyrox.	Xa	Xb	Xc	Xd	Xe

* 873 specimens were examined.

excluded, because the glassy groundmass may not represent true assemblage which would obtain after complete crystallization. Microphenocrysts are disregarded because most of them may have been formed in the intermediate stage between intratelluric and effusive.

Microscopical observation reveals that there are rock types in which mafic minerals show all the features transitional from those of type b to type c (type b→c), and from type d to type c (d→c). In the tables, percentages of the rocks of these transitional types are given at the intermediate positions.

No great weight, needless to say, can be placed upon the individual figures, but the percentage ratio may afford a rough measure of the relative frequency of the different types of assemblage. The relative frequency of the types depends upon the phase equilibrium relations which obtained in the course of the whole magmatic history.

Nature of the various types of assemblage

The most striking fact seen from Tables 9 and 10 is the absence of the types belonging to columns a and b and those of lines IX and X. These types are also absent among the glassy rocks. Non-occurrence of such types as VIc, VIIc, and VIIIc has an important bearing on the genesis of rocks with hornblende phenocrysts.

The rocks belonging to the same type of assemblage exhibit definite mineralogical characteristics and also similar textural habit. Therefore, the essential characters of the rocks can be best shown by describing the characteristics of the mineral assemblage.

Basalts of types IIIb→c and IVb→c (Pl. 3, figs. 5, 6) comprise the basic end members of the rock suite of this region (Table 14, column D), characterized by the presence of varying amounts (usually less than 5%) of olivine formed evidently during the groundmass crystallization. The olivine is either euhedral with slightly rounded outline, or in acicular and skeletal crystals, or ophitic with included laths of plagioclase. It always shows incipient traces of marginal resorption with concomitant formation of narrow reaction rim of pigeonite. Thus there is much indication that olivine continued to crystallize from the intratelluric to the effusive stage, until it was replaced by pigeonite along the margin of the crystals due to reaction with the magma. This distinguishes these basalts from those of types IIIb and IVb (Table 16) in which olivine is entirely free from the reaction rim.

In these basalts, pyroxene of the groundmass is largely augite or pigeonitic augite, accompanied with some pigeonite, but in a few cases simply pigeonite. Larger grains of the groundmass pyroxene are generally augitic with larger optic angles; smaller grains in the same groundmass and also marginal zones of the larger ones have smaller optic angles.

The groundmass is usually intergranular and sometimes ophitic. Interstitial cristobalite is reduced to minimum, but present in almost all rocks.

Most of the rocks of type Vb→c differ from the basalts just mentioned only by containing sporadic crystals of hypersthene which are in all probability xenocrysts, being surrounded by aggregates of augite and olivine (Fig. 15). However, only a few basalts and basic andesites assigned to type Vb→c contain crystals of hypersthene which are free from reaction rim.

Basalts (partly basic andesites) of types IIIc and IVc (Pl. 4, Figs. 1, 2) are generally slightly more acidic than the preceding types (Table 12, columns 1, 2, 4, 5). Olivine is either entirely absent in the groundmass or rarely present as small relics of resorbed microphenocrysts with thick reaction rim of pigeonite. Monoclinic pyroxene of the groundmass is usually pigeonitic augite but sometimes pigeonite either with or without accompanying the former pyroxene. The relation between augitic and pigeonitic pyroxenes and the texture of the groundmass are similar to those in the basalts of types IIIb→c and IVb→c. The interstitial cristobalite is increased in amount, sometimes attaining to about 10% of the groundmass.

Some of the basalts of type Vc (Table 12, column 3) contain xenocrysts of hypersthene, otherwise they might be classified as type IVc.

Basalts and andesites (rarely dacites) of type Vc (Pl. 3 figs. 1, 2; Pl. 4, figs. 3, 5; Pl. 5, figs. 1, 2, 3), the commonest type, cover a wide range of chemical composition and textural variation. Most of the rocks are andesites (Table 12, columns 7, 9, 10, 11, 13, 17; Table 14, column 23); some basalts (Table 12, columns 3, 8) and a few dacites are represented. Toward the basic members of this type, olivine increases progressively in amount, while hypersthene decreases to minimum, and the rocks grade in to basalts to type IVc. Olivine disappears in most of the intermediate to acid andesites where hypersthene tends to become dominant ferromagnesian phenocrysts.

Pigeonite prevails in the groundmass more than pigeonitic augite. In basic to intermediate andesites, they occur side by side; in more acidic rocks, pigeonite with a rather uniform optic angle (2V nearly 0°) tends to become the dominant or even the only pyroxene. In the acid members, the groundmass pigeonite is notably rich in $FeSiO_3$ (Table 14, columns 17, 23). The last-formed pigeonite in druses of a dacite of this type has the composition represented by P_8 of Figure 12.

In some basalts of this as well as of the preceding types, minute needles of hypersthene occur in microscopical cavities and pegmatitic patches of the groundmass.

Andesites (partly basalts) of types IIc and Ic (Pl. 4, fig. 6) are characterized by the common occurrence of microphenocrysts of lime-poor pigeonite and/or hypersthene. The groundmass pyroxene is always pigeonitic augite or pigeonite with higher $CaSiO_3$ content than the microphenocrystic pyroxenes, as judged from its moderate optic angle in 010 plane. In other respects, except for the absence of augite phenocrysts, these rocks do not differ essentially from those of type Vc. The rocks of type IIc are generally more basic than those of type Ic, but are more acidic than types IIIc and IVc.

Andesites of type Vd (Pl. 5, figs. 4, 5, 6; Pl. 6, figs. 1, 2) range from basic to acid andesites (rarely dacites), intermediate and acid andesites being the most predominant (Table 12, columns 14, 16).

Olivine is present both in the basic and intermediate members, often in considerable quantity.

This type is characterized by the presence of hypersthene in the groundmass without any trace of marginal replacement by pigeonite. Monoclinic pyroxene of the groundmass is in most cases simply augite, sometimes augite plus pigeonite, and in rare cases simply pigeonite. Hypersthene of the groundmass occurs usually as long prisms, but sometimes as short prismatic crystals, or as irregular-shaped ones including poikilitically grains of plagioclase and iron ore.

There is a wide variation in the ratio between the amounts of orthorhombic and monoclinic pyroxenes present in the groundmass. The latter mineral tends to decrease toward the acid rocks so that the andesites of this type show complete gradation to the dacites of type Ve. Type Vd is connected with type Vc through the transitional type Vd→c. The augite and hypersthene in the rocks of type Vd show all the features indicating parallel crystallization continued from the intratelluric to effusive stage.

From the data so far obtained, the ratios $FeSiO_3/MgSiO_3$ in the bulk compositions of the groundmass pyroxenes (augite + hypersthene) of the rocks of this type are rarely higher than unity—a strong contrast to the iron-rich compositions of the groundmass pigeonite of the rocks of type Vc.

Type IIId of Table 17 is represented by basic andesites, while types IId and Id of Tables 16 and 17 are encountered in andesites. Again, by the gradual decrease of phenocrysts of hypersthene and the corresponding increase of those of olivine, type Vd passes into type IVd. A few andesites belong to the latter type.

Andesites of type Vd→c (Table 12, column 12) show all the features transitional from type Vd to type Vc. The distinctive character is the presence of hypersthene in the groundmass which is always surrounded by pigeonite in the same manner as that already described for porphyritic hypersthene. The two pyroxenes are usually in parallel intergrowth. Monoclinic pyroxene of the groundmass consists either of augite (or pigeonitic augite) plus pigeonite, the former more common in coarser grains, or simply of pigeonite. It is highly probable that the hypersthene, which was separated in the earlier stage of the groundmass formation was marginally replaced by pigeonite in the later stage due to the reaction with the magma.

Acid andesites and dacites of type VId resemble closely those of type Vd except for the presence of hornblende phenocyrsts. That the two types are genetically related is also indicated by their close association in the field. Thus the rocks of these types occur side by side as flows and pyroclastics interbedded with the sediments of the Asigara Beds, and also with the Haya-kawa Tuff Breccias and the Sukumo-gawa Andesite Group, or small intrusive masses related to these formations. Olivine or quartz may be present as phenocrysts. In the groundmass hypersthene usually exceeds monoclinic pyroxene which is always augitic. With decrease of augite in the groundmass, this type passes into the more acidic types VIe and VIIe.

Acid andesites and dacites of types Ve, VIe, VIIe, and VIIIe (Pl. 6, figs. 3, 4, 5) have many textural and mineralogical characters in common, and are closely associated with one another in the field and also with andesites of types VId and Vd. Olivine is absent, while quartz may occur as phenocrysts. Hypersthene

forms prismatic or slender needle-like crystals embedded in felsitic groundmass (Pl. 6, fig. 4).

The most acidic dacites of the region (Table 12, column 18) show assemblage of phenocrysts either belonging to type I, V, or VII. However, their groundmasses are either glassy (obsidian) or crystalline with flakes of biotite, instead of pyroxene, as the only ferromagnesian silicate mineral (Pl. 6, fig. 6).

Basalt of type IIIa→d, though not shown in the tabular scheme, comprises two specimens from the Yugawara volcano, possibly constituting a single flow. The rock cosely resembles the common basalts of type IIIb→c. It carries sporadic phenocrysts of olivine and plagioclase in an intergranular groundmass with some glass and cristobalite. In the groundmass are found grains of olivine, augite, and a few pigeonite, together with short prisms of hypersthene. The groundmass olivine, which is largely replaced by dust of iron ore, is surrounded by reaction rim of hypersthene and/or pigeonite, while the hypersthene is free from rim of pigeonite. It may be inferred that, in the earlier stage of groundmass formation of this type, olivine and augite were separated together, whereas in the later stage, olivine was resorbed to form hypersthene, and monoclinic pyroxene, still continuing to crystallize, gradually changed its composition to that of pigeonite.

Basic andesites of type Va→c (not shown in tabular scheme) comprise two specimens, one (Table 12, column 6) collected by Tsuya from a lava of the Taga volcano, and another by the writer from a lava of the Yugawara volcano. They carry rounded grains of olivine in the groundmass together with those of pigeonite and prisms of hypersthene. Cristobalite is present in considerable quantity. Both olivine and hypersthene are marginally replaced by pigeonite. These rocks may be classified as a variety of type Vd→c, in which olivine was separated in the earlier stage of the groundmass formation. The andesites of this type are comparatively rich in olivine phenocrysts.

Andesite of type Va→d (not shown in tabular scheme) is a scoriaceous rock which constitutes the deposit of nuée ardente from one of the central cones of the Hakone volcano and shows a peculiar mineral composition. Fibrous or skeletal crystals of olivine occur in the groundmass along with laths of plagioclase, long prisms of hypersthene, and a few grains of augite and magnetite. Distinct phenocrysts of olivine are rarely found, and the mineral ranges from microphenocrysts 0.3 mm. long to tiny needles. It is always surrounded by reaction rim of hypersthene. Its optic angle is approximate to 90°.

Because of the presence of an appreciable amount of glass base, the mineral assemblage of the groundmass cannot be regarded as what would have obtained after complete crystallization. Possibly, complete equilibrium would have resulted in type Vd.

The other andesites of the central cones of Hakone, from which this rock does not differ in general composition, all belong to type Vd. Why then did magnesian olivine appear in such a siliceous groundmass (probably of a composition not far from that given in Table 14, column 14)?

A tentative explanation is that the olivine was separated temporarily, probably due to a sudden change of physico-chemical condition of the extruded magma, say, a rise of temperature by gaseous combustion or an escape of volatiles. That the volatiles may have played an important role is suggested by the fact that this andesite forms the deposit of nuée ardente.

Order of Crystallization of the Minerals and Reaction Series

The order of crystallization of the principal minerals and the reaction relations as determined under the microscope are shown in Figure 19.

Continuous reaction series

The feldspar group forms a simple continuous reaction series, ranging from pure anorthite to anorthoclase.

Each mafic mineral group forms a continuous reaction series which is connected with other groups by a discontinuous reaction relation. The continuous reaction series are: magnesian olivine, hypersthene, monoclinic pyroxene, and cummingtonitic to green hornblende. The first two groups have rather simple compositions, both changing from Mg-rich to Fe-rich as the crystallization proceeds.

The crystallization of monoclinic pyroxene proceeds generally from diopsidic augite, passing through pigeonitic augite, to iron-rich pigeonite, both under the intratelluric and effusive conditions (Fig. 12). This course of crystallization prevails in a series of rocks in which augite was separated as phenocrysts prior to hypersthene. This is in good agreement with the observations of Barth (1931, p. 195) and Benson (1944, p. 81–84). The same course of crystallization was also found in "hypersthene-augite" (pigeonitic augite of the present writer) of Palisade diabase (Walker, 1940, p. 1090) and of Karroo dolerites (Walker and Poldervaart, 1940, p. 168; 1941, p. 436; Poldervaart, 1944, p. 96).

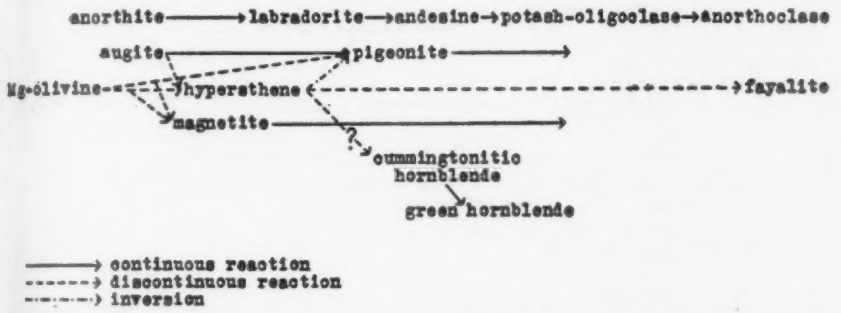

FIGURE 19.—ORDER OF CRYSTALLIZATION OF THE PRINCIPAL MINERALS AND REACTION RELATIONS

The pigeonite formed under the intratelluric condition is limited in composition, being more enriched in $FeSiO_3$ than the ratio $MgSiO_3$: $FeSiO_3 \doteq 1:1$; the groundmass pigeonite covers a wider range of composition.

In some cases, however, the crystallization under the effusive condition proceeds from Ca-poor pigeonite to Ca-rich pigeonite or pigeonitic augite, as indicated by the occurrence of microphenocrysts of Ca-poor pigeonite. This course of crystallization prevails in rocks in which hypersthene was formed as phenocrysts prior to augite. These microphenocrysts of pigeonite correspond in composition almost exactly to pigeonites described from doleritic rocks such as Hunnediabase (Wahl, 1907, p. 40), Semi dolerite (Sugi, 1937, p. 259), Palisade diabase (Walker, 1940, p. 1072), Tasmanian dolerites (Edwards, 1942, p. 586), and Karroo dolerites (Walker and Poldervaart, 1940, p. 163; 1941, p. 436; Poldervaart, 1944, p. 91, 93). In these dolerites, the pigeonite (the "early pigeonite" of Walker and Poldervaart) is always surrounded by pigeonitic augite (the "hypersthene-augite"). In Tasmanian and Karroo dolerites, orthorhombic pyroxene is the only pyroxene separated before the intrusion of the dolerite magmas. These features indicate that the "early pigeonite" has the same genetical significance as the microphenocrystic pigeonite of Hakone and Izu. Although Walker and Poldervaart emphasize that the "early pigeonite" was always formed in volatile-rich parts of magmas, the writer could not find such indications in Hakone and Izu.

The existence of a limited solid solution in monoclinic pyroxenes has been emphasized by Hess (1941, p. 519–525) and by Edwards (1942, p. 596). The last-named author mentioned however (p. 602) that the immiscibility gap narrows as the temperature of crystallization rises or the rate of cooling increases and finally disappears. A quite similar view was expressed by Benson (1944, p. 116). Macdonald (1944a, p. 627) also maintains that a complete gradation does exist between augite and pigeonite occurring in extrusive rocks.

The belief in the existence of the gap is based chiefly on the rarity of pyroxenes with 2V about 30° in spite of the common occurrence of those with 2V about 40° and about 0° in the same rock. However, certain members of a solid solution system may be formed less frequently than the other members according to the shapes of solidus and liquidus curves (or surfaces) for that system. Thus, those members having com-

positions between the points a and b of diagram D in Fig. 25 may often escape notice as they usually occur as very rare grains, or as very narrow zones in zoned crystals in which case the earlier members (lying to the right of b) may appear to be sharply bounded from the later members (lying to the left of a).

A good illustration is the zoned relation between andesine and anorthoclase of the Hakone and Izu rocks. The boundary appears quite sharp in the groundmass grains (Pl. 1, fig. 6), while completely gradual zoning can be seen in the feldspars of quartz-diorites (Pl. 1, figs. 1, 2).

The monoclinic pyroxenes of the present region offer no conclusive evidence of the limited solid solution. They rather suggest a complete gradation from augite to iron-rich pigeonite.

In phenocrysts of pigeonite-andesite from Weiselberg, Germany (Kuno, 1947), and also in coarse-grained crystals in pegmatitic facies of dolerite from Semi, Japan, the writer found completely gradual zoning between augite and pigeonite. These pyroxenes are comparatively rich in iron. Therefore a complete gradation between augite and iron-rich pigeonite both under the intratelluric and effusive conditions is concluded. However, the possibility cannot be excluded of the existence of the gap between pigeonitic augite and Mg-rich pigeonite ("early pigeonite") such as those occurring as microphenocrysts.

The crystallization of the hornblende group proceeds from cummingtonitic hornblende, passing through common green hornblende, to a deep-green, possibly iron-rich variety.

TABLE 11.—GROUNDMASS PYROXENES THAT FORM RIMS AROUND PORPHYRITIC OLIVINE AND PYROXENES

Porphyritic minerals	Mineral assemblage of the groundmass			
	Type c	Type d		Type e
	(pigeonitic augite and/or pigeonite)	(augite + pigeonite + hypersthene)	(augite + hypersthene)	(hypersthene only)
Olivine	Rimmed usually with pigeonite, and rarely with hypersthene or with hypersthene inside and pigeonite outside.	Rimmed with pigeonite plus some hypersthene.	Rimmed with hypersthene.	
Augite	No reaction rim.	No reaction rim.	No reaction rim.	Rimmed with hypersthene.
Hypersthene	Rimmed with pigeonite.	No reaction rim.	No reaction rim.	No reaction rim.

Note: the natures of the reaction rims in types b→ c and d→ c are entirely same as those in type c.

Discontinuous reaction series

Porphyritic olivine is surrounded by rim of porphyritic hypersthene, but not of augite. Groundmass pyroxenes that form the rims around porphyritic olivine and pyroxenes differ according to the kinds of pyroxenes of the groundmass (Table 11).

Hypersthene which forms the reaction rim around olivine is more enriched in $MgSiO_3$ than the isolated hypersthene in the same rock, and pigeonite which forms the reaction rim around olivine is poorer in $CaSiO_3$ than the average isolated monoclinic pyroxenes. It follows then that the reaction rims around crystals of olivine are formed by using materials introduced both from the crystals and from the magma.

It may be concluded that reaction relations exist between magnesian olivine and hypersthene, between magnesian olivine and pigeonite, and between augite and hypersthene only

when the pyroxenic components of the magma become largely hypersthenic.

The reaction relation between magnesian olivine and hypersthene is also suggested by the antipathetic relation between porphyritic olivine and hypersthene in the rocks of types Vc and Vd. If olivine and hypersthene underwent parallel crystallization, the occurrence of olivine in the groundmasses of rocks with hypersthene phenocrysts (rocks of types Ia, Ib, IIa, IIb, Va, Vb) would be quite general.

Pigeonite which forms rim around hypersthene is always nearly uniaxial, probably close to the hypersthene in composition. Such pigeonite is formed by inversion of the hypersthene when the hypersthene crosses the hypersthene-pigeonite inversion curve during the cooling of magma as will be discussed later. But it is quite likely that this inversion is not merely an atomic rearrangement within the solid pyroxene but is accompanied by reaction with the liquid magma, because the pigeonite rim around the hypersthene does not show the appearance of a simple pseudomorph after the latter mineral.

From the structure illustrated in Figure 9 and also from the fact that phenocrysts of magnetite tend to associate with those of hypersthene, it is concluded that magnetite is the joint product of the reaction between olivine, hypersthene (or pigeonite), and liquid magma.

The iron-rich hypersthene bears a reaction relation to fayalite (Fig. 11).

The relation between pyroxene and hornblende is somewhat ambiguous. Hornblende grows sometimes around augite and sometimes around hypersthene. Hypersthene may bear a reaction relation to cummingtonitic hornblende which is however formed temporarily and is readily converted to green hornblende (continuous reaction). Hornblende is unstable under the effusive condition, so that the ferromagnesian components of the magma with which the mineral is in equilibrium split up into hypersthene and augite, instead of combining to form hornblende, during the groundmass formation (type VId, etc.). In more acid magmas, however, the augite thus separated is resorbed to form hypersthene by discontinuous reaction, resulting in types VIIe, VIIIe, etc.

Magnesian olivine and augite crystallize side by side (see Kuno, 1935, p. 162) until hypersthene or pigeonite begins to separate. This is indicated by the absence of the reaction rim of augite around olivine, and by the absence of the types Xa—Xe of Tables 9 and 10. In type IVb→c, both olivine and augite continue to crystallize until the beginning of the groundmass stage. At this stage, olivine begins to be resorbed by the magma containing excess silica, with concomitant separation of pigeonite. Whether the ferromagnesian components of the groundmass crystallize as olivine + augite (type b), or simply monoclinic pyroxene with low $CaSiO_3$ content (type c) likely depends entirely on the amount of excess silica contained in the residual magma. The occasional association olivine + augite + pigeonite + silica mineral (type b→c) is therefore a result of incomplete equilibrium.

Augite and hypersthene also undergo parallel crystallization, except in the acid magma where the pyroxenic components become largely hypersthenic. The common occurrence of type Vd strongly indicates that the two minerals continue to crystallize until the final stage of the groundmass formation.

One might interpret the frequent occurrence of the mantle of augite around hypersthene as showing a reaction relation. In some instances, however, this may be better explained as developed around resorbed xenocrysts of hypersthene, and, in others, as due merely to parallel crystallization because there is scarcely any indication of the mutual reaction.

Order of crystallization

Judged from the microscopical observation, the earliest mineral to separate from the magma of this region is picotite, which is succeeded by Mg-rich olivine. Anorthite begins to crystallize usually later than olivine. Augite is next, succeeded by hypersthene. Magnetite begins to crystallize almost contemporaneously with hypersthene. In some cases, however, hypersthene begins to crystallize next to olivine, and may or may not be succeeded by augite. Hornblende is still later than hypersthene. Toward the later stage, the order of crystallization of minerals becomes more complicated. Anorthoclase, quartz or tridymite, and hypersthene or iron-rich pigeonite, together with some biotite, are

the last minerals to crystallize from the residual magma of pegmatitic composition. Crystallization of fayalite is still later, and may more properly be assigned to deuteric stage.

Comparison with artificial systems

The reaction relations between olivines and pyroxenes show a close resemblance to the behavior of these minerals in the laboratory dry melts.

That a reaction relation exists between magnesian olivine and pigeonite, but not between magnesian olivine and augite, is quite analogous to the relation of forsterite to various members of the diopside-clino-enstatite series in the ternary system diopside-forsterite-silica (Bowen, 1914, p. 207).

Again, in the rocks of this region, magnesian olivine bears a reaction relation to hypersthene having compositions more magnesian than about En_1 Fs_1, while iron-rich hypersthene (about $En_{63}FS_{37}$) bears a reaction relation to fayalite (about Fo_2Fa_{98}). Quite similar relations are demonstrated in the investigated system MgO-FeO-SiO_2 (Bowen and Schairer, 1935, p. 187), although the pyroxenic phases formed directly from the melt of this system are monoclinic and the composition ranges of olivines and pyroxenes which bear different relations do not agree exactly with those found in natural rocks.

Parallel crystallization of olivine and hypersthene (or pigeonite), demonstrated in the investigated system but not found in these rocks, has been noted in some ferriferous andesites of Japan (Kuno, unpublished data).

It might be expected from the experiments by Bowen and Schairer that pigeonite appears first and upon cooling is inverted to hypersthene. Textural relation of the two pyroxenic forms in the rocks of this region shows however that the reverse is always the case and only in rare instances, pigeonite (groundmass grains) is succeeded by hypersthene where volatile substances are concentrated (in pegmatitic patches and cavities). Barth and Holmsen (1939, p. 16) suggested that phenocrysts of hypersthene in andesites from the Antarctandes may "represent porphyroblasts formed metasomatically at a late stage of the congealing process" and therefore later than the general groundmass. However, most of the hypersthene phenocrysts in Japanese andesites appear to represent really early-formed crystals.

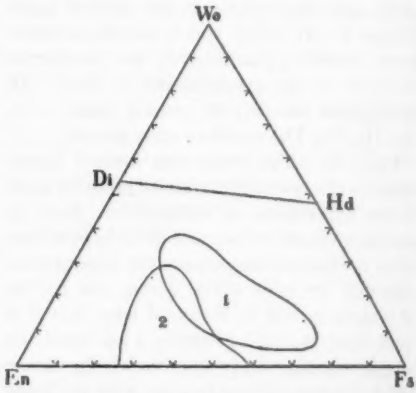

FIGURE 20.—DIAGRAM SHOWING THE CHEMICAL COMPOSITIONS OF THE GROUNDMASS PYROXENES OF THE TWO ROCK GROUPS

1. the area for the monoclinic pyroxenes of the first group. 2. the area for the pyroxenes (orthorhombic ± monoclinic) of the second group

The crystallization relation between these two pyroxenes will be discussed later.

ORIGIN OF THE ROCK SERIES

Distinction of the two rock series

The rocks of the present region may be classified into two major groups according to the kind of their groundmass pyroxenes. One contains monoclinic pyroxene as the only pyroxenic phase, and another is characterized by the presence of orthorhombic pyroxene, either with or without monoclinic.

To the first group belong types IIIb→c, IVb→c, IIIc, IVc, Vc, IIc, and Ic, and to the second, types IIIa→d, Vd, VId, VIe, VIIe, VIIIe, and Ve (rare types being omitted).

From the natures of the pyroxenes contained in these rock types (p. 68–74) and also from chemical analyses of the rocks, it is inferred that the groundmass pyroxenes of the respective rock groups have compositions differentiated into two areas when plotted in the ternary diagram (Fig. 20).

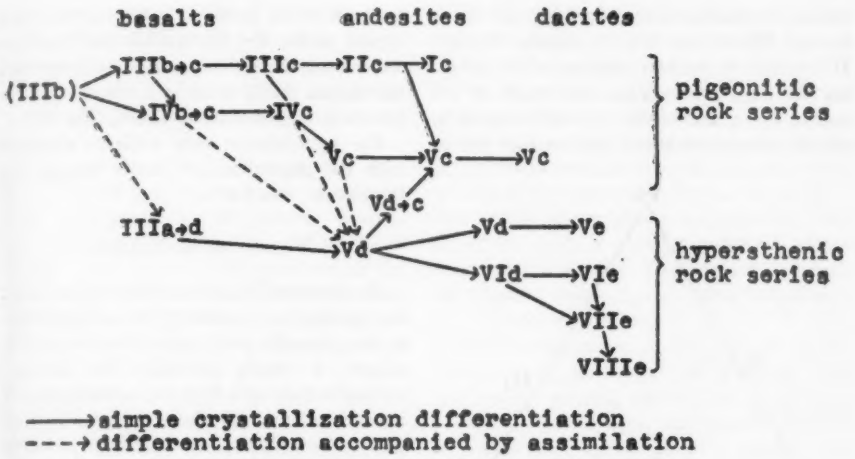

FIGURE 21.—EVOLUTION OF THE PRINCIPAL ROCK TYPES

The following facts have an important bearing upon the genetical relationship between the two groups:

(1) Porphyritic plagioclase contained in the second group carries dust inclusions more commonly than that in the first group. Thus plagioclase with this type of inclusion is encountered in nearly a half of the rocks of the second group but in nearly a quarter of the rocks of the first.

(2) Porphyritic hornblende is confined to the second group.

(3) The rapidly cooled portion of any lava or dike does not show any difference in the kinds of the groundmass pyroxenes from the slowly cooled portion of the same mass. For example, if the interior of any lava or dike shows the assemblage of type d (or type e), the chilled margin (usually finer-grained or more glassy than the interior) of the same mass also shows the assemblage of type d (or type e).[4]

(4) The various rock types belonging to the same group are closely associated with one another in the field. Thus, for example, the rock types carrying porphyritic hornblende tend to occur in those suites of volcanic rocks in which types Vd and Ve predominate over types IVc, Vc, IIc, etc.

These facts lead us to the conclusion that the two rock groups were formed from magmas of differing physico-chemical conditions which determined the kinds of groundmass pyroxenes and the appearance or non-appearance of porphyritic hornblende.

The two rock groups are designated here as "pigeonitic rock series" and "hypersthenic rock series" respectively according to the pyroxenes which characterize the groundmass.

Within each series, one rock type passes into another by the appearance or disappearance of any one of the ferromagnesian silicate minerals belonging to the discontinuous reaction series. Any pair of rock types showing such a relation resemble one another texturally as well as mineralogically. In this way, the evolution of the various rock types can be traced (Fig. 21).

Evolution of the ferromagnesian components

The fact that the rocks belonging to the different series were erupted alternately from one and the same volcanic center strongly indicates derivation from a common parental magma through different courses (Fig. 21). This magma is assumed to have a composition of an undersilicated olivine-basalt, corresponding to type IIIb in mineral assemblage.

Beginning with this assemblage, the main

[4] Throughout the whole region, no regular relationship appears to exist between the crystallinity or granularity of the groundmass and the kinds of its pyroxenes. The writer's previous statement (1936b, p. 142) that, when both augite and hypersthene occur in the groundmass, the groundmass tends to be higher in crystallinity should be revised.

course of evolution of the pigeonitic rock series is from IIIb→ c or IVb→ c, passing through IIIc or IVc, to the acid members of Vc, covering the most predominant rock types of the region. Along this course, the ferromagnesian silicate components of the liquid magma change

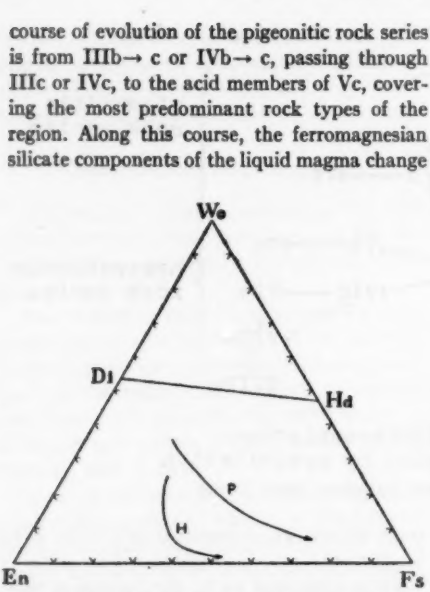

FIGURE 22.—EVOLUTION OF PYROXENIC COMPONENTS OF THE TWO ROCK SERIES

P: pigeonitic rock series: H: hypersthenic rock series.

from a mixture of augite plus some olivine in the basic end, passing through monoclinic pyroxene with moderate contents of lime and iron, to iron-rich pigeonite in the acid end (Fig. 22). The subsidiary course from IIIc to Ic differs from the preceding in the non-appearance of augite phenocrysts and in the generally lime-poor nature of the groundmass pyroxene. In this course, the pyroxenic components separated from the magma during the effusive stage change from lime-poor (hypersthene or pigeonite with optic plane perpendicular to 010) to lime-rich (pigeonitic augite).

The hypersthenic rock series shows the evolution from IIIa→d, passing through Vd, to Ve or to VIIIe. In the basic end of this series, the ferromagnesian silicate components of the magma consist of a mixture of augite and hypersthene, together with some olivine; in the intermediate members, olivine disappears completely; and to the acid end, augite is successively replaced by hypersthene until finally hypersthene becomes the only ferromagnesian silicate. In the later stage, cummingtonitic and common green hornblende may or may not appear under the intratelluric condition. In either case, the ferromagnesian components of the magma finally attain a composition of hypersthene approximate to En_1Fs_1 (Fig. 22).

The hypersthenic rock series is connected with the pigeonitic rock series through the transitional type Vd→c.

Origin of the two rock series

The essential features of these two series can be explained by assuming that the derivation of the pigeonitic rock series from the parental magma is chiefly controlled by fractional crystallization, and that the contamination of igneous rocks by more basic magmas is an important factor in the genesis of the hypersthenic rock series.

The formation of the oversilicated rock types (such as IIIc, IVc, Vc, IIc, Ic, etc.) from the undersilicated basaltic magma (IIIb) is possible by the early separation of olivine more than its stoichiometric amount. In the later stage of the evolution of the pigeonitic rock series, the separation of augite, combined with hypersthene, pushes the residual magma toward a composition relatively enriched in $FeSiO_3$ in its pyroxenic components (Fig. 22). Silica and alkalies are also concentrated in this residual magma by the separation of olivine, pyroxenes, and calcic plagioclase.

The contamination of igneous rocks by more basic magmas accounts for the presence of the dust inclusions in plagioclase characteristic of the hypersthenic rock series.

The dust inclusions are formed in plagioclase xenocrysts enclosed by a magma saturated with more calcic plagioclase (or yet unsaturated with this mineral). The origin of such xenocrysts may be either crystals suspended in another part of the magma differing in composition from the enclosing one or detached crystals from cognate inclusions (or "autolith") which are usually found in the hypersthenic rock series. Crystals which appear derived directly from foreign igneous rocks, say granitic, are quite rare.

However, it is not improbable that the local heterogeneity in composition within a single magma reservoir and the formation of the

cognate inclusions result from the assimilation of the wall rocks (possibly granitic) of the reservoir. Therefore, the ultimate cause of the formation of the hypersthenic rock series may be ascribed to the assimilation of granitic and related rocks.

The contamination, whether of the substances of the cognate or of the accidental origin, may occur in the parental basaltic basaltic magma as well as in more differentiated magmas. It is likely that the members of the hypersthenic rock series are generated through the contamination at various stages in the course of the evolution of the magmas of the pigeonitic rock series (Fig. 21).

The inclusions of picotite in olivine tend to occur in rocks in which dust inclusions are found in plagioclase, which strongly suggests that the formation of picotite is also related to the assimilation.

If the magma which captures the xenocrysts of plagioclase is saturated only with olivine, but not yet with plagioclase, or even in a slightly superheated condition, the plagioclase will suffer complete resorption with concomitant precipitation of olivine. After the addition of the plagioclase components, the magma will attain to such a composition as to precipitate a new phase spinelid, along with olivine, as has been discussed by Bowen (1928, p. 277) with the aid of the investigated system anorthite-forsterite-silica. The picotite included in olivine may be formed in this way.

It is further assumed that volatile substances are concentrated in the assimilated magma. The concentration of volatile substances around or within xenoliths is suggested by a number of examples in other regions, especially in xenoliths in plutonic rocks. This necessarily lowers the crystallization temperatures of the various components of the magma and thus favours the formation of hypersthene instead of pigeonite in the effusive stage. That the concentration of volatiles favours the formation of hypersthene is strongly indicated by the occurrence of hypersthene in microscopical druses and pegmatitic patches of some basalts of the pigeonitic rock series.

The separation of porphyritic hornblende in the hypersthenic rock series is also attributable to the abundance of volatiles.

The crystallization temperatures of the pigeonitic rock series are always kept high, because of the poverty of the volatiles. This gives rise to the formation of pigeonite in the effusive stage, as will be discussed later.

In the hypersthenic rock series, not only do the pyroxenic components of the magma suffer a notable change in composition by the assimilation of the foreign substances, but also their future evolution is greatly controlled by the action of the volatiles concentrated, although the effect of the fractional crystallization cannot entirely be ruled out.

Thus granitic rocks are always poorer in Wo component in their normative pyroxenes than the basaltic magma, yielding in many cases even normative corundum. Where the granites are assimilated by the basaltic magma, the resulting products will be comparatively impoverished in Wo in their pyroxenic components.

In the later stage of evolution of this hybrid magma, the separation of augite and hypersthene pushes the residual liquid toward a composition enriched in Fs in the pyroxenic components. On the other hand, this is compensated by the action of the volatiles, which changes a part of FeO in the liquid to Fe_2O_3, resulting in the formation of magnetite or hematite in greater amount than otherwise. The content of Fs in the pyroxenic components is thus reduced.

Phemister (1934, p. 40) discussed the oxidation of FeO to Fe_3O_4 in the magma through the action of H_2O gas contained there and arrived at the conclusion that "the ratio Fe_3O_4/FeO will be increased during those stages of the cooling of the magma when the escape of gas (H_2O) is accelerated." Taneda (1943b, p. 94) emphasized the enrichment of $MgSiO_3$ relative to $FeSiO_3$ in the groundmasses of hornblende-andesites from Haruna volcano, central Japan, and attributed the cause of this enrichment of $MgSiO_3$ to the separation of magnetite from the magma.

Again, some parts of Na_2O and K_2O in the magma may be transferred by the volatiles into the country rocks which make up the wall of the magma chamber. Excess alumina is then left in the magma, and combines with CaO to form anorthite. This also reduces the Wo component in the pyroxene.

There is another possible way of changing the composition of the residual liquid in the same direction. Among the volatile components may be present a notable amount of phosphorus which combines with CaO to form apatite. Microscopical observation shows that this mineral is conspicuous in the hypersthenic rock series rather than in the pigeonitic.

Obviously, these processes are more effective in the acid magma where the ferromagnesian components are reduced in amount and the subtraction of even an infinitesimal amount of CaO and FeO from the liquid should notably change the ratio Wo:En:Fs in the remaining pyroxenic components.

The net result of these processes is the successive enrichment of both En and Fs in the pyroxenic components of the magma.

The distribution of the two rock series in the field is also worthy of note. The hypersthenic rock series tends to associate with the thick deposits of geosyncline (the Asigara Beds), whereas the pigeonitic rock series predominates over the hypersthenic in the volcanic suites developed in the area which has not undergone geosynclinal subsidence (for example, rocks of the Quaternary volcanoes).

It is quite likely that the contamination of the granitic crust (sial) by the basaltic magma (sima) takes place in the area which suffers subsidence for a long period.

Crystallization of pyroxenes

The writer (1936b, p. 141) formerly advanced the view that pyroxenes of igneous rocks crystallize either as augite plus hypersthene or as single monoclinic pyroxene (pigeonite) according to whether their compositions lie within his "two-pyroxene field" or within his "pigeonite field." The boundary between the two fields is located at about En:Fs = 1:1.

In regard to the physico-chemical meaning of this conclusion, Tsuboi (1936, p. 405) offered the following view:

The inversion curve for the pyroxenes of the system $MgSiO_3$—$FeSiO_3$ was determined by Bowen and Schairer (1935, p. 196) as shown by the curve AB of Figure 23. Consider first only the $MgSiO_3$ and $FeSiO_3$ components of natural magmas, and assume that pyroxenes of this series crystallize from the magmas at temperatures indicated roughly by the curve CD of Fig. 23.[5]

On the left-hand side of point E, the intersection of the two curves, the crystallization takes place below the inversion temperatures, so

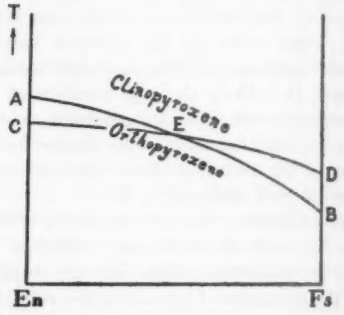

FIGURE 23.—STABILITY FIELDS OF CLINO- AND ORTHOPYROXENES (AB BEING THE INVERSION CURVE) AND THE AVERAGE TEMPERATURES OF CRYSTALLIZATION OF PYROXENES IN NATURAL MAGMAS (SHOWN BY THE CURVE CD)
After Tsuboi.

that orthorhombic pyroxenes are normally formed. However, if a rapid cooling obtains, such as in the groundmass formation, monoclinic pyroxenes may result as a metastable phase. On the contrary, the crystallization on the right-hand side of E takes place above the inversion temperatures, so that monoclinic pyroxenes are formed in rapid as well as in slow cooling.

Consider next the ternary system $CaSiO_3$—$MgSiO_3$—$FeSiO_3$ and suppose two curved surfaces produced from the curves AB and CD of Figure 23 toward the Wo apex of the triangular diagram. The intersection of the two curved surfaces corresponds to the boundary line between Kuno's "two-pyroxene field" and "pigeonite-field," having the same significance as point E.

Since 1936, four examples of porphyritic pigeonites have been discovered: (1) in andesite from Patagonia (Larsson, 1941, p. 267); (2) in andesite from Minami-aizu, Japan (Kuno,

[5] Hess (1941, p. 583) constructed a similar diagram quite independently for explaining the hypersthene with oriented plates of augite as an inversion product of pigeonite.

1940d, p. 180); (3) in weiselbergite from Weiselberg, Germany (Kuno, in press); (4) in dacite from Asio, Japan (Kuno, unpublished data). More data have been accumulated on the composition range of orthorhombic pyroxenes in volcanic rocks, and detailed observations have been made on pyroxenes in gabbroic and doleritic intrusives from various parts of the world. Hess (1941, p. 578–591) and Edwards (1942, p. 593–602) drew almost the same conclusions as regard to the crystallization of pyroxenes in gabbroic and doleritic rocks. But a slight modification of their theories is necessary to explain the pyroxene relations observed in volcanic rocks.

The porphyritic pigeonites are all found in rocks of the pigeonitic rock series so far as can be judged from the nature of their groundmasses. The mineral has compositions more ferriferous than the ratio $FeSiO_3:MgSiO_3 \doteqdot 1:1$ (Minami-aizu pigeonite, $Wo_{11}En_{37}Fs_{52}$; Weiselberg pigeonite, $Wo_{10}En_{37}Fs_{53}$; Asio pigeonite, $Wo_{10}En_{13}Fs_{78}$). Hypersthene phenocrysts in these pigeonite-andesites (including those already described from Scotland and Hakone) are found as relics surrounded by the pigeonite, having compositions between Fs_{46} and Fs_{55}. It is evident that the inversion from hypersthene to pigeonite occurs within a narrow composition interval around En_{50} Fs_{50}.

However, some hypersthenes in Japanese volcanic rocks have compositions between Fs_{60} and Fs_{93}. Such ferriferous hypersthenes are found in rocks of hypersthenic rock series.

Since the crystallization temperatures of pyroxenes in magmas are supposed to be lower in the hypersthenic rock series than in the pigeonitic, it is reasonable to substitute for the curve CD of Figure 23 two sets of liquidus and solidus curves, one for the pigeonitic rock series (CED and CFD) and another for the hypersthenic (C′E′D′ and C′F′D′) (Fig. 24). In the same figure, curves AB show the inversion temperatures for the ortho- and clinopyroxenes. The two points (F and a point between F and E) at which the solidus curve CFD and the inversion curves AB intersect have the same significance as the point E of Figure 23.

The circles lettered 1 and 2 represent two types of Vc. The phenocrysts crystallize below the inversion temperatures so that hypersthenes are formed along with augites. The groundmass pyroxenes crystallize rapidly from the liquids. In such a case, the solidus curve is assumed to approach the liquidus and take the position somewhat above the broken line CGD. The

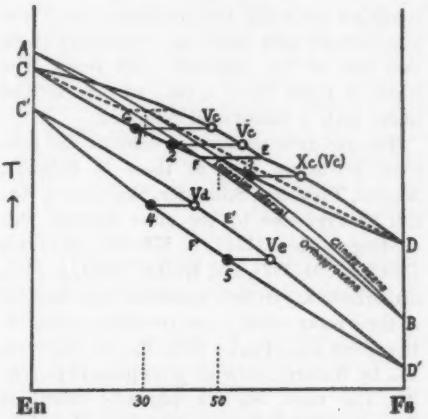

FIGURE 24.—RELATIONS BETWEEN THE CLINO- AND ORTHOPYROXENE INVERSION CURVES (AB) AND THE LIQUIDUS AND SOLIDUS CURVES FOR THE CRYSTALLIZATION OF PYROXENES FROM MAGMAS

CED and CFD: pigeonitic rock series; C′E′D′ and C′F′D′: hypersthenic rock series. Broken lines, CGD: solidus curve for gabbroic and doleritic intrusives. Solid circles: phenocrysts. Open circles: liquid in equilibrium with the phenocrysts. The types of mineral assemblage which will result from solidification upon extrusion of the liquids carrying the phenocyrsts are shown by the marks Vc, Vd, etc.

pyroxenes then crystallize above the inversion temperatures so that pigeonites are formed. The rocks whose pyroxenes have the compositions represented by the circles 2 are much more common in Hakone and Izu than those represented by circles 1.

In type Xc (Circles 3), both the phenocrysts and groundmass grains are pigeonites, and are all formed above the inversion temperatures. Typical examples are pigeonite-andesites from Mull (Bailey *et al.*, 1924, p. 283), Weiselberg, and Minami-aizu. These rocks contain a little phenocrysts (relics) of hypersthene so that the actual assemblage belongs to type Vc.

In types Vd and Ve (4 and 5), both the phenocrysts and the groundmass grains crystallize below the inversion temperatures, so that hy-

persthenes are always formed either alone or together with augite.

In Figure 24, the curves C'E'D' and C'F'D' are located too low in order to avoid confusion of lines. They are probably closer to but do not cross the inversion curves. Moreover, the condition attending the crystallization of the hypersthenic rock series may sometimes grade into that of the pigeonitic rock series. The rocks of types Vd→ c, etc., may be formed under such a transitional condition.

The pyroxene relations in doleritic and gabbroic intrusives such as those of Palisade, Karroo, Tasmania, Stillwater, Skaergaard, etc., can be explained by the same diagram. According to Hess (1941, p. 578–591), Edwards (1942, p. 593–597), and Walker (1943, p. 519), orthorhombic pyroxene separates from magmas of these rocks which, upon reaching a composition about Fs_{30} (Fs_{35} by Hess, Fs_{30} by Edwards, Fs_{28} by Walker), abruptly gives place to pigeonite. The most Mg-rich pigeonite found in Karroo dolerites has a composition Wo_{14} En_{61} Fs_{25} (Walker and Poldervaart, 1941, p. 438), being close to the hypersthene separated immediately before this change takes place. Afterwards pigeonite continues to crystallize side by side with augite which also joins in crystallization, and after reaching a composition about En:Fs = 30:70, the two pyroxenes give place to a single monoclinic pyroxene (ferroaugite). In the gabbroic rocks, pigeonite always invert to hypersthene with oriented plates of augite so that no pigeonite is found as such in the final consolidation products. In the doleritic rocks, inversion of pigeonite to hypersthene with oriented plates takes place only within a composition range from En:Fs = 70:30 to about En:Fs = 50:50.

The course of crystallization of monoclinic pyroxenes was traced more fully by Walker and Poldervaart (Walker, 1940, p. 1089–1092, Walker and Poldervaart, 1940, p. 167–168; 1941, p. 436–440; Poldervaart, 1944, p. 95–97). Thus, in Palisade and Karroo dolerites, magnesian pigeonite (early pigeonite) is followed by pigeonitic augite (hypersthene augite) which is in turn followed by less magnesian pigeonite (late pigeonite), there being little evidence of the simultaneous crystallization of pigeonites and pigeonitic augite. This course is somewhat similar to that found in the groundmass monoclinic pyroxenes of Hakone and Izu.

Hess, Edwards, Walker, and Poldervaart all believe that the pigeonites in the dolerites are formed as a stable phase.

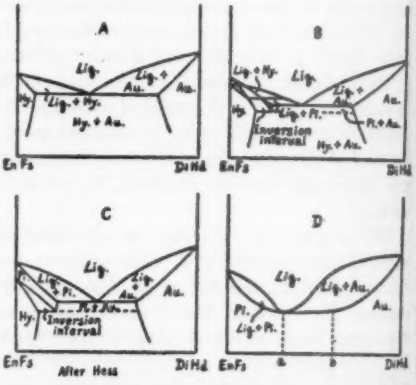

FIGURE 25.—HYPOTHETICAL EQUILIBRIUM DIAGRAMS FOR PYROXENES

What has been summarized above can be explained by assuming that the solidus curve for these doleritic and gabbroic pyroxenes crosses the inversion curves at a composition about Fs_{30} (Fig. 24, CGD), corresponding to the curve drawn by Hess (1941, p. 583) to represent the temperature of magmas. This solidus curve is situated very close to that assumed for the groundmass pyroxenes of the pigeonitic rock series.

A more complete picture of the behaviour of pyroxenes can be obtained by a series of hypothetical equilibrium diagrams (A to D of Fig. 25) representing cross-sections of the ternary diagram Wo-En-Fs. The diagram A shows the equilibrium relation for those parts of Figure 24 where the solidus curves lie below the inversion curves, while the diagrams B to D for those parts where the solidus curves lie above the inversion curves.

During the crystallization of the dolerites and gabbros, the change of the equilibrium relation from A to B takes place when the ratio En:Fs in the separating pyroxenes reaches 70:30, that from B to C at about a ratio En:Fs = 50:50 (or 60:40), that from C to D at about a ratio En:Fs = 30:70 (Hess, 1941, p. 584–

591). The possible appearance of fayalitic olivine is disregarded in the equilibrium diagram D.

It appears possible to the writer that, at least in doleritic pyroxenes, the change of the equilibrium relation from C to D sometimes occurs at about a ratio En:Fs = 50:50.

In the pigeonitic rock series, porphyritic pyroxenes more ferriferous than En:Fs = 50:50 crystallize according to the equilibrium relation D, whereas nearly all the groundmass pyroxenes do so according to the same relation, although comparatively magnesian pyroxenes of the groundmass, say En:Fs < 55:45 (see point P_1 of Fig. 12), may crystallize according to the relation C. Inversion from pigeonite to hypersthene does not take place in these pyroxenes because of rapid cooling.

Evidences of contamination in the hypersthenic rock series in other regions of Japan

In other volcanic fields of Japan, rocks belonging to the hypersthenic rock series exhibit all the features just described. Some of them afford more direct evidences of contamination of acid igneous rocks (rarely sandstone) than in the rocks of the present region.

In some basalts of the Ômuro-yama volcano group, lying south of the Usami volcano, xenocrysts of andesine and quartz were found by Tsuya (1930, p. 421; 1937, p. 300) which he considered derived from some dacite mass underlying the volcano. Specimens collected by the writer show that the basalts represent the most basic members of the hypersthenic rock series, having the mineral assemblage of types IIIa→d and IIId. Phenocrysts of olivine include small octahedrons of picotite, and the xenocrysts of plagioclase are full of dust inclusions.

Near the mouth of the Tone river, Tiba Prefecture, bronzite-andesite is exposed (Yamane, 1927), which includes occasional fragments of sandstone. The mineral assemblage of this rock belongs to type Ie.

In Nasu and Zaô volcanoes, northeastern Japan, some lavas of andesites carry xenocrysts of quartz associated with crystals of plagioclase rich in dust inclusions. All of them belong to type Vd in mineral assemblage.

Among the Tertiary volcanic rocks of Sidara basin, Aiti Prefecture, the rocks of the most basic composition are olivine-basalts of type IIIb which include xenoliths of granites and biotite-gneisses. Olivine phenocrysts in these basalts carry inclusions of picotite, sometimes attaining to 0.1 mm. in diameter.

Sugi (1938, p. 17) studied the behaviour of granitic xenoliths captured by "sanukite" and associated andesitic rocks in Kagawa Prefecture, Sikoku Island. He concluded that the chemical compositions of these andesitic rock were affected by the contamination of the granitic rocks which were in all probability derived from the basement of the area. It is well known that "sanukite" and the associated andesites are characterized by the predominance of bronzite both as phenocrysts and as groundmass grains, belonging to types Vd, Id, and Ie.

He (1942, p. 69) also showed that the "quartz-basalt" in the vicinity of Hagi, Yamaguti Prefecture was derived from an olivine-basalt magma (approaching in composition to the parental magma of the Circum Japan Sea Province) through the assimilation of granitic rock, the quartz crystals in the basalt being the resorption remnants of the xenoliths. Dr. Sugi kindly placed the specimens at the writer's disposal, and microscopical examination shows that the quartz-basalt belongs to type IIa→d, carrying phenocrysts of olivine which include numerous grains of picotite.

Sugi also reported that one of the undersilicated olivine-basalts near Hagi contains partly remelted granitic xenoliths, around which hypersthene is formed as a groundmass constituent. Thus the groundmass adjacent to the xenoliths closely resembles the quartz-basalt in mineral composition. Again hornblende-andesites, which are closely associated with the quartz-basalt, carry xenocrysts of quartz and feldspar. The groundmass pyroxene of this rock consists almost exclusively of hypersthene.

Chemical Compositions of the Rocks

Bulk compositions and modes

The porphyritic rocks are notably rich in CaO and poor in alkalies as compared with the average basalt-andesite-rhyolite series of the world (Table 12).

TABLE 12.—BULK COMPOSITIONS AND NORMS OF PORPHYRITIC ROCKS

	1	2	3	4	5	6	7	8
Type of mineral assemblage	IIIc	IVc	Vc	IVc	IVc	Va → c	Vc	Vc
SiO_2	49.62	50.17	50.37	50.38	50.45	50.71	50.94	51.10
Al_2O_3	20.37	19.65	19.07	20.36	19.45	18.84	19.32	18.90
Fe_2O_3	2.61	2.54	2.25	2.86	2.27	2.42	4.14	3.56
FeO	6.71	7.92	8.66	7.26	8.41	7.13	5.52	6.52
MgO	4.05	4.54	4.19	4.45	3.73	6.08	4.20	5.03
CaO	11.97	11.29	11.30	11.28	11.23	10.05	10.62	10.80
Na_2O	1.89	1.66	1.96	1.95	1.75	2.03	2.15	2.14
K_2O	0.31	0.29	0.32	0.33	0.33	0.24	0.32	0.32
$H_2O(+)$	0.39	0.41	0.30	0.36	0.42	0.69	0.73	0.50
$H_2O(-)$	0.71	0.20	0.27	0.25	0.30	0.38	1.04	0.28
TiO_2	0.87	0.87	1.01	0.84	1.04	0.67	0.78	0.83
P_2O_5	0.07	0.10	0.08	0.10	0.09	0.13	0.07	0.13
MnO	0.17	0.17	0.21	0.15	0.20	0.15	0.18	0.13
Total	99.74	99.81	99.99	100.57	99.67	99.52	100.01	100.24
Q	4.93	5.70	4.68	4.80	6.12	4.44	8.16	6.48
Or	1.67	1.67	1.67	1.67	1.67	1.67	1.67	1.67
Ab	15.73	14.15	16.77	16.77	15.20	17.29	18.34	17.82
An	46.45	45.31	42.26	45.87	43.92	41.42	41.98	41.14
Wo	5.11	4.18	5.45	3.94	4.52	3.13	4.06	4.87
En	10.04	11.40	10.50	11.10	9.30	15.10	10.50	12.60
Fs	8.97	11.22	12.67	9.90	12.28	10.30	5.68	7.66
Mt	3.71	3.71	3.25	4.18	3.25	3.48	6.03	5.34
Il	1.67	1.67	1.98	1.52	1.98	1.22	1.52	1.52
Hm	—	—	—	—	—	—	—	—
Ap	0.34	0.34	0.34	0.34	0.34	0.34	0.34	0.34
Wt% Or	2	3	3	3	3	2	3	3
Wt% Ab	24	23	28	26	25	29	30	29
Wt% An	74	74	69	71	72	69	67	68
Wt% Wo	21	16	19	16	17	11	20	20
Wt% En	42	42	37	44	36	53	52	50
Wt% Fs	37	42	44	40	47	36	28	30

	9	10	11	12	13	14	15
Type of mineral assemblage	Vc	Vc	Vc?	Vd → c	Vc	Vd	d
SiO_2	51.68	52.35	52.85	54.00	55.83	57.07	57.22
Al_2O_3	19.70	20.23	18.37	18.84	17.75	17.53	17.46
Fe_2O_3	2.69	2.28	3.48	2.07	2.76	2.59	2.45
FeO	6.78	6.25	7.83	7.71	6.01	5.44	6.15
MgO	4.15	3.72	2.96	2.72	3.90	3.87	3.77
CaO	10.78	9.62	10.12	9.74	8.62	8.77	7.93
Na_2O	1.94	2.74	2.07	2.95	2.98	2.80	2.87
K_2O	0.32	0.44	0.36	0.41	0.55	0.52	0.75
$H_2O(+)$	0.22	0.90	0.39	0.30	0.19	0.27	0.30
$H_2O(-)$	0.20	0.41	0.16	0.20	0.17	0.12	0.23
TiO_2	0.81	1.19	0.93	1.02	0.61	0.77	0.73

TABLE 12—BULK COMPOSITIONS AND NORMS OF PORPHYRITIC ROCKS (*Continued*)

	9	10	11	12	13	14	15
Type of mineral assemblage	Vc	Vc	Vc?	Vd → c	Vc	Vd	d
P_2O_5	0.13	0.15	tr.	0.11	0.13	0.08	0.11
MnO	0.16	0.13	0.17	0.29	0.17	0.14	0.16
Total	99.56	100.41	99.69	100.36	99.67	99.97	100.13
Q	8.04	6.72	11.10	7.86	10.68	13.68	12.96
Or	1.67	2.22	2.22	2.22	3.34	2.78	4.45
Ab	16.24	23.06	17.29	25.15	25.15	23.85	24.10
An	44.20	41.70	39.75	36.97	33.64	33.92	32.80
Wo	3.60	2.09	4.29	4.41	3.48	3.60	2.44
En	10.40	8.36	7.40	6.80	9.80	9.70	9.40
Fs	9.24	9.12	10.16	11.22	7.79	6.73	8.32
Mt	3.94	3.25	5.10	3.02	4.18	3.71	3.71
Il	1.52	2.28	1.82	1.98	1.22	1.52	1.37
Hm	—	—	—	—	—	—	—
Ap	0.34	0.34	0.00	0.34	0.34	0.34	0.34
Wt% Or	3	4	4	4	6	5	8
Wt% Ab	26	34	29	39	40	39	39
Wt% An	71	62	67	57	54	56	53
Wt% Wo	15	10	20	20	16	18	12
Wt% En	45	43	34	30	47	48	47
Wt% Fs	40	47	46	50	37	34	41

	16	17	18	A	B
Type of mineral assemblage	Vd	Vc	VII	IIc	Ic?
SiO_2	57.85	59.77	76.05	48.02	51.45
Al_2O_3	16.94	17.00	12.79	20.48	16.84
Fe_2O_3	2.23	2.49	1.47	2.13	1.49
FeO	5.30	5.59	0.31	7.05	10.95
MgO	4.34	2.24	0.08	5.79	4.48
CaO	7.80	7.05	1.60	14.14	10.71
Na_2O	3.32	3.29	3.89	1.28	1.23
K_2O	0.60	0.62	1.82	0.30	0.37
$H_2O(+)$	0.26	0.41	0.74	n.d.	0.72
$H_2O(-)$	0.32	0.51	0.52	n.d.	
TiO_2	0.80	0.63	0.19	0.78	1.27
P_2O_5	0.13	0.10	tr.	0.01	0.26
MnO	0.15	0.16	0.05	0.26	0.19
Total	100.04	99.86	99.51	100.36*	99.96
Q	12.36	17.94	42.96	0.12	8.76
Or	3.34	3.34	10.56	1.67	2.22
Ab	27.77	27.77	33.01	11.00	10.48
An	29.75	30.02	8.06	49.21	39.20
Wo	3.36	1.74	C = 1.43	8.82	5.10
En	10.90	5.60	0.20	14.50	11.20
Fs	6.86	7.39	0.00	10.43	17.16

TABLE 12—BULK COMPOSITIONS AND NORMS OF PORPHYRITIC ROCKS (*Concluded*)

	16	17	18	A	B
Type of mineral assemblage	Vd	Vc	VII	IIc	Ic?
Mt	3.25	3.71	0.46	3.02	2.09
Il	1.52	1.22	0.46	1.52	2.43
Hem	—	—	1.12	—	—
Ap	0.34	0.34	—	—	0.67
Wt% Or	5	6	20	2	4
Wt% Ab	46	45	64	18	20
Wt% An	49	49	16	80	76
Wt% Wo	16	12	—	26	16
Wt% En	52	38	—	43	33
Wt% Fs	32	50	—	31	51

* Including (Ce, Y)$_2O_3$ 0.003, ZrO_2 0.002, BaO 0.010, S (total) 0.108.

1. Olivine-basalt, a block in tuff breccia of the Yugasima Series. Loc., south of Uomi-saki, near Atami (Tsuya, 1937, p. 235). The rock is slightly altered.

2. Augite-olivine-basalt (with microphenocrysts of hypersthene), a lava of the Taga volcano. Loc., a quarry near Takyô, south of Nirayama (Tsuya, 1937, p. 273).

3. Hypersthene-bearing augite-olivine-basalt (H.K. 37112107b), an upper porphyritic part of a composite lava flow of the Hata Basalt Group. Loc., west of Simotanna.

4. Augite-bearing olivine-basalt, a lava of the Taga volcano (TV_1). Loc., a valley south of Tawarano (Tsuya, 1937, p. 273).

5. Augite-bearing olivine-basalt (H.K. 31041812), a lava of the Taga volcano. Loc., a valley northwest of Usami (Kuno, 1936c, p. 55).

6. Augite-hypersthene-olivine-andesite, a lava of the Taga volcano. Loc., south of Kameisi-tôge, west of Usami (Tsuya, 1937, p. 273).

7. Olivine-augite-hypersthene-andesite, a lava interbedded with the tuff breccias of the Taga volcano. Loc., immediately southwest of Uomi-saki, near Atami (Tsuya, 1937, p. 273).

8. Hypersthene-augite-olivine-basalt (51227), an upper porphyritic part of a composite lava flow of the Aziro Basalt Group. Loc., immediately southeast of Aziro (Kuno, 1933 b, p. 396).

9. Hypersthene-augite-olivine-basalt (H.K. 31050201), a lava of the Taga volcano. Loc., a valley northeast of Kameisi-tôge (Kuno, 1936 c, p. 55).

10. Olivine-bearing augite-hypersthene-andesite (H.K. 31041909), a lava of the Taga volcano. Loc., a valley east of Kameisi-tôge (Kuno, 1936 c, p. 55). The analysis was made on the material in which large phenocrysts (3–10 mm.) of pyroxenes were taken off.

11. Andesite (olivine-two pyroxene-bearing andesite according to Tsuya), a lava of the Taga volcano. Loc., near Ôno, south of Nirayama (Tsuya, 1937, p. 273).

12. Augite-hypersthene-andesite (H.K. 32090104), a lava of the Taga volcano. Loc., midway between Simotaga and Yamabusi-tôge.

13. Augite-hypersthene-andesite (H.K. 33022003), a lava of the old somma of the Hakone volcano. Loc., a quarry northwest of Kurakake-yama (Kuno, 1936 a, p. 120).

14. Olivine-bearing hypersthene-augite andesite (H.K. 33082410), the lava of Simohutago-yama, one of the central cones of Hakone. Loc., eastern foot of Simohutago-yama (Kuno, 1936 c, p. 55).

15. Quartz-bearing augite-pigeonite-hypersthene-andesite (H.K. 33022001), a lava of the old somma of the Hakone volcano. Loc., near Hakone-tôge, south of Hakone-mati (Kuno, 1936 a, p. 132).

16. Olivine-augite-hypersthene-andesite (H.K. 32082002), a lava of the Taga volcano. Loc., midway between Tanna and Wada (Atami) (Kuno, 1936 c, p. 55).

17. Augite-hypersthene-andesite (H.K. 31072908), a lava of the old somma of the Hakone volcano. Loc., immediately southeast of the summit of Iwato-san, north of Atami (Kuno, 1936 a, p. 114).

18. Hypersthene-hornblende-quartz-dacite, the dacite dome near Kamitaga. Loc., immediately north of Kamitaga (Kuno, 1936 c, p. 55).

A. Hypersthene-bearing olivine-basalt (H.K. 35101901), a lava (or a dike?) of the Okata Basalt Group. Loc., sea-cliff near Okata, Ô-sima (Iwasaki, 1935, p. 1511).

B. "Miharaite" or hypersthene-bearing (?) basalt, a lava (erupted in 1912–1914) of the central cone of the Ô-sima volcano. Loc., Mihara-yama, Ô-sima (Tsuboi, 1920, p. 139). Average of four analyses.

Analysts, 1–18; Senzaburô Tanaka, A; Iwazi Iwasaki, B; Okamura.

Note: The mineral assemblages of the rocks of columns 2, 4, 6, 7, and 11 were determined on thin sections placed at the writer's disposal through the kindness of Dr. Tsuya to whom his thanks are due.

Not a single instance is known in which excess silica does not appear in the norm. The normative quartz increases in amount toward the acid end, attaining as much as 43% in the most acid dacite (Table 12, column 18). The excess silica in the norm is largely attributable to the presence of silica minerals, although it may be partly occult in the interstitial glass or make up micropegmatitic intergrowth with feldspar (see Table 13).

Compositions of normative feldspars are markedly calcic, being rarely more sodic than An_{50} in basalts and andesites. Five basalts and one basaltic andesite show normative feldspars even more calcic than An_{70}. In an extreme case, it is as calcic as An_{80} (column A).

These two characters have been already pointed out by Tsuboi (1920, p. 139) for the recent lavas of the Ô-sima volcano, and the name "miharaite" was given to these rocks so as to emphasize their peculiarity in chemical composition (see column B).

Phenocrysts of plagioclase are exceedingly abundant as compared with those of mafic minerals, especially in basic rocks (Table 13). This feature can be correlated with the high content of Al_2O_3 and CaO in the bulk compositions of these rocks.

TABLE 13.—MODES (WT.%) OF THE ROCKS OF TABLE 12

		3	5	8	9	10	12	13	14	15	16	17	A
Phenocrysts	Plagioclase	25.6	30.3	25.4	30.1	34.9	21.1	31.4	27.1	24.2	15.0	13.5	32.3
	Olivine	1.4	0.9	2.3	1.9	tr.	—	—	tr.	—	0.7	—	2.5
	Augite	2.0	0.1	0.8	0.5	0.5	0.2	1.8	3.8	0.3	2.0	0.6	—
	Hypersthene	0.1	—	0.1	0.1	2.1	0.7	5.5	2.8	6.0	2.9	1.8	0.3
	Pigeonite	—	—	—	—	—	—	—	—	1.3	—	—	—
	Hornblende	—	—	—	—	—	—	—	—	0.2**	—	—	—
	Magnetite	—	—	—	—	0.5	0.3	1.6	1.8	0.5	0.5	1.4	—
	Quartz	—	—	—	—	—	—	—	—	0.1	—	—	—
Groundmass	Plagioclase	24.2	24.4	25.4	26.1	24.7	31.5	17.2		22.6	33.7	31.5	21.3
	Pigeonite*	30.7	26.2	22.5	22.2	18.4	26.6	13.0		—	—	12.6	34.0
	Augite	—	—	—	—	—	—	—		13.9	17.2	—	—
	Hypersthene	—	—	—	—	—	—	—		0.2		—	—
	Magnetite	8.2	7.0	12.4	6.9	5.4	5.4	8.3	64.5†	7.0	5.8	6.0	6.3††
	Ilmenite	—	—	—	—								—
	Cristobalite	5.5	6.2	5.2	5.5	2.6	8.3	—		5.1	—	—	3.4
	Tridymite	—	—	—	—	—	—	10.4			11.1	6.3	—
	Quartz	—	—	—	—	—	—	10.8		18.6	11.1	26.3	—
	Anorthoclase	—	—	—	—	—	—						—
	Glass	2.2	4.9	6.0	6.9	10.9	5.8	—		—	—	—	—
	Micropegmatite	—	—	—			—	—		—	—	—	—
Total		99.9	100.0	100.1	100.2	100.0	99.9	100.0	100.0	100.0	100.0	100.0	100.1

* Including pigeonitic aguite.
† Groundmass constituents are plagioclase, augite, hypersthene, magnetite, cristobalite, and glass.
** Replaced by minute grains of pigeonite.
†† Including limonite 2.4%.

Compositions of aphyric rocks and those of groundmasses

The most striking fact seen in Table 14 is that the calculated compositions of the groundmasses agree closely with the analyses of the aphyric rocks. The features common to these compositions are the relatively low content of Al_2O_3 and high content of FeO. Normative quartz is somewhat more plentiful than in the bulk analyses of the porphyritic rocks, and

TABLE 14.—CHEMICAL COMPOSITIONS AND NORMS OF APHYRIC ROCKS AND THE CALCULATED GROUNDMASS COMPOSITIONS OF THE PORPHYRITIC ROCKS OF TABLE 12

	19	3	20	8	5	10	9	12
Type of mineral assemblage	c	Vc	c	Vc	IVc	Vc	Vc	Vd → c
SiO_2	52.13	52.2	52.80	53.4	53.5	55.1	55.4	56.6
Al_2O_3	15.68	14.7	14.60	14.4	13.1	14.6	13.8	14.8
Fe_2O_3	4.36	3.2	4.30	5.1	3.3	3.2	4.1	2.4
FeO	9.81	11.6	9.64	8.4	12.4	9.6	9.6	10.0
MgO	4.08	4.7	4.16	5.7	5.0	5.0	5.0	3.2
CaO	8.87	9.4	8.75	8.9	8.5	6.9	8.0	7.6
Na_2O	2.44	2.2	2.28	2.4	2.0	2.8	2.3	3.5
K_2O	0.32	0.4	0.47	0.4	0.4	0.6	0.4	0.5
$H_2O(+)$	0.67	—	0.51	—	—	—	—	—
$H_2O(-)$	0.50	—	0.60	—	—	—	—	—
TiO_2	0.74	1.5	1.40	1.1	1.5	2.0	1.2	1.3
P_2O_5	tr.	0.1	0.08	0.2	0.2	0.2	0.2	0.1
MnO	0.32	—	0.22	—	—	—	—	—
Total	99.92	100.0	99.81	100.0	99.9	100.0	100.0	100.0
Q	8.52	7.56	10.68	9.84	10.68	11.22	13.56	10.32
Or	1.67	2.22	2.78	2.22	2.22	3.34	2.22	2.78
Ab	20.44	18.34	19.39	20.44	16.77	23.58	19.39	29.34
An	31.14	29.19	28.08	27.24	25.58	25.58	26.13	23.35
Wo	5.34	6.96	6.03	6.73	6.61	3.25	5.34	5.68
En	10.20	11.80	10.40	14.30	12.50	12.50	12.50	8.00
Fs	13.60	16.10	12.14	9.37	17.42	11.62	12.14	14.26
Mt	6.50	4.64	6.26	7.42	4.87	4.64	6.03	3.48
Il	1.37	2.89	2.74	2.13	2.89	3.80	2.28	2.43
Ap	—	0.34	0.34	0.34	0.34	0.34	0.34	0.34
Wt.% Or	4	5	6	4	5	7	5	6
Wt.% Ab	38	37	39	41	38	44	41	53
Wt.% An	58	58	55	55	57	49	54	41
Wt.% Wo	18	20	21	22	17	11	17	20
Wt.% En	35	34	36	47	35	46	42	29
Wt.% Fs	47	46	43	31	48	43	41	51
Color index	37	42	38	40	45	36	38	34

	21	22	16	15	13	14	17	23
Type of mineral assemblage	c	c	Vd	d	Vc	Vd	Vc	Vc
SiO_2	56.62	56.70	60.5	60.5	60.6	62.7	63.6	67.37
Al_2O_3	15.49	15.90	15.5	14.8	13.5	13.8	15.3	15.28
Fe_2O_3	4.58	2.94	2.4	3.3	3.0	1.9	2.0	1.13
FeO	7.09	7.74	5.5	6.3	7.1	6.3	6.0	3.86
MgO	3.00	3.34	3.8	3.3	3.9	4.1	2.1	1.20
CaO	7.33	7.77	6.8	6.6	6.6	6.1	5.9	4.46
Na_2O	2.95	3.13	3.5	3.0	3.2	3.1	3.7	4.67
K_2O	0.55	0.74	0.8	1.2	1.0	0.8	0.7	0.92

TABLE 14—CHEMICAL COMPOSITIONS AND NORMS OF APHYRIC ROCKS AND THE CALCULATED GROUNDMASS COMPOSITIONS OF THE PORPHYRITIC ROCKS OF TABLE 12 (*Continued*)

	21	22	16	15	13	14	17	23
Type of mineral assemblage	c	c	Vd	d	Vc	Vd	Vc	Vc
$H_2O(+)$	0.35	0.36	—	—	—	—	—	0.14
$H_2O(-)$	0.72	0.09	—	—	—	—	—	0.09
TiO_2	0.96	1.24	1.0	1.0	1.0	1.3	0.7	0.72
P_2O_5	0.08	0.16	0.1	0.1	0.1	0.2	0.1	0.18
MnO	0.22	0.18	—	—	—	—	—	0.15
Total	99.94	100.29	99.9	100.1	100.0	100.3	100.1	100.17
Q	15.48	11.82	16.20	18.36	16.98	20.76	21.54	24.06
Or	3.34	4.45	5.00	7.23	6.12	5.00	3.89	5.56
Ab	25.15	26.72	29.34	25.15	27.25	26.20	31.44	39.30
An	27.24	26.97	24.19	23.35	19.18	21.13	23.07	18.07
Wo	3.48	4.52	3.60	3.60	5.34	3.48	2.20	1.39
En	7.50	8.40	9.50	8.30	9.80	10.30	5.30	3.00
Fs	8.06	10.16	6.34	7.13	8.84	7.92	8.05	5.28
Mt	6.73	4.18	3.48	4.87	4.41	2.78	3.02	1.62
Il	1.82	2.43	1.98	1.98	1.98	2.43	1.37	1.37
Ap	0.34	0.34	0.34	0.34	0.34	0.34	0.34	0.34
Wt.% Or	6	8	7	12	11	8	7	9
Wt.% Ab	45	46	51	45	51	51	53	62
Wt.% An	49	46	42	43	38	41	40	29
Wt.% Wo	19	20	17	17	23	16	12	14
Wt.% En	39	36	50	44	40	47	35	31
Wt.% Fs	42	44	33	39	37	37	53	55
Color index	28	30	25	26	30	27	20	13

Rock	A	C	D	E	F	G
Type of Mineral assemblage	IIc	IId → c	b → c	Ic	Ic	?
SiO_2	49.9	51.23	51.25	52.45	52.53	53.01
Al_2O_3	13.7	15.24	14.73	13.48	15.25	14.73
Fe_2O_3	3.2	4.18	3.82	4.60	2.69	3.38
FeO	10.4	8.99	10.22	10.02	10.57	9.42
MgO	7.2	4.85	5.47	4.78	4.54	4.97
CaO	12.3	11.14	11.73	10.23	10.76	9.09
Na_2O	1.7	2.19	1.85	1.99	1.89	2.09
K_2O	0.4	0.54	0.26	0.52	0.43	0.44
$H_2O(+)$	—	n.d.	0.11	n.d.	n.d.	1.22
$H_2O(-)$	—	n.d.	0.02	n.d.	n.d.	
TiO_2	1.2	0.83	0.81	1.39	0.74	1.03
P_2O_5	tr.	0.03	0.13	0.33	0.41	0.11
MnO	—	0.33	0.28	0.31	0.24	0.34
Total	100.0	99.680*	100.838†	100.319**	100.157††	99.87***

TABLE 14—CHEMICAL COMPOSITIONS AND NORMS OF APHYRIC ROCKS AND THE CALCULATED GROUNDMASS COMPOSITIONS OF THE PORPHYRITIC ROCKS OF TABLE 12 (*Concluded*)

Rock	A	C	D	E	F	G
Type of mineral assemblage	IIc	IId → c	b → c	Ic	Ic	?
Q	2.04	5.46	5.34	9.84	7.80	9.84
Or	2.22	2.78	1.67	2.78	2.22	2.22
Ab	14.15	18.34	15.72	16.77	16.24	17.82
An	28.63	30.30	30.86	26.41	31.97	29.47
Wo	13.57	10.44	11.14	9.51	7.89	6.26
En	18.00	12.10	13.70	12.00	11.40	12.40
Fs	14.39	12.41	14.78	12.67	16.37	13.46
Mt	4.64	6.03	5.57	6.73	3.94	4.87
Il	2.28	1.52	1.52	2.74	1.37	1.98
Ap	—	0.00	0.34	0.67	1.01	0.34
Wt.% Or	5	5	3	7	5	4
Wt.% Ab	32	36	33	36	32	36
Wt.% An	63	59	64	57	63	60
Wt.% Wo	29	29	28	28	22	19
Wt.% En	39	35	35	35	32	39
Wt.% Fs	32	36	37	37	46	42
Color index	53	43	47	44	41	40

* Including (Ce, Y)$_2O_3$ 0.003, ZrO_2 0.002, BaO 0.025, S(total) 0.100.
† Including (Ce, Y)$_2O_3$ 0.002, ZrO_2 0.005, BaO 0.014, S(total) 0.137.
** Including (Ce, Y)$_2O_3$ 0.003, ZrO_2 0.004, BaO 0.030, S(total) 0.182.
†† Including (Ce, Y)$_2O_3$ 0.004, ZrO_2 0.002, BaO 0.023, S(total) 0.078.
*** Including ZrO_2 0.04.

19. Aphyric basalt (with a few phenocrysts of plagioclase), a lava of the Taga volcano. Loc., east of the Smelting Furnace, south of Nirayama (Tsuya, 1937, p. 273).

20. Aphyric basalt (with a few microphenocrysts of olivine) (H.K. 31082204b), the base of a composite lava flow of the Hata Basalt Group. Loc., west of Simotanna. The analysis of the upper porphyritic part of the same flow is given in column 3 of Table 12.

21. Aphyric andesite (with a few phenocrysts of plagioclase and hypersthene) (H.K. 31041419), the base of a composite lava flow of the Aziro Basalt Group. Loc., immediately southeast of Aziro (Kuno, 1936 c, p. 60).

22. Aphyric andesite (H.K. 33081909a), a lava of the old somma of the Hakone volcano. Loc., middle course of Saru-sawa, south of Yumuto (Kuno, 1936 c, p. 60).

23. Augite-hypersthene-andesite (H.K. 33090504), a lava of the young somma of the Hakone volcano. Loc., a cliff southeast of Byôbu-yama, east of Hakone-mati (Kuno, 1936 c, p. 60). The rock carries phenocrysts of plagioclase 3.4%, hypersthene 0.3%, augite 0.2%, and magnetite 0.1% (in volume).

C. Hypersthene- and olivine-bearing basalt (H.K. 35101903), a somma lava of the Ô-sima volcano. Loc., a point where the road from Mihara-yama to Nomasi crosses the somma (Iwasaki, 1935, p. 1511). The rock carries phenocrysts of plagioclase 5.1%, olivine 0.1%, and hypersthene 0.1% (in volume).

D. Aphyric basalt (H.K. 33060701), a dike related to the Okata Basalt Group. Loc., sea-cliff near Okata, Ô-sima (Iwasaki, 1935, p. 1511).

E. Hypersthene-basalt (H.K. 35101904), a lava (erupted in 1778) of the central cone of the Ô-sima volcano. Loc., midway between Mihara-yama and Kagamihata, Ô-sima (Iwasaki, 1935, p. 1511). The phenocrysts of plagioclase and hypersthene of this rock are slightly less abundant than those of rock F.

F. Hypersthene-basalt (H.K. 35101905), a lava (erupted in 1912–1914) of the central cone of the Ô-sima volcano. Loc., northwestern part of the lava field of Mihara-yama crater, Ô-sima volcano (Iwasaki, 1935, p. 1511). The rock carries phenocrysts of plagioclase 5.8% and hypersthene 0.1% (in volume).

G. "Basaltic bandaite" or olivine-bearing basalt, a somma lava of the Ô-sima volcano. Loc., near Habu (?), Ô-sima (Tsuboi, 1920, p. 71).

Analysts, 19–23; Senzaburô Tanaka, C–F; Iwazi Iwasaki, G; Ôhasi.

Note: Columns 3, 5, 8, 9, 10, 12, 13, 14, 15, 16, 17, and A give the calculated compositions of the groundmasses of the rocks of the respective numbers in Table 13.

normative feldspar is not so calcic. In most cases, the feldspar is sodic labradorite or andesine, although calcic labradorite is encountered in a few basalts of the Ô-sima volcano. The

The two different curves for each oxide, except those for Al_2O_3, show a similar shape, and the curves for Na_2O and K_2O are nearly straight lines without intersecting to one another as in

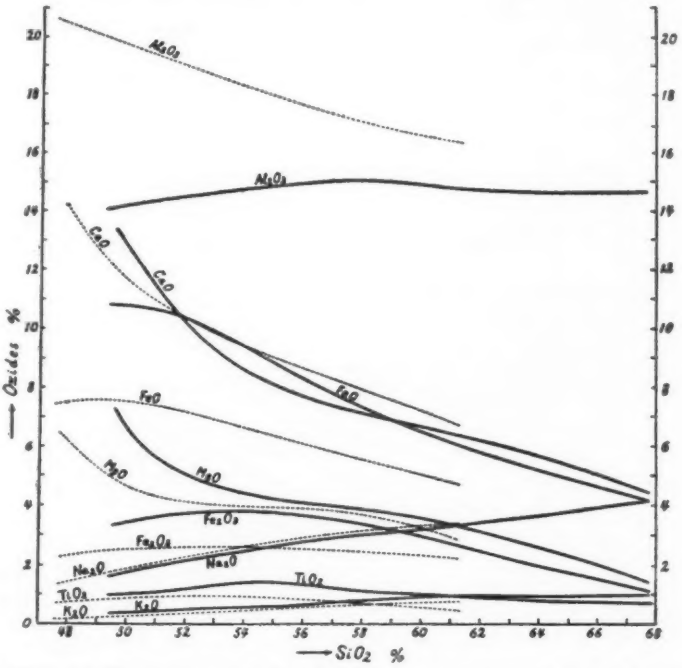

FIGURE 26.—VARIATION DIAGRAMS FOR THE OXIDE COMPOSITIONS OF THE ROCKS OF IZU AND HAKONE
Broken lines: bulk compositions of the porphyritic rocks. Full lines: compositions of the aphyric rocks and those of the groundmasses of the porphyritic rocks.

sum of normative femic minerals attains about 50% in the basic rocks.

Relations between the bulk and the groundmass compositions

It will be seen from Figure 26 that the bulk compositions are decidedly higher in Al_2O_3, especially in the low silica side, and lower in FeO and Fe_2O_3 than the groundmass compositions (including those of the aphyric rocks). Slight differences may also be noted in MgO, CaO, and TiO_2, but the curves for Na_2O and K_2O of the bulk compositions nearly coincide with the respective curves of the groundmass compositions.

the average variation diagram for the calc-alkaline suite. The same feature for alkalies was noted in the volcanic rocks of the whole Izu region (Tsuya, 1937, p. 342).

The normative feldspars of the porphyritic rocks are generally more calcic than those of the groundmasses (Fig. 27). The compositions of all the feldspars are included within a narrow zone stretched from the anorthite corner to an area corresponding to the composition of anorthoclase.

The normative pyroxenes of the porphyritic rocks are slightly more enriched in En than those of the groundmasses (Fig. 28).

The porphyritic rocks are higher in the feldspar content than the groundmasses, this tend-

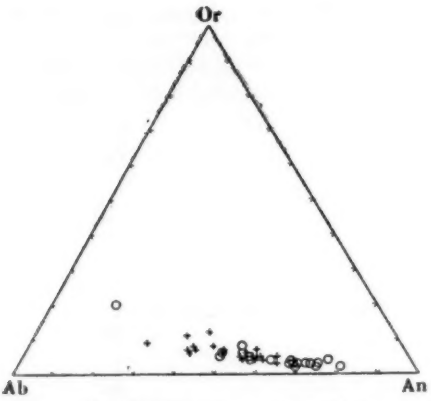

FIGURE 27.—COMPOSITIONS OF THE NORMATIVE FELDSPARS OF THE ROCKS OF IZU AND HAKONE

Circles: bulk compositions of the porphyritic rocks. Crosses: compositions of the aphyric rocks and those of the groundmasses of the porphyritic rocks.

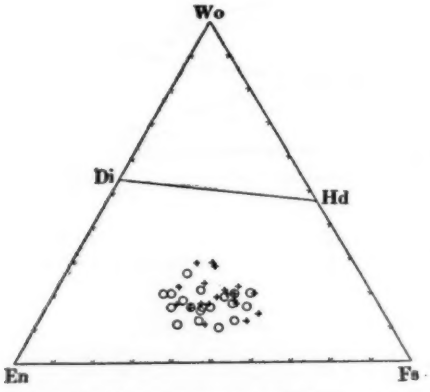

FIGURE 28.—COMPOSITIONS OF THE NORMATIVE PYROXENES OF THE ROCKS OF IZU AND HAKONE

Symbols same as in Figure 27.

ency being more pronounced toward the basic end of the series (Fig. 29).

The differences between the bulk and the groundmass compositions are due to the presence of abundant phenocrysts of calcic plagioclase and a few of mafic minerals in the porphyritic rocks.

Whether the bulk compositions of the porphyritic rocks represent the compositions of true magmatic liquids (Tsuboi, 1925, p. 77; Bowen, 1928, p. 93) is open to discussion. The writer has not observed even a single instance of aphyric rocks or groundmasses of porphyritic rocks which contain as much as 60% calcic plagioclase in their general fabric, namely, a mineral composition approximating the norms

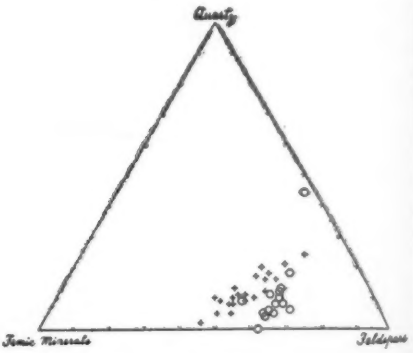

FIGURE 29.—RATIO NORMATIVE QUARTZ: NORMATIVE FEMIC MIMERALS: NORMATIVE FELDSPARS OF THE ROCKS OF IZU AND HAKONE

Symbols same as in Figure 27.

of the porphyritic basalts shown in Table 12; in all the cases, the mineral compositions of such rocks are close to the norms of Table 14. It is highly probable that the bulk compositions of the porphyritic rocks represent those of magmas plus various amounts of plagioclase crystals, and that the compositions of the true magmatic liquids fall within the narrow limit represented by those of the aphyric rocks and the groundmasses as shown in Table 14. The accumulation of phenocrysts in some parts of magmas is strongly indicated by the occurrence of composite lava flows and composite dikes in the region (compare Pl. 4, figs. 3, 4).

COMPARISON WITH ROCKS OF OTHER REGIONS

Comparison with basalts and dolerites of the tholeiitic magma-type

In their chemical and mineral compositions, the basalts of Izu and Hakone closely resemble those of the tholeiitic magma-type of Kennedy (1933, p. 239). The groundmass composition of the Izu basalts agrees generally with the

TABLE 15.—COMPOSITIONS OF BASALTS AND DOLERITES OF THE THOLEIITIC MAGMA-TYPE FROM VARIOUS LOCALITIES OF THE WORLD

Rocks	I Oregonian basalts	II Hawaiian basalts	III Deccan traps	IV Huzi basalts	V Whin sill dolerites	VI Izu basalts	VII Tholeiites of England	VIII Karroo dolerites
SiO_2	50.62	51.11	51.3	51.6	51.92	52.3	52.68	52.69
Al_2O_3	13.92	12.65	13.9	14.7	14.12	14.5	14.56	14.73
Fe_2O_3	2.40	1.90	3.3	4.5	3.96	3.8	2.91	0.85
FeO	11.75	9.40	10.1	9.1	8.73	10.2	7.70	9.97
MgO	4.79	7.59	5.5	5.1	5.56	5.1	6.15	7.00
CaO	8.32	10.65	9.8	8.5	9.35	10.0	10.98	9.79
Na_2O	2.96	2.26	2.8	2.7	2.49	2.1	2.39	2.22
K_2O	1.31	0.44	0.7	1.1	0.98	0.4	0.89	0.97
TiO_2	2.91	3.54	2.0	2.0	2.46	1.1	1.23	1.11
P_2O_5	0.78	0.34	0.3	0.3	0.27	0.2	0.19	0.22
MnO	0.24	0.12	0.3	0.3	0.16	0.3	0.32	0.45
Total	100.00	100.00	100.0	99.9	100.00	100.0	100.00	100.00
Q	2.04	4.68	3.24	5.04	6.30	7.68	3.90	1.86
Or	7.78	2.22	3.89	6.67	6.12	2.22	5.56	6.12
Ab	25.15	18.86	23.58	23.06	20.96	17.82	20.44	18.34
An	20.57	23.63	23.35	24.46	24.19	28.91	26.13	27.24
Wo	6.26	11.73	9.86	6.84	8.58	8.35	11.48	8.58
En	12.00	19.00	13.80	12.80	13.90	12.80	15.40	17.50
Fs	15.31	10.03	12.94	10.16	8.84	14.26	10.30	16.63
Mt	3.48	2.78	4.87	6.50	5.80	5.57	4.18	1.39
Il	5.47	6.69	3.80	3.80	4.71	2.13	2.28	2.13
Ap	2.02	0.67	0.67	0.67	0.67	0.34	0.34	0.34
Wt.% Or	15	5	8	12	12	5	11	12
Wt.% Ab	47	42	46	43	41	36	39	35
Wt.% An	38	53	46	45	47	59	50	53
Wt.% Wo	18	28	27	23	28	24	31	20
Wt.% En	36	47	38	43	44	36	41	41
Wt.% Fs	46	25	35	34	28	40	28	39
Color index	43	50	46	40	42	43	44	46

I. Average of 6 Oregonian basalts (Washington, 1922, p. 797).
II. Average of 13 aphyric basalts from Kilauea (8) and Mauna Loa (5), Hawaii (Washington, 1923, p. 109 and 338).
III. Average of 16 Deccan traps (Tyrrell and Sandford, 1933, p. 312).
IV. Average of the groundmass compositions of 4 basalts from the Huzi volcano (Tsuya, 1935, p. 655).
V. Average of 6 dolerites of Whin sill and adjacent dikes (Holmes and Harwood, 1928, p. 493).
VI. Average of the groundmass compositions of 11 basalts from Izu. Data are given in columns 19, 3, 20, 8, 5, A, C, D, E, F, G of Table 14.
VII. Average of 8 tholeiites of Brunton type and Talaidh type, north England (Holmes and Harwood, 1929, p. 1).
VIII. Average of 5 Karroo dolerites (Daly and Barth, 1930, p. 97).

compositions of the other basalts and dolerites (Table 15), provided that alkalies are slightly lower. A striking similarity is found especially between the average composition of the Izu basalts and that of the Deccan traps.

The most conspicuous characters of the Izu basalts are the high content of An in the normative feldspars and the high content of quartz against the sum of feldspars and femic minerals (Figs. 30, 31, 32).

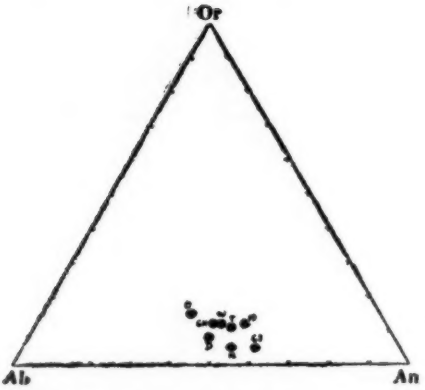

FIGURE 30.—COMPOSITIONS OF THE NORMATIVE FELDSPARS OF THE BASALTS AND DOLERITES OF THE THOLEIITIC MAGMA TYPE

O: Oregonian basalts. H: Hawaiian basalts. D: Deccan traps. GH: groundmass of Huzi basalts. W: Whin sill dolerites. GI: groundmass of Izu basalts. K: Karroo dolerites. T: Tholeiites of England

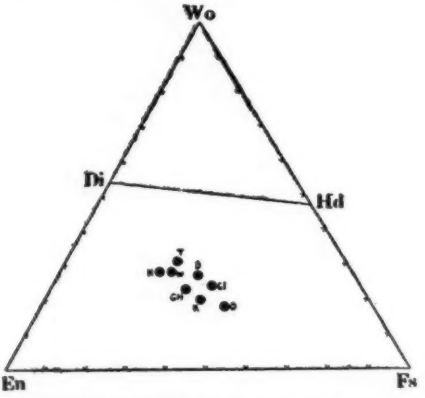

FIGURE 31.—COMPOSITIONS OF THE NORMATIVE PYROXENES OF THE BASALTS AND DOLERITES OF THE THOLEIITIC MAGMA TYPE

Symbols same as those in Figure 30.

Compared with the Huzi basalts, the Izu basalts are high in CaO and low in alkalies, notably rich in An in normative feldspars, rich in Fs in normative pyroxene, and rich in normative quartz. The Izu basalts deviate from the Huzi basalts in the same direction as from the other basalts and dolerites of the tholeiitic magma-type (Tsuya, 1935, p. 656; 1937, p. 334).

That the Japanese basalts are markedly more siliceous and calcic than the common basalts of the world has been pointed by many authors, by comparing the bulk compositions of porphyritic rocks. It is now clear that the groundmasses of the Izu basalts show the same departure from the average basalts of the world.

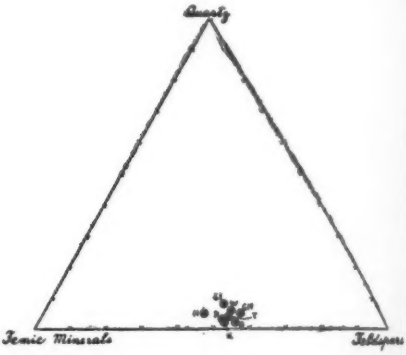

FIGURE 32.—RATIO NORMATIVE QUARTZ: NORMATIVE FEMIC MINERALS: NORMATIVE FELDSPARS OF THE BASALTS AND DOLERITES OF THE THOLEIITIC MAGMA TYPE

Symbols same as in Figure 30.

However, for the groundmasses compared with the tholeiitic basalts and dolerites, the departure is not so great as previously emphasized.

Comparison with rocks of other volcanoes of Japan and adjacent regions

No systematic comparison can yet be made between the groundmass compositions of the rocks of Izu and Hakone and those of other volcanoes of Japan and adjacent islands. However, Tsuya (1937, p. 345) compared the bulk compositions of porphyritic rocks of the whole Izu region (including the southern islands) with those of the Nasu volcanic zone of northeastern Japan and also with those of the Ryûkyû zone, south of Kyûsyû. He found that the rocks of Izu differ scarcely from the others except that they are slightly higher in Na_2O and lower in K_2O.

An attempt is made here to compare the mineral assemblages of the rocks of north Izu and Hakone with those from other Quaternary volcanoes of the Huzi zone, of northeastern

TABLE 16.—TYPES OF ASSEMBLAGE OF THE CHIEF FERROMAGNESIAN SILICATE MINERALS IN ROCKS OF THE VOLCANOES OF THE HUZI ZONE (EXCLUDING VOLCANOES OF NORTH IZU AND HAKONE), OF NORTHEASTERN JAPAN, AND OF KURILE ISLANDS*

Groundmass / Phenocrysts	Olivine Mono. pyrox. Orth. pyrox.	Olivine Mono. pyrox.	Mono. pyrox.	Mono. pyrox. Orth. pyrox.	Orth. pyrox.
Orth. pyrox.	Ia	Ib	Ic 2 <1	Id <1	Ie 1
Olivine Orth. pyrox.	IIa	IIb	IIc 2 1	IId <1	IIe
Olivine	IIIa <1	IIIb <1 3	IIIc 5 <1	IIId 4	IIIe
Olivine Mono. pyrox.	IVa <1	IVb 5 2	IVc 5 <1	IVd 2	IVe
±Olivine Mono. pyrox. Orth. pyrox.	Va <1	Vb <1	Vc 11 6	Vd 26	Ve <1
±Olivine Mono. pyrox. Orth. pyrox. Hornblende	VIa	VIb	VIc	VId 9	VIe <1
±Olivine Orth. pyrox. Hornblende	VIIa	VIIb	VIIc	VIId 1	VIIe 4
±Olivine Hornblende	VIIIa	VIIIb	VIIIc	VIIId <1	VIIIe <1
±Olivine Mono. pyrox. Hornblende	IXa	IXb	IXc	IXd	IXe
Mono. pyrox.	Xa	Xb	Xc <1?	Xd <1?	Xe

* Each figure represents the percentage of the specimens belonging to each type. 436 specimens from the following volcanoes were examined:
Kurile zone:—Alaid, Iwô-yama (Paramusil Island), Tyatyanupuri, Daisetu.
Nasu zone:—Usu, Komaga-take, Towada, Iwate, Hunakata, Gando, Zaô, Adatara, Bandai, Nasu, Takahara, Nikkô, Hodaka, Akagi, Haruna, Asama, Azumaya.
Tyôkai zone:—Ôsima (west of Hokkaidô), Kampû, Tyôkai.
Huzi zone:—Kiriga-mine, Yatuga-take, Kayaga-take, Huzi, Asitaka, Daruma, Ômuro-yama, Amagi, Ô-sima, Miyake-zima, Hatizyô-zima, Kita-Iwô-zima.

Japan, and of Kurile Islands. Rocks included are basalts, andesites, and dacites from widely scattered volcanoes.

In Table 16, nearly the same types prevail as those in the rocks of north Izu and Hakone (Tables 9, 10). The presence of types IIIb and IVb in Table 16 is a marked difference.

The types IIIb and IVb are found in some basic basalts from Alaid volcano, north Kurile (Kuno, 1935, p. 153), and Ô-sima volcano,

west of Hokkaidô (Kuno, 1936d, p. 392), as well as in a few basalts from the Huzi volcano. The basalts from the former two volcanoes carry euhedral crystals of olivine and augite in the groundmass, the olivine being entirely free from reaction rim of pyroxene. Interstitial anorthoclase is present in these basalts instead of the silica minerals so common in the basalts of types IIIb→c and IVb→c from Izu and Hakone.

In the rocks of north Izu and Hakone, there are three or four times as many Vc type as Vd; in the other rocks, the number of Vc is less than half that of Vd. This fact, in conjunction with the abundance of hornblende-bearing rocks in the other regions, indicates that the hypersthenic rock series prevails there. This character is especially marked in the northern part of the Huzi zone and in the Nasu and Tyôkai zones. In these areas, the assimilation of granitic crust by basaltic magmas may have taken place more generally there than in north Izu and Hakone.

A comparative study of the geologic structures underlying these different volcanic fields might throw some light upon the problem of genesis of the Japanese volcanic rocks.

Problem of the Parental Magma

The parental magma of north Izu and Hakone is assumed to have a composition of an undersilicated olivine-basalt, consisting of calcic labradorite or sodic bytownite, augite, olivine, and iron ore. The closest approach to this mineral composition is found in the basalts of type IIIb→c which actually occur in the region.

The usage of the term "olivine-basalt magma" may be confusing, since this term was already introduced by Kennedy (1933, p. 239) to designate the parental magma of the alkaline rock suite. Recent petrologists incline to the opinion that the "olivine-basalt magma-type" gives rise to the "tholeiitic magma-type" through the assimilation of granitic rocks.

If the "olivine-basalt magma-type" of Kennedy is taken as including the "olivine-basalt" of north Izu and Hakone, its parental position to the "tholeiitic magma-type" is justified from the present study.

While some rocks of the "tholeiitic magma-type" are generated from the "olivine-basalt magma" through the assimilation of granitic rocks (the hypersthenic rock series), others of the former magma-type are formed chiefly through the simple fractional crystallization (the pigeonitic rock series). However, most of the basalts generally considered typical of the "olivine-basalt magma-type" are definitely more alkaline than the parental "olivine-basalt" of Izu and Hakone. For example, the basalts of the Circum Japan Sea Province contain as much as 3% Na_2O and 1.5% K_2O. There appears to exist a complete gradation in mineralogical and chemical compositions between these extreme "olivine-basalts."

The genetical relation between these different types of "olivine-basalts" cannot be solved by the present study. It is hoped that a detailed petrological study will be made on some region where the different types of "olivine-basalts" occur side by side.

References Cited

Bailey, E. B., et al. (1924) *Tertiary and post-Tertiary geology of Mull, Loch Aline, and Oban*, Geol. Survey Scotland, Mem.

Barth, T. F. W. (1931) *Crystallization of pyroxenes from basalts*, Am. Mineral., vol. 16, p. 195–208.

———, and Holmsen, P. (1939) *Rocks from the Antarctandes and the Southern Antilles*, Det Norske Vid.-Akad. i Oslo, p. 7–64.

Benson, W. N. (1944) *The basic igneous rocks of eastern Otago and their tectonic environment*, Royal Soc. New Zealand, Tr., vol. 74, p. 71–123.

Bowen, N. L. (1914) *The ternary system: diopside–forsterite—silica*, Am. Jour. Sci., vol. 38, p. 207–264.

——— (1928) *The evolution of the igneous rocks*, Princeton.

——— (1935) *"Ferrosilite" as a natural mineral*, Am. Jour. Sci., vol. 30, p. 481–494.

———, and Schairer, J. F. (1935) *The system, MgO—FeO—SiO_2*, Am. Jour. Sci., vol. 29, p. 151–217.

Daly, R. A., and Barth, T. F. W. (1930) *Dolerites associated with the Karroo System, South Africa*, Geol. Mag., vol. 67, p. 97–110.

Edwards, A. B. (1942) *Differentiation of the dolerites of Tasmania*, Jour. Geol., vol. 50, p. 451–610.

Harada, Z. (1933) *On some minerals from Japan* (in Japanese), Geol. Soc. Tokyo, Jour., vol. 40, p. 341–345.

——— (1936) *Chemische Analysenresultate von japanischen Mineralien*, Fac. Sci., Hokkaidô Imp. Univ., Jour., ser. IV, vol. 3, nos. 3–4, p. 221–362.

Hess, H. H. (1941) *Pyroxenes of common mafic magmas*, Am. Mineral., vol. 26, p. 515–535 and p. 573–594.

———, and Phillips, A. H. (1938) *Orthopyroxenes of the Bushveld type*, Am. Mineral., vol. 23, p. 450–456.

Holmes, A., and Harwood, H. F. (1928) *The age and composition of the Whin Sill and the related dikes of the north of England*, Mineral. Mag., vol. 21, p. 493–542.

——— (1929) *The tholeiite dikes of the north of England*, Mineral. Mag., vol. 22, p. 1–52.

Iwasaki, I. (1935) *Geochemical study of Japanese volcanoes, part 2. Chemical compositions of lavas of Ôsima volcano, Izu* (in Japanese), Chem. Soc. Japan, Jour., vol. 56, p. 1511–1522.

Kennedy, W. Q. (1933) *Trends of differentiation in basaltic magmas*, Am. Jour. Sci., vol. 25, p. 239–256.

Kikuchi, Y. (1889) *On anorthite from Miyakejima*, Coll. Sci., Imp. Univ. Tokyo, Jour., vol. 2, p. 31–47.

Kôzu, S. (1914) *Optical, chemical and thermal properties of anorthite from three localities of Japan*, Sci. Rep. Tôhoku Imp. Univ., ser. II, vol. 2, no. 1, p. 7–33.

———, and Tsurumi, S. (1933) *Triangular biotitic phlogopite in basalt from Mutsure-jima and its chemical composition*, Imp. Acad., Tokyo, Pr., vol. 9, p. 269–272.

———, and Yoshiki, B. (1933) *Mica basalt from Mutsure-jima*, Imp. Acad., Tokyo, Pr., vol. 9, p. 265–268.

———, Seto, K., and Ueda, J. (1928) *Optical and chemical properties of diopside from Sano and influence of temperature on the change in the volume of the crystal* (in Japanese), The Globe, vol. 9, p. 406–423.

Kuno, H. (1933a) *On silica minerals occurring in the groundmass of common Japanese volcanic rocks*, Earthquake Res. Inst., Bull., vol. 11, p. 382–390.

——— (1933b) *Preliminary note on basalt from Aziro, Idu*, Earthquake Res. Inst., Bull., vol. 11, p. 391–401.

——— (1935) *Petrology of Alaid volcano, north Kurile*, Jap. Jour. Geol. Geogr., vol. 12, p. 153–162.

——— (1936a) *Petrological notes on some pyroxene-andesites from Hakone volcano, with special reference to some types with pigeonite phenocrysts*, Jap. Jour. Geol. Geogr., vol. 13, p. 107–140.

——— (1936b) *On the crystallization of pyroxenes from rock-magmas, with special reference to the formation of pigeonite*, Jap. Jour. Geol. Geogr., vol. 13, p. 141–150.

——— (1936c) *Chemical compositions of volcanic rocks from Izu and Hakone* (in Japanese), Volc. Soc. Japan, Bull., vol. 3, p. 53–71.

——— (1936d) *On the lavas of Ôsima volcano, Hokkaidô* (in Japanese), Geol. Soc. Japan, Jour., vol. 43, p. 392–393.

——— (1938a) *Hypersthene from Odawara-mati, Japan*, Imp. Acad., Tokyo, Pr., vol. 14, p. 218–220.

——— (1938b) *On the occurrence of a primary cummingtonitic hornblende in some dacites from Japan*, Imp. Acad., Tokyo, Pr., vol. 14, p. 221–224.

——— (1940a) *On pigeonite-quartz-diorite, an ejected block found in Hakone volcano* (in Japanese), Geol. Soc. Japan, Jour., vol. 47, p. 175–179.

——— (1940b) *Occurrence of fayalite in some dacites from north Izu and adjacent area*, Geol. Soc. Japan, Jour., vol. 47, p. 228–232.

Kuno, H. (1940c) *Pigeonite in the groundmass of some andesite from Hakone volcano*, Geol. Soc. Japan, Jour., vol. 47, p. 347–351.

——— (1940d) *On pigeonite-andesite from Minami-aizu-gun, Hukusima Prefecture* (in Japanese), Geol. Soc. Japan, Jour., vol. 47, p. 180–182.

——— (1941a) *Dispersion of optic axes in the orthorhombic pyroxene series*, Imp. Acad., Tokyo, Pr., vol. 17, p. 204–209.

——— (1941b) *Studies on orthorhombic pyroxenes of Japan* (in Japanese), Geol. Soc. Japan, Jour., vol. 48, p. 277–279.

——— (in press) *Occurrence of porphyritic pigeonite in weiselbergite from Weiselberg, Germany*, Imp. Acad., Tokyo, Pr.

———, and Sawatari, M. (1934) *On the augites from Wadaki, Izu, and from Yoneyama, Eligo, Japan*, Jap. Jour. Geol. Geogr., vol. 11, p. 327–343.

Larsen, E. S., Irving, J., Gonyer, F. A., and Larsen, E. S. 3rd. (1936, 1937, 1938) *Petrologic results of a study of the minerals from the Tertiary volcanic rocks of the San Juan region, Colorado*, Am. Mineral., vol. 21, p. 677–701; vol. 22, p. 889–905; vol. 23, p. 417–429.

Larsson, W. (1941) *Petrology of interglacial volcanics from the Andes of northern Patagonia*, Geol. Inst. Univ. Upsala, Bull., vol. 28, p. 190–405.

Macdonald, G. A. (1944a) *Pyroxenes in Hawaiian lavas*, Am. Jour. Sci., vol. 242, p. 626–629.

——— (1944b) *Petrography of the Samoan islands*, Geol. Soc. Am., Bull., vol. 56, p. 1333–1362.

MacGregor, A. G. (1938) *The volcanic history and petrology of Montserrat, with observations on Mt. Pelé, in Martinique*, Royal Soc. London, Philos. Tr., ser. B, vol. 229, no. 557, p. 1–90.

Phemister, T. C. (1934) *The role of water in basaltic magma, part I*, Mineral. Petro. Mitt., vol. 45, p. 19–77.

Poldervaart, A. (1944) *The petrology of the Elephant's Head dike and the New Amalfi sheet (Matatiele)*, Royal Soc. South Africa, Tr., vol. 30, p. 85–119.

Seto, K. (1929) *Chemical composition of olivine from Miyake-zima*, Jap. Ass. Mineral. Petro. Econ. Geol., Jour., vol. 1, p. 23–24.

Sueno, T. (1933) *On the use of standard glass powders in refractive index determinations*, Am. Mineral., vol. 18, p. 421–430.

Sugi, K. (1931) *On the metamorphic facies of the Misaka Series in the vicinity of Nakagawa, Prov. Sagami*, Jap. Jour. Geol. Geogr., vol. 9, p. 87–142.

——— (1937) *On the occurrence of zoned pigeonitic augite in the dolerite from Semi, near Sinzyô, Uzen*, Geol. Soc. Japan, Jour., vol. 44, p. 255–261.

——— (1938) *On sanukitic rocks in the vicinity of Takamatu, Sikoku, with special reference to xenocrysts contained in them* (in Japanese) Volc. Soc. Japan, Jour., vol. 4, p. 17–33.

——— (1942) *Petrological studies on the basaltic rocks from Sanin and northern Kyûsyû, southwestern Japan*, Fac. Sci., Kyûsyû Imp. Univ., Mem., part 1, ser. D, vol. 1, no. 3, p. 69–90.

Tanakadate, H. (1935) *A volcanological and petrographical note of the new volcanic islet near Iô-zima*, Imp. Acad., Tokyo, Pr., vol. 11, p. 370–372.

Taneda, S. (1943a) *Occurrence of olivine at the peripheral zone of hypersthene phenocryst*, Imp. Acad., Tokyo, Pr., vol. 19, p. 31–36.

——— (1943b) *Petrographic notes on the volcanic rocks from Haruna, central Japan, part 3*, Fac. Sci., Kyûsyû Imp. Univ., Mem., ser. D, vol. 2, p. 1–96.

Tomita, T. (1931) *Geological and petrological study of Dôgo, Oki Islands, parts 11, 12, and 13*, Geol. Soc. Tokyo, Jour., vol. 38, p. 203–222, p. 413–431, p. 461–479.

——— (1933) *Olivine-trachyandesitic basalt from Hsueh-hua-shan Hill, Ching-Hsing district, north China*, Shanghai Sci., Inst., Jour., sec. II, vol. 1, p. 1–10.

Tsuboi, S. (1920) *Volcano Ôshima, Idzu*, Coll Sci., Tokyo Imp. Univ., Jour., vol. 43, part 6, p. 1–146.

——— (1925) *The genetical interpretation of extrusive rocks*, Fac. Sci., Imp. Univ. Tokyo, Jour., vol. 1, part 2, p. 77–86.

——— (1934) *A straight-line diagram for determining plagioclase by the dispersion method*, Jap. Jour. Geol. Geogr., vol. 11, p. 325–326.

——— (1936) *Some notes on the crystallization of pyroxenes* (in Japanese), Geol. Soc. Japan, Jour., vol. 43, p. 405–406.

Tsuya, H. (1930) *On the geologic structure of Itô district, Idu*, Earthquake Res. Inst., Bull., vol. 8, p. 409–426.

——— (1935) *On some lavas of volcano Huzi (Fuji)*, Earthquake Res. Inst., Bull., vol. 13, p. 645–659.

——— (1937) *On the volcanism of the Huzi volcanic zone, with special reference to the geology and petrology of Idu and Southern Islands*, Earthquake Res. Inst., Bull., vol. 15, p. 213–357.

Tyrrell, G. W., and Sandford, K. S. (1933) *Geology and petrology of the dolerites of Spitzbergen*, Royal Soc. Edinburgh, Pr., vol. 53, part 3, p. 284–343.

Wahl, W. (1907) *Die Enstatitaugite*, Mineral. Petr. Mitt., vol. 26, p. 1–131.

Walker, F. (1940) *Differentiation of the Palisade diabase, New Jersey*, Geol. Soc. Am., Bull., vol. 51, p. 1059–1106.

——— (1943) *Note on the pyroxenes of basaltic magma*, Am. Jour. Sci., vol. 241, p. 517–520.

———, and Poldervaart, A. (1940) *The petrology of the dolerite sill of Downes Mountain, Calvinia*, Geol. Soc. South Africa, Tr., vol. 43, p. 157–173.

——— ——— (1941) *The Hangnest dolerite sill, S. A.*, Geol. Mag., vol. 78, p. 429–450.

Washington, H. S. (1922) *Deccan traps and other plateau basalts*, Geol. Soc. Am., Bull., vol. 33, p. 765–803.

——— (1923) *Petrology of the Hawaiian Islands, III. Kilauea and general petrology of Hawaii*, Am. Jour. Sci., vol. 6, p. 338–367.

Wentworth, C. K., and Williams, H. (1932) *The classification and terminology of the pyroclastic rocks*, Nat. Res. Council, Bull., no. 89, p. 43–53.

Winchell, A. N. (1933) *Elements of optical mineralogy*, part 2.

Yamane, S. (1927) *Explanatory text for geologic map "Tyôsi"* (1:75,000) (in Japanese), Imp. Geol. Surv. Japan.

GEOLOGICAL INSTITUTE, TOKYO UNIVERSITY, JAPAN.

MANUSCRIPT RECEIVED BY THE SECRETARY OF THE SOCIETY, JUNE 24, 1948.

Plate 1.—PHOTOMICROGRAPHS OF THE ROCKS OF IZU AND HAKONE

FIGURE 1. AUGITE- AND HYPERSTHENE-BEARING PIGEONITE-QUARTZ-DIORITE (H.K. 37090503)

Showing potash-oligoclase (Po) with fine microcline-like structure, pigeonite (Pi), and glass (dark). A block ejected from a central cone of Hakone. Crossed nicols. × 65.

FIGURE 2. SAME AS FIGURE 1, SHOWING QUARTZ (Q) AND ZONED FELDSPAR (ANDESINE Ad) TO POTASH-OLIGOCLASE (Po)

Crossed nicols. × 65

FIGURE 3. GROUNDMASS INCLUSION IN PLAGIOCLASE IN HYPERSTHENE-AUGITE-ANDESITE (H.K. 33082502c)

AN ACID MEMBER OF TYPE Vc

A lava of the young somma of Hakone. × 20.

FIGURE 4. HONEY-COMBED STRUCTURE IN PLAGIOCLASE IN AUGITE-HYPERSTHENE-ANDESITE OF TYPE Vd→c (H.K. 32090104)

A lava of the Taga volcano. Crossed nicols. × 20.

FIGURE 5. AUGITE-BEARING HYPERSTHENE-ANDESITE (H.K. 33082702).

Needle-like crystals of cristobalite (C) in the glassy groundmass show fluidal arrangement and also project into cavities. A lava of the Sukumogawa Andesite Group. × 65.

FIGURE 6. COGNATE INCLUSION (H.K. 38110602b) IN ANDESITE

A dike related to the Haya-kawa Tuff Breccias, showing mesh of tridymite (T) and plagioclase (P) with rim of anorthoclase (A). Dark patches are opacitized hornblende. × 65.

FIGURE 1

FIGURE 2

FIGURE 3

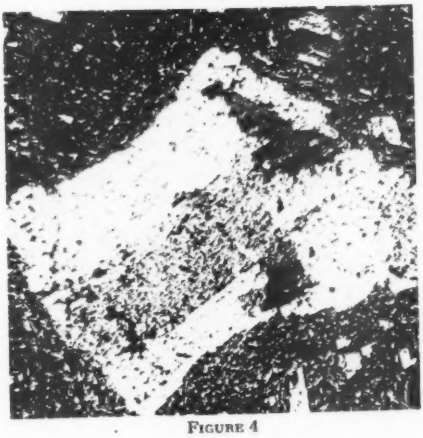

FIGURE 4

FIGURE 5

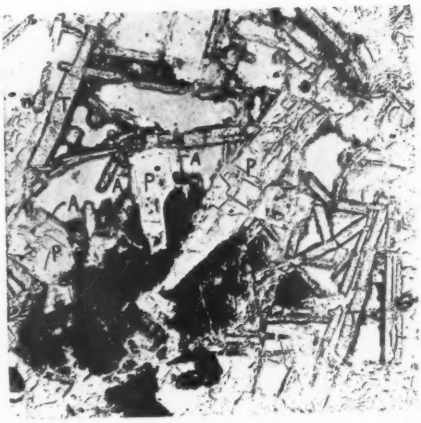

FIGURE 6

PHOTOMICROGRAPHS OF THE ROCKS OF IZU AND HAKONE

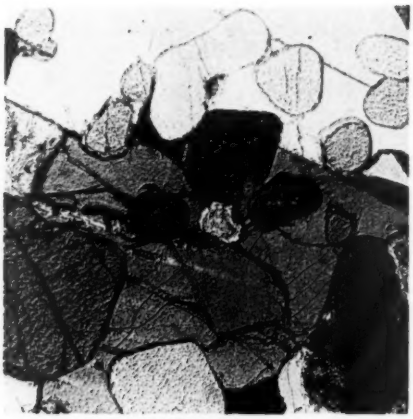

FIGURE 1

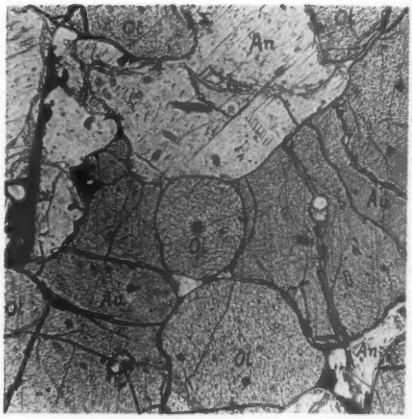

FIGURE 2

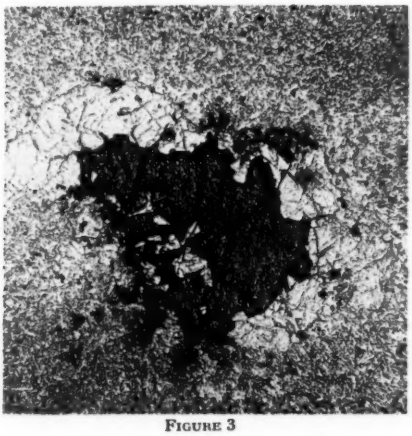

FIGURE 3

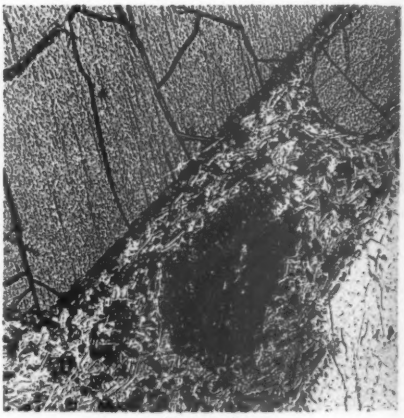

FIGURE 4

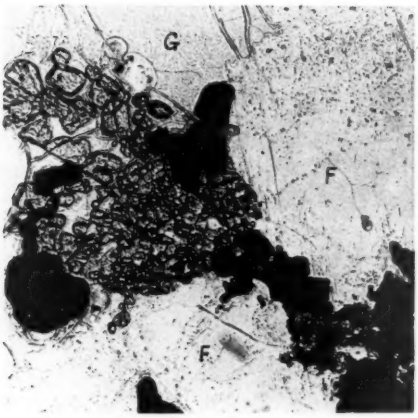

FIGURE 5

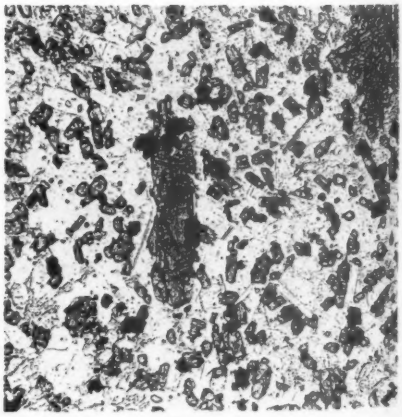

FIGURE 6

PHOTOMICROGRAPHS OF THE ROCKS OF IZU AND HAKONE

Plate 2.—PHOTOMICROGRAPHS OF THE ROCKS OF IZU AND HAKONE

FIGURE 1. ALLIVALITE (H.K. 33080805e)

Showing rounded crystals of olivine in a matrix of anorthite. A cognate block ejected from the Hakone volcano. Crossed nicols. × 65.

FIGURE 2. OLIVINE-EUCRITE (H.K. 33010901e)

Showing textural relation between olivine (Ol), augite (Au), and anorthite (An). A cognate block ejected from the Taga volcano. × 65.

FIGURE 3. ANHEDRAL CRYSTAL OF FAYALITE IN A DRUSE LINED WITH TRIDYMITE

Augite-bearing hypersthene-dacite (H.K. 39010903b). × 65.

FIGURE 4. QUARTZ-BEARING AUGITE-PIGEONITE-HYPERSTHENE-ANDESITE (H.K. 33022001)

Showing phenocrysts of plagioclase, hypersthene (a large crystal on the left), pigeonite (a rounded crystal), and hornblende (now completely pseudomorphed by pyroxene and magnetite). A lava of the old somma of Hakone. × 65.

FIGURE 5. AUGITE- AND HYPERSTHENE-BEARING PIGEONITE-QUARTZ-DIORITE

An aggregate of minute grains of pigeonite and magnetite passes into almost uniformly orientated, coarser crystals of pigeonite. G: glass. F: feldspar. The specimen same as that of Pl. 1, Fig. 1. × 65.

FIGURE 6. APHYRIC ANDESITE (H.K. 33081909a)

Showing plagioclase, pigeonite, magnetite, interstitial cristobalite (with a shagreened appearance), and apatite (fine needles). A lava of the old somma of Hakone. × 65.

Plate 3. PHOTOMICROGRAPHS OF THE ROCKS OF IZU AND HAKONE

FIGURE 1. PIGEONITE IN A DRUSE OF AUGITE-HYPERSTHENE-DACITE

The most acid member of type Vc (H.K. 40040801a). An essential block in pumice-tuff at the base o the young somma lavas of Hakone. × 80.

FIGURE 2. PHLOGOPITIC BIOTITE (right below) AND PIGEONITE (left above) IN DRUSES OF AUGITE-HY PERSTHENE-DACITE

Same as Pl. 3, Fig. 1. × 62.

FIGURE 3. PHENOCRYST OF HYPERSTHENE (IN AN EXTINCTION POSITION) WITH A RIM OF PIGEONIT

The two pyroxenes form a parallel intergrowth. Hypersthene-augite-olivine-basalt of type Vc (H.K 31050201). A lava of the Taga volcano. Crossed nicols. × 62.

FIGURE 4. PARGASITIC HORNBLENDE IN A DRUSE OF HYPERSTHENE-DACITE (H.K. 33090506d)

The clear area of the druse is occupied by tridymite. An essential block in pumice-tuff at the base of th young somma lavas of Hakone. × 62.

FIGURE 5. OLIVINE-BASALT

The most basic member of type IIIb→c (H.K. 32081806), showing phenocrysts of olivine and plagi clase. A lava of the Hata Basalt Group. × 62.

FIGURE 6. OLIVINE-BASALT OF TYPE IIIb→c (H.K. 33081401e)

Showing phenocrysts of olivine and plagioclase. A lava of the old somma of Hakone. × 62.

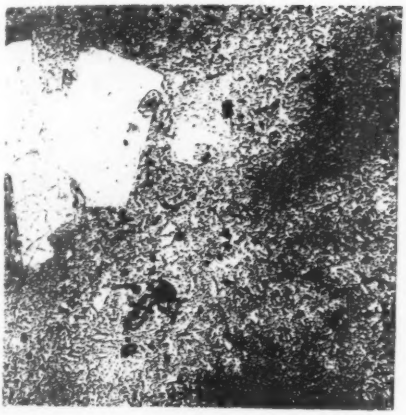

FIGURE 1

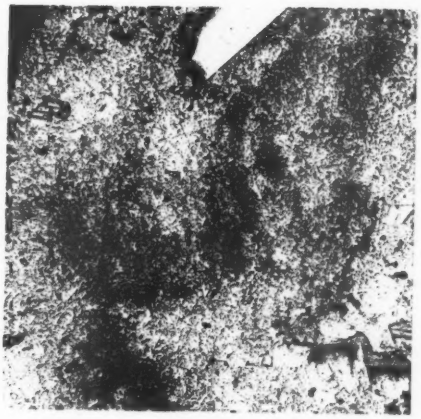

FIGURE 2

FIGURE 3

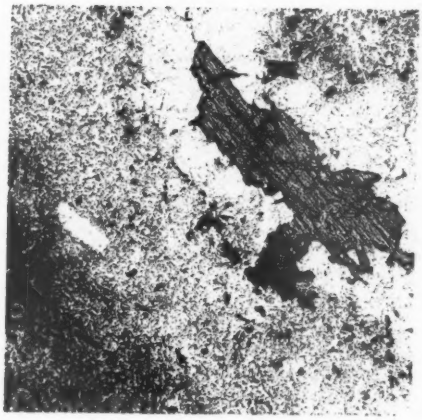

FIGURE 4

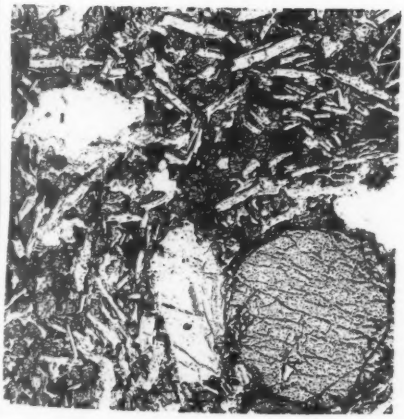

FIGURE 5

FIGURE 6

PHOTOMICROGRAPHS OF THE ROCKS OF IZU AND HAKONE

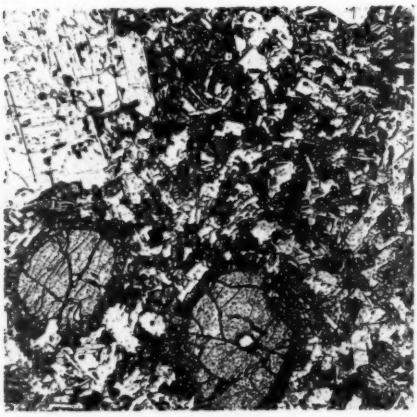

FIGURE 1

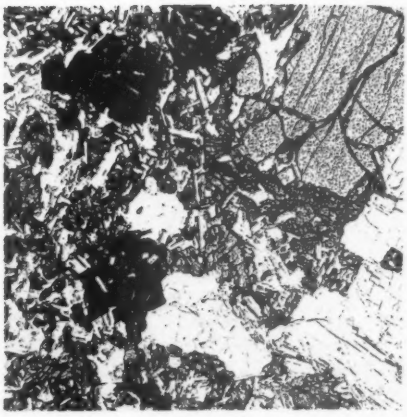

FIGURE 2

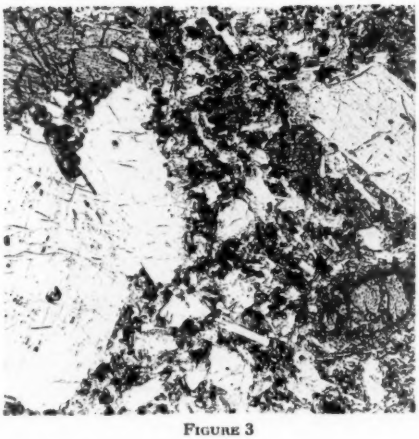

FIGURE 3

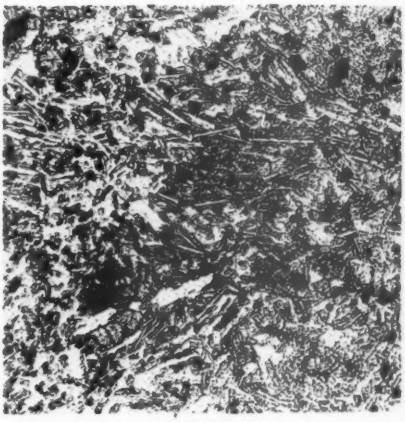

FIGURE 4

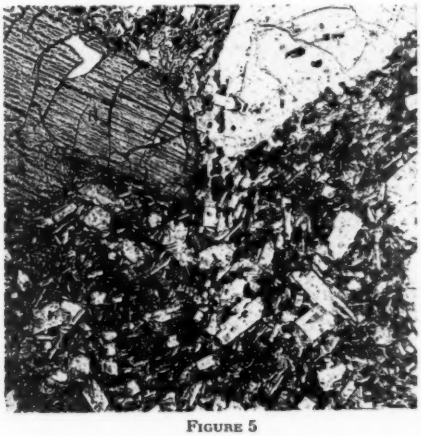

FIGURE 5

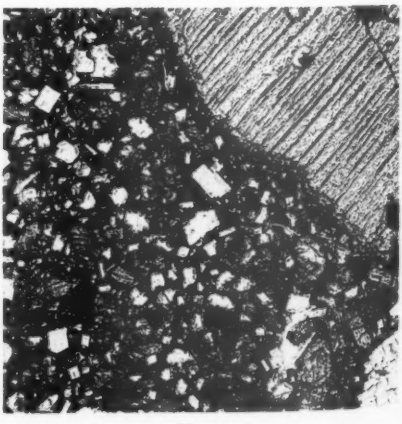

FIGURE 6

PHOTOMICROGRAPHS OF THE ROCKS OF IZU AND HAKONE

Plate 4. PHOTOMICROGRAPHS OF THE ROCKS OF IZU AND HAKONE

FIGURE 1. AUGITE-BEARING OLIVINE-BASALT OF TYPE IVc

(H.K. 31041812). Showing phenocrysts of bytownite and olivine (rimmed with pigeonite). A lava of the Taga volcano. × 62.

FIGURE 2. AUGITE-BEARING OLIVINE-BASALT OF TYPE IVc

(H.K. 32083005). Showing phenocrysts of olivine and anorthite in a coarse-grained groundmass. A lava of the Taga volcano. × 62.

FIGURE 3. HYPERSTHENE-BEARING OLIVINE-AUGITE-BASALT OF TYPE Vc

(H.K. 37112107b). An upper part of a composite lava flow, showing phenocrysts of bytownite, augite and resorbed olivine (rimmed with groundmass pigeonite). The Hata Basalt Group. × 65.

FIGURE 4. APHYRIC BASALT

(H.K. 31082204B). A lower part of the same composite lava flow as Pl. 4, Fig. 3. × 65.

FIGURE 5. HYPERSTHENE-AUGITE-OLIVINE-BASALT

Most basic member of type Vc (51227), showing phenocrysts of bytownite, hypersthene (h), and augite (A). A lava of the Aziro Basalt Group. × 62.

FIGURE 6. OLIVINE-BEARING/HYPERSTHENE-ANDESITE OF TYPE IIC

(H.K. 36090102). Showing phenocrysts of hypersthene and plagioclase and microphenocrysts of pigeonite. A lava of Kintoki-san volcano, Hakone. × 62.

Plate 5. PHOTOMICROGRAPHS OF THE ROCKS OF IZU AND HAKONE

FIGURE 1. AUGITE-HYPERSTHENE-ANDESITE OF TYPE Vc

(H.K. 31072908). Showing phenocrysts of hypersthene rimmed with granular pigeonite of the groundmass. A lava of the old somma of Hakone. × 62.

FIGURE 2. AUGITE-HYPERSTHENE-ANDESITE

An acid member of type Vc (H.K. 33090504), showing phenocrysts of plagioclase and augite (with a narrow marginal zone of quasi-uniaxial pigeonite) in a fine-grained holocrystalline groundmass. A lava of the young somma of Hakone. × 65.

FIGURE 3. HYPERSTHENE-AUGITE-ANDESITE

An acid member of type Vc (H.K. 33082502c), showing phenocrysts of plagioclase and augite (with a narrow marginal zone of quasi-uniaxial pigeonite). A lava of the young somma of Hakone. × 62.

FIGURE 4. HYPERSTHENE-BEARING OLIVINE-AUGITE-ANDESITE

A basic member of type Vd (H.K. 31071801c), showing phenocrysts of plagioclase (with dust inclusions), augite, and altered olivine. A lava of the Tensyô-zan Basalt Group. × 62.

FIGURE 5. OLIVINE-BEARING HYPERSTHENE-AUGITE-ANDESITE OF TYPE Vd

(H.K. 33082410). Showing phenocrysts of augite and labradorite (with dust inclusions). The lava of Simohutago-yama dome. × 62.

FIGURE 6. OLIVINE-AUGITE-HYPERSTHENE-ANDESITE OF TYPE Vd

(H.K. 32082002). Showing phenocrysts of plagioclase and olivine (rimmed with groundmass hypersthene) in a coarse-grained groundmass. A lava of the Taga volcano. × 65.

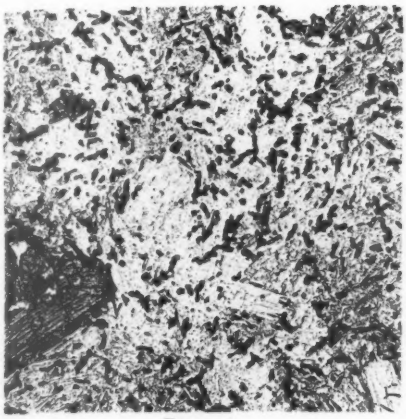

FIGURE 1

FIGURE 2

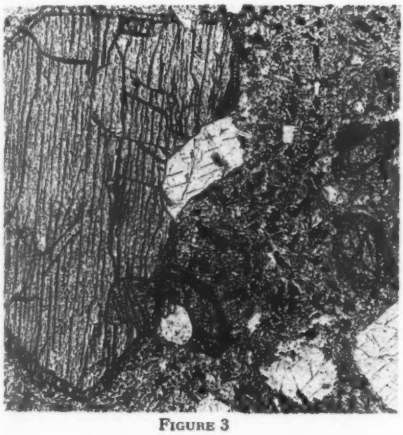

FIGURE 3

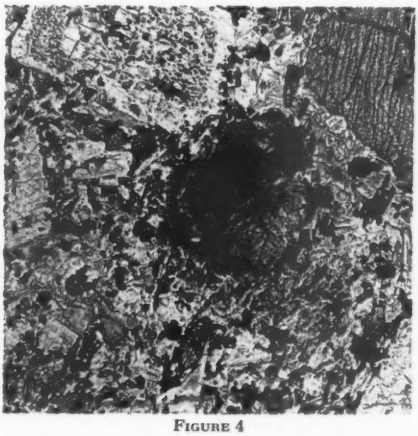

FIGURE 4

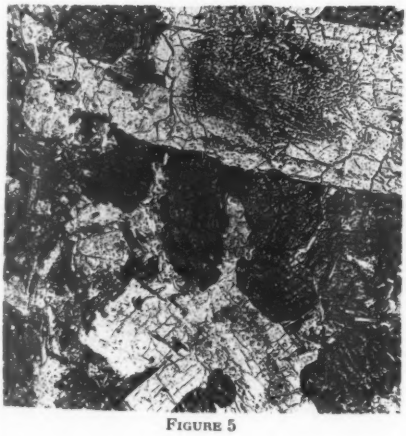

FIGURE 5

FIGURE 6

PHOTOMICROGRAPHS OF THE ROCKS OF IZU AND HAKONE

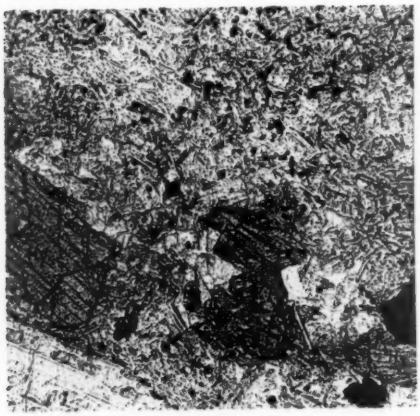

FIGURE 1

FIGURE 2

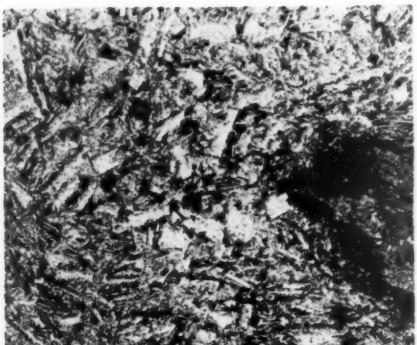

FIGURE 3

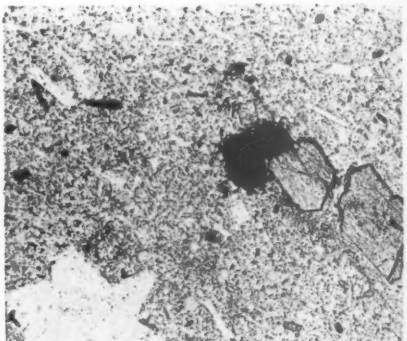

FIGURE 4

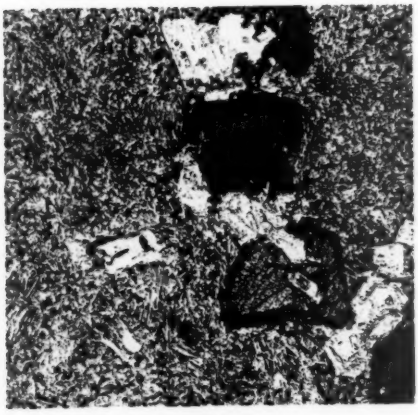

FIGURE 5

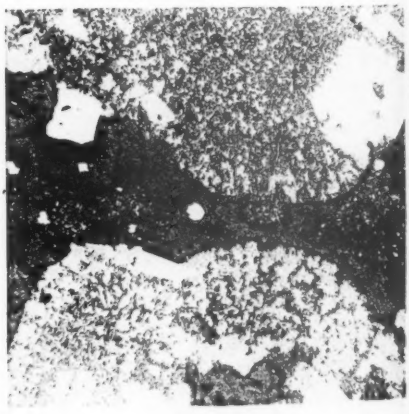

FIGURE 6

PHOTOMICROGRAPHS OF THE ROCKS OF IZU AND HAKONE

Plate 6. PHOTOMICROGRAPHS OF THE ROCKS OF IZU AND HAKONE

FIGURE 1. AUGITE-HYPERSTHENE-ANDESITE OF TYPE Vd

(H.K. 34081408). Showing pargasitic hornblende (Ho) and phlogopitic biotite (B), together with phenocrysts of hypersthene (Hy), plagioclase, and magnetite. Minute prisms of hypersthene are found in the groundmass. A lava of the old somma of Hakone. × 65.

FIGURE 2. HYPERSTHENE-AUGITE-DACITE

An acid member of type Vd (H.K. 33080906a). Showing phenocrysts of augite. A lava of the old somma of Hakone. × 62.

FIGURE 3. GREEN HORNBLENDE-DACITE OF TYPE VIIIe

(H.K. 33082408a). Showing phenocrysts of opacitized hornblende and plagioclase with dust inclusions in a groundmass consisting of tabular plagioclase, needle-like hypersthene, octahedral magnetite, and acid mesostasis. A dike related to the Haya-kawa Tuff Breccias. × 65.

FIGURE 4. AUGITE-BEARING HYPERSTHENE-DACITE OF TYPE Ve

(H.K. 32080904) Showing phenocrysts of plagioclase, hypersthene, magnetite, and apatite (Ap) in a groundmass carrying prisms of hypersthene and plagioclase in a felsitic matrix. A dike through the Tensyô-zan Basalt Group. × 65.

FIGURE 5. GREEN HORNBLENDE-AUGITE-HYPERSTHENE-DACITE OF TYPE VIe

(H.K. 33081708). Showing phenocrysts of magnetite, plagioclase, and augite (with a rim of groundmass hypersthene). Fine needles of hypersthene are scattered in the groundmass. A dike related to the Haya-kawa Tuff Breccias. × 62.

FIGURE 6. OXYHORNBLENDE-HYPERSTHENE-QUARTZ-DACITE (H.K. 38110301)

Showing phenocrysts of quartz (right and left above). The rounded patches of the groundmass are of higher crystallinity than the dark area, the former consisting of spherulitic growth of quartz, tridymite, acid feldspars, and a few biotite. The lava of the dacite dome near Kamitaga. × 21.

BULLETIN OF THE GEOLOGICAL SOCIETY OF AMERICA
VOL. 61, PP. 1021—1022 SEPTEMBER 1950

Short Notes

VOLCANIC GEOLOGY OF TOOWA VALLEY, SOUTHERN SIERRA NEVADA, CALIFORNIA

A REPLY

By Evans B. Mayo

Robert W. Webb (1950) has reported many welcome details concerning a fascinating area. The following comments are not intended to detract from the value of his work. They concern only the material under "Structural Setting" (Webb, 1950, p. 357). Under this caption he wrote: "Structural patterns are not evident in the relations of these volcanic centers, and no generalizations appear justified."

One may wonder just what Webb considers a structural pattern to be like. Any arrangement of points in space constitutes some sort of a pattern. It is assumed, however, that he meant that there appeared not to be in the arrangements or orientations of these volcanoes, either as individuals or as groups, any relation to any known pattern of regional structures. Because he did not reveal his concept of the regional pattern, it is necessary to furnish one in order that the above quotation may be tested.

In the paper cited by Webb (Mayo, 1947), an attempt was made to show that the regional pattern was dominated by four "framework" directions: (1) northwest, (2) northeast, (3) nearly north-south, and (4) west-northwest. As stated elsewhere (Mayo, 1941, p. 1050) these may not be the only directions important in the regional structure.

The writer has been impressed by a topographic map (Maxson, 1950, Pl. 1) on which the above directions stand in relief, thanks to diastrophism and erosion. Toowa Valley, together with related features to the east-southeast, stands out clearly. All these features combined are a west-northwest element.

The volcano map (Webb, 1950, Pl. 1) shows 33 vents. The vent, or vents, at the Tunnel center is not shown, therefore not counted. Of the 33 indicated outlets, most are arranged along Toowa Valley; at least 29 are within half a mile of the valley axis. The field, then, is elongated parallel to Toowa Valley which, as we have seen, is part of a west-northwest element of the regional framework.

It seems that the west-northwest direction afforded the dominant structural control; but this control was interfered with by structures following other regional directions. Seven of the outlets are elongated north-south (in regional direction 3). Thirteen of them, including the Little Whitney vent, are elongated northeast-southwest, a direction followed by some of the valleys tributary to Toowa Valley. Also, the two large cones are breached toward the northeast. Obviously, a structural pattern is evident in the relations of these volcanoes.

Concerning the breaching of the Groundhog and South Fork cones, Webb wrote (1950, p. 357):

> "Cones are commonly breached when flows emanating at or near the cone base cause collapse or breaching by engulfing part of the cone. Intersecting fissures, joints, faults, or other structures are not necessarily evidenced by breaching of cones in a given direction."

The first statement is elementary, and the mechanism was never questioned by this writer. But why should this process cause cones to breach in so nearly the same direction?

The direction of breaching could, of course, have been a function of slope. The possibility exists that, at the time the cones were breached, the surface sloped at both localities in exactly the same direction, causing the emerging lavas to breach the cones alike. It seems more probable, however, that the surface was different at the two places and that the cones should therefore be differently breached.

If, as previously suggested (Mayo, 1947, p. 501), the cones were built on intersections of east-west (west-northwest) and northeasterly fractures, might not adjustments on the northeasterly fractures have favored the escape of lavas on the northeastern sides of the outlets? Because no very great differences may be expected in the trends of the northeasterly fractures at the two sites, certainly it would not be surprising if the cones breached very nearly alike. Perhaps the Groundhog and South Fork outlets, if the cones were removed, would appear to be elongated to the northeast as the Little Whitney and certain other vents are shown to be.

The above argument does not prove that structure controlled the breaching, but to this writer the evidence still "suggests that the cones were erupted where northeast fissures intersected the east-west fissure."

References Cited

Maxson, John H. (1950) *Physiographic features of the Panamint Range, California*, Geol. Soc. Am., Bull., vol. 61, p. 99, Pl. 1.

Mayo, Evans B. (1941) *Deformation in the interior Mt. Lyell-Mt. Whitney, California*, Geol. Soc. Am., Bull., vol. 52, p. 1050.

—— (1947) *Structure plan of the southern Sierra Nevada, California*, Geol. Soc. Am., Bull., vol. 58, p. 495–504.

Webb, Robert W. (1950) *Volcanic geology of Toem Valley, southern Sierra Nevada, California*, Geol. Soc. Am., Bull., vol. 61, p. 349–357, esp. Pl. 1.

Kelowna Exploration Co., Nickel Plate, British Columbia, Canada